Universitat Politècnica de València
Departamento de Máquinas y Motores Térmicos

Implementation of a Combustion Model based on the Flamelet Concept and its Application to turbulent reactive Sprays

Doctoral Thesis

Presented by:
Johannes Franz Winklinger

Directed by:
Dr. Ricardo Novella Rosa

Valencia, December 2014

Doctoral Thesis

Implementation of a Combustion Model based on the Flamelet Concept and its Application to turbulent reactive Sprays

Presented by: Johannes Franz Winklinger

Directed by: Dr. Ricardo Novella Rosa

Evaluation board:

President: Prof. José M. Desantes
(Universitat Politècnica de València)

Secretary: Prof. Juan José Hernández Adrover
(Universidad de Castilla-La Mancha)

Examiner: Dr. Peter Priesching
(AVL List GmbH, Graz)

External examiners:

Prof. Tommaso Lucchini
(Politecnico di Milano)

Dr. Peter Priesching
(AVL List GmbH, Graz)

Prof. Pedro Acisclo Rodríguez Aumente
(Universidad Carlos III de Madrid)

Valencia, December 2014

Abstract

The main objective of this work is the modeling of the turbulent combustion process of diesel-like sprays including the autoignition event and the quasi-steady flame structure. For this purpose, a combustion model based on the flamelet concept and embedded in a RANS environment is implemented in the CFD platform OpenFOAM. The implemented modeling approach follows the idea of an unsteady flamelet/progress variable (UFPV) model. In such models, the underlying assumption is to suppose that the structure of a turbulent flame can be described by a set of laminar diffusion flames (flamelets). Igniting and extinguishing solutions of such flamelets in opposed jet configuration are studied. The mixture fraction Z, the scalar dissipation rate χ, and the progress variable Y_c are key parameters in the description of unsteady flamelets. The transition of the mixture from the inert state to the stable reactive state is described unequivocally by Y_c. Moreover, an interesting method to calculate approximated diffusion flames (ADF) is studied with the objective to reduce the computational effort especially for complex fuels.

The subgrid turbulence-chemistry interaction is accounted for by means of presumed PDF modeling. In doing so, the joint statistical distribution of the mixture fraction, the stoichiometric scalar dissipation rate, and the progress variable is assumed. The outcome of this *a priori* calculation step is stored in a turbulent flamelet database. Four lookup parameters are required during a calculation run to obtain thermochemical properties from this pre-calculated table: the mean mixture fraction and its variance, the mean stoichiometric scalar dissipation rate, and the mean progress variable. Furthermore, two different ways of coupling combustion model and CFD code are presented.

First, the model is applied to the turbulent lifted H_2/N_2 jet flame experiment from Berkeley University. This laboratory flame is a widely used test case in the area of turbulent combustion modeling. Good agreement between computational results and experimental data is observed. Moreover, also the simplified version of the combustion model based on ADF solutions is successfully tested and encouraging results are obtained.

Finally, the simplified combustion model is applied to the experimental series of "Spray H" from the Engine Combustion Network (ECN). The calculated ignition delay and lift-off length are compared with experimental data, and the influence of ambient temperature on these two characteristic flame parameters is studied. Furthermore, the quasi-steady flame structure, predicted heat release rates, and species mass fractions are analyzed in detail.

Resumen

El objetivo principal de este trabajo es la modelización del proceso de combustión turbulenta de chorros diésel, incluyendo el evento de autoencendido y la estructura de la llama cuasi-estacionaria. Para este fin, se implementa un modelo de combustión basado en el concepto de *flamelets* en un entorno RANS en la plataforma CFD OpenFOAM.

El enfoque de modelado aplicado aquí sigue la idea de un modelo del tipo *flamelets* no-estacionarias/variable de progreso (UFPV). En estos modelos, la hipótesis subyacente es que se asume que la estructura de una llama turbulenta puede ser representada por un conjunto de llamas de difusión laminares (*flamelets*). Se han estudiado soluciones de encendido y apagado de estas llamas en configuración de flujo opuesto. La fracción de mezcla Z, la tasa de disipación escalar χ y la variable de progreso Y_c son parámetros clave en la descripción de tales llamas no-estacionarias. La transición de la mezcla desde el estado inerte hasta el estado reactivo estable está descrita unívocamente por Y_c. Además se estudia un método interesante para calcular llamas de difusión aproximadas (ADF) con el objetivo de reducir el coste computacional especialmente para combustibles complejos.

La interacción sub-malla de turbulencia-química está tomada en cuenta por medio de modelado de PDF presumido, de forma que se asume la distribución estadística conjunta de la fracción de mezcla, la tasa de disipación escalar estequiométrica y la variable de progreso. El resultado de esta operación *a priori* se almacena en una base de datos de *flamelets* turbulentas. Para obtener las propiedades termoquímicas de esta base de datos durante un cálculo, se requieren cuatro parámetros de busqueda: la media de la fracción de mezcla y su varianza, la media de la tasa de disipación escalar estequiométrica y la media de la variable de progreso. Además, se presentan dos diferentes formas de acoplamiento entre el modelo de combustión y el código CFD.

En primer lugar, el modelo se ha aplicado al experimento de la llama turbulenta despegada de H_2/N_2 de la Universidad de Berkeley. Esta llama de laboratorio es un caso de prueba ampliamente utilizado en el área de modelado de combustión turbulenta. Los resultados obtenidos representan un buen acuerdo entre la simulación y los experimentos. Por otra parte, la versión simplificada del modelo de combustión basado en soluciones ADF también se ha aplicado con éxito y se han obtenido resultados alentadores.

Finalmente, el modelo simplificado de combustión se aplica al "Spray H" del Engine Combustion Network (ECN). El tiempo de retraso y la longitud de despegue calculados se comparan con los datos experimentales. También se estudia la influencia de temperatura ambiente sobre estos dos parámetros característicos de llama. Además, se analiza con detalle la estructura de la llama cuasi-estacionaria, la predicción de las tasas de liberación de calor y las fracciones másicas de las especies.

Resum

L'objectiu principal d'aquest treball és la modelització del procés de combustió turbulenta de dolls dièsel, incloent l'esdeveniment d'autoignició i l'estructura de la flama quasi-estacionària. Amb aquesta finalitat, s'implementa un model de combustió basat en el concepte de *flamelets* en un entorn RANS a la plataforma CFD OpenFOAM.

L'enfocament de modelatge aplicat ací segueix la idea d'un model del tipus *flamelets* no-estacionàries/variable de progrés (UFPV). En aquests models, la suposició subjacent és que s'assumeix que l'estructura d'una flama turbulenta pot ser representat per un conjunt de flames de difusió laminars (*flamelets*). S'han estudiat solucions d'encesa i apagada d'aquestes flames en configuració de fluxos oposats. La fracció de mescla Z, la taxa de dissipació escalar χ i la variable de progrés Y_c són paràmetres clau en la descripció d'aquestes flames no-estacionarias. La transició de la mescla des de l'estat inert fins a l'estat reactiu estable està marcada unívocament per Y_c. A més s'estudia un mètode interessant per calcular flames de difusió aproximades (ADF) amb l'objectiu de reduir el cost computacional especialment per a combustibles complexos.

La interacció subgrid de turbulència-química està presa en compte per mitjà de modelatge de PDF presumit, per tal d'assumir la distribució estadística conjunta de la fracció de mescla, de la taxa de dissipació escalar estequiomètrica i de la variable de progrés. El resultat d'aquest pas de càlcul a priori s'emmagatzema en una base de dades de *flamelets* turbulentes. Per obtenir les propietats termoquímiques d'aquesta base de dades durant un càlcul es requereix quatre paràmetres de cerca, la mitjana de la fracció de mescla i la seva variància, la mitjana de la taxa de dissipació escalar estequiomètrica i la mitjana de la variable de progrés. A més, es presenten dues formes diferents d'acoblament entre el model de combustió i el codi CFD.

En primer lloc, el model està aplicat a l'experiment de la flama turbulenta enlairada d'H_2/N_2 de la Universitat de Berkeley. Aquesta flama de laboratori és un cas de prova àmpliament utilitzat en l'àrea de modelatge de combustió turbulenta. Els resultats obtinguts representen un bon acord entre la simulació i els experiments. D'altra banda, la versió simplificada del model de combustió basat en solucions ADF està també aplicat amb èxit i s'obtenen resultats encoratjadors.

Finalment, el model simplificat de combustió s'aplica al "Spray H" de l'Engine Combustion Network (ECN). El temps de retard i la longitud d'enlairament computacionalment obtinguts es comparen amb les dades experimentals. També s'estudia la influència de la temperatura ambient sobre aquests dos paràmetres característics de flama. A més, s'analitza amb detall l'estructura de la flama quasi-estacionari, taxes d'alliberament de calor calculades i fraccions màssiques d'espècies.

Zusammenfassung

Das Ziel dieser Arbeit ist die Modellierung turbulenter Verbrennungsprozesse Diesel-ähnlicher Sprays einschließlich der Selbstzündung und der quasi-stationären Flammenstruktur. Zu diesem Zweck wurde ein Verbrennungsmodell basierend auf dem *Flamelet*-Konzept – eingebettet in eine RANS Umgebung – in die CFD Plattform OpenFOAM implementiert.

Der gewählte Modellierungsansatz folgt der Idee eines sogenannten *unsteady flamelet/progress variable (UFPV) model* (zu Deutsch etwa: instationäres Flämmchen/ Fortschrittsvariable-Model). Der solchen Modellen zugrunde liegende Ansatz beruht auf der Annahme, dass eine turbulente Flamme durch ein Ensemble laminarer Diffusionsflammen (*Flamelets*) repräsentiert werden kann. Zu Beginn werden numerische Lösungen solch entzündender und erlöschender Flamelets in Gegenstromkonfiguration untersucht. Der Mischungsbruch Z, die skalare Dissipationsrate χ und die Fortschrittsvariable Y_c stellen die Schlüsselparameter bei der Beschreibung instationärer Flamelets dar. Der Übergang des Gemisches vom inerten in den stabilen, reaktiven Zustand wird dabei durch Y_c eindeutig beschrieben. Mit dem Ziel den Rechenaufwand, speziell im Fall komplexer Kraftstoffe, zu verringern, wird zusätzlich eine attraktive Methode zur Berechnung approximierter Diffusionsflammen (ADF) implementiert und untersucht.

Die vom Rechennetz nicht aufgelöste Turbulenz-Chemie-Interaktion wird durch Modellierung mittels vorausgesetzter Wahrscheinlichkeitsdichtefunktionen berücksichtigt, mit welchen die gemeinsame statistische Verteilung des Mischungsbruchs, der skalaren Dissipationsrate und der Fortschrittsvariablen beschrieben wird. Das Ergebnis dieses vorab durchgeführten Berechnungsschritts wird in einer Datenbank turbulenter *Flamelets* gespeichert. Zur Ermittlung thermochemischer Eigenschaften aus dieser Datenbank während einer Berechnung sind vier Eingabeparameter nötig: der Mittelwert des Mischungsbruchs und dessen Varianz sowie die Mittelwerte der stöchiometrischen, skalaren Dissipationsrate und der Fortschrittsvariable. In der Modellbeschreibung werden abschließend zwei unterschiedliche Methoden zur Kopplung des Verbrennungsmodells mit dem CFD Code vorgestellt.

Als erster Testfall für das Verbrennungsmodell dient das Experiment einer turbulenten, abgehobenen H_2/N_2 Gasflamme, durchgeführt an der Universität Berkeley. Diese Laborflamme stellt einen viel beachteten Testfall im Bereich der Modellierung turbulenter Verbrennungsvorgänge dar. Die Simulationsergebnisse zeigen sehr gute Übereinstimmung mit diesen experimentell ermittelten Daten. Zusätzlich zur Standardimplementierung wurde auch die vereinfachte Version des Verbrennungsmodells basierend auf ADF-Lösungen erfolgreich auf diese Gasflamme angewandt und damit vielversprechende Ergebnisse erzielt.

Abschließend werden mit dem vereinfachten Verbrennungsmodell Sprays in unter-

schiedlicher Umgebungstemperatur simuliert. Als Anwendungsbeispiel dient die "Spray H" Experimentreihe des Engine Combustion Networks (ECN). Die berechnete Zündverzögerung sowie die Abhebelänge werden mit den vorhandenen experimentellen Daten verglichen. Außerdem wird der Einfluss der Umgebungstemperatur auf diese beiden charakteristischen Flammenparameter untersucht. Darüber hinaus werden die quasi-stationäre Flammenstruktur, prognostizierte Wärmefreisetzungsraten und die Verteilung der Massenanteile der chemischen Komponenten einer detaillierten Analyse unterzogen.

Acknowledgment

The development of a PhD thesis goes along with quite a number of frustrating days where you feel pretty lonesome. Fortunately, I had a lot of people around me who helped me to get over those difficult days. Since it is not my intention to state a long list of names here, I rather mention some of them as representatives for quite a few more.

First of all, I would like to thank Prof. José M. Desantes for his personal interest in my work, and his support with the paper work at the end of my PhD. I always enjoyed our conversations that often spilled over to German and lead us far away from professional matters.

Quite at the beginning of my research work I got stuck the first time with some programming issues that exceeded my former knowledge in this field. Luckily I met Eloy Romero in a meeting some weeks before. The helping "programmer fingers" of—in the meantime Dr.—Eloy represented my salvation at this point and I learned a lot about classes, hash functions, and so on from him. Thank you Eloy!

About midway of my PhD, I participated in a series of lectures given by Dr. Bertrand Naud, another fortune "coincidence". Thenceforth, our group entered a highly interesting and profitable collaboration with him, which resulted in joint publications and over all in a sharp increase of my knowledge of combustion modeling. It is not always easy to maintain a close cooperation when the workplaces are separated by several hundred kilometers, however, our mutual effort made that possible. Thank you very much Bertrand for all the lively discussions we had, for your active support, for sharing your knowledge, and for throwing light on some dark areas of combustion modeling.

Above all, I want to thank two people, my adviser Dr. Ricardo Novella and my co-adviser Dr. José Manuel Pastor, who guided me in and sometimes pushed me through these four years. In the end, I even owe them the fact that I could do my PhD here, since they decided to choose me as their new collaborator. At this time I hardly spoke Spanish, but they evidently understood that I only wanted to work within their field of research. At the beginning everything was really new to me somehow, as usual when starting new challenges. I had to learn many things apart from my actual research work such as Spanish, the quite different mentality, and sometimes also the different way of getting things done. Both, Ricardo and José Manuel, had a lot of patience with me and we soon became a real team. Although we are three quite different characters, it was always congenial to work together with them. Ricardo has an extremely wide range of knowledge and an impressively quick and analytic

mind. Additionally, he seems to have an endless source of energy with which he often pushed me to try harder and do better. José Manuel often dropped in with his selective comments that were especially welcome when Ricardo and I run out of ideas. His great experience in CFD and the fact that he is something like a walking library were particularly helpful to me. I absolutely enjoyed working together with Ricardo and José Manuel. Looking back, I feel really lucky to have had them by my side. ¡Muchísimas gracias Ricardo! ¡Muchísimas gracias José Manuel!

Last but not least, sincere thanks to all my valuable colleagues. You great guys are responsible for many hours of fun, witty conversations and some unforgettable "torràs". But they were also good to share common sorrows. Our after-work sessions over beer and some delicious tapas were very valuable to me. The best thing is that most of these colleagues turned into friends. I clearly remember when Chris, the crazy American with some Polish cells and "guiri" like me, inducted me to some peculiarities of the department in the first week of this long journey. Thanks Chris for your extraordinary parties! Special thanks goes to Walter and Adrián for being such helpful and congenial office mates. I will never forget the big support I received from Edu during my first weeks, when I was completely lost with all the paper work. Thank you so much Edu for becoming such an honest and precious friend. And not to forget, I enjoyed our staircase-coffee breaks. Danke, euch drei! All the best to you Eduardo for carrying on this work and thank you for the interesting time that we worked together. I learned a lot, I hope you too.

At this point I would like to mention two further important aspects that influenced me and my work over the last four years. The first one is the amazing campus of the UPV and the lovely, virtually always sunny city of Valencia. It is a great place to live with nice people and an excellent cuisine. Moreover, they know how to celebrate a festival that has no equal, the "Fallas", where the most beautiful occurrence of combustion is happening. The second one refers to free and/or open source tools such as OpenFOAM, Gnuplot, LaTeX, Ubuntu, Linux, etc. A lot of people work hard to develop such powerful instruments. Thanks to all of you!

Danke – Gracias

In der Wissenschaft spielen Konstanten oft eine sehr wichtige Rolle, so auch in dieser Arbeit. Sie sind mathematisch betrachtet einfach zu handhaben und für korrekte Ergebnisse oft unumgänglich. Auch im Leben ist es wichtig Konstanten zu haben. Ich habe das große Glück viele solcher Konstanten an meiner Seite zu wissen. Diesen Menschen möchte ich hier noch einige Worte in meiner bzw. deren Muttersprache widmen.

Meine Freunde aus der Heimat und vom Studium stellen eine ganz außerordentliche Klasse von Konstanten dar. Das Nennen von Namen ist hier nicht notwendig, da jeder einzelne von ihnen weiß, dass er gemeint ist. Eine Gruppe sei aber doch erwähnt. Diese feine Runde verbindet nämlich interessanter Weise etwas, wo auch Verbrennung in einer ihrer schönsten Formen eine Rolle spielt, unsere "Kistnsau". Danke all jenen, die schöne und lustige Tage mit mir in Valencia verbracht haben. Meine Freunde sind ein sehr bunter Mix aus Menschen, die mich durchs Leben begleiten und es gewaltig bereichern. Sie alle haben für mich einen unermesslichen Stellenwert, den sie selbst manchmal gar nicht kennen. Ohne sie hätte ich so manche Dinge vielleicht nicht geschafft. Danke, dass ihr meine Freunde seid!

Die Entscheidung das Doktorat (relativ) weit weg von daheim anzustreben war kein einfacher Schritt. Er hat mich sicherlich verändert und auch meine Umgebung, vor allem meine Familie, beeinflusst. Ich weiß, dass meine Entscheidung gerade anfangs nicht leicht für sie war. Aber als wahre Konstanten haben sie mich auch dabei unterstützt. Danke euch allen für eure Besuche. Noch viel mehr Dank jedoch dafür, dass ihr mich immer wieder mit offenen Armen und einem breiten Lächeln empfängt. Diese Momente des Wiedersehens gehören zu den glücklichsten in meinem Leben!

Dass es überhaupt so weit gekommen ist, und ich hier diese Zeilen am Ende meiner Dissertation schreibe, verdanke ich meinen Eltern. Ich hatte das große Glück in einem liebevollen Zuhause aufzuwachsen. Meine Eltern haben mich zu einem offenen und interessierten Menschen erzogen. Sie haben mir gute Werte vermittelt, mir stets Rückhalt gegeben und mich unterstützt. Für alles, was ihr je für mich getan habt und hoffentlich noch tun werdet, danke ich euch aus tiefstem Herzen! Meine Sch(w)ester und mein B(r)uder sollen wissen, dass ich sehr stolz auf sie bin. Ich bin so froh, dass ich euch habe! Ihr seid alle immer für mich da, auch wenn ich nicht da bin.

Al final fue una persona, la que tuvo que soportarme incluso en mis peores momentos durante estos cuatro años, cuando me tomé la tesis demasiado en serio. María es más que solo una increíble pareja para mi, gracias a ella somos un equipo extraordinario que funciona ya muchos años. Te doy mis más sinceras gracias por todo lo que haces por mi y a la vez espero que sigamos de esta manera muchos años más. ¡Un abrazo y un beso muyyy fuerte!

Ich habe in diesen vier Jahren sehr viel gelernt, nicht nur fachlich sondern vor allem auch menschlich. Manchmal habe ich meine Arbeit zu wichtig genommen und ihr einen zu hohen Stellenwert eingeräumt. Gegen Ende meiner Dissertation wurde mir auf wunderbare Weise gezeigt, dass es im Leben aber viel wichtigere Dinge gibt. Danke!

Table of contents

Index of figures

Index of tables

Acronyms

ADF	Approximated diffusion flame
ASI	After start of injection
ASC	After start of combustion
CFD	Computational fluid dynamics
CMC	Conditional moment closure
CRT	Chemical reduction technique
DF	Diffusion flame
DI	Direct injection
DNS	Direct numerical simulation
EU	European Union
ECN	Engine Combustion Network
EGR	Exhaust gas recirculation
EVM	Eddy viscosity model
FANS	Favre-averaged Navier-Stokes
FGM	Flame generated manifold
FPI	Flame prolongation of ILDM
HR	Homogeneous reactor
HRR	Heat release rate
ICE	Internal combustion engine
ID	Ignition delay
ILDM	Intrinsic low dimensional manifold
ISAT	In-situ adaptive tabulation
LES	Large eddy simulation
LOL	Lift-off length

MMC	Multi mapping conditioning
PEA	Partial equilibrium approximation
PCM	Presumed conditional moment
PDF	Probability density function
PV	Progress variable
RANS	Reynolds-averaged Navier-Stokes
REDIM	Reaction diffusion manifold
ROI	Rate of injection
RSM	Reynolds stress model
TFC	Total final consumption
TPDF	Transported probability density function
TPES	Total primary energy supply
UDF	Unsteady diffusion flame
UFPV	Unsteady flamelet progress variable
QSSA	Quasi steady-state approximation

Chapter 1

Introduction

Contents

1.1 Combustion – Look back and outlook

For some one million years men make use of fire—the most common form of combustion—as evidenced by archaeological artifacts found all over the world. But it took mankind hundreds of thousands of years to take advantage of fire apart from cooking, illumination or pottery. Steam engines are one of the first attempts to convert the energy released by fire into controlled and continuously generated work. The atmospheric engine invented by the English forger Thomas Newcomen (1664–1729) around 1712 can be considered as the first serious example of an engine, though still at a very low efficiency it was used to pump water. From about 1769 the Scottish engineer James Watt (1736–1819) made some fundamental modification to Newcomen's engine

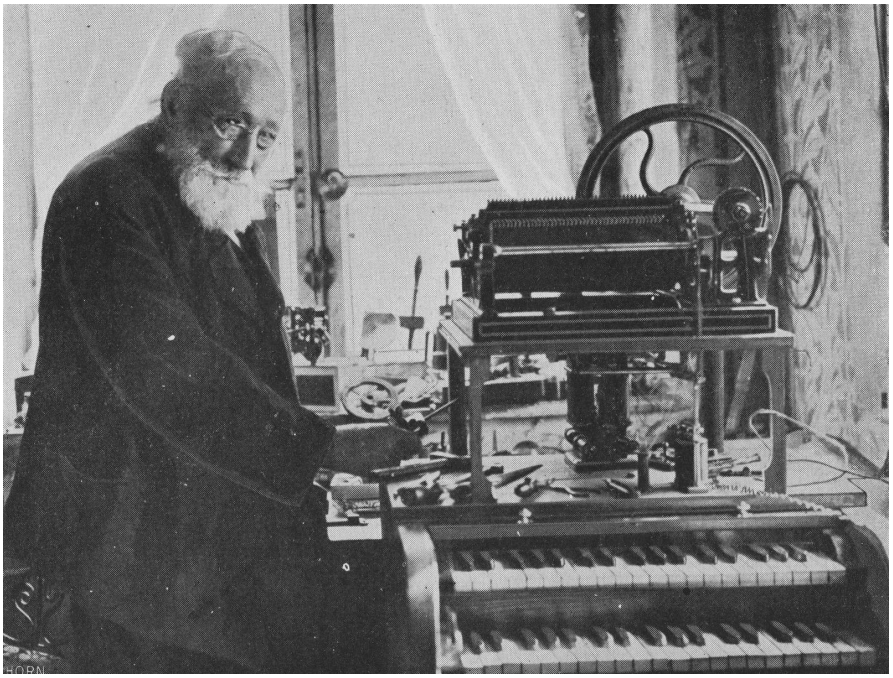

Figure 1.1. *Tyrolean clockmaker Christian Reithmann, the first to take a patent on a four–stroke engine.*

which resulted in an improved steam engine and marked the beginning of the industrial revolution. Almost at the same time the English inventor John Barber (1734 – 1801) presented a detailed description of a gas turbine, virtually including all features of today's gas turbines for which he was granted a patent in 1791. In 1858 the Belgian engineer Jean Joseph Étienne Lenoir (1822–1900) developed the first functional and commercially successful internal combustion engine (ICE) which was fired with a mixture of coal gas and air. Right in the middle of the industrial age dropped one of the key inventions of this time which has an enduring impact on the world. On the 26th of October 1860 the Tyrolean clockmaker Christian Reithmann (1818–1909), shown in Fig. 1.1 taken from [1], took out the first patent for an engine running on the four–stroke cycle. The engine had a stroke of 111 mm and a bore of 98 mm and it run on 200 min^{-1} in his workshop until 1881. More than 150 years later the principles of this engine are still in use in countless diesel and petrol engines running in cars, ships, aircraft, etc. All these engines and their respective enhancements used nowadays, have an internal or external combustion process in common where chemical reactions between a fuel and an oxidizer generate

thermal energy that is afterwards converted to mechanical work.

Since then, the developers spirit of engineers together with growing knowledge of thermodynamics and combustion contributed to the rapid improvement of internal combustion engines which made them more reliable and efficient to use. As a result, they quickly found application in many different fields such as pump stations or transportation during the industrial revolution in Europe and North America. This increasing use of ICEs also marked the beginning of a steep rise of consumption of fossil fuels which is, although at lower rate, growing until now (see Fig. 1.2 taken from [2]) and has been the driving force behind the economic growth and the industrialisation of the modern world. Until today the world total primary energy supply (TPES) has reached about 13100 Mtoe of which more than 81% is produced from fossil fuels [3, 4]. The TPES is foreseen to rise up to approximately 14000–17000 Mtoe till 2035, depending on the underlying scenario, with an predicted share of oil, coal and natural gas of around 70% [3]. This primary energy stored in fossil fuels, virtually without exception, is transformed to thermal energy in different combustion devices to be afterwards directly used as heat or converted to other forms of energy.

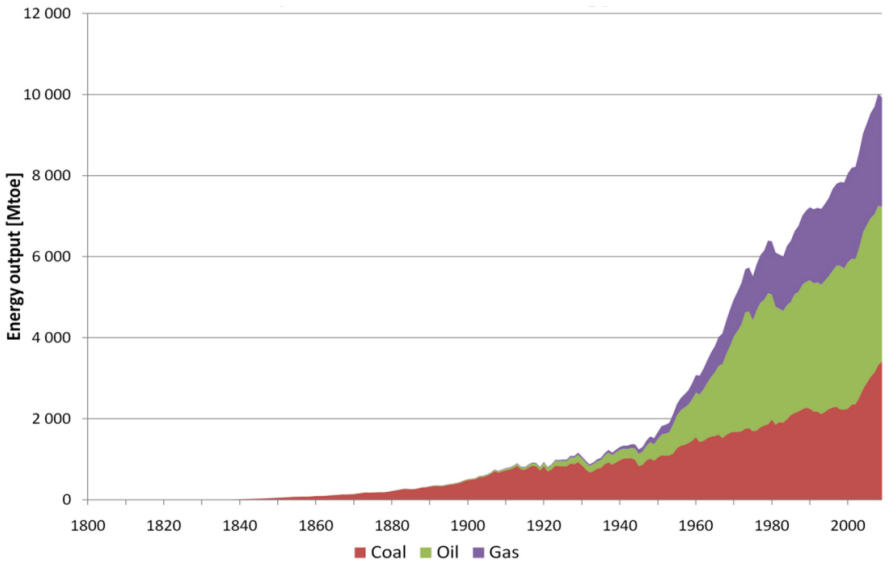

Figure 1.2. *Historical production of fossil energy from 1800 to 2009.*

In the European Union (EU) for example, one-third of the final energy consumption of 1103 Mtoe was used in the transport sector in 2011 [4]. The main power source in this sector are ICEs such gas turbines or reciprocating internal combustion engines with oil being by far the most important fuel type. In Germany for instance, almost 93% of the total final consumption (TFC) in the transport sector come from petroleum products (with a split of 48.5% diesel, 28.8% gasoline and 14.4% aviation petrol), 4.6% from biofuels and around 2% is electric energy mainly used in rail traffic [5]. Road transport accounts for more then 80% of the energy use within the transport sector in the EU, however, aviation currently at about 14% is growing rapidly [6]. It is expected that the global passenger volume will grow to around 16 billion passengers compared to 2.5 billion passengers in 2011 [7]. Consequently, there is also an important demand on new passenger and freighter aircraft summing up to more than 29200 aircraft deliveries until 2032 (considering only air planes with more than one hundred seats) according to a current estimate [8]. Moreover, the motorization rates in countries like France or Germany for example are estimated to increases by about 24% and 19%, respectively, until 2035 based on the respective levels of 2005 [9]. On a global perspective, it is even expected that the total number of passenger cars nearly doubles to almost 1.7 billion in 2035 [10].

All these figures underline the need of efficient combustion systems for the next decades. The continuously growing economic wealth in a globalized world stimulates the demand of energy, private mobility and transportation of goods. In order to overcome these challenges with a reduced use of limited resources in the future, unceasing efforts to improve existing devices as well as new strategies will be necessary. This includes for instance the development of modern light-weight materials and their application in cars and aircraft which contributes to further reduction of specific fuel consumption. However, the combustion process in itself will certainly remain the key factor of an efficient and clean engine, but at the same time also the most sophisticated process due to multiple reasons as addressed in the next section.

1.2 Particular challenges of thermal engines

Thermal engines such as reciprocating internal combustion engines or gas turbines are sophisticated machines having their origins hundreds of years ago as reminded in section 1.1. During this long period of continuous development, engineers tried to better understand the complex physical and

chemical phenomena that occur in the interior of thermal engines. Needless to say, these phenomena did not change over the time and neither did the basic principles of operation of many of these engines. Therefore, some main challenges still remain which will be discussed below. The first topic is valid in general for combustion devices whereas all other mentioned challenges are maybe not present in every type of combustion device but are specific to a certain range of devices this work is focused on.

- **Turbulent flow.** Just as the vast majority of technical applications, thermal engines are working virtually without exception (besides some domestic furnaces) in a turbulent flow regime. This fact has some far–reaching consequences on the combustion process. Turbulence has influence on the stratification of the reactive mixture and consequently on the flame structure, it may increase chemical reaction but also prevent the progression of chemical reaction and lead to quenching of the flame. Moreover, there exists a two–way coupling between turbulence and chemistry which means that turbulence is on the other hand influenced by strong heat release from chemical reactions. The heat transfer on walls is also strongly affected by turbulence.
  Apart from the mentioned physical aspects, turbulence also has a great impact when it comes to its numerical treatment. Turbulent flow is chaotic and its structure is always three–dimensional making it difficult to simulate.

- **Non–premixed combustion.** A large number of industrial applications make use of non–premixed combustion where fuel and oxidizer enter separately the combustion device. There are two main reasons for the use of this combustion regime instead of premixed combustion being the second regime [1]. First, non–premixed burners are simpler to design since no prior reactant mixing is required and, second, non–premixed flames do not propagate which makes them safer to operate. The fact of the separate existence of fuel and oxidizer in the combustion chamber requires their mixing before combustion. This mixing process is significantly influenced by turbulent fluctuations present in such devices. The time needed to bring together fuel and oxidizer in the reaction zone becomes a key parameter in this combustion regime. This additional aspect makes non–premixed combustion more difficult to understand and

[1] Partially premixed combustion is actually a combination of the two above–named combustion regimes and therefore not considered as a third regime though sometimes different classifications are used.

describe than premixed combustion, but it also attracts more interest due to its wider range of application.

- **Multiphase mixture.** In many mobile applications of combustion devices like cars or aircraft, liquid fuel is carried aboard and consequently introduced in liquid form into the combustion chamber. Hence, it has to be evaporated before it can be burned. This phase–change process usually occurs simultaneously with the mixing process mentioned above and consists of several sub–processes such as droplet breakup, atomization or coalescence. Moreover, these processes occur within a turbulent flow environment.

- **Unsteady conditions.** Internal reciprocating combustion engines (e.g. Diesel engines) in particular do not posses a continuous combustion process like for instance gas turbines. There is only limited range of time—the combustion stroke—for the evaporation, mixing and combustion processes to take place. This means that there is no steady state during the whole process and unsteady effects may become more important. Moreover, applications like Diesel engines do not work in a constant operating point, on the contrary, conditions like pressure, temperature or oxygen level (e.g. due to the use of EGR) can change rapidly.

- **Complex fuels.** Gasoline, diesel and jet fuel are the most common liquid fuels and together they represent by far the biggest share of fuels used in thermal engines applied in the transport sector. These fuels are not pure fuels but blends of different hydrocarbons with a complex chemical structure that is difficult to describe. Moreover, usually hundreds of species and thousands of reactions are involved in the reaction of such fuels which makes their modeling complicated. In general chemical reactions are highly non–linear, strongly dependent on temperature and proceed on a different time scale compared to other physical phenomena involved in the combustion process.

Apart from many other issues concerning the design of thermal engines, the above–mentioned challenges can be considered as the most characteristic and important ones without the claim to completeness. All of them are treated in more or less detail in this work.

1.3 Motivation and objectives

1.3.1 Motivation

Combustion processes provide about 90% of the worldwide energy support and accompany people in everyday's life. They represent the driving source in countless applications reaching from furnaces to aircraft. At present there is an ongoing demand for clean and efficient combustion devices arising for instance from the continuously growing demand for mobility and transportation of goods. This fact as well as ecological reasons—due to environmental considerations and limited resources—to design improved combustion systems are pointed out in section 1.1. Additionally to ecological causes and legal exigency (e.g. emission standards) exist economical concerns to improve the efficiency of combustion systems. Fuel costs often represent the main part of the operating costs in the aviation industry, the transport sector or for private vehicles, etc.
Today's thermal engines are highly developed devices unifying a lot of know–how which makes improvements challenging. Moreover, the physical and chemical phenomena involved in turbulent combustion processes are very complex and their interaction is still not entirely understood. Advancements in this complicated field of science are only possible through the combined adoption of experimental and numerical tools. Computer simulations became therefore an integral part in the design process of combustion systems and are indispensable in the investigation of turbulent combustion. They can drastically speed up the design process at reduced costs, and numerical simulations furthermore can provide additional information about the underlying problem, difficult or even impossible to obtain with experiments. This additional insight allows to study the different complex phenomena and hence increase the understanding of the sophisticated combustion process which is in turn the basis for improvements.
However, numerical simulation always goes along with modeling of parts of the real process since an exact numerical description is usually not possible. The further development of advanced combustion models is therefore crucial in the investigation of turbulent combustion and for the design process of modern combustion devices.

1.3.2 Objectives

The final objective of this work is the numerical simulation of the turbulent combustion process of fuel sprays as it occurs similarly in diesel engines or

aircraft engines. This implies the reproduction of the structure of a lifted diffusion flame in a turbulent environment. Additionally, the modeling of the autoignition event becomes a further issue in transient combustion problems. The reliable prediction of characteristic parameters like ignition delay and lift–off length is thus an important measure for combustion models applied in this area.
As a consequence, the implementation and validation of an advanced combustion model in a CFD platform represents the core task to accomplish these targets. This also implies the development of the necessary numerical tools. Primary due to the reduced computational cost, a RANS approach is chosen as working environment. However, the planned modeling strategy is extendable to LES approach.

1.4 Methodology and outline

1.4.1 Methodology

The global methodology of this work is briefly outlined in the following. At the beginning a bibliographic review is made to find the state of the art of combustion modeling and to detect future trends. As a conclusion of the review it was decided to implement a model based on laminar diffusion flames (flamelet concept). Hence, in a first step some basic investigations on unsteady flamelets in an opposed jet configuration are carried out using hydrogen as a simple test fuel. Moreover, an useful and interesting approximation of such laminar diffusion flames is analyzed.
Then a modeling strategy that accounts for the influence of turbulence-chemistry interaction based on presumed probability density functions (PDFs) is developed and implemented. At the same time a progress variable is introduced that describes the transition from the inert to the fully burned state of the reactive mixture. The resulting unsteady flamelet progress variable model is applied to simulate the turbulent lifted H_2/N_2 jet flame from Berkeley University, a relatively simple test case specially designed for validation of numerical models in the field of turbulent combustion. Different studies including model parameters and boundary condition variations are conducted in order to test the implemented model. Furthermore, the combustion model based on approximated diffusion flames is also assessed by means of this test case to verify its potential. Such a simplified version is of particular interest for combustion problems with more complex fuels, since it may further reduce the comparatively laborious calculation process of unsteady flamelet solutions in such cases. On an industrial level with more complex fuels and

variable operating conditions the conventional flamelet calculation process could rapidly become too expensive.
The simplified and adapted combustion model based on approximated diffusion flames is finally applied to diesel-like reactive sprays. The spray test cases are taken from the data base of the Engine Combustion Network and reflect operating conditions similar to those of modern diesel engines. The influence of varying ambient temperature is studied in order to assess the predictive capabilities of the simplified version of the combustion model.

1.4.2 Outline of this work

A brief outline of the contents of the following chapters is given below:

- **Chapter 2.** The second chapter consists of comprehensive bibliographic review that starts with some physical basics of combustion, followed by the basics of CFD modeling and ends with an overview of trends in combustion modeling.
- **Chapter 3.** The actual description of the implemented turbulent combustion model is given in this chapter. First, laminar diffusion flames in opposed jet configuration are discussed in detail and then an interesting approximation of such flamelets is introduced. Then, the turbulence-chemistry interaction modeling by means of a presumed-PDF approach is properly described. The chapter is closed with the presentation of two possible ways of coupling between the combustion model and the CFD code.
- **Chapter 4.** A first application of the combustion model to simulate a turbulent lifted H_2/N_2 jet flame is presented in this chapter. Both versions of the combustion model are studied on the basis of this test case. The chapter ends with some preliminary conclusions.
- **Chapter 5.** In this chapter, the application of the simplified model to reactive n-heptane sprays of the ECN is presented. Model predictions of the flame structure in transient and quasi-steady state are investigated and key flame parameters are compared to experimental data. Conclusions of the obtained findings close this chapter.
- **Chapter 6.** The document is closed with some general conclusions about the present work as well as the proposal of potential future works including possible further enhancements of the implemented combustion model.

Bibliography

[1] Dietzschold C. *Der Cornelius Nepos der Uhrmacher.* C. Dietzschold's Verlag, 1910.

[2] Höök M. *Fuelling Future Emissions - Examining fossil fuel production outlooks used in climate models.* InTech, 2011.

[3] IEA. *Key World Energy Statistics 2013.* International Energy Agency (IEA), 2013.

[4] European Comission. *EU Energy in Figures - Statistical Pocketbook 2013.* Publications Office of the European Union, 2013.

[5] DIW Berlin and Energy Analysis Environment Forecast. *Auswertungstabellen zur Energiebilanz fur die Bundesrepublik Deutschland 1990 bis 2012.* Arbeitsgemeinschaft Energiebilanzen e.V., 2013.

[6] European Comission. *Panorama of Energy - Energy statistics to support EU policies and solutions.* Office for Official Publications of the European Communities, 2009.

[7] European Comission. *Flightpath 2050 Europe's Vision for Aviation.* Publications Office of the European Union, 2011.

[8] Airbus S.A.S. *Global Market Forecast Future Journeys 2013 2032.* 2013.

[9] Bodek K. and Heywood J. *Europe's evolving passenger vehicle fleet: Fuel use and GHG emissions scenarios through 2035.* Laboratory for Energy and Environment, Massachusetts Institue of Technology, 2008.

[10] IEA. *World Energy Outlook 2011.* International Energy Agency (IEA), 2011.

Chapter 2

Bibliographic review

Contents

2.1 Introduction

Combustion processes consist of a combined sequence of physical and chemical phenomena that are involved when chemical reactions proceed in fluid flows. The presence of interrelated processes of fluid dynamics, thermodynamics, heat and mass transfer and chemical kinetics underline the complexity of this field of study. Moreover, in most practical applications the combustion process takes place in a turbulent environment which additionally increases the difficulty of this subject. Turbulence is probably the most complex topic in fluid mechanics with still many unanswered questions and an immense range of literature covering this area of physics.
This enumeration of issues finally makes clear that a wide range of knowledge is necessary when attempting to model turbulent combustion processes. A clear view of the considered problem with all its facets and an understanding of the influence they have on each other is essential. In order to be able to develop an adequate combustion model it is in addition wise to find out the state of the art of combustion modeling. Therefore, a detailed bibliographic review is fundamental not only to list the most recent trends in combustion modeling but also to keep hold of some basics of the problem in hand.
The bibliographic review presented in this chapter starts with a common classification of combustion regimes, followed by a brief recapitulation of the basics of CFD for reactive flows including the most important equations as well as the major issues of turbulence modeling. In the last decades many different strategies to describe chemical kinetics and to model turbulent combustion were developed. Hence, this chapter also tries to give a brief overview of existent models and resume the most important trends of combustion modeling. The given information finally allows to better define the scope of this investigation and sketch the chosen modeling strategy.

2.2 Combustion regimes

2.2.1 Basic concepts

Combustion is the event of a chemical reaction between a fuel and an oxidant that goes along with the conversion of chemical species accompanied by the emission of heat (and usually but not necessarily light). This process can occur in a flame or a non-flame mode [1], whereupon the latter is outside the scope of this work. Flame refers to the spatially limited zone of reaction and is commonly divided into two different types, premixed and nonpremixed

flames, which represent the most usual classification of combustion regimes. As denoted by their names, the classification is made due to the state of the fuel and the oxidant before reaction. In case of nonpremixed combustion the involved chemical species have to reach the reaction zone by molecular diffusion, this is why nonpremixed flames are also called diffusion flames. Needless to say, both combustion regimes can occur in laminar flow as well as in turbulent flow.
A wide range of characteristic time and length scales are involved in turbulent combustion processes. First, the size of eddies present in turbulent flows can range over several orders of magnitude and consequently also the characteristic times of those eddies. Second, the characteristic time of chemical reaction, which shows high nonlinearity with the temperature, is usually different from the turbulent time scale. Two characteristic numbers, which compare those significant time scales, are commonly used in the field of turbulent combustion,

- the turbulent Damköhler[1] number Da
- the Karlovitz[2] number Ka.

The Damköhler number

$$Da = \frac{\tau_t}{\tau_c} \tag{2.1}$$

compares the macroscopic time scale of a turbulent flow (corresponding to the large eddies in the turbulent flow field) with the time scale of a chemical reaction.
The Karlovitz number

$$Ka = \frac{\tau_c}{\tau_k} \tag{2.2}$$

relates the time scale of the laminar flame to the smallest turbulent time scale, the Kolmogorov time (corresponding to the smallest eddies in the turbulent flow field).
Statements about the spatial structure and temporal behavior of a flame can be made based on these two dimensionless numbers. For instance, the inner structure of a turbulent flame that posses much shorter chemical time than integral turbulence time and thus high Damköhler numbers ($Da \gg 1$), is not strongly affected by turbulence. The inner structure remains close to a laminar flame with a thin reaction zone, although the flame front is wrinkled by turbulent motion. On the other hand, when chemical reactions are slow compared to turbulent fluctuations, this means low Damköhler numbers

[1] Named after the German chemist Gerhard Damköhler (1908–1944)
[2] Named after the Hungarian physicist Béla Karlovitz (1904–2004)

($Da \ll 1$), reacting species and products are mixed by turbulence before reaction. This is referred to as the *perfecty stirred reactor* limit [2].
The scale analyses are graphically represented in so-called *turbulent combustion diagrams* where various types of flames according to turbulence interaction can be identified. Models are always based on assumptions which restrict their validity. That is why these diagrams are useful to clarify the extent of validity of a combustion model for a certain type of flame. Different versions of such diagrams based on various parameter definitions can be found in the literature depending on the author. In the corresponding sections of premixed and nonpremixed combustion, the different characteristic flame types are discussed more in detail.
Both regimes and a combination of the two extremes in terms of mixing are addressed in the following sections with a focus on the nonpremixed regime due to the scope of this work as already mentioned in Section 1.3.2. The objective here is to briefly describe the characteristic nature of each combustion regime, not concrete modeling approaches. Modeling strategies primary applied to nonpremixed combustion problems will be addressed in section 2.4.

2.2.2 Premixed combustion

In the premixed combustion regime fuel and oxidizer are completely mixed before the combustion process takes place. The most well-known application of turbulent premixed combustion is the spark ignition engine, beyond that, lean-burn gas turbine and house hold burners are further examples for the use of this combustion regime. The Bunsen burner is another example which is furthermore used to study laminar and turbulent premixed combustion.
In order to avoid uncontrolled combustion, mixing has to be done at sufficiently low pressure and temperature where no chain-braking reactions occur which is referred to the "frozen" state of reactions [3]. In order to describe the state of the mixture, the equivalence ratio

$$\phi = \frac{Y_F/Y_O}{(Y_F/Y_O)_{st}}, \tag{2.3}$$

is defined, which compares the fuel-to-oxidizer ratio to the stoichiometric fuel-to-oxidizer ratio. Hence, when the mixture is at stoichiometry, the equivalence ratio equals unity. A heat source, such as a spark, can ignite the homogeneously mixed fuel and oxidizer if the mixture is within the flammability limits. These limits usually move in the order between $\phi = 0.5$ and $\phi = 2$ for hydrocarbons, but vary with the fuel [4]. In mixtures within the flammability limits the chemical reaction can occur anywhere in the domain

and even propagate upstream the feeding system. This property of premixed combustion is an important safety issue in industrial applications. Measures have to be made to avoid unwanted propagation of combustion. This can be achieved with a strong local heat loss in order to quench the flame or just with a too rich or too lean mixture such that the flame reaches its flammability limits.

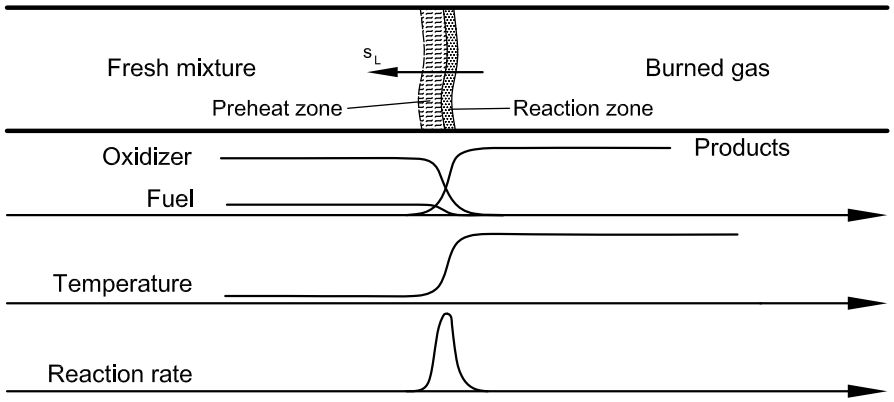

Figure 2.1. *Sketch of premixed flame structure and profiles of fuel, oxidizer and products as well as the temperature and reaction rate profiles.*

Once the combustion is started, a flame front propagates through the mixture. This characteristic nature of premixed flames is sketched in a simplified manner in Fig. 2.1. Chemical reactions are limited to a thin reaction zone where the conversion of the fresh mixture of fuel and oxidizer to burnt gas occurs. Thus, the flame front separates the fresh gas from the combustion products. The reaction rate is zero outside the reaction zone and shows a Dirac-like shape within the reaction zone. There is a steep temperature rise in this zone as the gas rapidly approaches the burnt state close to the chemical equilibrium.

Two stable states can be identified, the unburnt and the burnt gas state, and the flame propagates from the latter to the first one. The speed of this propagation is a key feature of premixed flames. The laminar flame speed s_L, marked in Fig. 2.1, primarily depends on the equivalence ratio ϕ, the temperature in the unburnt mixture, the pressure and certainly on the fuel determining the chemical kinetics [4]. Zeldovich's analysis made for a one-step global reaction

$$fuel + oxidizer \longrightarrow products$$

gives an analytical expression for the laminar flame speed

$$s_L = \sqrt{\frac{\alpha}{\tau}} \tag{2.4}$$

with the characteristic time of reaction

$$\tau = \frac{1}{A \exp(-E/RT)}. \tag{2.5}$$

In this analysis the thermal diffusivity α is equal to the mass diffusivity [5], so the Lewis number is supposed to be unity. An extensive discussion on analytical solutions for laminar flame speed can be found in [2].
In a turbulent flow regime the flame is affected by turbulence, thus the resulting turbulent flame speed is different from the laminar flame speed. The first to describe a turbulent flame velocity was Damköhler [6] in 1940 who identified wrinkling as the main mechanism controlling turbulent flames. Wrinkling increases the area of the flame front (A_t in equation 2.6) compared to the laminar flame front area and he assumed that this increase is proportional to the velocity increase

$$\frac{s_t}{s_L} = \frac{A_t}{A_L}. \tag{2.6}$$

But turbulence not only affects the flame front, the flame front in turn also affects turbulence [2]. A stabilization of the flame in space can be achieved when the turbulent flame speed equals the mean flow velocity oriented in the opposite direction. The key issue in premixed combustion modeling is then the prediction of the turbulent flame speed which is influenced by the laminar flame speed and flame front wrinkling and stretching by large eddies, as well as flame thickening by small eddies.

In order to distinguish different flame regimes (or flame types), the time and length scales involved in the premixed combustion process are compared. Such a physical analysis of the problem leads to the above mentioned combustion diagrams, which can support the development of combustion models. This diagram for premixed combustion is sometimes called *Borghi diagram* since he was among the first to propose such a representation [7], but similar diagrams have been proposed by many other authors too [8–12].
First, turbulent flow is characterized by the turbulent Reynolds number defined as

$$Re_t = \frac{u' \, l_0}{\nu} = \frac{u' \, l_0}{s_L \, \delta_L}, \tag{2.7}$$

which is the ratio of the inertial forces due to the flow to the viscous forces determined by the fluid. This number is based on the turbulent integral length

scale l_0 and the velocity fluctuation u'. For homogeneous, isotropic turbulence $u' = \sqrt{2k/3}$, which, related with the turbulent kinetic energy k, represents the turnover velocity of integral scale eddies [3]. The kinematic viscosity ν of the gas can be expressed with the laminar flame speed s_L and the flame thickness δ_L assuming the flame Reynolds number to be unity ($Re_f = (\delta_L\, s_L)/\nu = 1$ compare e.g. [2]).
Figure 2.2 represents a classical turbulent combustion diagram (adapted from [2, 3, 5]) where the logarithm of u'/s_L is plotted versus the logarithm of l_t/δ_L. A first important observation can be made considering the turbulent Reynolds number. When $Re_t < 1$ laminar combustion occurs (sketched in Fig. 2.2) and indeed turbulent combustion is observed for $Re_t > 1$ reflecting the more probable case in practical applications. The latter regime is further subdivided by the use of additional characteristic numbers.
According to the basic definition given in Eq. (2.1), the Damköhler number is defined as

$$Da = \frac{l_0/u'}{\delta_L/s_L} = \frac{l_0}{\delta_L}\frac{s_L}{u'}. \tag{2.8}$$

The chemical time τ_c is defined as the time need by the flame to propagate over a distance of its own thickness δ_L at the laminar flame speed s_L. The turbulent time scale is given by turbulent integral length scale l_0 and the velocity fluctuation u', i.e. the velocity fluctuation of the turbulent flow. In a similar way the Karlovitz number (see Eq. (2.2)) is calculated according to [2] as

$$Ka = \frac{\delta_L/s_L}{\eta/\upsilon} = \frac{\delta_L}{\eta}\frac{\upsilon}{s_L} = \frac{\delta_L^2}{\eta^2}, \tag{2.9}$$

where η and υ are the characteristic length and velocity of the Kolmogorov structures, respectively. These determining properties of the smallest structures present in turbulent flows are given by Eq. (2.28a) and Eq. (2.28b). These two additional characteristic numbers now allow to make further classifications of the turbulent premixed combustion regime as represented in Fig. 2.2.

First, for $Da \ll 1$ the chemical time is slower than the turbulent motions, resulting in continuous mixing of reactants and products before chemical reactions occur. Thus, the term *flame front* is not adequate here and this zone is referred to as the *well-mixed* or *perfectly stirred reactor regime*. As a consequence the mean reaction rate can be estimated from the mean values of the mixture.

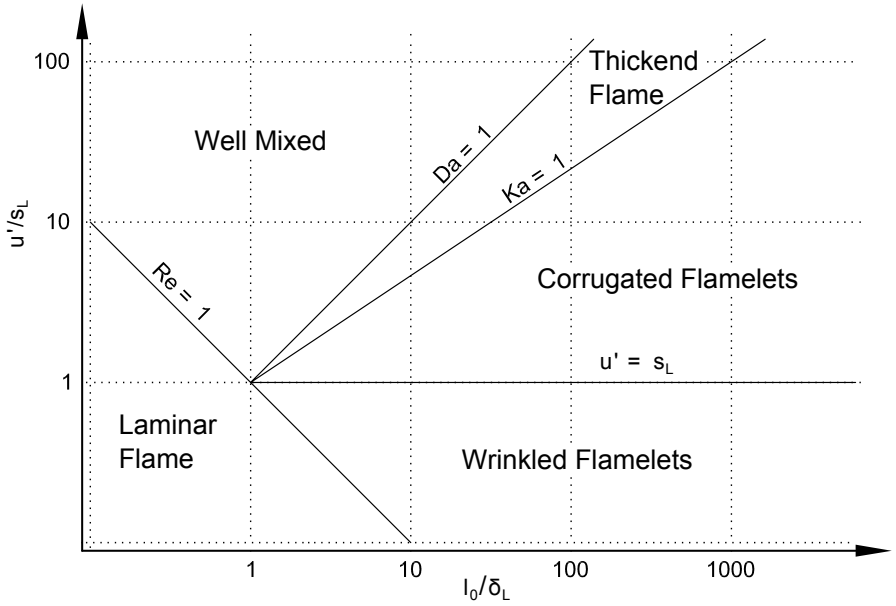

Figure 2.2. *Turbulent combustion diagram for premixed combustion. Identification of combustion regimes based on length and velocity ratios.*

On the contrary, for $Da \gg 1$ the chemical reaction rates are fast compared to the fluid mixing rates dominated by turbulent fluctuations. This corresponds to a thin reaction zone with a preserved internal structure of the flame that can be described by a laminar flame element, a so-called *flamelet*. Turbulent motions wrinkle the flame front which leads to an increase of the flame area. In this *flamelet limit* the ratio of turbulent to laminar flame speed is simply given by the ratio of wrinkled flamelet area to the time-mean flame area [1]. These two limiting cases are determined by estimations based on the macroscopic turbulent time scale.
Below the line $Da = 1$, various flame types may be distinguished upon considerations of the Karlovitz number and the turbulent intensity. For values of $Ka < 1$, the chemical time scale is shorter than the fastest turbulent time and the flame thickness is smaller than the size of the smallest eddy given by the Kolmogorov length. This means that the reactive-diffusive flame structure is embedded within eddies of the order of the Kolmogorov scale where the flow is considered quasi-laminar. Turbulence affects the flame in a way that it wrinkles the flame front, but the thin reaction zones retain locally the structure of a laminar premixed flame.
This *flamelet regime* is further divided into two zones depending on a flame

speed to turbulence velocity ratio. In the *wrinkled flamelet regime*, when $(u'/s_L) < 1$, the speed of the large eddies is not fast enough to lead to frame front interaction. The laminar flame propagation is dominant over the wrinkle formation caused by turbulence. This zone is not of high practical interest. The zone above the line $(u'/s_L) = 1$ is referred to the *corrugated flamelet regime* because the turbulent motion velocities are large enough to wrinkle the flame front up to flame front interaction. This means that a formation of pockets of fresh and burnt gases may occur.
For values of $Ka > 1$ and $Da > 1$ the macroscopic turbulent time scale is still larger than the chemical time scale, but the smallest eddies can enter the reactive-diffusive flame structure since the Kolmogorov scales are smaller than the flame thickness. In this so-called *thin reaction zones* or *thickened flame regime* the reaction zone remains thin but turbulence is able to thicken the flame preheat zone. The line $Ka = 1$, separating this regime from the flamelet regime, is known as the Klimov-Williams criterion.
The above observations are based on strong assumptions, such as homogeneous and isotropic turbulence and one-step reactions, and thus provide only a simplified overview of the different turbulent combustion regimes. More advanced combustion diagrams with refined definitions of flame types have been proposed by [13–15] as well as the characterization of combustion regimes introducing a second thicknesses [12].

2.2.3 Nonpremixed combustion

In nonpremixed combustion, as foretold by its name, fuel and oxidizer are not premixed, they rather enter separately the combustion chamber. The fuel typically issues from a nozzle into the domain where mixing and reaction with the oxidizer takes place. Candle and lighter are well-known examples for this combustion regime which in addition can be found in important industrial applications such as diesel engines, aircraft gas turbines or furnaces. A great advantage of nonpremixed combustion is the fact that the operation of a combustion device in this regime is much safer than applying premixed combustion.
Combustion can only occur in limited regions where fuel and oxidizer are present in certain proportions. In the reaction zone fuel and oxidizer are consumed and converted into products by chemical reactions. The combustion process is sustained by continuous diffusion of fuel and oxidizer to the reaction zone. This diffusion process occurs simultaneously to the sequence of chemical reactions and represents a key issue in nonpremixed combustion. Nonpremixed

flames are therefore also called diffusion flames [3] since diffusion is a dominant phenomenon in this combustion regime. A simplified representation of the local structure of a diffusion flame is shown in Fig. 2.3 including the principle profiles of the most important properties.

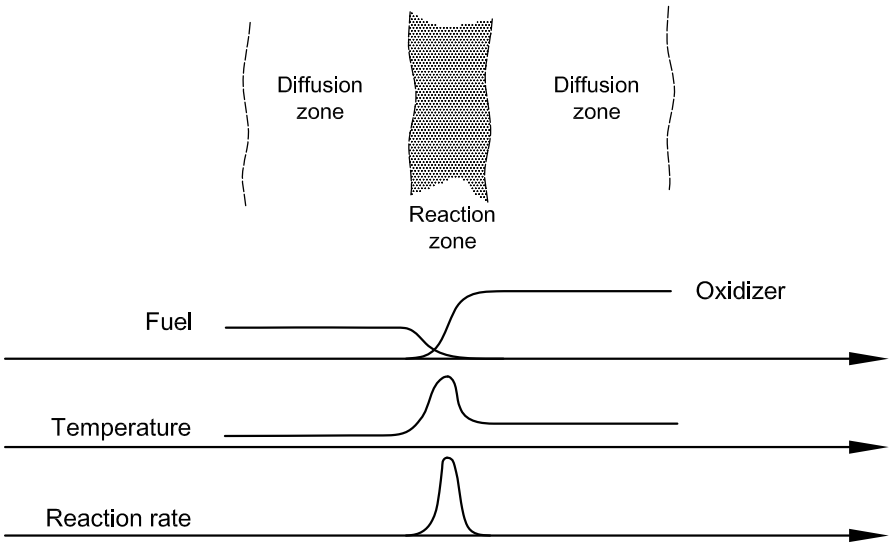

Figure 2.3. *Structure of diffusion flame with profiles of main properties.*

Diffusion flames in contrary to premixed flames do not exhibit a flame speed since the flame is always located close to stoichiometric mixture representing the most favorable proportion of fuel and oxidizer. The profiles of fuel and oxidizer mass fraction sketched in Fig. 2.3 illustrate that moving away from the reaction zone leads to an increase of either fuel or oxidizer. Hence, when departing from the stoichiometric proportion the mixture becomes either too rich or too lean for combustion to continue. In fact the flame separates the fuel side from the oxidizer side and is not able to propagate towards any of the two sides, resulting in the safety feature mentioned above. Since diffusion flames can not propagate against the flow, unlike premixed flames, they are more sensible to fluctuations in the flow introduced by turbulence. Like in premixed flames, burning occurs at the highest temperature since the reaction rate is very sensitive to temperature as known from the Arrhenius equation $k = A\exp(-E/RT)$. Hence, in the high temperature region fast transformation of species occurs resulting in local gradients of fuel and oxidizer

[3] Some authors (e.g. [5]) avoid the term *diffusion flame* arguing that all flames require diffusion and thus this term is not unique.

(see profiles in Fig. 2.3) which in turn are the driving force for the diffusion of fresh reactants towards the reaction zone. The structure of a diffusion flame as shown in Fig. 2.3 can only be maintained in steady state by a constant fuel and oxidizer stream feeding the flame from either side. The strain imposed on the flame by such species streams leads to a stretched flame structure, whereas without strain the flame grows infinitely in perpendicular direction until it goes out due to lack of fuel and oxidizer. As a consequence of this behavior, diffusion flames in contrast to premixed flames do not posses a reference flame thickness. The thickness of a stretched flame is basically determined by the strain imposed on it.

The state of the mixture is fundamental in diffusion flames as may be concluded from above. Therefore, the *mixture fraction*, which relates the fuel stream to the oxidizer stream, plays a key role in the description of nonpremixed combustion. The basic idea is to define a conservative quantity, i.e. independent of chemical reactions, that describes the state of the mixture. The mixture fraction Z (sometimes also denominated f) is commonly defined to be zero in the oxidizer stream and unity in the fuel stream.
Slightly different formulations of the mixture fraction based on mass fractions or specific enthalpy exist [2, 3, 16, 17], though all represent the same physical meaning. An established definition is

$$Z = \frac{\nu Y_F - Y_O + Y_O^0}{\nu Y_F^0 + Y_O^0}, \tag{2.10}$$

where $\nu = \nu_O' W_O / \nu_F' W_F$ is the stoichiometric mass ratio with the stoichiometric coefficients ν_i' and the molecular weights W_i. In Eq. 2.10 Y_F^0 and Y_O^0 are the fuel and oxidizer mass fractions of the corresponding fuel and oxidizer streams respectively, and moreover it is assumed that all scalars diffuse at the same rate ($D_i = D$). The stoichiometric mixture fraction Z_{st} can be expressed with the stoichiometric mass ratio as

$$Z_{st} = \frac{1}{1 + \frac{\nu Y_F^0}{Y_O^0}}. \tag{2.11}$$

The mixture fraction follows the transport equation

$$\frac{\partial \rho Z}{\partial t} + \frac{\partial \rho u_i Z}{\partial x_i} = \frac{\partial}{\partial x_i}\left(\rho D \frac{\partial Z}{\partial x_i}\right), \tag{2.12}$$

where no source term appears, since Z is a passive scalar and only changes due to convection and diffusion. This equation describes the state of the mixture

and the iso-surface of $Z(\mathbf{x}, t) = Z_{st}$ can be interpreted as a tracer of the flame sheet which is located close to the stoichiometric mixture.

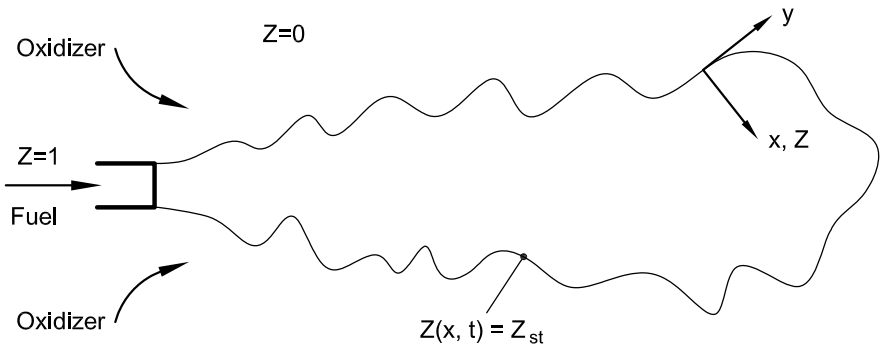

Figure 2.4. *Iso-surface of stoichiometric mixture fraction of a jet diffusion flame.*

In the following the main ideas of a fundamental concept of how to describe laminar diffusion flames are outlined. This concept is widely used in combustion modeling and is also applied in this work. The concept is based on the representation of the reactive-diffusive structure of the flame's close environment by means of the mixture fraction Z. First a coordinate transformation from physical space to mixture fraction space is made. The local coordinate x normal to the surface of stoichiometric mixture (see Fig. 2.4 adapted from [3]) is replaced by Z. Furthermore it is assumed that gradients of the reactive scalars tangential to the stoichiometric surface are negligible compared to gradients normal to the iso-surface of Z_{st} (in Z direction). This can be expressed in other words that one expects temperature or species mass fraction to vary hardly along the surface of stoichiometric mixture. In doing so, the description of a laminar diffusion flame is reduced to an one-dimensional problem with the new independent variable Z and is given for any reactive scalar ψ_i (species mass fractions, temperature) by

$$\rho \frac{\psi_i}{\partial t} = \rho \frac{\chi}{2} \frac{\partial^2 \psi_i}{\partial Z^2} + \dot{\omega}_i. \tag{2.13}$$

These are the so-called *unsteady flamelet equations* which were derived independently by [18, 19] and where "flamelet" refers to the thin reaction-diffusion structure described by the equations. In this version of the equations unity Lewis number is assumed, but extended versions of the flamelet equations have been derived including effects such as differential diffusion ($Le \neq 1$) or radiative heat losses [20, 21].

The scalar dissipation rate χ is introduced in Eq. (2.13) which is defined as

$$\chi = 2D \left(\frac{\partial Z}{\partial x_i} \right)^2, \tag{2.14}$$

where D is the diffusion coefficient of mixture fraction. The scalar dissipation rate is another fundamental property, besides the mixture fraction, in the description of nonpremixed flames. It represents the inverse of a diffusion time scale and can be interpreted as the diffusivity in the mixture fraction space. The scalar dissipation rate therefore determines the feeding rate of the reaction zone due to diffusion and it is linked to the spatial gradients of Z. The mixture fraction field in turn is determined by the flow field and the mixing of fuel and oxidizer and thus the scalar dissipation rate represents an external parameter imposed by the flow on the structure of a flamelet.

Williams [22] proposed to describe turbulent diffusion flames as an ensemble of laminar flamelets. Many models for turbulent nonpremixed combustion are based on this assumption together with the adoption of the flamelet equations. Indeed, this concept requires the existence of certain conditions concerning both chemistry and turbulent flow.

Two important length scales may be identified in turbulent diffusion flames, the diffusion layer thickness l_d and the reaction zone thickness l_r, both plotted in Fig. 2.5. The conditional mean value $\widetilde{\chi}_{st}$ of the scalar dissipation rate at $Z = Z_{st}$ together with the molecular diffusivity D is used to estimate l_d by

$$l_d \approx \sqrt{\left(\frac{D}{\widetilde{\chi}_{st}} \right)}. \tag{2.15}$$

In this region mixing due to diffusion occurs and fuel and oxidizer coexist along with combustion products. The thickness of the reaction zone is given by non zero reaction rate. In the theoretical case of infinitely fast chemistry l_r would be zero. A local Damköhler number comparing local flow time τ_f and chemical time τ_c is estimated as

$$Da^{fl} = \frac{\tau_f}{\tau_c} \approx \frac{1}{\widetilde{\chi}_{st}\tau_c}. \tag{2.16}$$

In case of high Damköhler numbers, which means fast chemical reactions compared to a characteristic flow time, the reaction zone is thin ($l_r \ll l_d \sim \eta$). If the thickness of the reaction layer is small compared to the smallest structures of the turbulent flow, i.e. eddies of the size of the Kolmogorov length, the layer is embedded in a quasi-laminar flow. Then the internal

structure of the flamelet is furthermore considered intact and not affected by turbulence.

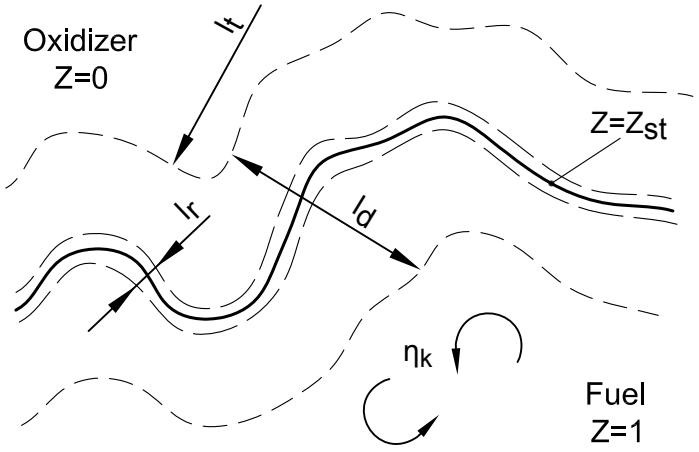

Figure 2.5. *Characteristic length scales in turbulent diffusion flames.*

The validness of the concept finally adds up to a competition between chemical scales and turbulent scales. Combustion diagrams for nonpremixed combustion have therefore been developed, similar to those of the premixed combustion regime, with the aim to classify different flame regimes comparing chemical and turbulent time and length scales. However, since nonpremixed flames do not exhibit a characteristic flame velocity nor a flame thickness, the definition of characteristic scales is not straight forward and various definitions have been proposed [17, 23–25]. As a consequence of this difficulty, the classification of turbulent nonpremixed combustion remains still vague.

Here a classification based on the turbulent Reynolds number Re_t to reflect the turbulent flow and the Damköhler number as a ratio of time scales is reproduced. This valuation is presented in [2], where a quite extensive disquisition on this issue can be found. The Damköhler number can be expressed as

$$Da = \frac{\tau_t}{\tau_c} = \frac{\tau_t}{\tau_k}\frac{\tau_k}{\tau_c} \approx \frac{\tau_t}{\tau_k}\frac{2}{\widetilde{\chi}_{st}\tau_c} \approx 2\sqrt{Re_t}\,Da^{fl} \tag{2.17}$$

with the relation $\tau_t/\tau_k = \sqrt{Re_t}$ of the integral turbulent time τ_t and the Kolmogorov time τ_k. Different regimes may be identified based on this two characteristic numbers as shown in the combustion diagram in Fig. 2.6 using log-log axes. A simple observation is the line $Re_t = 1$ separating

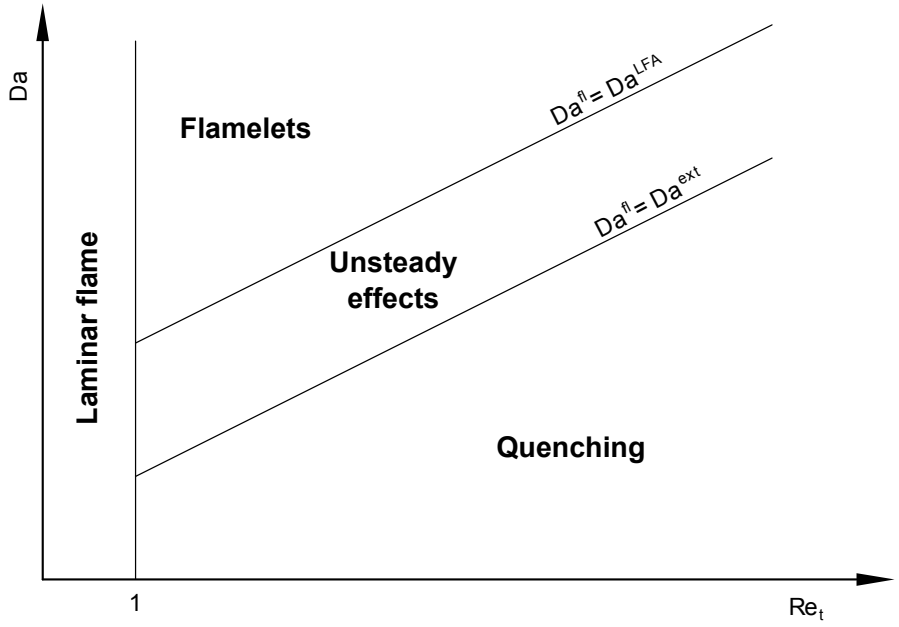

Figure 2.6. *Flame regimes in turbulent nonpremixed combustion.*

the laminar from the turbulent combustion regime at which the latter is further subdivided. First, the flame is considered to have a laminar flame structure when chemistry is fast, corresponding to large values of Damköhler numbers as already mentioned above. This flamelet region is limited by the criterion $Da > Da^{LFA}$. On the contrary, flame extinction occurs when chemistry is relatively slow which can be expressed with $Da < Da^{ext}$. The Damköhler numbers Da^{LFA} and Da^{ext} separating the different flame zones have been found in numerical studies [25]. In the intermediate zone between this transition Damköhler numbers unsteady effects are important. Otherwise identified classifications of diffusion flames may be found in the literature based on other combinations of characteristic ratios [23, 24, 26]. Such combustion diagrams in general can only give an approximate overview of flame regimes since they are based on several strong assumptions, for instance the local diffusion layer thickness is assumed to be of the order of the Kolmogorov length ($l_d \approx \eta$). That is to say that they can not be directly used to identify a flame regime in a combustion device as local flame speed and thickness depend on the local flow conditions.
However, one can deduce the influence of the scalar dissipation rate linked to the strain imposed on the flame. Too high values of scalar dissipation rate

lead to local extinction as the combustion can not be sustained against strong heat loss due to diffusion. The role of the scalar dissipation rate will be further discussed in Chapter 3.

2.2.4 Partially premixed combustion

The partially premixed combustion regime is some kind of a hybrid of the two previous combustion regimes. Gasoline direct injection engines represent a known industrial application where partially premixed flame propagation takes place. Such flames can furthermore be found in industrial burners where flames are stabilized by recirculation of hot combustion products and therefore locally partial premixing of fuel and oxidizer together with burnt gas occurs. Moreover, this combustion regime is important in lifted turbulent jet flames. If the exit velocity of the fuel stream exceeds a certain value, the flame detaches from the rim of the nozzle and a characteristic lift-off length between nozzle and flame base can be observed. In this region fuel and oxidizer have time to mix and thus the flame base develops in a partially premixed mixture. Downstream of the flame base a diffusion flame as described in Section 2.2.3 spreads out. The lift-off length increases with increasing exit velocity until a critical value of this velocity where the flame extinguishes.
The stabilization of the flame lift-off is a complex issue, extensively studied with experimental and numerical methods, and therefore controversial discussion on this topic can be found in the literature [27–30]. Many questions in this field remain open until today and a more recent review on this topic with respect to fuel sprays was presented in [31], where different theories are discussed. In the field of reactive sprays the relation between ignition processes and lift-off length was amongst others investigated in [32].
Another important flame type in relation with partially premixed combustion are the so-called triple flames. These flames are considered to play an important role during the ignition phase of the combustion process in diesel engines which is supported by DNS results [33]. In the first instants after the autoignition of the inhomogeneous, partially premixed mixture, flame propagation normal to iso-mixture fraction surfaces occurs. Moreover, triple flames seem to play a role in the stabilization process of lifted flames [34] and represent therefore an interesting model problem. What is usually called *triple flame* refers to a structure of a rich and a lean premixed flame front together with a diffusion flame and such structures have first been observed in experiments by [35]. A common configuration to study such a flame is a shear layer of mixing fuel and oxidizer streams [36], where diffusion flame evolves at the stoichiometric mixture. On both sides of the diffusion flame, i.e. the

fuel and oxidizer side, a reach and a lean partially premixed flame propagate, respectively, starting from the triple point. The partially premixed flames of triple flames exhibit a typical curvature of the flame front since the burning velocity decreases moving away from the stoichiometric mixture towards very reach and lean mixtures.
Triple flames (in relation with lifted flames) have been and are still intensively studied by investigators using theoretical and numerical methods and an extensive literature is available on this topic [33, 37–39]. The interaction of nonpremixed turbulent flames with partial premixing and triple flames was closely reviewed in [40].

2.3 CFD modeling of turbulent reactive flows

The basic equations that describe the fundamental physics of turbulent reactive flows will be covered in this subsection. The problem can basically be divided in three main areas, first the fluid dynamics describing the fluid flow including important conservation laws, second the treatment of turbulence[4], and third the chemistry covering the conversion of species by chemical reactions. The most important aspects of all three areas will be recapitulated without going into deeper details, rather references to helpful and extensive literature are given.

2.3.1 Basic equations of fluid flow

The basic equations of fluid flow are the mathematical description of the physical principles obeyed by any fluid, which are condensed in the three fundamental conservation laws:

- The mass is conserved, the increase of mass in a closed fluid element equals to the net rate of flow into the fluid element.
- The momentum is conserved, the sum of forces acting on a fluid element equals to the change of momentum. Newton's second law.
- The energy is conserved, the change of energy of a fluid element must equal to the heat change of the fluid element and the work done on it. First law of thermodynamics.

[4]Fluid dynamics actually includes turbulent flows, but since turbulence by its own is such a complex field and its treatment needs special attention, it is considered separately in this context.

The conservation of mass for a compressible fluid is represented by the *continuity equation*

$$\frac{\partial \rho}{\partial t} + \frac{\partial}{\partial x_j}(\rho u_j) = 0 \tag{2.18}$$

with the density ρ of the fluid and the velocity u_i of the component i.

Applying Newton's second law to a fluid element, one obtains the *momentum equation*

$$\frac{\partial}{\partial t}(\rho u_i) + \frac{\partial}{\partial x_j}(\rho u_i u_j) = -\frac{\partial p}{\partial x_i} + \frac{\partial \tau_{ij}}{\partial x_j} + \rho g_i \tag{2.19}$$

which describes the motion of fluid. In this equation p is the pressure, τ is the viscous stress tensor and g is the gravitational acceleration. So the terms on the right-hand side of the momentum equation represent the forces acting on a fluid element, while the two terms on the left-hand side are the local rate of change and the convection of momentum, respectively. The indexes i and j in the component of the stress tensor τ_{ij} indicate that the stress component acts in the j-direction on a surface normal to the i-direction.
The stress tensor τ is unknown at this point, so a model describing viscous stress in a fluid is required. In late 17^{th} century, Sir Isaac Newton (1642–1727) stated that a linear relationship between shear stress in a fluid and strain rate, i.e. velocity gradients, exists. This can be understood as an analogy to Hook's law which describes the linear-elastic behavior of solids. Fluids that follow this simple law are called *newtonian* fluids which include common and industrially important liquids (e.g. water) and virtually all gases (e.g. air). On the contrary, non-newtonian fluids are for example blood, paint, starch suspensions, etc. The assumption of newtonian behavior, with respect to the gases considered in reacting flows, represents a credible approximation in this field. In 1845 Stokes gave a mathematical formulation for the shear stress in newtonian fluids:

$$\tau_{ij} = \mu \left(\frac{\partial u_i}{\partial x_j} + \frac{\partial u_j}{\partial x_i} \right) + \lambda \frac{\partial u_k}{\partial x_k} \delta_{ij} \tag{2.20}$$

where μ is the dynamic molecular viscosity relating stresses to linear deformations (velocity gradients) and a second viscosity λ relates stresses to volumetric deformations. The second viscosity is therefore also called bulk viscosity and commonly assumed

$$\lambda = -\frac{2}{3}\mu, \tag{2.21}$$

which is referred to as Stoke's hypothesis [41]. The Kronecker delta, defined as $\delta_{ij} = 0$ if $i \neq j$ and $\delta_{ij} = 1$ if $i = j$, was used in the last term of Eq. (2.20)

to rewrite the volume expansion $div(u)$. This last term is often suggested to be negligible, since the volumetric deformation is usually very small (cp. $div(u) = 0$ for incompressible flow according to the continuity equation).
Finally, the equations describing the motion of netwonian fluid, written as a single equation using index notation, are given by

$$\begin{aligned}\frac{\partial}{\partial t}(\rho u_i) + \frac{\partial}{\partial x_j}(\rho u_i u_j) = & \\ & - \frac{\partial p}{\partial x_i} \\ & + \frac{\partial}{\partial x_j}\left[\mu\left(\frac{\partial u_i}{\partial x_j} + \frac{\partial u_j}{\partial x_i}\right) - \frac{2}{3}\mu\frac{\partial u_k}{\partial x_k}\delta_{ij}\right] \\ & + \rho g_i, \end{aligned} \tag{2.22}$$

where Eq. (2.20) together with Eq. (2.21) are applied in Eq. (2.19).

These equations (three in a three-dimensional case) are in a strict sense referred to as the *Navier-Stokes equations* dating from Claude Louis Marie Henri Navier[5] and Sir George Gabriel Stokes[6] who independently formulated them in the first half of the 19$^{\text{th}}$ century.

The conservation of energy is ensured by the *energy equation*

$$\frac{\partial}{\partial t}(\rho h_t) + \frac{\partial}{\partial x_j}(\rho h_t u_j) = \frac{\partial p}{\partial t} + \frac{\partial}{\partial x_j}(\tau_{ij} u_i) + \frac{\partial}{x_j}\left(k\frac{\partial T}{\partial x_j}\right) + S_h, \tag{2.23}$$

which is here stated in the form of an equation of total enthalpy $h_t = e + p/\rho$. Especially for compressible flows this represents a common choice. Fourier's law $q_i = -k\frac{\partial T}{\partial x_i}$ was applied in Eq. (2.23) to connect heat flow to temperature gradients with the thermal conductivity k acting as proportionality factor. This is in analogy to the dynamic viscosity μ in Eq. (2.20). The second term on the right-hand side of the energy equation represents the work done on a fluid particle by surface forces τ_{ij} and is denoted viscous dissipation term. In the area of computational fluid dynamics Eq. (2.18), (2.22) and (2.23) are in a wider sense sometimes referred to as Navier-Stokes equations. All three equations are shown in conservation form here but may also be written in non-conservation or integral form, e.g. [42].
Further relations are necessary in addition to the five conservation equations in order to obtain a mathematically closed system. Two equations of state for ideal gas, a common and suitable model concept for real gases, represent these

[5] French mathematician and physicist (1785–1836).
[6] Irish mathematician and physicist (1819–1903)

supplementary relations. Those relations are the thermal state equation

$$p = \rho\, R\, T, \tag{2.24}$$

relating pressure p with density ρ and temperature T, and the caloric state equation

$$h = c_p\, T \tag{2.25}$$

relating enthalpy h with temperature T through the specific heat capacity at constant pressure c_p. This relation together with the Prandtl number allows to rewrite the third term on the right-hand side of the energy equation (Eq. (2.23)) such as

$$k\frac{\partial T}{\partial x_j} = \frac{\mu}{Pr}\frac{\partial h}{\partial x_j}. \tag{2.26}$$

The Prandtl[7] number represents the ratio of momentum diffusivity to thermal diffusivity:

$$Pr = \frac{\nu}{\alpha} = \frac{\mu c_p}{k}, \tag{2.27}$$

where ν and $\alpha = k/(\rho c_p)$ are the kinematic viscosity and thermal diffusivity. This set of equations allows a complete description of compressible, viscous fluid flow and heat transfer. Derivations and more detailed discussion of the conservation equations of fluid flow are given in abundant literature about this topic, e.g. [41, 43]. Indeed, the consideration of chemical reaction processes needs further relations presented in section 2.3.3.

2.3.2 Treatment of turbulence

In the great majority of industrial applications turbulent flow is the dominant flow regime and applications with laminar flow represent rare exceptions. Though there does not exist an exact description of turbulence, it can be best described by its known properties [44]. Indeed, some of the turbulence' properties may be considered favorable whereas others may introduce additional challenges, depending on the respective application.

- First, turbulence only appears in a flow and is therefore a property of the flow and not the fluid.

[7] Named after the German engineer Ludwig Prandtl (1875–1953)

- A well-known, easily observable property of turbulence is its chaotic behavior. Therefore the prediction of turbulent flow is impossible and statistical methods are adopted to describe the effects of turbulence. This is probably the worst feature of turbulence from the point of view of design engineers trying to model turbulent flows.
- Turbulent flow causes in general an increase in momentum, mass and heat transfer rates and boosts mixing. The fluctuations present in turbulent flow yield to high diffusivity. This is a very important property of turbulence regarding to combustion processes especially in case of mixing controlled combustion.
- Moreover, turbulent flow is always dissipative. Turbulent kinetic energy is dissipated at small turbulent scales leading to an increase of internal energy in the flow. Turbulence decays rapidly without energy supply. Hence, turbulent flow goes along with increased energy losses.
- Turbulence is a three-dimensional phenomenon and large eddies are highly anisotropic. This means that fluctuations are different in different directions. However, at the lower end of length scales present in turbulent flow, molecular viscosity gains importance and reduces the directionality, so that eddies of the smallest scales appear to be isotropic.

Today's comprehension of turbulence is characterized by the concept of the energy cascade that was introduced by Lewis Fry Richardson[8] in 1922 [45]. In short, a continuous energy transfer occurs in turbulent flow over a wide range of scales from large eddies to small eddies. Large scale eddies, arising from instabilities in the flow, take energy from the mean flow which is referred to the injection range. The characteristic size l_0 of such large eddies is of the same order as the mean flow scale or the problem geometry (e.g. the diameter in pipe flow). Large eddies are instable and break up into smaller eddies, thereby transporting kinetic energy over the inertial subrange down to scales of the order of the Kolmogorov length η, the smallest scale in turbulent flow. These smallest length, velocity and time scales only depend on the kinematic viscosity ν and the dissipation rate ε and are given according to [46] as:

$$\eta = \left(\frac{\nu^3}{\varepsilon}\right)^{1/4} \tag{2.28a}$$

$$\upsilon = (\nu\,\varepsilon)^{1/4} \tag{2.28b}$$

$$\tau = \left(\frac{\nu}{\varepsilon}\right)^{1/2} \tag{2.28c}$$

[8] English physicist and meteorologist (1881–1953)

They are named after Andrey Nikolaevich Kolmogorov[9] who found these relations and further developed the idea of the energy cascade [47, 48]. At those smallest turbulent scales, the inertial and viscous forces balance. The Reynolds number, representing the ratio of before mentioned forces, of an eddy of characteristic length η and characteristic velocity υ is unity, $Re_\eta = (\upsilon\,\eta)/\nu = 1$. In the dissipation range at the end of the energy cascade the turbulent kinetic energy is dissipated by viscous forces into heat.

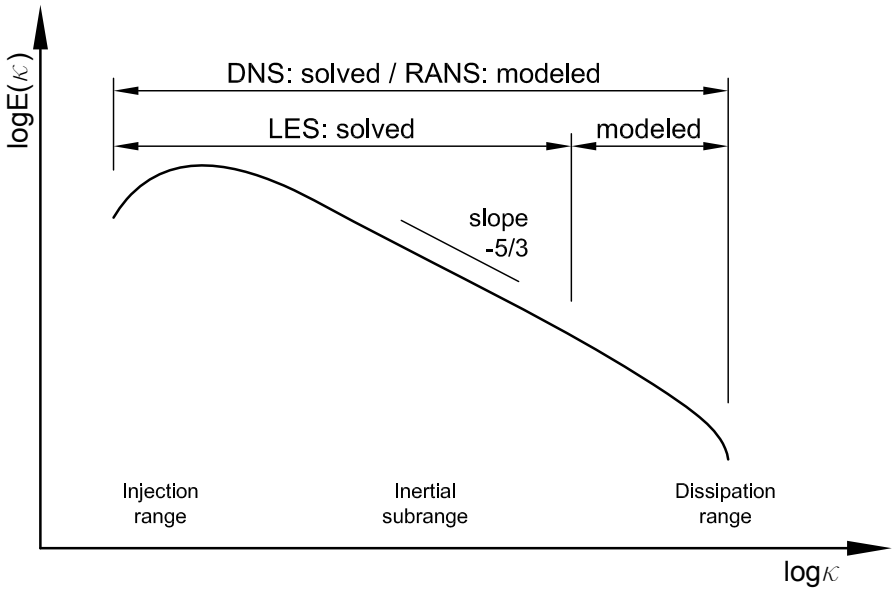

Figure 2.7. *Energy spectrum of turbulent flow.*

A schematic representation of the energy cascade is given in Fig. 2.7, where the spectral energy is plotted against the range of wavenumbers on double logarithmic axes. The wavenumber κ is connected to eddies of the length scale λ by $\kappa = 2\pi/\lambda$. The energy containing injection range is found at low wavenumbers, i.e. large eddies. Kolmogorov also found, that the spectral energy follows $E(k) \sim \kappa^{-5/3}$ in the inertial subrange.

Three approaches are available for the numerical treatment of turbulent flow, in which two approaches represent limit cases of the range of possible methods and the third can be considered as a compromise of the other two.

[9] Russian mathematician (1903–1987)

All three methods are addressed below and the basics of the method selected (the last in this listing) in this work are treated in more detail.

Direct numerical simulation (DNS). The first approach describes turbulent flow without the need of any model, which marks the great advantage of this method. This means that the whole energy spectrum is resolved in the calculation process as indicated in Fig. 2.7. In order to do so, the basic equations of fluid flow (Eq. (2.18), (2.22) and (2.23)) have to be solved on a numerical mesh fine enough to resolve all turbulent length scales. Moreover, the time step of a DNS has to be small enough to resolve all turbulent time scales. At this point the mean drawback of this method gets clear, the computational effort is more than challenging with today's computing power. The computational cost increases with Reynolds number Re^3 [46]. Due to this fact it is not affordable to apply DNS on an industrial level. However, DNS is adopted in simple, academic cases and gives there support to fundamental research. In the area of reactive flows, DNS is a powerful tool in the investigation of the complex turbulence-chemistry interaction processes [49–51].

Large eddy simulation (LES). The second approach is a compromise in every sense. As can be suspected from its name, in LES large scales are directly resolved whereas the smallest scales of the turbulent flow are modeled. The cell size of the calculation mesh is usually the determining factor of what scales may be resolved (spatial filtering). Filter functions are adopted to separate resolved scales from modeled subgrid-scales. The effect of the modeled scales on the resolved ones has to be taken into account by the subgrid-scale model. As indicated in Fig. 2.7, great part of turbulent energy is still resolved in LES, though the computational cost is reduced since the smallest scales are not directly calculated. Moreover, the isotropic nature of small scale eddies possibly facilitates the formulation of models for this range of turbulence. Many structural details of turbulent flow can be retained with LES at reasonable effort. This method is therefore increasingly applied even on an industrial level recently. But calculation times still may become not acceptable in problems where combustion processes occur in turbulent flow together with complex geometry. Several approaches for modeling combustion in combination with LES are available today but many open questions remain in this field [52]. Another issue is the comparability of LES results with experimental data which often represent mean values of flow variables. This means that several LES runs have to be done in order to obtain statistically significant mean values. Furthermore, huge amount of data may be generated

by LES making its postprocessing challenging (the same is certainly true for DNS).

Reynolds averaged Navier-Stokes (RANS). The last option are RANS computations where the whole range of turbulent scales are modeled (see Fig. 2.7). Equations for the mean values of the flow are solved, which are obtained by Reynolds (or Favre) averaging of the instantaneous balance equations. The advantage of this approach is the relatively low computational cost even for great and complex problems, hence being still the most widely applied method for CFD calculations. The disadvantage of RANS is that new unknowns arise during the averaging process why additional equations are necessary to overcome this closure problem. For this purpose a variety of turbulence models have been developed with the attempt to best describe the effect of turbulent motion, which is not directly calculated by the solved equations, on the mean flow properties. All of these models are based on strong simplifications and no universal turbulence model exists. However, some models are operative since almost four decades, where lot of experience was gained with those well tested numerical tools. Each model has its pros and cons and a limited range of applicability. The mean flow properties obtained from RANS calculations represent sufficient information in many cases. Moreover, mean values usually can be directly compared with experimental data.

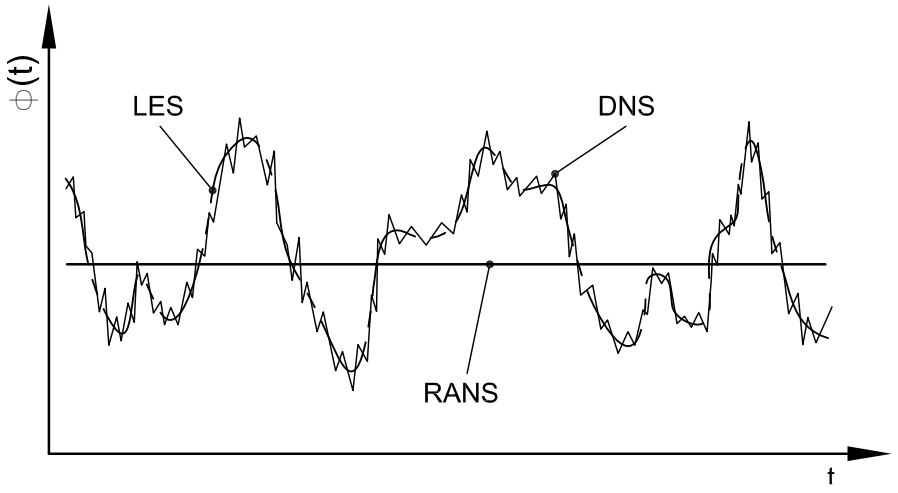

Figure 2.8. *Temporal evolution of a variable in turbulent flow calculated with different numerical approaches.*

The type of results which can be expect from each numerical method is clarified in Fig. 2.8, where the temporal evolution of a property (e.g. velocity, temperature) at a point in a turbulent flow is shown schematically. The effort of resolving turbulent scales is directly reflected in the details of the obtained results. DNS reproduces even the fastest and smallest turbulent fluctuations, LES retains great part of turbulent motion but omits fast and small fluctuations, and finally RANS represents the (here temporal) mean value of the flow variable $\phi(t)$.

In this work a RANS approach is adopted according to common nomenclature, although it correctly concerns a FANS approach as discussed below. The averaging process, the governing equations for the mean flow properties and the closure of the system with the standard $k-\varepsilon$ turbulence model are reminded in the following.

Reynolds and Favre averaging. The averaging concept introduced by Reynolds in 1895 usually refers to a time average, but may also be a spatial or ensemble average [53]. The basic idea of Reynolds averaging is the decomposition of any instantaneous flow variable $\phi(t)$ (e.g. velocity, temperature) into a mean part Φ and a fluctuating part $\phi'(t)$[10] , such that

$$\phi(t) = \Phi + \phi'(t). \tag{2.29}$$

The time average is then defined by

$$\Phi = \lim_{T\to\infty} \frac{1}{T} \int_t^{t+T} \phi(t)\, dt. \tag{2.30}$$

This definition of decomposition and Reynolds (time) averaging marked with an overbar ($\bar{}$) gives the two relations $\overline{\Phi} \equiv \Phi$ and $\overline{\phi'} \equiv 0$.
In reactive flows however, density variations have to be expected arising from steep temperature variations due to local heat release. This leads to additional terms during Reynolds averaging of the instantaneous balance equations as shown exemplary for the continuity equation below. Applying Reynolds decomposition ($\rho(t) = \overline{\rho} + \rho'(t)$ and $u(t) = \overline{u} + u'(t)$) to Eq. (2.18) gives

$$\frac{\partial}{\partial t}\left(\overline{\rho} + \rho'\right) + \frac{\partial}{\partial x_j}\left(\overline{\rho}\,\overline{u_j} + \rho'\,\overline{u_j} + \overline{\rho}\,u_j' + \rho' u_j'\right) = 0 \tag{2.31}$$

[10] This nomenclature is used here for clarity in the definition of the Reynolds averaging process. Though, in the literature this form $\phi(t) = \overline{\phi} + \phi'(t)$ of writing the decomposition can be found. The overbar may lead to an ambiguity here, when the averaging is also marked with an overbar. The Reynolds average is then $\overline{\overline{\phi} + \phi'(t)}$ and $\overline{\overline{\phi}} \equiv \overline{\phi}$.

and after time averaging, the Reynolds averaged continuity equation for compressible flow is obtained

$$\frac{\partial \bar{\rho}}{\partial t} + \frac{\partial}{\partial x_j}\left(\overline{\rho u_j} + \overline{\rho' u_j'}\right) = 0. \tag{2.32}$$

The additional term with the correlation of density and velocity fluctuations $\overline{\rho' u_j'}$ represents a new unknown which requires closure. In the momentum equation (see Eq. (2.22)) appear triple correlations $\rho u_i u_j$ making this problem even worse. In order to avoid such additional terms, a density-weighted averaging procedure is commonly used when modeling reactive flows as suggested by Favre [54, 55]. A variable $\phi(t)$ is then decomposed into a density-averaged mean part and a fluctuation part as $\phi(t) = \widetilde{\phi} + \phi''(t)$. The Favre average is defined by

$$\widetilde{\phi} = \lim_{T\to\infty} \frac{1}{\overline{\rho}} \int_t^{t+T} \rho(t)\phi(t)\, dt = \frac{\overline{\rho\phi}}{\overline{\rho}}, \tag{2.33}$$

where $\overline{\rho}$ is the Reynolds averaged density according to Eq. (2.30).

Averaged governing equations. Applying this procedure to the instantaneous balance equations (Eq. (2.18), (2.22) and (2.23)), one obtains the Favre averaged form of:

- Continuity equation

$$\frac{\partial \overline{\rho}}{\partial t} + \frac{\partial}{\partial x_j}(\overline{\rho}\widetilde{u_j}) = 0 \tag{2.34}$$

- Momentum equation

$$\frac{\partial}{\partial t}\left(\overline{\rho}\widetilde{u_i}\right) + \frac{\partial}{\partial x_j}\left(\overline{\rho}\widetilde{u_i}\widetilde{u_j}\right) = -\frac{\partial \overline{p}}{\partial x_i} + \frac{\partial}{\partial x_j}\left(\overline{\tau_{ij}} - \overline{\rho}\widetilde{u_i'' u_j''}\right) + \overline{\rho} g_i \tag{2.35}$$

- Energy equation (total enthalpy)

$$\frac{\partial}{\partial t}(\overline{\rho}\widetilde{h_t}) + \frac{\partial}{\partial x_j}(\overline{\rho}\widetilde{h_t}\widetilde{u_j}) = \frac{\partial \overline{p}}{\partial t} + \frac{\partial}{x_j}\left(\alpha_{eff}\frac{\partial \widetilde{h_t}}{\partial x_j}\right) + \overline{S_h} \tag{2.36}$$

Note that no additional term appears in the Favre averaged continuity equation (2.34) in contrast to the Reynolds averaged continuity equation (2.32). Minor simplifications were introduced in Eq. (2.36) based on the

assumption that no extreme pressure gradients (e.g. shock waves) are present in the flow [5]. Moreover, another common closure approximation is used in the averaged energy equation where the turbulent heat flux is assumed to be proportional to the mean temperature gradient [53]. This is reflected by the effective thermal diffusivity α_{eff} composed of a laminar and a turbulent contribution with the turbulent thermal diffusivity $\alpha_t = \mu_t/Pr_t$. A constant value is usually used for the turbulent Prandtl number Pr_t. The eddy viscosity μ_t is discussed further below in the paragraph about the Boussinesq hypothesis.
A new term with the quantity $\overline{\rho}\widetilde{u_i''u_j''}$ arises in the averaged momentum equation compared to its instantaneous counterpart given by Eq. (2.19). This quantity is called the Reynolds stress tensor

$$\tau_{ij} = \overline{\rho}\widetilde{u_i''u_j''} = \overline{\rho}\begin{pmatrix} \widetilde{u''u''} & \widetilde{u''v''} & \widetilde{u''w''} \\ \widetilde{v''u''} & \widetilde{v''v''} & \widetilde{v''w''} \\ \widetilde{w''u''} & \widetilde{w''v''} & \widetilde{w''w''} \end{pmatrix}, \tag{2.37}$$

composed of correlations of velocity fluctuations that are associated with momentum transfer due to turbulent fluctuations. The Reynolds stress tensor is symmetric, as can be seen from Eq. (2.37), and hence six unknown Reynolds stresses appear.

Reynolds stress models. One possibility to overcome this closure problem is to solve additional transport equations for the Reynolds stresses, one for each component of the Reynolds stress tensor [56]. This approach is referred to as Reynolds stress model (RSM) or second-order closure model and represents the most elaborate type of RANS turbulence models. This type of model accounts more rigorously for effects such as streamline curvature, swirl, rotation, and rapid changes in strain rate. Indeed, closure assumptions are required for several unknown terms in the exact equations of the Reynolds stresses which is a challenging task and often considered to compromise the accuracy of RSM predictions. The number of additional equations, seven in three-dimensional problems including the equation for turbulent dissipation, leads to an elevated computational costs and marks the main drawback of RSM. Moreover, the stability of the calculation process is another concern when using RSM. The additional effort is often not justified by improved quality of the obtained results. Reynolds stress models are therefore rarely adopted and rather used in a limited range of special flow problems.

Eddy viscosity models. Another very important and commonly used group of turbulence models are eddy viscosity models (EVM). These models are based on the Boussinesq hypothesis[11] which introduces the concept of an eddy viscosity. The Reynolds stresses are here treated in an analogous manner to the stresses caused by molecular viscosity and linked to the mean rate of deformation:

$$-\overline{\rho}\widetilde{u_i''u_j''} = \mu_t\left(\frac{\partial\widetilde{u}_i}{\partial x_j}+\frac{\partial\widetilde{u}_j}{\partial x_i}-\frac{2}{3}\frac{\partial\widetilde{u}_k}{\partial x_k}\delta_{ij}\right)-\frac{2}{3}\overline{\rho}\,k\delta_{ij} \tag{2.38}$$

where μ_t is the eddy viscosity (or turbulent viscosity) and $k=\frac{1}{2}\left(\widetilde{u_k''u_k''}\right)$ is the turbulent kinetic energy. The eddy viscosity can be interpreted as the increase in viscosity due to turbulent fluctuations and is usually clearly greater than the molecular viscosity. The last term in Eq. (2.38) is necessary in order to ensure correct results for the normal Reynolds stresses [43].

k − ε turbulence model. The $k-\varepsilon$ model, member of the two-equation models subgroup of EVM, is the most widely used turbulence model and can be considered as an industrial standard. Many derivatives of this model are available today, but the origins of the $k-\varepsilon$ model go back to the work of Jones and Launder in 1972 [57]. Other important contributions to the further development of the model are due to [58, 59]. The model is based on the eddy viscosity assumption described above and additionally consists of two transport equations for the turbulent kinetic energy k and its rate of dissipation ε and the following specification of the eddy viscosity [46]:

$$\mu_t = \overline{\rho}\,C_\mu\frac{k^2}{\varepsilon}. \tag{2.39}$$

The transport equation for the turbulent kinetic energy is given by

$$\frac{\partial\bar{\rho}k}{\partial t}+\frac{\partial\bar{\rho}\widetilde{u}_j k}{\partial x_j}=\frac{\partial}{\partial x_j}\left[\left(\mu+\frac{\mu_t}{\sigma_k}\right)\frac{\partial k}{\partial x_j}\right]+P_k-\bar{\rho}\varepsilon \tag{2.40}$$

and for its rate of dissipation by

$$\frac{\partial\bar{\rho}\varepsilon}{\partial t}+\frac{\partial\bar{\rho}\widetilde{u}_j\varepsilon}{\partial x_j}=\frac{\partial}{\partial x_j}\left[\left(\mu+\frac{\mu_t}{\sigma_\varepsilon}\right)\frac{\partial\varepsilon}{\partial x_j}\right]+C_{\varepsilon1}\frac{\varepsilon}{k}P_k-C_{\varepsilon2}\bar{\rho}\frac{\varepsilon^2}{k}-C_{\varepsilon3}\bar{\rho}\varepsilon\frac{\partial\widetilde{u}_j}{\partial x_j}. \tag{2.41}$$

The production term P_k in the above equations is defined as

$$P_k=-\overline{\rho}\widetilde{u_i''u_j''}\,\frac{\partial\widetilde{u}_i}{\partial x_j}, \tag{2.42}$$

[11] Proposed in 1877 by the French mathematician and physicist Joseph Valentin Boussinesq (1842–1929)

where the Boussinesq hypothesis given by Eq. (2.38) is adopted to determine the Reynolds stresses $\widetilde{\overline{\rho} u_i'' u_j''}$. Equation (2.41) is stated here as it is implemented in OpenFOAM, where the last term on the right-hand side, other than in its original version, is added. Deeper insight to the above model equations is given for instance in [46]. The coefficients of the standard $k-\varepsilon$ model are summarized in Table 2.1. The Prandtl numbers σ_k and σ_ε link the diffusivity of k and ε to the eddy viscosity μ_t.

Despite the known drawbacks of the model arising from the underlying

Table 2.1. *Coefficients of the standard $k-\varepsilon$ turbulence model.*

C_μ	σ_k	σ_ε	$C_{\varepsilon 1}$	$C_{\varepsilon 2}$	$C_{\varepsilon 3}$
0.09	1.0	1.3	1.44	1.92	0

assumptions, such as high Reynolds number flow and homogeneous, isotropic turbulence, it is still very popular and widely employed due to its low computational cost, robustness and simplicity. The closure problem that appeared in the averaging process of the governing equations is now solved with the additional model equations. This model will be used throughout the whole work.

Averaged species transport equation. A closed set of equations is now available to describe the mean properties of turbulent flow. However, in reactive flows chemical species are present which require additional transport equations. The Favre averaged form of the transport equation of species α is:

$$\frac{\partial \overline{\rho} \widetilde{Y}_\alpha}{\partial t} + \frac{\partial \overline{\rho} \widetilde{u}_j \widetilde{Y}_\alpha}{\partial x_j} = -\frac{\partial}{\partial x_j}\left(\overline{V_{\alpha,j} Y_\alpha} + \overline{\rho} \widetilde{u_j'' Y_\alpha''}\right) + \overline{\dot{\omega}}_\alpha, \tag{2.43}$$

where $V_{\alpha,j}$ is the j-component of the diffusion velocity V_α of species α and $\dot{\omega}_\alpha$ is the corresponding reaction rate. In multiphase flows such as sprays an additional source term due to evaporation may appear in Eq. (2.43). The species laminar diffusion fluxes are typically modeled as:

$$\overline{V_{\alpha,j} Y_\alpha} = -\overline{\rho D_\alpha \frac{\partial Y_\alpha}{\partial x_j}} \approx -\overline{\rho} \overline{D}_\alpha \frac{\partial \widetilde{Y}_\alpha}{\partial x_j}, \tag{2.44}$$

where $\overline{D}_\alpha$ is a mean species molecular diffusion coefficient [2]. The coefficient D_α is an equivalent diffusion coefficient of species α into the rest of the mixture that dates from the approximation of Hirschfelder [60]. The gradient-diffusion

hypothesis is used

$$\overline{\rho}\widetilde{u_i''Y_\alpha''} = -D_{t,\alpha}\frac{\partial \widetilde{Y}_\alpha}{\partial x_j} \tag{2.45}$$

according to which the scalar flux $\widetilde{u_i''Y_\alpha''}$ is connected to the mean scalar gradient by the turbulent diffusion coefficient $D_{t,\alpha}$ of species α [46]. The turbulent version of the Schmidt number $Sc_t = \frac{\mu_t}{D_t}$ which represents the ratio of turbulent viscosity (momentum diffusivity) to mass diffusivity, allows to estimate $D_{t,\alpha}$ as

$$D_{t,\alpha} = \frac{\mu_t}{Sc_{t,\alpha}}. \tag{2.46}$$

The turbulent Schmidt number is of the order of unity in simple shear flows. Indeed, the main challenge remains the determination of the mean reaction rate $\overline{\dot{\omega}}_\alpha$ in Eq. (2.43). This is in fact the core task of combustion modeling and therefore represents the focus of this work.

2.3.3 Chemical kinetics

This section outlines how to obtain the instantaneous reaction rate $\dot{\omega}_\alpha$ of species α mentioned at the end of the previous section. This chemical source term describes the rate of change of a species due to its participation in chemical reactions.
The stoichiometric reaction of a general hydrocarbon of the form C_mH_n in air is given by

$$C_nH_m + l\,O_2 + 3.71l\,N_2 \longrightarrow n\,CO_2 + \frac{m}{2}\,H_2O + 3.71l\,N_2, \tag{2.47}$$

where $l = n + {}^1\!/_4 m$. As a first approach, the inert species nitrogen does not contribute in the reaction and could be omitted here. Furthermore, Eq. (2.47) describes a complete combustion, which means an entire oxidation of fuel to its final products carbon dioxide and water. The global reaction of n-heptane for example is described by

$$C_7H_{16} + 11\,O_2 + 40.81\,N_2 \longrightarrow 7\,CO_2 + 8\,H_2O + 40.81\,N_2. \tag{2.48}$$

The global reaction in Eq. (2.48) is actually a result of a set of elementary reactions that occur between several (intermediate) species.

Such a system of N_s species reacting through N_r reactions can be written as

$$\sum_{\alpha=1}^{N_s} \nu'_{\alpha,r}\mathcal{S}_\alpha \rightleftarrows \sum_{\alpha=1}^{N_s} \nu''_{\alpha,r}\mathcal{S}_\alpha, \qquad r = 1, N_r \tag{2.49}$$

where $\mathcal{S}_\alpha$ is a symbol for species α, $\nu'_{\alpha,r}$ and $\nu''_{\alpha,r}$ are the species stoichiometric coefficients of species α that is consumed and produced in reaction r. According to the conservation of mass it is

$$\sum_{\alpha=1}^{N_s} \nu_{\alpha,r} W_\alpha = 0, \qquad r = 1, N_r \tag{2.50}$$

where $\nu_{\alpha,r} = \nu''_{\alpha,r} - \nu'_{\alpha,r}$ represents a net stoichiometric coefficient and W_α is the molecular weight of species α.

The reaction rate $\dot{\omega}_\alpha$ of species α is the sum of the reaction rates contributions $\dot{\omega}_{\alpha,r}$ produced by N_r reactions:

$$\dot{\omega}_\alpha = \sum_{r=1}^{N_r} \dot{\omega}_{\alpha,r} = W_\alpha \sum_{r=1}^{N_r} \nu_{\alpha,r} \Omega_r \tag{2.51}$$

The rate of progress Ω_r of reaction r was introduced in the equation above. This rate of progress is given by

$$\Omega_r = k_{fr} \prod_{\alpha=1}^{N_s} [X_\alpha]\nu'_{\alpha,r} - k_{br} \prod_{\alpha=1}^{N_s} [X_\alpha]\nu''_{\alpha,r}, \tag{2.52}$$

where k_{fr} and k_{br} are the forward and backward rate constants of the chemical reaction r. Furthermore, the rate of progress is calculated with the molar concentration $[X_\alpha] = \rho \frac{Y_\alpha}{W_\alpha}$, where Y_α is the mass fraction of species α in the mixture. The rate constants are estimated adopting the empirical Arrhenius' equation [61]:

$$k_{fr} = A_{fr} T^{n_r} e^{-\frac{E_r}{RT}} \tag{2.53}$$

In this equation, A_{fr}, n_r and E_r are prexponential factor, temperature exponent and the activation energy of reaction r, respectively, which have to be provided for each reaction. The backward rate constants are obtained from forward rates through equilibrium constants [2, 62].

The Arrhenius' equation is the mathematical evidence of the temperature dependence and the high non-linearity of chemical reactions. A further difficulty in the description of chemical reactions is to obtain the constants needed in Eq. (2.53). Moreover, for complex fuels more reactions have to be considered with an increased number of involved species in order to correctly describe the chemical process. So the system of equations may increase rapidly making its solution process costly. Chemical mechanisms describing

the reaction of everyday fuels such as diesel or gasoline are not even available. Finally, note that the above set of equations enable the calculation of the reaction rate $\dot{\omega}_\alpha$, which is not the averaged source term (i.e. averaged reaction rate) required in Eq. (2.43).

2.4 Tools for combustion modeling

The combustion model has to provide the average reaction rate of species representing the source term of its corresponding transport equation. As already pointed out in previous sections, this is a challenging and multidisciplinary task. A vast number of models have been developed over the last decades which in part is certainly attributed to the complexity of the problem. They all share common targets such as splitting and simplifying the complex problem, attempting to decrease the computational effort to solve it, but at the same time trying to retain important and necessary chemistry and physics of the problem. Most of the models only cover a certain combustion regime (see Section 2.2) and are not valid in general. The limitations arise from the underlying assumptions made for a particular type of combustion.
A global classification of combustion models, apart from their area of application, is not straightforward, however, the differences between various models are sometimes marginal. Furthermore, combustion models are commonly composed of two main components, where one is responsible for the treatment of chemistry, while the other one ensures the correct coupling of chemistry with turbulent flow. Different approaches exist for each of the two subtasks and different combinations of those approaches are possible. Therefore a brief overview of some methods that received attention by the scientific community is given here. More information on this extensive topic can be found in the comprehensive literature, where [5, 63] could be a good starting point.

2.4.1 Treatment of chemistry

A reliable prediction of consumption rates of fuels, formation of combustion products, ignition delays or flame lift-off in a wide range of conditions requires detailed chemical reaction schemes [50]. Such detailed mechanisms may consist of hundreds of species and thousands of elementary reactions. For instance, a detailed oxidation mechanism for n-heptane, a primary reference fuel (PRF) for diesel, presented by Curran et al. [64] includes more than 2400 reactions and 550 species. One transport equation for each of the involved species has

to be solved apart from solving for the system of chemical equations (Section 2.3.3), whose size depends on the number of reactions. The direct use of such detailed mechanisms for the simulation of combustion processes in practical applications is simply not feasible with todays computational resources. In order to overcome this problem, different strategies have been followed by the scientific community.

2.4.1.1 Chemical based reduction

The first one applies chemical reduction techniques (CRT) with the aim to reduce the number of species and/or reactions in a chemical mechanism. A common idea of different techniques is based on the separation of chemical time scales. Chemical time scales typically span a much larger range than physical time scales (e.g. mixing times). The quasi steady-state approximation (QSSA) and the partial equilibrium approximation (PEA) are traditionally used to obtain simplified chemical kinetics [5, 65, 66]. Returning to the before mentioned example of n-heptane oxidation, a skeletal mechanism with 110 species and 1170 reactions was obtained by chemical lumping and species removal [67]. These techniques might be attractive for simple, basic studies, but they do not lead to the expected saving in computational cost and, furthermore, they show certain difficulties. First, some experience is required for these techniques, since the identification of quasi steady-state species and equilibrated species is complicated task especially for extensive chemical schemes. Species may participate in several reactions but at different time scales. Moreover, it is a priori not clear if the QSSA is valid in the whole range of the mechanism. Concluding, the relatively poor cost-benefit ratio of these methods pushed the further research towards manifold generation and tabulated chemistry.

2.4.1.2 Manifold generation and tabulated chemistry

Further possibilities to reduce computational costs include tabulation of chemistry, manifold generation and flamelet methods. First, an interesting attempt is the in situ adaptive tabulation (ISAT) [68], where a chemistry table is created during the CFD calculation process. Chemical information can then be obtained from the table generated “on the fly” taking into account an estimated interpolation error. Based on this error control a decision is made whether a new point in the composition space has to be calculated or not. The great advantage of this method is that the data base size is restricted to the actually necessary composition space. This is in contrast to methods that

use pre-tabulation (addressed further below), where it is a priori not known which part of the composition space is accessed.

The Intrinsic Low Dimensional Manifold (ILDM) approach [69] is another popular reduction method that is based on the analysis of the eigenstructure of the Jacobian of the local source terms to identify slow chemical processes. The ILDM, a small subset of variables that evolve slowly during combustion, is found with this analysis and consequently parametrized with controlling variables and stored in a database. So this method combines reduction of degrees of freedom of the system by manifold generation and the tabulation of the obtained results. The ILDM approach has been adopted for example to simulate turbulent diffusion flames [70, 71] and it has also been used with DNS [72]. It was found to be effective at high temperature, but does not show good results at low temperatures since the number of slow time scales increases. Furthermore, the method fails in regions where diffusion processes are as important as chemical processes, when the composition may be modified faster by transport effects than by slow chemical time scales. Such effects can not be captured, since only the chemical system is taken into account like it is done in the techniques presented in the previous section. The reaction diffusion manifold (REDIM) approach [73] for example, which is an extension of the ILDM approach, takes into account additional transport effects.

Transport due to convection and diffusion occurs in flames together with chemical reactions. Therefore, two quite similar reduction approaches combine CRT and the flamelet approach in order to overcome the problems of the ILDM approach. The first one is flame prolongation of ILDM (FPI) [74] and the second one is flamelet generate manifold (FGM) [75, 76], both based on laminar premixed flames. The use of these approaches in turbulent combustion modeling is based on the flamelet assumption (presented in Section 2.2). The basic idea of this assumption is that the turbulent flame front can be represented by an ensemble of laminar flamelets embedded in turbulent flow. These flamelets have one-dimensional structure and can be calculated with detailed chemical mechanisms. The solution can then be stored in a look-up table as function of a limited set of variables. Both methods originally use a pair of parameters, enthalpy and a progress variable in FGM and a linear combination of species mass fractions FPI. Consequently, the computational times can be reduced significantly compared to full integrated chemistry which makes them very attractive. Moreover, they have received great attention due to their applicability to the full range of combustion regimes, i.e. premixed, partially premixed and nonpremixed flames [77–81].

The FPI as well as the FGM approach were adapted and applied to three-dimensional ICE simulations [82, 83].

Over the last years, models based on the flamelet approach are extensively used to model turbulent flames and are still of great interest and under continuous development. The laminar flamelet method was proposed by Peters for nonpremixed turbulent combustion [84]. In [85] this model is used in a RANS environment to simulate lifted turbulent jet diffusion flames. Additionally to the flamelet assumption, these models commonly adopt pre-tabulation of detailed chemistry results in a limited composition space with the mixture fraction as a key parameter. A flamelet model in combination with a progress variable approach was presented by Pierce and Moin [86] and used to model a coaxial jet combustor. A flamelet/progress variable approach is used by Ihme and Pitsch to model extinction and re-ignition of the Sandia laboratory flames [87, 88].

Concepts like the flamelet assumption, the mixture fraction and the progress variable together with pre-tabulation of results obtained with the use of detailed chemistry are applied in the combustion model implemented in this work. A detailed description of the implemented modeling strategy is given in the next chapter.

2.4.2 Chemistry-turbulence interaction

The consideration of turbulence-chemistry interaction is an important but complex part of combustion modeling. Averaged or filtered equations of flow and thermodynamic properties are solved in RANS or LES approaches. These averaging or filtering process leaves unclosed terms that need to be modeled. This means that instantaneous chemical source terms obtained from chemical kinetics relations can not be used directly. Instead, mean or filtered chemical source terms need to be provided for a consistent consideration of turbulent effects on the combustion process. Different approaches have been proposed and are still developed. Statistical approaches making use of probability density functions (PDF) play an important role in this area [89–91]. Some important concepts are briefly presented below, whereas for more detailed and extensive reviews the reader is referred to [63] or [3] for instance.

2.4.2.1 Conditional moment closure

The conditional moment closure method was introduced in the early 1990's [92, 93], originally for nonpremixed combustion. Although the method was independently proposed based on two different approaches, the main idea is the same. Conditional averaging is used based on the fact that a strong correlation between reactive scalars and the mixture fraction exists. Hence, variables are split into a conditional mean and fluctuations around this mean value instead of traditional averaging. It is experimentally observed that these new fluctuations around the conditional mean are then smaller than conventional fluctuations. Furthermore, equations for the conditional mean values $\langle Y_k|z\rangle$ are solved. In the first order CMC method it is consequently assumed that conditional fluctuations are negligible and that the mean chemical source terms only depend on the first order moments. A detailed review on CMC and a discussion about the differences of the two different original approaches is given in [94]. CMC has been applied to a wide range of combustion problems [95–99],and it was further developed for spray combustion [100]. The use of second order moments [101, 102] marks an improvement for the closure of the chemical source terms especially important for more complex problems such as flame stabilization and autoignition. Peters claims that CMC for nonpremixed combustion follows closely the flamelet concept [3]. A further development of CMC is multi mapping conditioning (MMC) introduced by [103], which combines PDF and CMC models.

2.4.2.2 Transported probability density functions

Probability density function methods are powerful approaches and today widely adopted methods in combustion modeling. The work presented in [90] can be considered as the starting point for virtually all PDF methods. In these methods transport equations for joint scalar or joint velocity-scalar PDF are solved. The main advantage of PDF methods is that the chemical source term appears in closed form and thus no modeling is required. However, a closure problem exists for molecular mixing, which needs to be modeled. This fact represents the weak point or challenge of PDF methods and its predictive performance mainly depends on the quality of the mixing models. The commonly adopted mixing models are the Interaction by Exchange with the Mean (IEM) [104] or the Linear Mean-Square Estimation (LMSE) [105] as well as variants of Curl's model (modified Curl mixing model) [106–108] and the Euclidean minimum spanning tree (EMST) model [109]. The performance of different mixing models was for instance investigated in [110, 111]. PDF

methods suffer from excessive memory requirements which is why solution algorithms for PDF transport equations use a Lagrangian particle Monte Carlo algorithm [112] to overcome this problem. In doing so, the particles may be considered as different realizations of the turbulent combustion problem but do not represent real fluid elements. The Langrangian algorithm is commonly coupled with an Eularian CFD code [63]. The computational effort of transported PDF methods though remains still too high for many industrial applications. A current review on PDF methods is given in [113].

2.4.2.3 Presumed probability density functions

A second way to use PDF to build a numerical model is to presume the PDF shape through the information from available quantities such as mean and variance of mixture fraction [50]. Presumed PDF are commonly used together with flamelet models to account for turbulent fluctuations of key parameters such as mixture fraction, scalar dissipation rate and/or progress variable. The main advantage of presumed PDF approaches is their relatively low computational effort since PDF shape is known a priori and does not have to be transported over the whole simulation run. In this work, such a presumed PDF approach is applied, so it is described in detail in the next chapter.

Bibliography

[1] Turns S. R. *An Introduction to Combustion.* MacGraw–Hill, 2000.

[2] Poinsot T. and Veynante D. *Theoretical and Numerical Combustion.* Edwards, 2005.

[3] Peters N. *Turbulent Combustion.* Cambridge University Press, 2000.

[4] K. Kuan–yun Kuo. *Principles of Combustion.* John Wiley & Sons, 1986.

[5] Warnatz J., Maas U. and Dibble R. W. *Combustion.* Springer, 2006.

[6] Damköhler G. "Der Einfluss der Turbulenz auf die Flammengeschwindigkeit in Gasgemischen". *Z. Elektrochem. Angew. Phys. Chem.*, Vol. 46, pp. 601–626, 1940.

[7] Borghi R. "On the structure and morphology of turbulent premixed flames". In Casci C., editor, *Recent Advances in the Aerospace Science*, pp. 117–138. Plenum Press, New York, 1985.

[8] Bray K. N. C. "Turbulent flows with premixed reactants in turbulent reacting flows". In Libby P. A. and Williams F. A., editors, *Topics in Applied Physics*, pp. 115–183. Springer Verlag, New York, 1980.

[9] Williams F. A. *Combustion Theory.* Addison-Wesley, 1985.

[10] Abdel-Gayed R. G. and Bradley D. "Combustion regimes and the straining of turbulent premixed flames". *Combust. Flame*, Vol. 76, pp. 213–218, 1989.

[11] Poinsot T., Veynante D. and Candel S. "Diagrams of premixed turbulent combustion based on direct simulation". *Proc. Combust. Inst.*, Vol. 23, pp. 613–619, 1990.

[12] Peters N. "The turbulent burning velocity for large–scale and small–scale turbulence". *J. Fluid Mech.*, Vol. 384, pp. 107–132, 1999.

[13] Poinsot T., Veynante D. and Candel S. "Quenching process and premixed turbulent combustion diagrams". *J. Fluid Mech.*, Vol. 228, pp. 561–605, 1991.

[14] Roberts W. L., Driscoll J. F., Drake M. C. and Goss L. P. "Images of the quenching of a flame by a vortex—To quantify regimes of turbulent combustion". *Combust. Flame*, Vol. 94, pp. 58–69, 1993.

[15] Borghi R. and Destriau M. *Combustion and flames.* (Translated from French). Editions Technip, 1998.

[16] Burke S. P. and Schumann T. E. W. "Diffusion flames". In *1st Symposium (Int.) on Combustion*, pp. 2–11, Pittsburgh, 1928. The Combustion Institute.

[17] Bilger R. W. "The structure of turbulent nonpremixed flames". In *22nd Symposium (Int.) on Combustion*, pp. 475–488, Pittsburgh, 1988. The Combustion Institute.

[18] Peters N. "Local quenching of diffusion flamelets and non-premixed turbulent combustion". In *Western States Section of the Combustion Institute*, WSS 80-4, Spring Meeting, Irvine, CA, 1980.

[19] Kuznetsov V. R. "Effect of turbulence on the formation of large superequilibrium concentration of atoms and free radicals in diffusion flames". *Mehan. Zhidkosti Gasa*, Vol. 6, pp. 3–9, 1982.

[20] Pitsch H. and Peters N. "A consistent flamelet formulation for non-premixed combustion considering differential diffusion effects". *Combust. Flame*, Vol. 114, pp. 26–40, 1998.

[21] Pitsch H. and Peters N. "Unsteady flamelet modeling of turbulent hydrogen-air diffusion flames". In *27th Symposium (Int.) on Combustion*, pp. 1057–1064, Pittsburgh, 1998. The Combustion Institute.

[22] Williams F. A. "Turbulent Mixing in Nonreactive and Reactive Flows". In Murthy S. N. B., editor, *Recent advances in theoretical descriptions of turbulent diffusion flames*, pp. 189–208. Plenum Press, New York, 1975.

[23] Borghi R. "Turbulent combustion modelling". *Prog. Energy Combust. Sci.*, Vol. 14, pp. 245–292, 1988.

[24] Bray K. N. C. and Peters N. "Laminar Flamelets in turbulent Flames". In Libby P. A. and Williams F. A., editors, *Turbulent reacting flows*, pp. 63–113. Academic Press, London, 1994.

[25] Cuenot B. and Poinsot T. "Effects of curvature and unsteadiness in diffusion flames. Implications for turbulent diffusioncombustion". In *25th Symposium (Int.) on Combustion*, Pittsburgh, 1994. The Combustion Institute.

[26] Libby P. A. and Williams F. A. "Turbulent combustion: fundamental aspects and a review". In Libby P. A. and Williams F. A., editors, *Turbulent reacting Flows*, pp. 2–61. Academic Press, London, 1994.

[27] Pitts W. M. "Assessment of theories for the behaviourand blowout of lifted turbulent jet diffusion flames". In *22nd Symposium (Int.) on Combustion*, pp. 809–816, Pittsburgh, 1988. The Combustion Institute.

[28] Chen T. H., Goss L. P., Talley D. G. and Mikolaitis D. W. "Dynamic Stabilization Zone Structure of Jet Diffusion Flames from Liftoff to Blowout". *J. of Propulsion and Power*, Vol. 8, pp. 548–552, 1992.

[29] Brown C. D., Watson K. A. and Lyons K. M. "Studies on Lifted Jet Flames in Coflow: The Stabilization Mechanism in the Near– and Far–Fields". *Flow Turb. Combust.*, Vol. 62, pp. 249–273, 1999.

[30] Ghosal S. and Vervisch L. "Stability Diagram for Lift-Off and Blowout of a Round Jet Laminar Diffusion Flame". *Combust. Flame*, Vol. 123, pp. 646–655, 2001.

[31] Venugopal R. and Abraham J. "A Review of Fundamental Studies Relevant to Flame Lift–off in Diesel Jets". *SAE Technical Paper 2007–01–0134*, 2007.

[32] Pickett L. M., Siebers D. L. and Idicheria C. A. "Relationship Between Ignition Processes and the Lift-Off Length of Diesel Fuel Jets". *SAE Technical Paper 2005–01–3843*, 2005.

[33] Domingo P. and Vervisch L. "Triple flames and partially premixed combustion in autoignition of non–premixed mixtures". In *26th Symposium (Int.) on Combustion*, pp. 233–240, Pittsburgh, 1996. The Combustion Institute.

[34] Chen Y.-C. and Bilger R. W. "Stabilization Mechanisms of Lifted Laminar Flames in Axisymmetric Jet Flows". *Combust. Flame*, Vol. 123, pp. 23–45, 2000.

[35] Phillips H. "Flame in a buoyant methane layer". In *10th Symposium (Int.) on Combustion*, pp. 1277–1283, Pittsburgh, 1965. The Combustion Institute.

[36] Liñán A. "Ignition and flame spread in laminar mixing lauyers". In Buckmaster J., Jackson T. L. and Kumar A., editors, *Combustion in High–Speed Flows*, pp. 461–476. Kluwer Academic, Dordrecht, 1994.

[37] Plessing T., Terhoeven P., Peters N. and Mansour M. S. "An Experimental and Numerical Study of a Laminar Triple Flame". *Combust. Flame*, Vol. 115, pp. 335–353, 1998.

[38] Bourlioux A., Cuenot B. and Poinsot T. "Asymptotic and Numerical Study of the Stabilization of Diffusion Flames by Hot Gas". *Combust. Flame*, Vol. 120, pp. 143–159, 2000.

[39] Boulanger J., Vervisch L., Reveillon J. and Ghosal S. "Effects of heat release in laminar diffusion flames lifted on round jets". *Combust. Flame*, Vol. 134, pp. 355–368, 2003.

[40] Vervisch L. "Using numerics to help the understanding of non–remixed turbulent flames". *Proc. Combust. Inst.*, Vol. 28, pp. 11–24, 2000.

[41] White F. M. *Viscous Fluid Flow*. McGraw-Hill, 1991.

[42] Anderson J. D. *Computational Fluid Dynamics*. McGraw-Hill, 1995.

[43] Versteeg H. K. and Malalasekera W. *An Introduction to Computational Fluid Dynamics*. Pearson, 2007.

[44] Tennekes H. and Lumley J. L. *A first course in turbulence*. MIT Press, 1972.

[45] Richardson L. F. *Weather Prediction by Numerical Process*. Cambridge University Press, 1922.

[46] Pope S. B. *Turbulent Flows*. Cambridge University Press, 2000.

[47] Kolmogorov A. N. "The Local Structure of Turbulence in Incompressible Viscous Fluid for Very Large Reynolds Numbers". *Proc. R. Soc. London*, Vol. 434, pp. 9–13, 1991.

[48] Kolmogorov A. N. "A refinement of previous hypotheses concerning the local structure of turbulence in a viscous incompressible fluid at high Reynolds number". *J. Fluid Mech.*, Vol. 13, pp. 82–85, 1962.

[49] Vervisch L. and Poinsot T. "Direct numerical simulation of non-premixed turbulent flames". *Ann. Rev. Fluid Mech.*, Vol. 30, pp. 655–691, 1998.

[50] Veynante D. and Vervisch L. "Turbulent combustion modeling". *Prog. Energy Combust. Sci.*, Vol. 28, pp. 193–266, 2002.

[51] Hawkes E. R., Sankaran R., Sutherland J. C. and Chen J. H. "Direct numerical simulation of turbulent combustion: fundamental insights towards predictive models". *J. Phys.: Conf. Ser.*, Vol. 16, pp. 65–79, 2005.

[52] Pitsch H. "Large-Eddy Simulation of Turbulent Combustion". *Ann. Rev. Fluid Mech.*, Vol. 38, pp. 453–482, 2006.

[53] Wilcox D. C. *Turbulence Modeling for CFD*. DCW Industries, 1994.

[54] Favre A. "Équations des gaz turbulents compressibles". *Jour. Méc.*, Vol. 4, pp. 361–390, 1965.

[55] Favre A. "Statistical equations of turbulent gases". In *Problems of Hydrodynamics and Continuum Mechanics*, pp. 231–266, Philadelphia, 1969. Soc. for Ind. and Appl. Mathematics.

[56] Launder B. E., Reece G. J. and Rodi W. "Progress in the Development of a Reynolds-Stress Turbulence Closure". *J. Fluid Mech.*, Vol. 68, pp. 537–566, 1975.

[57] Jones W. P. and Launder B. E. "The prediction of laminarization with a two–equation model of turbulence". *International Journal of Heat and Mass Transfer*, Vol. 15, pp. 301–314, 1972.

[58] Launder B. E. and Spalding D. B. "The Numerical Computation of Turbulent Flows". *Comput. Methods Appl. Mech. Eng.*, Vol. 3, pp. 269–289, 1974.

[59] Launder B. E. and Sharma B. I. "Application of the Energy Dissipation Model of Turbulence to the Calculation of Flow Near a Spinning Disc". *Letters in Heat and Mass Transfer*, Vol. 1, pp. 131–138, 1974.

[60] Hirschfelder J. O., Curtiss C. F. and Byrd R. B. *Molecular theory of gases and liquids*. John Wiley & Sons, New York, 1969.

[61] Arrhenius S. "On the reaction rate of the inversion of non-refined sugar upon souring". *Z. Phys. Chem.*, Vol. 4, pp. 226–248, 1889.

[62] Connors K. A. *Chemical Kinetics*. VCH Publishers, 1990.

[63] Echekki T. and Mastorakos E. *Turbulent Combustion Modeling*, volume 95. Springer, 2011.

[64] Curran H. J., Gaffuri P. and Westbrook C. K. "A Comprehensive Modeling Study of n-Heptane Oxidation". *Combust. Flame*, Vol. 114, pp. 149–177, 1998.

[65] Bodenstein M. and Lind S. C. "Geschwindigkeit der Bildung des Bromwasserstoffs aus seinen Elementen". *Z. Phys. Chem.*, Vol. 57, pp. 168, 1906.

[66] Law C. K. *Combustion Physics*. Cambridge University Press, New York, 2006.

[67] Zeuch T., Moréac G., Ahmed S. S. and Mauss F. "A comprehensive skeletal mechanism for the oxidation of n-heptane generated by chemistry-guided reduction". *Combust. Flame*, Vol. 155, pp. 651–674, 2008.

[68] Pope S. B. "Computationally efficient implementation of combustion chemistry using in situ adaptive tabulation". *Combust. Theory Modelling*, Vol. 1, pp. 41–63, 1997.

[69] Maas U. and Pope S. B. "Simplifying chemical kinetics: Intrinsic low-dimensional manifolds in composition space". *Combust. Flame*, Vol. 88, pp. 239–264, 1992.

[70] Norris A. T. and Pope S. B. "Modeling of Extinction in Turbulent Diffusion Flames by the Velocity-Dissipation-Composition PDF Method". *Combust. Flame*, Vol. 100, pp. 211–220, 1995.

[71] Xiao K., Schmidt D. and Maas U. "PDF simulations of turbulent non-premixed CH4/H2-air flames using automatically reduced chemical kinetics". *Proc. Combust. Inst.*, Vol. 27, pp. 1073–1080, 1998.

[72] Gicquel O., Thévenin D., Hilka M. and Darabiha N. "Direct numerical simulation of turbulent premixed flames using intrinsic low-dimensional manifolds". *Combust. Theory Modelling*, Vol. 3, pp. 479–502, 1999.

[73] Bykov V. and Maas U. "The extension of the ILDM concept to reaction–diffusion manifolds". *Combust. Theory Modelling*, Vol. 11, pp. 839–862, 2007.

[74] Gicquel O., Darabiha N. and Thévenin D. "Laminar premixed hydrogen/air counterflow flame simulations using flame prolongation of ILDM with differential diffusion". *Proc. Combust. Inst.*, Vol. 28, pp. 1901–1908, 2000.

[75] van Oijen J. A. and de Goey L. P. H. "Modelling of premixed laminar flames using flamelet-generated manifolds". *Combust. Sci. Technol.*, Vol. 161, pp. 113–137, 2000.

[76] van Oijen J. A., Lammers F. A. and de Goey L. P. H. "Modeling of Complex Premixed Burner Systems by Using Flamelet-Generated Manifolds". *Combust. Flame*, Vol. 127, pp. 2124–2134, 2001.

[77] van Oijen J. A. and de Goey L. P. H. "Modelling of premixed counterflow flames using the flamelet-generated manifold method". *Combust. Theory Modelling*, Vol. 6, pp. 463–478, 2002.

[78] van Oijen J. A. and de Goey L. P. H. "A numerical study of confined triple flames using a flamelet-generated manifold". *Combust. Theory Modelling*, Vol. 8, pp. 141–163, 2004.

[79] Bongers H. *Analysis of Flamelet-Based Methods to Reduce Chemical Kinetics in Flame Computations*. Doctoral Thesis, Technische Universiteit Eindhoven, 2005.

[80] Vreman A. W., Albrecht B. A., van Oijen J. A., de Goey L. P. H. and Bastiaans R. J. M. "Premixed and nonpremixed generated manifolds in large-eddy simulation of Sandia flame D and F". *Combust. Flame*, Vol. 153, pp. 394–416, 2008.

[81] Vervisch L., Hauguel R., Domingo P. and Rullaud M. "Three facets of turbulent combustion modelling: DNS of premixed V-flame, LES of lifted nonpremixed flame and RANS of jet-flame". *Journal of Turbulence*, Vol. 4, pp. 1–36, 2004.

[82] Colin O., Pera C. and Jay S. "Detailed chemistry tabulation based on a FPI approach adapted and applied to 3-D internal combustion engine calculations". In *Third European Combustion Meeting*, 2007.

[83] Bekdemir C., Somers L. M. T. and de Goey L. P.H. "Modeling diesel engine combustion using pressure dependent Flamelet Generated Manifolds". *Proc. Combust. Inst.*, Vol. 33, pp. 2887–2894, 2011.

[84] Peters N. "Laminar diffusion flamelet models in non-premixed turbulent combustion". *Prog. Energy Combust. Sci.*, Vol. 10, pp. 319–339, 1984.

[85] Chen M., Herrmann M. and Peters N. "Flamelet modeling of lifted turbulent methane/air and propane/air jet diffusion flames". *Proc. Combust. Inst.*, Vol. 28, pp. 167–174, 2000.

[86] Pierce C. D. and Moin P. "Progress–variable approach for large–eddy simulation of non–premixed turbulent combustion". *J. Fluid Mech.*, Vol. 504, pp. 73–79, 2004.

[87] Ihme M. and Pitsch H. "Prediction of extinction and reignition in nonpremixed turbulent flames using a flamelet/progress variable model 1. A priori study and presumed PDF closure". *Combust. Flame*, Vol. 155, pp. 70–89, 2008.

[88] Ihme M. and Pitsch H. "Prediction of extinction and reignition in nonpremixed turbulent flames using a flamelet/progress variable model 2. Application in LES of Sandia flames D and E". *Combust. Flame*, Vol. 155, pp. 90–107, 2008.

[89] O'Brien E. E. "The probability density function (PDF) approach to reacting turbulent flows". In Libby P. A. and Williams F. A., editors, *Turbulent reacting flows*, pp. 185–218. Academic Press, London, 1980.

[90] Pope S. B. "PDF method for turbulent reacting flows". *Prog. Energy Combust. Sci.*, Vol. 11, pp. 119–192, 1985.

[91] Dopazo C. "Recent developments in PDF methods". In Libby P. A. and Williams F. A., editors, *Turbulent reacting flows*, pp. 375–474. Academic Press, London, 1994.

[92] Klimenko A. Y. "Multicomponent diffusion of various scalars in turbulent flows". *Fluid Dyn.*, Vol. 25, pp. 327–334, 1990.

[93] Bilger R. W. "Conditional moment closure for turbulent reacting flows". *Phys. Fluids*, Vol. A5, pp. 436–444, 1993.

[94] Klimenko A. Y. and Bilger R. W. "Conditional moment closure for turbulent combustion". *Prog. Energy Combust. Sci.*, Vol. 25, pp. 595–688, 1999.

[95] Kim W. T. and Huh K. Y. "Numerical simulation of spray autoignition by the first order conditional moment closure model". *Proc. Combust. Inst.*, Vol. 29, pp. 569–576, 2002.

[96] Martin S. M., Kramlich J. C., Kosály G. and Riley J. J. "The premixed conditional moment closure method applied to idealized lean premixed gas turbine combustors". *J. Eng. Gas Turb. Power*, Vol. 125, pp. 895–900, 2003.

[97] Fairweather M. and Woolley R. M. "First-order conditional moment closure modeling of turbulent, nonpremixed hydrogen flames". *Combust. Flame*, Vol. 133, pp. 393–405, 2003.

[98] Devaud C. B. and Bray K. N. C. "Assessment of the applicability of conditional moment closure to a lifted turbulent flame: first order model". *Combust. Flame*, Vol. 132, pp. 102–114, 2003.

[99] Fairweather M. and Woolley R. M. "First- and second-order elliptic conditional moment closure calculations of piloted methane diffusion flames". *Combust. Flame*, Vol. 150, pp. 92–107, 2007.

[100] Mortensen M. and Bilger R. W. "Derivation of the conditionalmoment closure equations for spray combustion". *Combust. Flame*, Vol. 156, pp. 62–72, 2009.

[101] Kronenburg A., Bilger R. W. and Kent J. H. "Second Order Conditional Moment Closure for Turbulent Jet Diffusion Flames". *Proc. Combust. Inst.*, Vol. 29, pp. 1097–1104, 1998.

[102] Mastorakos E. and Bilger R. W. "Second-order conditional moment closure for the auto-ignition of turbulent flows". *Physics of Fluids*, Vol. 10, pp. 1246–1248, 1998.

[103] Klimenko A. Y. and Pope S. B. "A model for turbulent reactive flows based on multiple mapping conditioning". *Phys. Fluids*, Vol. 15, pp. 1907–1925, 2003.

[104] Villermaux J. and Devillon J. C. "Représentation de la coalescence et de la redispersion des domaines de ségrégation dans un fluide par un modèle d'interaction phénoménologique". In *Proc. Second Intern'l. Symp. on Chemical Reaction Engineering*, pp. 1–13, New York, 1972. Elsevier.

[105] Dopazo C. and O'Brien E. E. "An approach to the autoignition of a turbulent mixture". *Acta Astronaut.*, Vol. 1, pp. 1239–1266, 1974.

[106] Curl R. L. "Dispersed phase mixing: I. Theory and effects of simple reactors". *AIChE J.*, Vol. 9, pp. 175–181, 1963.

[107] Janicka J., Kolbe W. and Kollmann W. "Closure of the transport equation for the probability density function of turbulent scalar fields". *J. Non-Equilib. Thermodyn.*, Vol. 4, pp. 47–66, 1977.

[108] Nooren P. A., Wouters H. A., Peeters T. W. J., Roekaerts D., Maas U. and Schmidt D. "Monte Carlo PDF modeling of a turbulent natural-gas diffusion flame". *Combust. Theory Modelling*, Vol. 1, pp. 79–96, 1997.

[109] Subramaniam S. and Pope S. B. "A mixing model for turbulent reactive flows based on Euclidean minimum spanning trees". *Combust. Flame*, Vol. 115, pp. 487–514, 1998.

[110] Ren Z. and Pope S. B. "An investigation of the performance of turbulent mixing models". *Combust. Flame*, Vol. 136, pp. 208–216, 2004.

[111] Senouci M., Bounif A., Abidat M., Belkaid N. M., Mansour C. and Gokalp I. "Transported-PDF (IEM, EMST) micromixing models in a hydrogen-air nonpremixed turbulent flame". *Acta Mech*, Vol. 224, pp. 3111–3124, 2013.

[112] Pope S. B. "A Monte Carlo method for the pdf equations of turbulent reactive flow". *Combust. Sci. Technol.*, Vol. 25, pp. 159–174, 1981.

[113] Haworth D. C. "Progress in probability density function methods for turbulent reacting flows". *Prog. Energy Combust. Sci.*, Vol. 36, pp. 168–259, 2010.

Chapter 3

Combustion model description and aspects of laminar flamelets

Contents

3.1 Introduction

The combustion model implemented and applied in this work is detailed in the following sections. The chosen modeling strategy can be classified as an Unsteady Flamelet/Progess Variable (UFPV) approach. Such an approach was originally presented for LES [1, 2]. The implemented approach of this work is somehow similar to the one in [3] using a RANS environment too. Though coupled with a LES code, the combustion model in [4] also shows some similarities.
First, the general characteristics of the combustion problem of interest are recapitulated in order to make clear the requirements for the model. Then a short overview of the fundamentals and key concepts used in the present combustion model is given.
After this introductory part, characteristics, calculation and parametrization of laminar steady and unsteady diffusion flames, which are the basis of the implemented model, are introduced. Furthermore, an interesting approximation of such laminar diffusion flames is presented with the aim of reducing computational effort in case of complex combustion problems.
Both versions of diffusion flames are equally applicable in the combustion model. This is shown in Chapter 4, where the H_2/N_2 flame from Berkeley University is modeled with both approaches. A more basic assessment of the approximated version of diffusion flames is made in Chapter 5 in a study of n-heptane sprays. Preliminary results of the different versions of laminar diffusion flames are presented in their corresponding sections of this chapter.
Then the consideration of turbulence effects by the adoption of probability density functions is explained. The rest of this chapter is dedicated to the coupling of the combustion model with the existent CFD code. Two different coupling methods, each adjusted for one of the two cases mentioned above, are presented.
Throughout this chapter (preliminary) results corresponding to the H_2/N_2 flame and the n-heptane sprays are shown to illustrate the different steps of the modeling strategy. Though, this does not mean any limitation of the combustion model to those cases or fuels.

3.1.1 Characteristics of the present combustion problem

The completion of the objective planned in Section 1.3, implies the consideration of some key features of turbulent lifted flames. These features are reminded with the help of a simplified representation of the combustion process of a fuel spray shown in Fig. 3.1. It should be noted that this representation is only exemplary, but the implemented model is not limited to this certain case of combustion. As shown later, the model is equally applicable to reactive gaseous jets and liquid sprays.

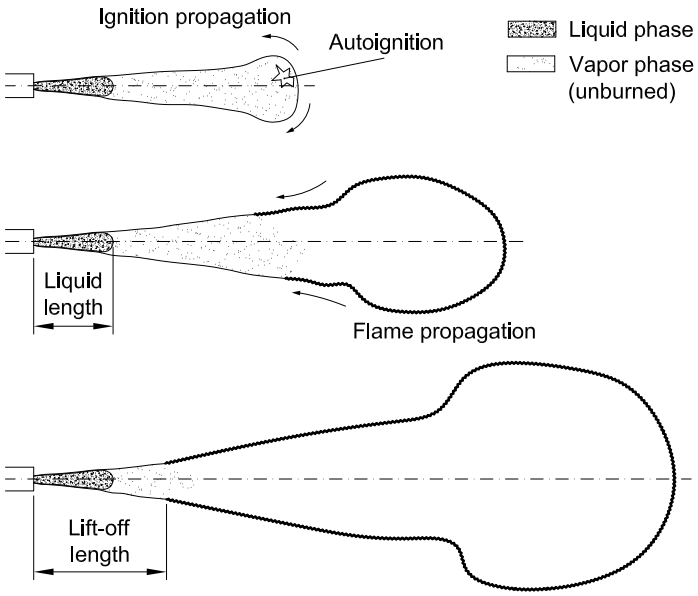

Figure 3.1. *Simplified representation of ignition and combustion process of reactive spray.*

The beginning of the combustion process is marked by an autoignition event taking place in a limited region within an inhomogeneous mixture. The combustion model therefore has to be capable to reproduce autoignition phenomena. Once the combustion has started the flame extends throughout a stratified, partially premixed mixture until a quasi-steady state is reached (sometimes referred to *burn out*). The transition from the inert to a quasi-steady burning state has to be captured by the model.
Subsequently, the combustion occurs mainly in a nonpremixed flame regime and a lifted turbulent diffusion flame is established. Mixing of fuel and oxidizer

plays an important role in this combustion regime as discussed in Section 2.2.3. That is why the mixture fraction plays a key role in the planned combustion model.
Indeed, in the region between the injection orifice and the flame base—this distance is the lift-off height—fuel and oxidizer have time and space for premixing to a certain level. Thus, the flame base is situated in a partially premixed mixture. The stabilization of the flame in this partially premixed region is still not totally understood. Quite the contrary, a lively discussion about the dominant phenomena in this particular zone of the flame exists in the scientific community. Peters [5] for instance gives an extensive disquisition about this topic and summarizes the mentioned discussion. Experimental as well as numerical investigations [6–10] about the stabilization mechanism of flame lift-off are still carried out to enhance the knowledge about this complex process. Certainly, unsteady effects need to be considered in the modeling strategy in order to correctly describe the structure of a lifted turbulent diffusion flame.

3.1.2 Model fundamentals

The fundamentals and key concepts adopted in the present modeling strategy, designed to describe the combustion problem considered, are briefly outlined here. These elements mark the cornerstones of the combustion model that is consequently implemented in the *dieselFoam* solver environment of OpenFOAM-1.6. OpenFOAM is an open source CFD package increasingly used and enhanced especially in the academic field over the last years. More precisely, it is an extensive collection of different solvers and libraries written in C++.
The implemented combustion model is based on the following concepts:

- **Flamelet concept.** The combustion model is based on the flamelet concepts which suggests that a turbulent flame can be represented by a set of laminar flamelets. Here in particular, it is assumed that the turbulent flame structure corresponds locally to a diffusion flame in opposed jet configuration.
- **Presumed PDF modeling.** In order to consider the effect of turbulence on the combustion process, presumed PDFs are adopted to describe the statistical distribution of the independent variables of the process. This approach allows a pre-integration of laminar flamelet results.

- **Flamelet manifold.** A flamelet manifold is generated which allows to store all properties involved in the combustion process as a function of reduced number of independent variables in a look-up table. Two different ways of tabulation will be applied.

- **Coupling with CFD code.** The coupling with existent CFD code describing fluid and thermodynamics depends on the independent variables and the before chosen manifold and tabulation strategy.

3.2 Laminar diffusion flames

The application of the flamelet concept reflects the quintessence of the implemented combustion model. The basic ideas of this concept are presented in Section 2.2.3, while the details of the geometrical configuration and the numerical resolution of steady and unsteady diffusion flames are discussed in this section.

3.2.1 Geometrical configuration and parametrization of flamelet space

An adequate and commonly used configuration for the representation of the local structure of a diffusion flame is a 1D laminar diffusion flame (DF) in opposed-jet configuration (also called counterflow diffusion flame). Figure 3.2 shows the geometrical arrangement of such a planar counterflow configuration. The local coordinate system (x, y) and the Z coordinate correspond to those shown in Fig. 2.3. A fuel and an oxidizer stream exit from two opposed nozzles at given velocities, which correspond to a strain rate a imposed on the laminar flame structure. The temperature and composition that are stated on either side represent the boundary conditions of this configuration. In the space between the two orifice mixing occurs and a flame front may establish at a certain distance from the nozzles. The mixture fraction Z increases monotonically from zero at the oxidizer boundary to unity at the fuel boundary. Any property $\mathcal{Q}^{\mathrm{DF}}$ of the reactive flow field such as species mass fraction or temperature can then also be represented against the mixture fraction instead of spacial coordinates. Given an initial solution at time τ along the center line (e.g. the adiabatic mixture), one can calculate igniting or extinguishing flamelets. These are the unsteady flamelets used to model the actual combustion problem including unsteady effects. They can be

parametrized in a 3D flamelet space defined by the independent variables mixture fraction Z, strain rate a and flamelet time $\Delta\tau$, so that any property of the unsteady diffusion flame is given by $\mathcal{Q}^{\mathrm{DF}}(Z,\, a,\, \Delta\tau)$.

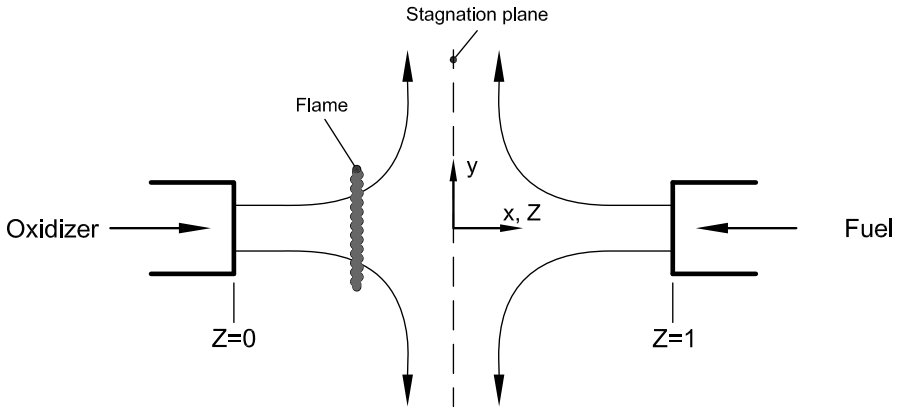

Figure 3.2. *Laminar diffusion flame in opposed jet configuration.*

However, a re-parametrization of this 3D space is made since the strain rate a and the flamelet time $\Delta\tau$ are not appropriate for a direct use in the combustion model. Instead of the strain rate a, defining the boundary condition of counterflow diffusion flame calculation, the scalar dissipation rate χ (see Eq. (2.14)) which can be obtained as a local value in turbulent flow is used. The flamelet time $\Delta\tau$ is replaced by a properly chosen progress variable (PV). A common choice for such a progress variable is a linear combination of species mass fractions in the same way as proposed for the generation of tabulated chemistry manifolds (e.g. FPI, FGM, etc. discussed in Section 2.4.1.2). In case of the lifted H_2/N_2 jet flame from Berkeley University [11], presented in Chapter 4, $Y_c = Y_{H_2O} + 10\, Y_{HO_2} + 3\, Y_{H_2}$ is chosen for instance.
In contrast, local values for mixture fraction $Z(\boldsymbol{x},\, t)$ can indeed be obtained from the local mixture composition. For instance, considering the mentioned case of the hydrogen flame by $Z = \frac{(Y_H - Y_{Hc})/2W_H - (Y_O - Y_{O,c})/W_O}{(Y_{H,f} - Y_{Hc})/2W_H - (Y_{O,f} - Y_{O,c})/W_O}$, where Y_H and Y_O are the elementary mass fractions of H and O atoms, W_H and W_O their respective atomic weight, and where the subscripts 'f' and 'c' refer to the fuel and coflow streams as stated in Table 4.2. Thus, no variable change for the mixture fraction is made.
Finally, the applied modeling assumption means that any property $\mathcal{Q}$ at location $\boldsymbol{x}$ and time t in a turbulent flame may be related to the corresponding property $\mathcal{Q}^{\mathrm{DF}}$ of the laminar diffusion flame for given values of $Z(\boldsymbol{x},\, t)$, $\chi(\boldsymbol{x},\, t)$

and $Y_c(\boldsymbol{x}, t)$ such that:

$$\mathcal{Q}(\boldsymbol{x}, t) = \mathcal{Q}^{\mathrm{DF}}(Z, \chi, Y_c). \tag{3.1}$$

3.2.2 Calculation of 1D diffusion flames

The steady and unsteady solutions of the counterflow diffusion flame configuration can be calculated in principle in two different ways. First, directly in the physical space or, second, after a variable transformation in the mixture fraction space. In general, the latter approach is used for flamelet models and is also chosen in this work. The main difference appears in the scalar dissipation rate $\chi(Z)$, which changes with time when solving in physical space, but is typically fixed in time when solving in mixture fraction space.

The calculations of the steady and unsteady flamelet solutions are carried out with the computer code LFLAM [1]. This code allows to resolve 1D diffusion flames in physical as well as in mixture fraction space.
The resolution of 1D flamelets in physical space is out of the scope of this work, however, the principle way of calculation is outlined briefly. A more detailed description of the two different calculation approaches as well as a comparison of the different flamelet solutions for the case of the "Berkeley flame" are presented in [13].

Resolution in physical space

In physical space, the continuity, momentum, temperature and species equation are solved as derived in [12, 14]. As a result, one obtains the composition $Y_i(x)$ and the temperature $T(x)$ in physical space at discrete times. The mixture fraction $Z(x)$ is retrieved from the composition. The instantaneous scalar dissipation rate $\chi(x)$ is calculated with Eq. (2.14). Finally, the results can then be expressed as a function of mixture fraction in the way: $Y_i(Z)$, $T(Z)$, $\chi(Z)$.

[1] The LFLAM code was developed at Ciemat in Madrid, Spain. It is a further development of the OPPDIF code [12] from Sandia NL, a Fortran program for calculating opposed flow diffusion flames.

Resolution in mixture fraction space

In the mixture fraction space, the flamelet equation is solved for each species i considered in the chemical reaction mechanism:

$$\frac{Y_i}{\partial t} = \frac{\chi(Z)}{2} \frac{\partial^2 Y_i}{\partial Z^2} + \dot{\omega}_i. \tag{3.2}$$

The reaction term $\dot{\omega}_i$ of species i is obtained from a chemical mechanism given in Chemkin format as function of composition Y_i and temperature T. Of course, the size of the provided mechanism, i.e. the number of species and reactions, has direct impact on the computational effort of the numerical resolution the system of flamelet equations. With the assumption of unity Lewis number, the total enthalpy of the mixture is approximated as $h = Z\,h_f + (1-Z)\,h_o$, where the subscripts 'f' and 'o' refer to the fuel and oxidizer. The temperature T is simply obtained as function of composition Y_i and total enthalpy h.
The profile of the scalar dissipation rate $\chi(Z)$ is prescribed as an fixed in time error function profile

$$\chi(a,\, Z) = \frac{a}{\pi} \exp\left[-2\left(\mathrm{erfc}^{-1}(2Z)\right)^2\right] = a\mathcal{F}(Z), \tag{3.3}$$

with the inverse of the complementary error function $\mathrm{erfc}(x) = 1 - \mathrm{erf}(x) = (2/\sqrt{\pi}) \int_x^\infty \exp\left(-y^2\right) \mathrm{d}y$. This commonly applied profile corresponds to the analytic solution of the steady-state profile of laminar counterflow diffusion flames in Z-space [5, 15]. A modified version of Eq. (3.3) that takes into account nonconstant density is presented in [16].
The strain rate a appears in Eq. (3.3), which can be rewritten in a strain rate-independent form. This is done by normalizing Eq. (3.3) with the value of the scalar dissipation rate at the stoichiometric mixture fraction in the way: $\chi_{st} = \chi(Z_{st},\, a) = a\mathcal{F}(Z_{st})$, which finally gives

$$\chi(Z,\, \chi_{st}) = \chi_{st} \frac{\mathcal{F}(Z)}{\mathcal{F}(Z_{st})}. \tag{3.4}$$

The system of equations (3.2)–(3.3) are solved in their steady form with the "Twopnt" algorithm for boundary value problems [17] and in their unsteady form with the DDASSL solver [18].

The flamelet equations given in Eq. (3.2) can obviously also be written for the progress variable Y_c, which is just a linear combination of species, as:

$$\dot{Y}_c = \frac{Y_c}{\partial t} = \frac{\chi(Z)}{2} \frac{\partial^2 Y_c}{\partial Z^2} + \dot{\omega}_{Y_c}. \tag{3.5}$$

The chemical source term $\dot{\omega}_{Y_c}$ as well as the combined source term $\dot{Y}_c$ of the progress variable Y_c play both an important role in the combustion model implemented in this work. The first source term includes only the chemical part, whereas the second one additionally includes the effect of local diffusion in the flamelet structure. Their characteristics are quite different as shown at the end of the next section. Both types of source terms are further compared when applied to model the H_2/N_2 flame in Chapter 4 .

3.2.3 Characteristics of 1D diffusion flames

Some preliminary results of steady and unsteady laminar diffusion flames are show in this section. The focus however does not only lie on the presentation of results of a particular case, rather than to serve as a graphical support for a description of some basic aspects and correlations of laminar flamelet solutions. The presented results correspond to the conditions of the "Berkeley flame" treated in detail in Chapter 4. The boundary conditions of this flame are listed in Tab. 4.2. The chemical mechanism of [19] used to calculate the laminar flamelets for this case involves 9 species (H_2, H, O_2, OH, O, H_2O, HO_2, H_2O_2 and N_2) and 21 reactions. Before presenting actual flamelet results, a visualization of Eq. (3.4) is shown in Fig. 3.3, where scalar dissipation rate profiles calculated with Eq. (3.3) for different strain rates a are plotted.

The steady flamelet solutions, which represent the physical limits for igniting and extinguishing flamelets, are shown at the top of Fig. 3.4. A 3D representation of the so-called S-curve is given in this figure. The red surface and the black surface represent the upper and lower stable branch and the blue, dash-dotted surface marks the unstable middle branch. The region below the stable branches and above the unstable branch corresponds to the zone of autoignition. Everywhere else—above the lower stable branch and below the middle unstable branch—extinction occurs. Thus, all unsteady flamelet solutions lie below the stable upper branch. A 3D representation of the S-curve plotting steady temperature values is shown at the bottom of Fig. 3.4. The temperature values at $Z = 0$ and $Z = 1$ correspond to the fuel stream temperature T_f and coflow temperature T_c of the "Berkeley flame" stated in Tab. 4.2.

A cross section of the steady flamelet solutions shown in Fig. 3.4 at a constant mixture fraction leads to the typical 2D representation of the S-curve. Such a representation is shown in Fig. 3.5 for the stoichiometric mixture fraction $Z_{st} = 0.4789$ of the "Berkeley flame" case. The coloring of the three

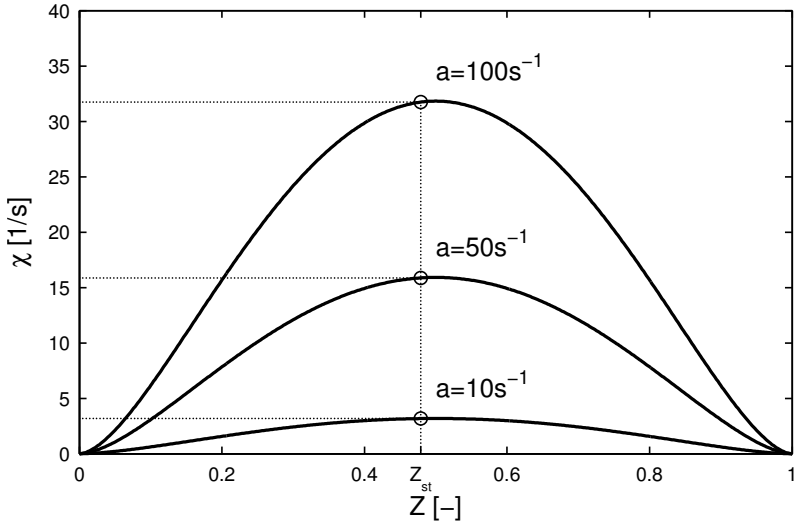

Figure 3.3. *Scalar dissipation rate profiles for different strain rates a. Stoichiometric scalar dissipation rate indicated for $Z_{st} = 0.4789$ of the H_2/N_2 flame.*

branches is identical to the one in Fig. 3.4. The gray, horizontal line marks the inert value of the progress variable Y_c, which is independent of scalar dissipation rate χ. Furthermore, two characteristic scalar dissipation rates are marked in Fig. 3.5. The first one is the scalar dissipation rate χ_{Q} where quenching of the laminar flame occurs. From this point on the combustion process cannot sustain the diffusion of hot combustion products from the reaction zone. The second one is the scalar dissipation rate χ_{AI} that marks the maximum scalar dissipation rate at which autoignition of the flame may occur. Hence, the region below χ_{AI}, which corresponds directly to the strain rate a_{AI} marking the autoignition limit, is referred to as *autoignition range*. The region with scalar dissipation rate above this characteristic value is referred to as *unstable range*. Inert mixtures at values of $\chi > \chi_{\mathrm{AI}}$ can not auto ignite. Consequently and as already mentioned, the region below the unstable middle branch (blue, dashed curve) corresponds to extinguishing flamelets. Though, there exists a small region below the stable lower branch, represented by the short black curve in Fig. 3.5, where some reaction occurs but which does not reach the upper steady solution.

The steady flamelet solutions presented above constitute starting points of the calculation of igniting and extinguishing unsteady flamelets. In the autoignition range—below χ_{AI}—igniting flamelet solutions are calculated

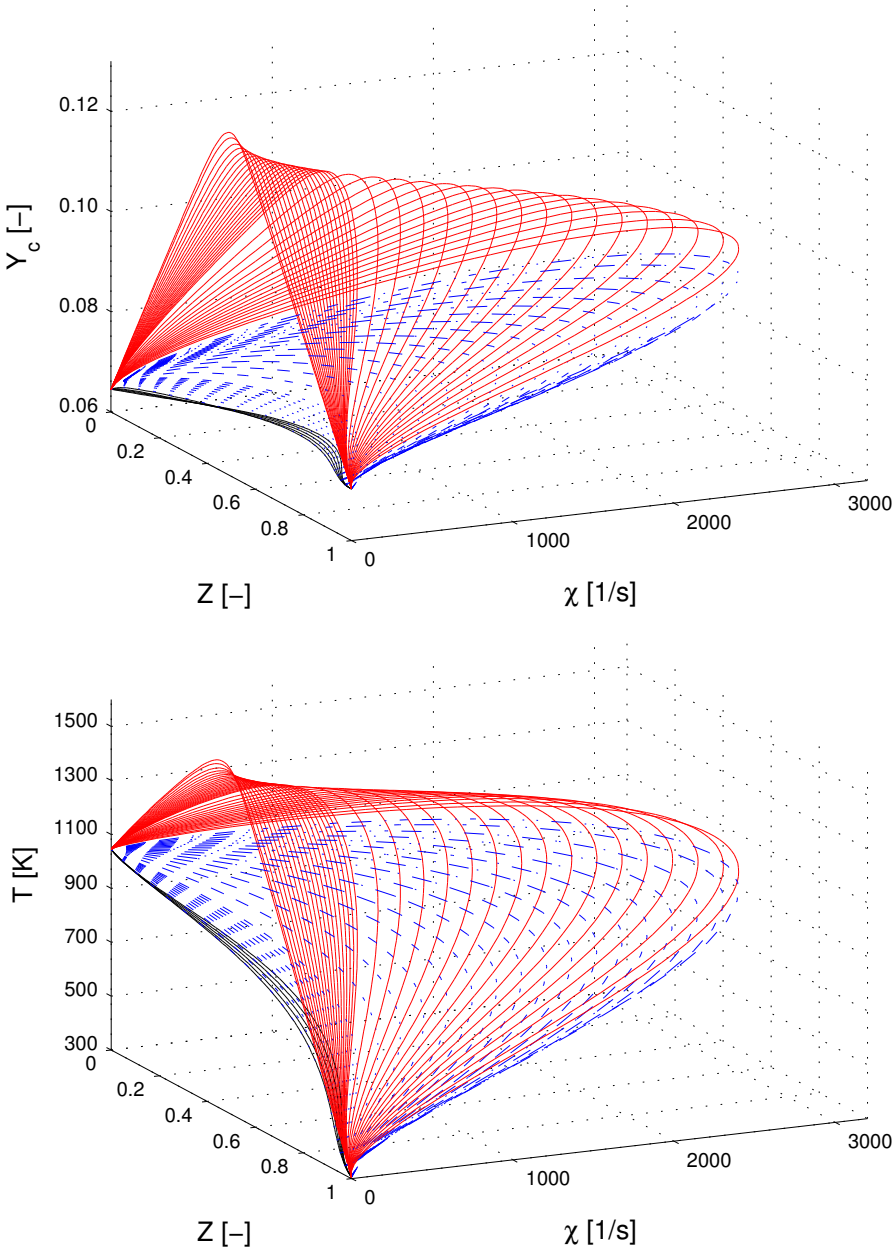

Figure 3.4. *Steady flamelet solutions. Top: S-curve represented in (Z, χ, Y_c)-space, with upper stable branch in red, middle unstable branch in blue and lower stable branch in black. Bottom: Temperature at steady flamelet solution.*

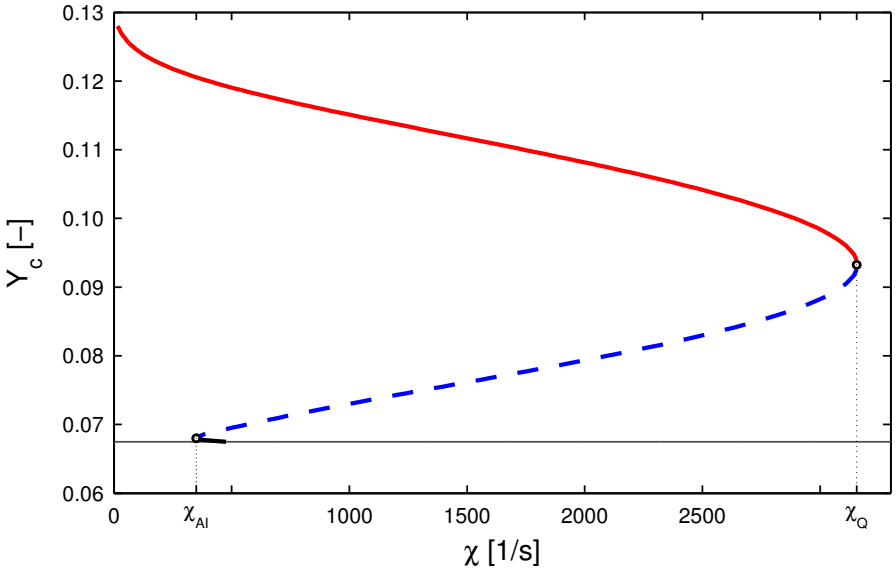

Figure 3.5. *Three branches of the steady flamelet solution. S-curve at stoichiometric mixture fraction Z_{st} = 0.4789 of the H_2/N_2 flame. Gray line: inert solution, solid lines: stable branches, dashed line: unstable branch.*

starting from the inert mixture. Igniting flamelet solutions are furthermore obtained above the unstable middle branch. The starting point of such an ignition path is a solution of this unstable branch with a slightly reduced strain rate. Starting from the same unstable solution with a slight increase in strain rate leads to an extinguishing flamelet solution below the unstable middle branch.

Unsteady flamelet solutions at different strain rates are shown in Fig. 3.6, where the progress variable Y_c is plotted at discrete instants versus mixture fraction Z. Unsteady solutions $Y_c(Z, t)$ are plotted every 0.1 ms for each of the four presented flamelets at strain rates indicated in the figure. The red curves represent the upper steady branch as in the figures before. The flamelets at strain rate a = 10, 100 and 1000 s^{-1} lie within the autoignition range and hence represent igniting flamelet solutions. The flamelet at strain rate a = 5000 s^{-1} however is situated in the unstable range and consists consequently of igniting and extinguishing flamelet solutions which are separated through the unstable middle branch marked by the blue curve in Fig. 3.6. Igniting flamelet solutions above the unstable branch are represented by the continuous, black lines, whereas extinguishing flamelet solutions below the unstable branch are plotted as dash-dotted lines.

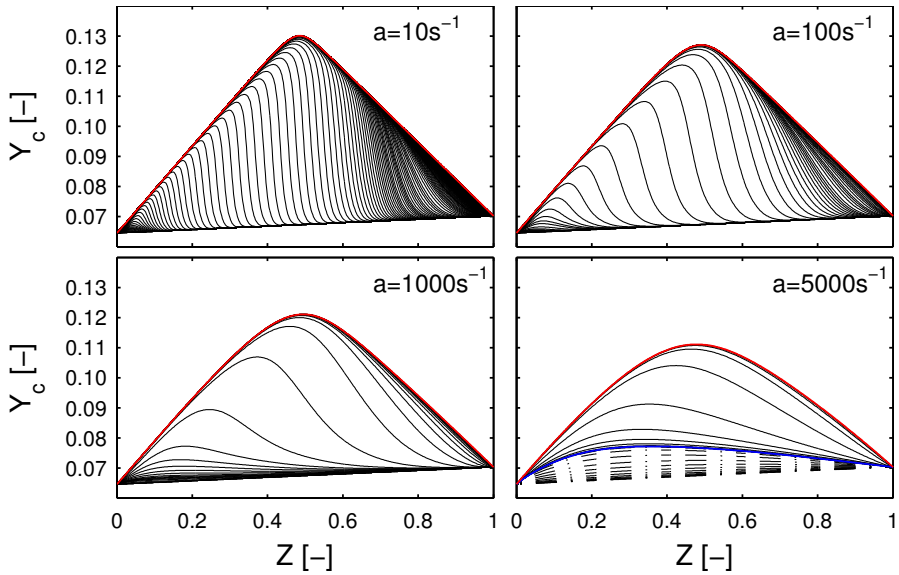

Figure 3.6. *Unsteady flamelet solutions at different strain rates. $Y_c(Z, t)$-profiles plotted at time increments of $\Delta t = 0.1$ ms.*

At a quick glance, one can easily note the different shapes of $Y_c(Z, t)$-profiles at different strain rates. At low strain rates and thus low values of scalar dissipation rate, reaction starts at very low mixture fraction values and propagates towards higher values of mixture fraction. The autoignition process shows a very heterogeneous behavior with a sequential ignition of different mixture fractions. In the upper left case it almost appears as each mixture fraction would react on its own.
In contrast, at higher strain rate values, for example at $a = 1000$ s^{-1} which in this case lies close to the upper autoignition limit a_{AI}, a more homogeneous propagation of the reaction can be observed. This means that higher scalar dissipation rates lead to a smoother ignition pattern in the sense of a more uniform reaction progress over a wide range of mixture fraction.
A further observation can be made by comparing the space between $Y_c(Z, t)$ curves. Since the time increment is constant and set to 0.1 ms for all four cases, the velocity of reaction progress at different strain rates can be estimated from Fig. 3.6. At low strain rates the progress of reaction is relatively fast after autoignition and gets slower when approaching higher mixture fractions. This is due to two main reasons. First, very rich mixture above stoichiometry exhibit in general lower chemical reactivity. Second, (in this case) higher mixture fractions are at lower temperature (compare Fig. 3.4) which leads to

a reduced chemical reaction rate. Therefore, the $Y_c(Z, t)$ curves, marking the progress of reaction, lie closer together on the rich side of the flame.
At high strain rates tough, the reaction progress behaves virtually the other way round. Increased diffusivity at higher strain rates leads to faster "diffusion of reactivity" towards the rich mixture. Note that Y_c represents a sum of combustion products that are diffused in mixture fraction space. Though, at the beginning of combustion—at low values of Y_c—the progress of reaction is slowed down due to higher diffusivity.

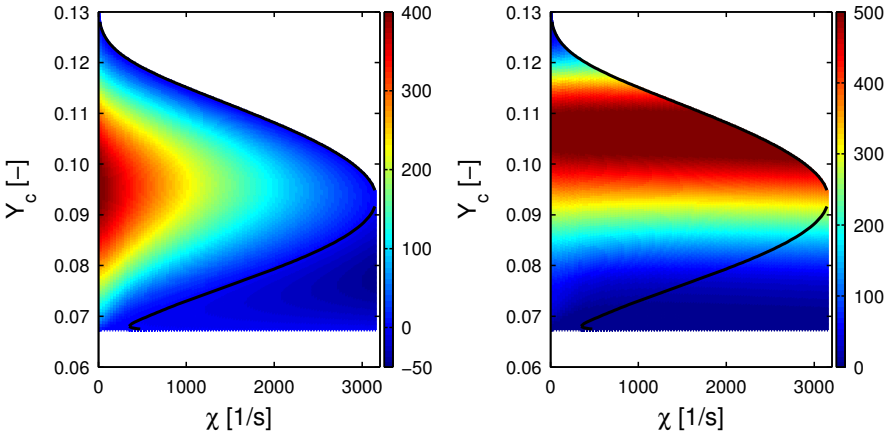

(a) Combined source term $\dot{Y}_c$ (b) Chemical source term $\dot{\omega}_{Y_c}$

Figure 3.7. *Comparison of the two possible source terms of progress variable Y_c at $Z = 0.4789$. Black line: steady flamelet solution.*

This section of preliminary flamelet results is closed with the comparison of two different types of source terms of the progress variable Y_c. Both source terms are shown in a contour plot in Fig. 3.7 as a function of scalar dissipation rate χ and progress variable Y_c at a constant mixture fraction $Z = 0.4789$. The two possible formulations are presented in the previous section and are obtained with Eq. (3.5). They are of quite different nature. The combined source term $\dot{Y}_c$ shown in Fig. 3.7(a) ranges from negative to positive values. Since $\dot{Y}_c$ represents the temporal term of the flamelet equation, it is obviously zero along the S-curve (black curve in Fig. 3.7), i.e. the steady solution. At the steady solution the diffusion term and the chemical source term balance. Below the unstable branch of the S-curve extinction occurs and consequently $\dot{Y}_c < 0$. The chemical source term $\dot{\omega}_{Y_c}$ shown in Fig. 3.7(b) however, is always positive and virtually independent of the scalar dissipation rate.

3.3 Approximated laminar diffusion flames

3.3.1 Need for approximated DF

For stationary flame configurations with simple fuels like the "Berkeley flame" presented in Chapter 4, the use of laminar diffusion flames is feasible. Constant boundary conditions are present in this case, such as constant, atmospheric pressure, fixed jet velocity and constant fuel and oxidizer temperature. Moreover, the chemical mechanism that describes the combustion of hydrogen consists only of 9 species and 21 reactions.
This situation changes drastically when considering internal combustion engines, where a wide range of variable operating conditions prevails and complex fuels are used. The simulation of the combustion process in an internal combustion engine is beyond the scope of this work. However, the implemented model is finally applied to a n-heptane spray in a constant volume vessel at diesel-like conditions—the so-called "Spray H" from the ECN database—in Chapter 5. The chemical mechanism [20] used to describe the combustion of n-heptane consists of 110 species and 1170 reactions. This means that, while flamelet equations for 9 species have to be solved when calculating laminar flamelet solutions for the H_2/N_2 flame, one would have to resolve more than ten times more equations in case of the n-heptane spray.
In order to reduce the computational effort for the calculation of flamelet solutions, an interesting approach has recently been presented in [21]. This modeling approach is followed closely in this work for the approximation of diffusion flames. The outcome of this approach are approximated diffusion flames (ADF) that may substitute the diffusion flames calculated in mixture fraction space (presented in the previous section). Hence, this new approach can be directly integrated in the implemented combustion model without any major changes. The "Berkeley flame" case is simulated with both, DF solutions as well as ADF solutions. For the "Spray H" case only ADF solutions are employed. The basic idea behind ADF and the implementation of this approach are presented below.

3.3.2 Calculation of approximated diffusion flames

The idea of the ADF model is to use solutions of auto-igniting, closed homogeneous reactors (HR) in combination with the flamelet equation solved for the progress variable only. So the chemical source term in Eq. (3.5)—the last term in that equation—is replaced by the source term obtained from HR solutions. The savings of this method arise therefore from the reduced cost of

HR calculations and the fact that the flamelet equations is just solved for one variable.
Thus, the first step of this method is the resolution of the autoignition process of a set of closed HRs at given initial conditions (e.g. different mixture fractions). These results can then be stored in a table as a function of a reduced number of independent variables similar to the FPI approach. In a last step, the flamelet equation for the progress variable is solved using the chemical information obtained with HR calculations. These steps are detailed in the following.
It shall be noted here that one may consider this method from a different point of view. When calculating the autoignition process of HRs at different mixture fraction, no diffusion in mixture fraction space is considered. However, this is an important characteristic of laminar diffusion flames and the combustion progress of flamelets changes with different strain rates as evidenced by Fig. 3.6. Diffusion in mixture fraction space is thus introduced a posteriori by solving the flamelet equation for the progress variable.

Autoignition of homogeneous reactors

A certain number of closed homogeneous reactors at constant pressure and enthalpy are considered to cover the whole range of mixture fraction. A reactor then represents the chemical transition from the initial state (fresh gases) to the equilibrium state (burned combustion products) for a given mixture fraction Z. For example in the case of the H_2/N_2 flame, the mixture fraction space is subdivided into 200 intervals. Thus, 199 HRs are calculated, each with different initial conditions. The required initial conditions for the autoignition calculations are the mixture fraction Z, though actually the initial composition $Y_i^{ini}(Z)$ in the reactor is stated, as well as the initial temperature $T^{ini}(Z)$ and the constant pressure p. The CHEMKIN-PRO package [22] is employed for the calculations which are relatively fast even with large chemical mechanisms such as the one used for n-heptane. For instance, calculating approximately 300 HRs for the base case of "Spray H" takes about a workday on a common PC. The chemical equilibrium of a HR at constant pressure and enthalpy is obtained with the same software package. Indeed, the equilibrium solutions are calculated for the same initial conditions as the corresponding HR. Since equilibrium solutions only depend on the initial composition $Y_i^{ini}(Z)$ and temperature $T^{ini}(Z)$ but not on time, they are consequently functions of mixture fraction Z only.

The results of the autoignition calculation, this means the temporal evolution of species mass fractions, species reaction rates, temperature, etc., can then be stored as a function of mixture fraction Z and a normalized progress variable $c(Z)$, such that any HR result is given by:

$$\mathcal{Q}^{\mathrm{HR}}(Z, c). \tag{3.6}$$

This tabulation method is actually inspired by the FPI [23] and FGM [24] approach, where the transition from unburned gas to burned combustion products is described by only one variable. Such a progress variable has to be chosen carefully in order to obtain an unequivocal relation. The normalized progress variable

$$c(Z) = \frac{Y_c(Z)}{Y_c^{eqi}(Z)} \tag{3.7}$$

thus goes from zero to unity in a strictly monotonic increasing way as the combustion progresses from the initial to the equilibrium state. The progress variable at equilibrium state $Y_c^{eqi}(Z)$ in Eq. (3.7) corresponds to the one obtained with the chemical equilibrium calculations mentioned before.

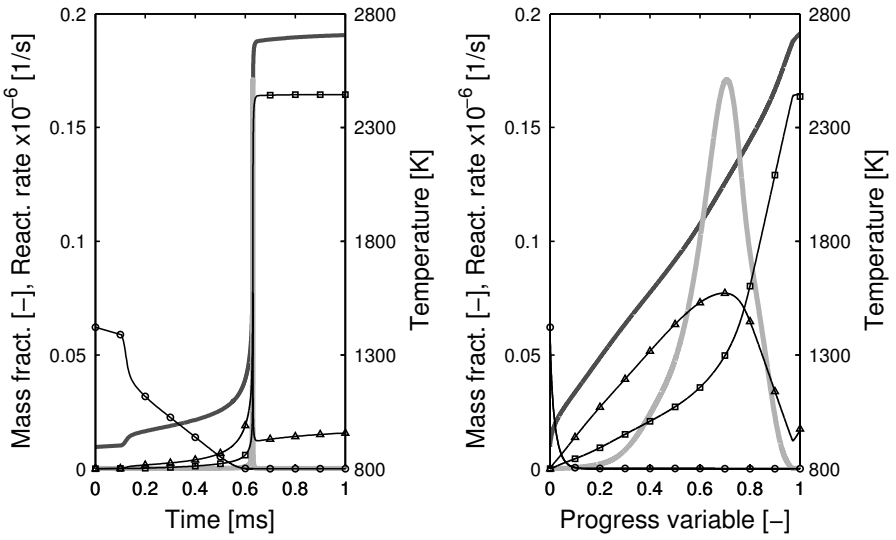

Figure 3.8. *Autoignition solution of HR at $Z = 0.062$ for "Spray H" base case ($T_{air} = 1000$ K) versus time (left) and progress variable (right). Dark gray line: temperature. Light gray line: PV reaction rate $\dot{\omega}_c$. Black lines: species mass fraction of C_7H_{16} (circles), CO (triangles) and CO_2 (squares).*

The progress of species mass fractions, temperature and PV reaction rate versus time during autoignition of a HR are shown on the left in Fig. 3.8 to give a concrete example of this step of the ADF method. The shown results correspond to the HR at Z=0.062—virtually the stoichiometric mixture fraction—of the "Spray H" base case (T_{air} = 1000 K, X_{O_2} = 21%). Species mass fractions are indicated by the black lines with symbols. The dark gray line shows the temperature trend and the light gray line the reaction rate of the normalized PV. The latter one has almost the shape of a Dirac delta function when represented over time. A common definition of the PV based on the combustion products CO and CO_2 [25] is retained in this work for n-heptane, so that $Y_c = Y_{CO} + Y_{CO_2}$. On the right of Fig. 3.8, the same properties of this HR are shown as a function of the normalized PV c as they are stored in the 2D lookup table. Especially the shape of the PV reaction rate appears to be much smoother when represented in the PV space.

Resolution of flamelet equation for PV

The computation of ADFs is not executed with the LFLAM code but with a proper Matlab routine. However, the calculation process itself is carried out in the same way. This means that first steady ADF solutions are calculated which gives the S-curve, and then, starting from those solutions, transient ADF solutions are computed.

The chemical reaction rates obtained for the whole range of mixture fraction by the HR calculations described above are now used in the resolution of the flamelet equation for the progress variable Y_c. This calculation process is similar to the one of DFs described in Section 3.2. The main difference is, as already mentioned, that for ADF only one flamelet equation has to be solved:

$$\frac{Y_c}{\partial t} = \frac{\chi(Z)}{2} \frac{\partial^2 Y_c}{\partial Z^2} + \dot{\omega}_{Y_c}^{\mathrm{HR}}(Z, c), \tag{3.8}$$

where the same fixed-in-time scalar dissipation rate profile $\chi(Z)$ given by Eq. (3.3) is used. The chemical source term $\dot{\omega}_{Y_c}^{\mathrm{HR}}(Z, c)$ in Eq. (3.8) is read from the 2D lookup table of the HR solutions for a given mixture fraction Z and a certain progress of combustion measured by the normalized PV c given by Eq. (3.7).
As a result of the resolution of Eq. (3.8), one obtains the time course of the progress variable $Y_c(Z, \chi, t)$ for all mixture fractions Z and its corresponding scalar dissipation rate $\chi(a, Z)$, at a given strain rate a. Any other properties,

such as species mass fractions, density or temperature, can then be looked up from the HR table $\mathcal{Q}^{\mathrm{HR}}(Z, c)$ for a given mixture fraction Z and normalized PV $c(Z, \chi, t)$ by

$$\mathcal{Q}^{\mathrm{ADF}}(Z, \chi, t) = \mathcal{Q}^{\mathrm{HR}}(Z, c(Z, \chi, t)), \tag{3.9}$$

where Eq. (3.7) is used to get $c(Z, \chi, t)$. Additionally, the term on the left-hand side of Eq. (3.8) represents the combined source term $\dot{Y}_c(Z, \chi, t)$ of the progress variable, which is the key property of the combustion model. It is the equivalent of ADFs to the one of DFs given by Eq. (3.5).
Finally, the relation (3.1) derived for DF can be simply replaced with solutions obtained for ADF such that

$$\mathcal{Q}(\boldsymbol{x}, t) = \mathcal{Q}^{\mathrm{ADF}}(Z, \chi, Y_c). \tag{3.10}$$

3.3.3 Characteristics of approximated diffusion flames

Steady and unsteady ADF solutions are exemplarily shown for the "Berkeley flame" case in the following, similar to the DF solutions shown in Section 3.2.3. First, steady approximated flamelet solutions are presented in form of the S-curve at $Z = 0.4789$ in Fig. 3.9. The shape of the S-curve is similar to the one of the DFs shown in Fig. 3.5 for the same boundary conditions.

Differences can though be observed for the values of χ_{AI} and χ_{Q}, which are found to be lower for ADF solutions compared to their equivalent DF solutions. This differences arise from the fact that the chemical source term used in Eq. (3.8) is obtained from closed HR calculations. More precisely, during the ignition of a HR, diffusion in mixture fraction space can not be taken into account. A HR may be interpreted as the hypothetical (and asymptotic) case of an igniting DF at scalar dissipation rate of zero, where each mixture evolves progresses separately with its inherent reactivity. The a posteriori consideration of diffusion in mixture fraction space does not lead to exactly the same reactivity of a certain mixture compared to the ignition of a DF. The differences between DF and ADF solutions become greater with increasing values of strain rate.

Unsteady solutions of ADFs are shown in Fig. 3.10 in the same way and for the same values of strain rate a as for DFs (compare Fig. 3.6). Profiles of $Y_c(Z)$ are again plotted for time increments of 0.1 ms, where igniting solutions are represented by continuous lines and extinguishing solutions by dash-dotted

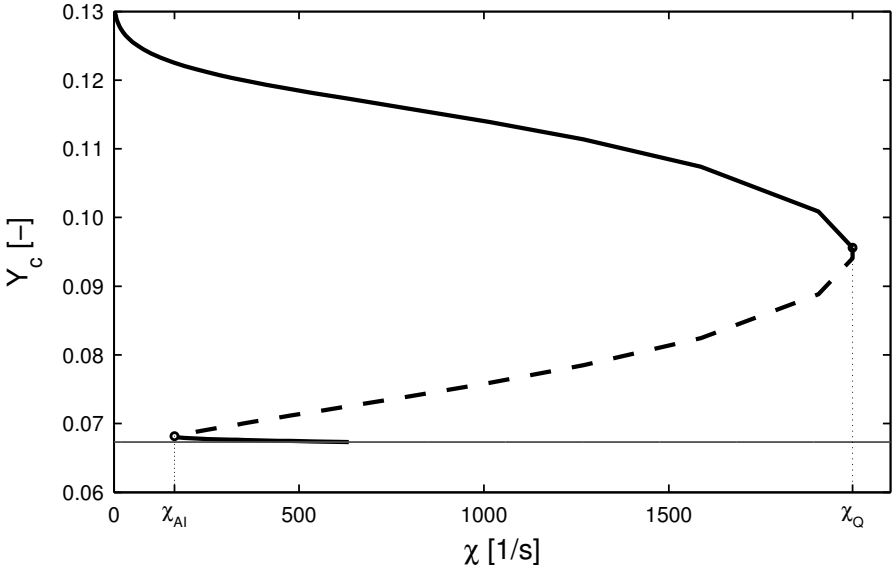

Figure 3.9. *Three branches of the steady approximated flamelet solution. S-curve at stoichiometric mixture fraction Z_{st} = 0.4789 of the H_2/N_2 flame. Gray line: inert solution, solid lines: stable branches, dashed line: unstable branch.*

lines. The unsteady solutions at $a = 10\ \mathrm{s}^{-1}$ and $a = 100\ \mathrm{s}^{-1}$ show virtually identical shape compared to those of laminar diffusion flames. Thus, the internal structure of flamelets, represented by the $Y_c(Z)$-profiles, appears to be very similar for DFs and ADFs at low strain rates. As already observed for the S-curve though, differences can be found at higher strain rate values. The ADF at strain rate $a = 1000\ \mathrm{s}^{-1}$ for example lies beyond the autoignition range and therefore extinction occurs at low values of PV. This means that for the ADF solution at this strain rate autoignition is not possible, while for the DF solution at the same strain rate autoignition still occurs. At an even higher strain rate of $a = 5000\ \mathrm{s}^{-1}$, it can be observed that the extinction zone of the ADF is greater than for its DF equivalent. However, the shape of the $Y_c(Z)$-profiles are also at high strain rates almost identical.

In the same manner as in the section about DFs, the chemical and the temporal term of the flamelet equation of Y_c are plotted in Fig. 3.11. These are the first and the last term in Eq. (3.8), respectively, where there first one is referred to as the combined source term $\dot{Y}_c$ and the second one as the chemical source term $\dot{\omega}_{Y_c}^{\mathrm{HR}}$. In general, the characteristics of both source terms are very similar to their counterparts of DFs.
Values of the combined source term $\dot{Y}_c$ shown in Fig. 3.11(a) range from

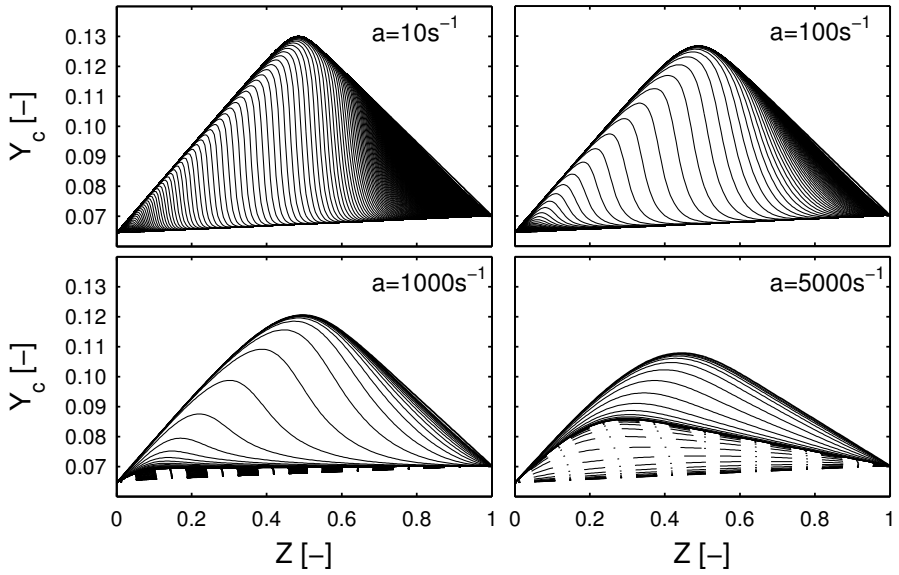

Figure 3.10. *Unsteady approximated flamelet solutions at different strain rates. $Y_c(Z, t)$-profiles plotted at time increments of Δt = 0.1 ms.*

negative to positive values as for DF solutions and $\dot{Y}_c$ becomes per definition zero along the steady solution (S-curve plotted as black line in Fig. 3.11). Zones of extinction are represented by negative values of $\dot{Y}_c$.
Indeed, the chemical source term $\dot{\omega}_{Y_c}^{\mathrm{HR}}$ of the ADF solution is per se independent of the scalar dissipation rate, since this is actually the chemical reaction rate of Y_c in a HR. The graphical representation of this term leads therefore to a horizontal band as shown in Fig. 3.11(b). Hence, the use of $\dot{\omega}_{Y_c}^{\mathrm{HR}}$ as source term for the progress variable in the final combustion model does not make sense. As suggested in [21], only the combined source term $\dot{Y}_c$ can be adopted in a combustion model when using the ADF approach.

Further conclusions regarding the comparison of ADFs with DFs can be drawn by means of the representations in Fig. 3.11. In fact, the shape of $\dot{Y}_c(Y_c, \chi)$ for a given mixture fraction obtained with the ADF method is similar to the equivalent DF results. However, the absolute values of $\dot{Y}_c$ of the ADF solution stay slightly below their DF counterpart. This finding could have been foreseen by a comparison of Fig. 3.11(a) with Fig. 3.7(a), where the distance between Y_c-profiles seperated by a constant time increment is smaller in case of the ADF solution. This suggests a slower progress of Y_c and consequently lower values of $\dot{Y}_c$. In a certain sense, the PV profiles shown in Fig. 3.11 are

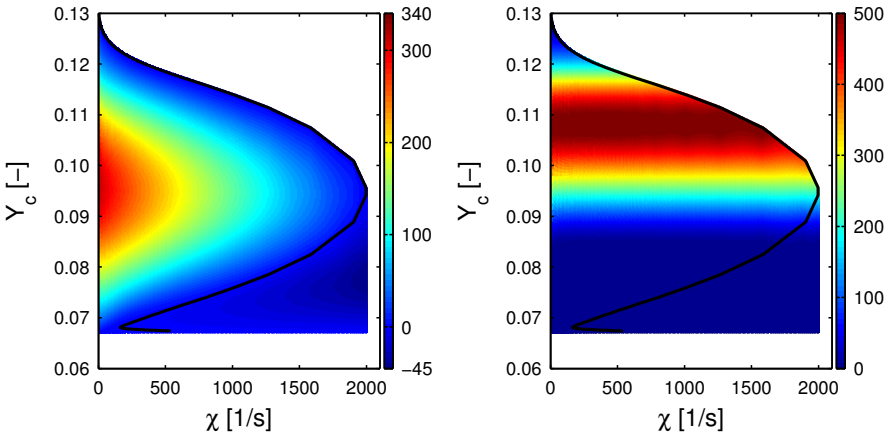

(a) Combined source term $\dot{Y}_c$ (b) Chemical source term $\dot{\omega}_{Y_c}$

Figure 3.11. *Comparison of the two possible source terms of progress variable Y_c at $Z = 0.4789$. Black line: steady approximated flamelet solution.*

implicitly a different representation of the combined source term $\dot{Y}_c$.
Concerning the chemical source term of Y_c, it can be observed that ADF and DF solutions reach similar values, but the noticeable onset of increase in $\dot{\omega}_{Y_c}^{\mathrm{HR}}$ occurs at higher values of Y_c compared to the DF solution of $\dot{\omega}_{Y_c}$. Though obvious and known a priori, this is a proof for different reactivity of the same mixture fraction depending on whether considered in the environment of a diffusion flame or in a homogeneous reactor. This fact plays along in the subsequent differences found for the combined source term.
At a first glance, the ADF approach can be considered capable to reproduce the structure of a 1D laminar diffusion flame. Further assessments of both versions of diffusion flames are made in Chapter 4.

3.3.4 Considerations on the computational effort

In order to evaluate the potential savings in computational effort by the adoption of the ADF method, it is interesting to have a look on the computing times required for the different solution approaches. Initially, two important issues concerning the following considerations have to be mentioned. First, two different tools are employed for the calculation of DF and ADF solutions, LFLAM written in Fortran and Matlab routines, respectively. Consequently, a direct comparison of the calculation processes may be questionable. Second, both approaches require manual interaction that consumes an important amount of the total time of the whole calculation process. The main contributor to this share is the calculation of the S-curve, which is not automated in neither of the two approaches. In case of the ADF method, the calculation process of homogeneous reactors carried out in Chemkin has to be additionally summed.
However, when focusing on the order of computing time needed for the calculation of a single flamelet, some significant estimations can be made. Considering first hydrogen as fuel, the calculation time of an unsteady DF solution lies in the order of some minutes. Approximately the same order of time is required when using the ADF method. In both approaches varies the computing time for an unsteady flamelet solution in a certain range depending on strain rate. This can be explained by the time required by a flamelet to get from the initial to the steady state which mainly depends on the strain rate. If this "flamelet time" is longer, obviously more CPU time is needed to numerically resolve it. So for the case of hydrogen, the ADF method does not represent an appreciable reduction of computational effort.
When considering more complex fuels such as n-heptane, the circumstances change significantly though. The calculation times for unsteady DF solutions literally explode and range in the order of weeks at least with the detailed mechanism adopted in this work. The observed order of CPU time goes along with values published in [21]. The computing time for unsteady ADF solution, however, range within some minutes to several hours depending on the strain rate again. This important difference clearly shows the benefit of the ADF method in case of complex fuels and represents a good example of use.
The numerical resolution of the flamelet equation in the ADF method was first based on an explicit scheme. Such an approach is accurate and efficient concerning main memory consumption. However, the inevitable stability criterion of such a scheme results in a strong restriction of the maximum admissible time step size. This fact represents an important drawback, for which reason the calculation process was eventually switched to an implicit

scheme. This leads to an appreciable reduction of computing time especially for ADF solutions at high strain rates, since the stability criterion imposes decreasing time step size for increasing strain rates. There exists a counter balancing effect to this trend, because higher strain rates and consequently intensified diffusion accelerates the approach of the stable state. In fact, all routines of the calculation process are still under continuous development (even beyond this work) in order to improve their numerical efficiency. Important issues of future improvements are discussed in Chapter 6.

3.4 Presumed PDF modeling

3.4.1 Outline of the presumed PDF modeling

The consideration of the influence of turbulence on the combustion progress will be treated in this section. From the modeling point of view this refers to the step which leads from the laminar flamelet property ϕ to the turbulent, mean property $\widetilde{\phi}$. In a RANS environment the use of probability density functions (PDFs) represents a common and adequate way to model turbulence effects. Two main possibilities exist for the employment of PDFs in a combustion model, (1) solve a balance equation for the PDF or (2) presume the shape of the PDF [26]. The latter one represents a more economic choice since no additional equations for the PDFs have to be solved. The modeling strategy used here is similar to the presumed conditional moment (PCM) approach [27, 28] which may be considered as a simplified version of CMC. This presumed PDF approach can of course be applied on both types of flamelet solutions—DF and ADF—regardless of the method of resolution. This is why in the following no differentiation between the two possible solutions is made, and instead the properties of unsteady flamelet solutions are referred to as $\mathcal{Q}^{\mathrm{UDF}}$.

The application of this approach in the present modeling strategy means to describe the statistical distribution of the three independent flamelet variables—mixture fraction, scalar dissipation rate and progress variable—by means of a PDF for one of each. So, z shall denote the sample space of possible values of $Z(\boldsymbol{x},\, t)$, ψ the sample space of possible values of $\chi(\boldsymbol{x},\, t)$ and y_c the sample space of possible values of $Y_c(\boldsymbol{x},\, t)$. Unsteady flamelet properties can then be represented in the sample space as $\mathcal{Q}^{\star}(z,\, \psi,\, y_c)$. The mean properties are obtained by integration over the whole range of each independent variable:

$$\widetilde{\mathcal{Q}} = \int\int\int \mathcal{Q}^{\star}(z,\, \psi,\, y_c)\, P_{Z,\chi,Y_c}(z,\, \psi,\, y_c;\, \boldsymbol{x},\, t)\, \mathrm{d}z\, \mathrm{d}\psi\, \mathrm{d}y_c, \tag{3.11}$$

where the joint PDFs are introduced in the sense of Favre averaged PDFs. Though discussed in detail further below, it may be anticipated here that for the PDF of Z the common assumption of a β-distribution is made [29, 30]. Moreover, a δ-PDF is simply used for the distribution of the progress variable, so it is assumed that there are no fluctuations of progress variable. A log-normal distribution is eventually used for the PDF of the scalar dissipation rate which was experimentally found to be appropriate by [31].

Finally, this leads to a 4D lookup table from which a turbulent mean flame property $\widetilde{\phi}$ can be obtained by the specification of:

- mean mixture fraction $\widetilde{Z}$,
- variance of mixture fraction $\widetilde{Z''^2}$,
- mean scalar dissipation rate $\widetilde{\chi}$,
- mean progress variable $\widetilde{Y}_c$.

The segregation factor

$$S = \frac{\widetilde{Z''^2}}{\widetilde{Z}(1-\widetilde{Z})} \tag{3.12}$$

is rather used as lookup parameter instead of the variance $\widetilde{Z''^2}$.

3.4.2 Reparametrization of unsteady flamelet solutions

Before turning to the detailed description of the presumed PDF modeling, a reparametrization is introduced in order to correctly describe the progress of the flamelet structure between the inert and the steady state. As mentioned before, the unsteady flamelet properties can be represented in the sample space as $\mathcal{Q}^\star(z,\, \psi,\, y_c)$. A function $\vartheta^\star(z,\, \psi,\, y_c)$ that is monotonic in y_c for fixed values of $(z,\, \psi)$ is defined such that there exists the unequivocal relation:

$$\mathcal{Q}^\star\left[z,\, \chi(z,\, a),\, y_c\right] = \mathcal{Q}^{\mathrm{UDF}}\left[z,\, a,\, \vartheta^\star(z,\, \psi,\, y_c)\right]. \tag{3.13}$$

While y_c can be seen as a local progress variable at a given mixture fraction and strain rate, $\vartheta^\star$ may be interpreted as a global progress variable of a flamelet at a given strain rate, which describes the state of progress of each mixture in the flamelet. A graphical representation of such a global PV is shown in Fig. 3.12, where unsteady flamelet solutions are plotted for discrete values of $\vartheta^\star$. This means that for a given value of $\vartheta^\star(z,\, \psi,\, y_c)$, one knows y_c for all z at a given ψ.

For flamelets in the autoignition range, $\vartheta^\star$ is monotonically increasing in time. However, $\vartheta^\star$ may either increase or decrease in time depending on whether one starts from a point $(z,\, \psi,\, y_c)^I$ in the ignition zone or a point $(z,\, \psi,\, y_c)^E$ in the extinction zone. This is indicated in Fig. 3.12(b) by black and gray lines which correspond to igniting and extinguishing flamelet solutions. The monotony in the autoignition range and the ambiguity in the unstable range with respect to time, plays an important role when integrating over a set of flamelets as discussed further below.

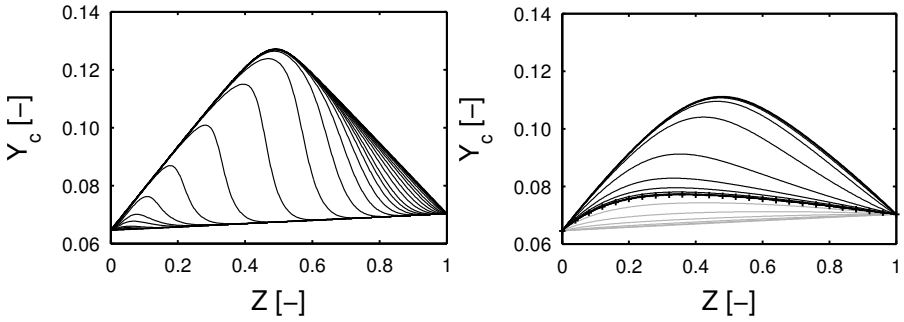

(a) Autoignition range ($\chi_{st} < \chi_{st,\mathrm{AI}}$) corresponding to low strain rates

(b) Unstable range ($\chi_{st} > \chi_{st,\mathrm{AI}}$) corresponding to high strain rates. Line with plus: Unstable middle branch

Figure 3.12. *Unsteady flamelet solutions at discrete values of $\vartheta^\star$.*

As indicated by Eq. (3.3) and (3.4), a and χ_{st} are directly related by a multiplicative constant. Therefore, a in Eq. (3.13) can be replaced by χ_{st} as commonly done in this type of models and also followed in this work. This allows to parametrize unsteady diffusion flame results finally as:

$$\mathcal{Q}^{\mathrm{UDF}}\left[z,\, \chi_{st},\, \vartheta^\star(z,\, \psi,\, y_c)\right]. \tag{3.14}$$

This parametrization is chosen for certain reasons, since it allows assumptions regarding the statistical relations between the different table parameters as detailed in the following section.

3.4.3 Detailed description of presumed PDF modeling

Joint PDF of independent variables

After the reparametrization, the mean properties can be obtained by integration over the three table parameters in the way:

$$\widetilde{\mathcal{Q}}(\boldsymbol{x},\, t) = \int\int\int \mathcal{Q}^{\mathrm{UDF}}(z,\, \psi_{st},\, \vartheta^{\star})\, P_{Z,\chi_{st},\vartheta^{\star}}(z,\, \psi_{st},\, \vartheta;\boldsymbol{x},\, t)\, \mathrm{d}z\, \mathrm{d}\psi_{st}\, \mathrm{d}\vartheta. \quad (3.15)$$

With the chosen representation of the unsteady flamelet space, one can reasonably assume statistical independence of the variables Z and χ_{st} on the one hand, and Z and $\vartheta^{\star}$ on the other hand. Nevertheless, $\vartheta^{\star}$ is indeed dependent on χ_{st} since the temporal evolution is obviously strongly related to the strain rate (see Fig. 3.6 or 3.10), which is directly related to χ_{st}. Consequently, the joint PDF $P_{Z,\chi_{st},\vartheta^{\star}}$ can be written as the product of the marginal Z-PDF and the joint $(\chi_{st}, \vartheta^{\star})$-PDF:

$$P_{Z,\chi_{st},\vartheta^{\star}} = P_Z\, P_{\chi_{st},\vartheta^{\star}} = P_Z(z)\, P_{\vartheta^{\star}|\chi_{st}}(\psi_{st},\, \vartheta)\, P_{\chi_{st}}(\psi_{st}). \quad (3.16)$$

As already outlined in the introductory part of this section, a β-PDF for P_Z, a δ-PDF for $P_{\vartheta^{\star}|\chi_{st}}$ and a log-normal-PDF for $P_{\chi_{st}}$ is employed.

Conditional mean properties $\langle \mathcal{Q}|\chi_{st}, \vartheta^{\star}\rangle$

The PDF of Z is modeled as a β-distribution based on the unconditional mean value $\widetilde{Z}(\boldsymbol{x},\, t)$ and its variance $\widetilde{Z''^2}(\boldsymbol{x},\, t)$:

$$\begin{aligned} P_Z(z;\boldsymbol{x},\, t) &= P^{\beta}_{\widetilde{Z},\widetilde{Z''^2}}(z;\boldsymbol{x},\, t) \\ &= \frac{1}{\mathrm{B}(\alpha,\beta,z_l,z_u)} \frac{(z-z_l)^{(\alpha-1)}(z_u-z)^{(\beta-1)}}{(z_u-z_l)^{(\alpha+\beta-1)}}. \end{aligned} \quad (3.17)$$

The above equation represent the general form of the β-PDF for values within the interval $[z_l,\, z_u]$, where the lower limit z_l usually takes zero and the upper limit z_u equals unity. However there exist cases where the upper limit of the mixture fraction might stay below unity, for instance in combustion processes of sprays (see Chapter 5). In Eq. (3.17) the beta function B appears, which is defined as

$$\begin{aligned} B(z_l, z_u, \alpha, \beta) &= \int_{z_l}^{z_u} (z-z_l)^{\alpha-1}(z_u-z)^{\beta-1}\mathrm{d}z \\ &= \frac{\Gamma(\alpha)\Gamma(\beta)}{\Gamma(\alpha+\beta)}(z_u-z_l)^{\alpha+\beta-1}, \end{aligned} \quad (3.18)$$

and can be further expressed with the gamma function Γ, especially useful for the implementation in computer codes. The shape parameters α and β are related to $\widetilde{Z}(\boldsymbol{x},\, t)$ and $\widetilde{Z''^2}(\boldsymbol{x},\, t)$ by:

$$\alpha = \frac{(z_u - z_l)^2\,\zeta - \widetilde{Z''^2}(1+\zeta)^2}{\widetilde{Z''^2}(1+\zeta)^3} \tag{3.19a}$$

$$\beta = \alpha\,\zeta, \tag{3.19b}$$

where $\zeta = \left(\frac{z_u - \widetilde{Z}}{\widetilde{Z} - z_l}\right)$.

Then, the conditional means are obtained by integration in Z-space for given values of $\widetilde{Z}(\boldsymbol{x},\, t)$ and $\widetilde{Z''^2}(\boldsymbol{x},\, t)$ together with the above relations:

$$\langle \mathcal{Q}|\chi_{st}, \vartheta^\star\rangle \left(\widetilde{Z}, \widetilde{Z''^2}, \psi_{st}, \vartheta\right) = \int_{[Z]} \mathcal{Q}^{\mathrm{UDF}}(z,\, \chi_{st},\, \vartheta)\, P^{\beta}_{\widetilde{Z},\widetilde{Z''^2}}(z)\,\mathrm{d}z. \tag{3.20}$$

Conditional mean properties $\langle \mathcal{Q}|\chi_{st}\rangle$

In the next step, the conditional PDF $P_{\vartheta^\star|\chi_{st}}(\psi_{st},\, \vartheta)$ is modeled and integrated over $\vartheta^\star$ in order to obtain the conditional means $\langle \mathcal{Q}|\chi_{st}\rangle$. Here it is assumed that there are no fluctuations of $\vartheta^\star$ for a given value of χ_{st} and the conditional expected value $\langle \vartheta^\star|\chi_{st}\rangle$ has to be specified. This is mathematically expressed by the use of a δ-PDF for $P_{\vartheta^\star|\chi_{st}}$. This assumption considerably simplifies the modeling and leads to an easier reparametrization in terms of the mean progress variable $\widetilde{Y}_c$. Fig. 3.12 may act as a visual support to better understand the meaning of the present assumption: for a specified value of χ_{st} (or a), which fluctuates in the turbulent flame, given profiles of $\vartheta^\star$ as function of Z are considered, without taking in to account fluctuations conditional on χ_{st}. With this assumption, in the final model all the fluctuations are due to fluctuations of mixture fraction and its scalar dissipation rate. By definition of the progress variable, for given values of z and ψ_{st}, Y_c^{UDF} is a monotonic function of ϑ in order to ensure relation (3.13). As a consequence $\langle Y_c|\chi_{st}\rangle$ there exists a bijective relation with $\langle \vartheta^\star|\chi_{st}\rangle$ for given values of $\widetilde{Z}$, $\widetilde{Z''^2}$ and ψ_{st}. With the assumption of a δ-PDF for $P_{\vartheta^\star|\chi_{st}}$, the conditional averages can be represented as functions

$$\langle \mathcal{Q}|\chi_{st}\rangle \left(\widetilde{Z}, \widetilde{Z''^2}, \psi_{st}, \hat{y}_c\right) = \langle \mathcal{Q}|\chi_{st}, \vartheta^\star\rangle \left(\widetilde{Z}, \widetilde{Z''^2}, \psi_{st}, \langle \vartheta^\star|\chi_{st}\rangle\right), \tag{3.21}$$

where $\hat{y}_c$ is the sample space of possible values of $\langle Y_c|\chi_{st}\rangle$. The value of $\langle \vartheta^\star|\chi_{st}\rangle$ is specified indirectly by assuming that $\langle Y_c|\chi_{st}\rangle$ satisfies the relation $\hat{y}_c =$

$\langle Y_c|\chi_{st}\rangle(\widetilde{Z}, \widetilde{Z''^2}, \psi_{st}, \hat{y}_c)$. The practical implementation of the modeling up to this point starts with the predetermination of pairs of values ($\widetilde{Z}$, S) where $\widetilde{Z''^2}$ is replaced by S using Eq.(3.12). The chosen pairs of values ($\widetilde{Z}$, S) already reflect the final discretization of the table in these two table dimensions. Note that a pair of values ($\widetilde{Z}$, S) together with Eq. (3.12), (3.19a) and (3.19b) determine the shape of the β-PDF. All unsteady flamelets at different χ_{st} and discrete values of $\vartheta^\star$ weighted with the given β-PDFs are then integrated. This results in intermediate tables of conditional properties $\langle\mathcal{Q}|\chi_{st}\rangle$ that are stored for every considered χ_{st} in a discretized ($\widetilde{Z}$, S, $\hat{y}_c$)-space. This first integration in Z-space can be illustrated by means of Fig. 3.12. The dependence of Y_c on Z is included in the model by the integration of the profiles of $Y_c(Z)$ at given levels of progress (that correspond to a certain value of ϑ or time τ) of the unsteady flamelet solutions for a given strain rate a.

Synchronization of flamelets with non-normalized PV

Before considering the final χ_{st}-PDF integration, a decision has to be made how to treat the conditional properties $\langle\mathcal{Q}|\chi_{st}\rangle$ of different flamelets at different values of χ_{st} with respect to their particular degree of reaction progress. This issue is referred to as the "synchronization" of flamelets in this work. No clear procedure is suggested in the literature (if even detailed in papers), quite the contrary, different approaches with e.g. a normalized progress variable or a progress parameter are used [2, 3, 32, 33].
Here, the non-normalized progress variable $\hat{y}_c$ is used to synchronize different transient flamelet solutions. This means that the final integration of $\langle\mathcal{Q}|\chi_{st}\rangle\left(\widetilde{Z}, \widetilde{Z''^2}, \psi_{st}, \hat{y}_c\right)$ in χ_{st}-space is done for given values of $\hat{y}_c$, which corresponds to horizontal lines in Fig. 3.13.
The domain of possible values of (ψ_{st}, $\hat{y}_c$) of χ_{st} and $\langle Y_c|\chi_{st}\rangle$ for a given pair of values ($\widetilde{Z}$, S) is shown in Fig. 3.13. This representation allows to make some important observations. The values of $\langle Y_c|\chi_{st}\rangle$ at different strain rates (i.e. different χ_{st}) are within the inert solution value $\langle Y_c^{\min}|\chi_{st}\rangle$ and the steady solution value $\langle Y_c^{\max}|\chi_{st}\rangle$, which are given by:

$$\left\langle Y_c^{\min}|\chi_{st}\right\rangle\left(\widetilde{Z},\, S,\, \psi_{st}\right) = \int_{[Z]} Y_c^{\min}(z,\, \psi_{st})\, P^{\beta}_{\widetilde{Z},\widetilde{Z''^2}}(z)\,\mathrm{d}z, \tag{3.22}$$

$$\left\langle Y_c^{\max}|\chi_{st}\right\rangle\left(\widetilde{Z},\, S,\, \psi_{st}\right) = \int_{[Z]} Y_c^{\max}(z,\, \psi_{st})\, P^{\beta}_{\widetilde{Z},\widetilde{Z''^2}}(z)\,\mathrm{d}z. \tag{3.23}$$

The minimum value is the inert value which is indeed the same for all strain rates:

$$Y_{c,\mathrm{MIN}}\left(\widetilde{Z},\, S\right) = \left\langle Y_c^{\min}|\chi_{st}\right\rangle\left(\widetilde{Z},\, S,\, \psi_{st}\right)\ \forall\,\psi_{st} \tag{3.24}$$

and there is a maximum value $Y_{c,\mathrm{MAX}}(\widetilde{Z},\, S)$ at the lowest considered strain rate ($\psi_{st} = \chi_{st,\mathrm{MIN}}$):

$$Y_{c,\mathrm{MAX}}\left(\widetilde{Z},\, S\right) = \langle Y_c^{\max}|\chi_{st}\rangle\left(\widetilde{Z},\, S,\, \chi_{st,\mathrm{MIN}}\right). \tag{3.25}$$

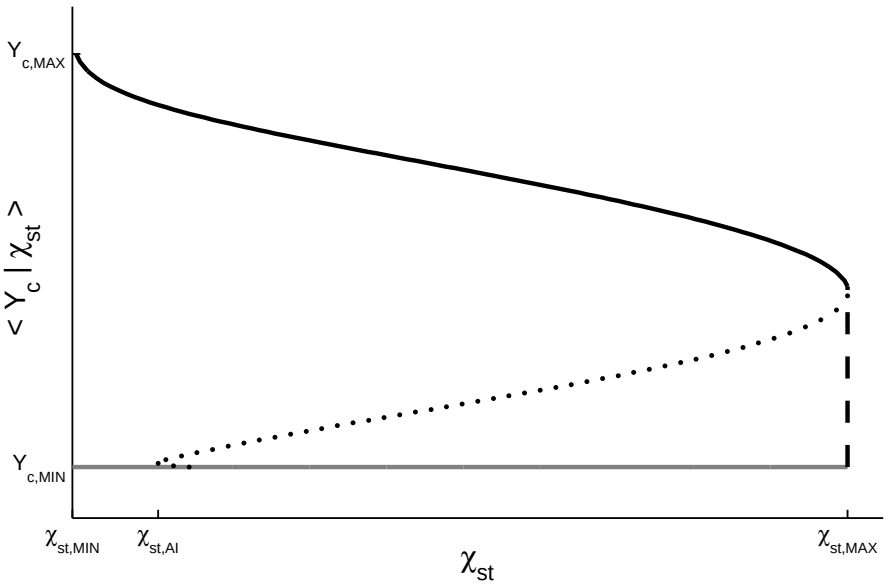

Figure 3.13. *Sketch of the domain of possible values $(\psi_{st},\, \hat{y}_c)$ of χ_{st} and $\langle Y_c|\chi_{st}\rangle$ for a given pair of values $(\widetilde{Z},\, S)$. Gray line: inert solution $Y_{c,\mathrm{MIN}}$. Black line: represents steady solution of $\langle Y_c^{\max}|\chi_{st}\rangle(\psi_{st})$, together with dashed black line it marks the limit $\chi_{st}^{\max}(\hat{y}_c)$. Black dots: conditional unstable branch $\hat{y}_c^{\mathrm{ust}}(\psi_{st})$.*

Synchronization of flamelets in time

Different ways of synchronizing transient flamelet solutions in presumed PDF approaches are used by different authors as already noted before. Besides the use of the non-normalized PV for this purpose, the synchronization in time of flamelet solutions at different strain rates represents certainly a physically reasonable approach.
However, synchronization in time can only be adopted to flamelets within the autoignition range, i.e for values of $\psi_{st} < \chi_{st,\mathrm{AI}}$ (marked in Fig. 3.13), where $\langle Y_c|\chi_{st}\rangle(\psi_{st})$ is monotonically increasing in time from $\langle Y_c^{\min}|\chi_{st}\rangle(\psi_{st})$ to $\langle Y_c^{\max}|\chi_{st}\rangle(\psi_{st})$. For flamelets within the unstable range (i.e. $\psi_{st} > \chi_{st,\mathrm{AI}}$) in contrary no such bijective function exists, since, starting from the unstable

middle branch, a flamelet may either ignite or extinguish. This fact is depicted in Fig. 3.12(b) where black curves correspond to igniting flamelet solutions and gray curves to extinguishing flamelet solutions.
Synchronization of flamelet solutions in time will in principle be quite different from synchronization with a non-normalized PV (or any other potential way of synchronization). The temporal evolution of a flamelet is strongly dependent on the strain rate (i.e. χ_{st}), and consequently $\langle Y_c|\chi_{st}\rangle(\psi_{st}, \tau)$ for a given time τ is indeed different for different values of ψ_{st}. This is clearly in contrast to a synchronization made with the non-normalized PV, which corresponds to horizontal lines in Fig. 3.13. Moreover, the time $\tau^{\mathrm{std}}_{|\chi_{st}}(\psi_{st})$ needed to reach $\langle Y_c^{\max}|\chi_{st}\rangle(\psi_{st})$ is also different for each flamelet.
Synchronization in time was also suggested for the ADF-PCM model [21]. This way of coupling the conditional properties at different values of ψ_{st} will be employed and investigated in the case of "Spray H" presented in Chapter 5.

Unconditional mean properties

The unconditional mean properties are finally obtained by the χ_{st}-PDF integration. A log-normal distribution is employed to model the PDF of the stoichometric scalar dissipation rate: $P_{\chi_{st}}(\psi_{st}) = P^{\log}_{\widetilde{\chi}_{st}}(\psi_{st})$. This means that a Gaussian distribution is assumed for the natural logarithm of χ_{st}. The log-normal PDF is given by

$$P^{\log}_{\widetilde{\chi}_{st}}(\psi_{st}) = \frac{1}{\psi_{st}\,\sigma\,\sqrt{2\pi}} \exp\left(-\frac{(\ln(\psi_{st}) - \mu)^2}{2\sigma^2}\right) \tag{3.26}$$

and depends only on $\widetilde{\chi}_{st}$ through

$$\mu = \ln(\widetilde{\chi}_{st}) - \frac{\sigma^2}{2}, \tag{3.27}$$

with a fixed variance σ^2. The variance of the log-normal PDF represents a parameter of the combustion model and usually takes values like $\sigma^2 = 1$ or $\sigma^2 = \sqrt{2}$. When $\sigma^2 = 0$ is chosen, the log-normal PDF changes to a δ-PDF, which is also tested in this work.

In the case of **synchronization with the non-normalized PV**, for given values of $\widetilde{Z}$, S and $\hat{y}_c$ (with $Y_{c,\mathrm{MIN}} < \hat{y}_c < Y_{c,\mathrm{MAX}}$), the unconditional

mean properties are then obtained as:

$$\widetilde{\mathcal{Q}}\left(\widetilde{Z},\, S,\, \widetilde{\chi}_{st},\, \hat{y}_c\right) = \int_0^{\chi_{st}^{\max}} \langle \mathcal{Q}|\chi_{st}\rangle \left(\widetilde{Z}, S, \psi_{st}, \hat{y}_c\right)\, P^{\log}_{\widetilde{\chi}_{st}}(\psi_{st})\,\mathrm{d}\psi_{st} + \int_{\chi_{st}^{\max}}^{\infty} \mathcal{Q}_{|\chi_{st}}\left(\widetilde{Z}, S, \psi_{st}\right)\, P^{\log}_{\widetilde{\chi}_{st}}(\psi_{st})\,\mathrm{d}\psi_{st}. \tag{3.28}$$

The notation $\mathcal{Q}_{|\chi_{st}}$ is introduced for $\psi_{st} > \chi_{st}^{\max}(\widetilde{Z}, S, \hat{y}_c)$, where the conditional averages $\langle \mathcal{Q}|\chi_{st}\rangle$ are not defined (above and on the right-hand side of the solid and dashed black lines in Fig. 3.13). The steady flamelet property values are used when $\psi_{st} > \chi_{st}^{\max}$ and $\psi_{st} \leqslant \chi_{st,\mathrm{MAX}}$:

$$\mathcal{Q}_{|\chi_{st}}\left(\widetilde{Z}, S, \psi_{st}\right) = \langle \mathcal{Q}|\chi_{st}\rangle \left(\widetilde{Z}, S, \psi_{st}, \langle Y_c^{\max}|\chi_{st}\rangle\right) \tag{3.29}$$

and the inert mixing property values above the extinction limit when $\psi_{st} > \chi_{st,\mathrm{MAX}}$:

$$\mathcal{Q}_{|\chi_{st}}\left(\widetilde{Z}, S, \psi_{st}\right) = \langle \mathcal{Q}|\chi_{st}\rangle \left(\widetilde{Z}, S, \chi_{st,\mathrm{MAX}}, Y_{c,\mathrm{MIN}}\right). \tag{3.30}$$

In the case of **synchronization in time**, for given values of $\widetilde{Z}$, S and τ (with $0 < \tau < \max\left(\tau^{\mathrm{std}}_{|\chi_{st}}(\psi_{st})\right)$, the time needed by the slowest flamelet to reach $\langle Y_c^{\max}|\chi_{st}\rangle(\psi_{st})$), the unconditional mean properties are then obtained as:

$$\widetilde{\mathcal{Q}}\left(\widetilde{Z},\, S,\, \widetilde{\chi}_{st},\, \tau\right) = \int_0^{\chi_{st,\mathrm{AI}}} \langle \mathcal{Q}|\chi_{st}\rangle \left(\widetilde{Z}, S, \psi_{st}, \tau\right)\, P^{\log}_{\widetilde{\chi}_{st}}(\psi_{st})\,\mathrm{d}\psi_{st} + \int_{\chi_{st,\mathrm{AI}}}^{\infty} \mathcal{Q}_{|\chi_{st}}\left(\widetilde{Z}, S, \psi_{st}\right)\, P^{\log}_{\widetilde{\chi}_{st}}(\psi_{st})\,\mathrm{d}\psi_{st}. \tag{3.31}$$

The notation $\mathcal{Q}_{|\chi_{st}}$ is introduced for $\psi_{st} > \chi_{st,\mathrm{AI}}$ in this case, since the conditional averages $\langle \mathcal{Q}|\chi_{st}\rangle$ of the unstable range (right of $\chi_{st,\mathrm{AI}}$ in Fig. 3.13) can not be considered. Instead, it is assumed that the flamelet remains in the initial state (i.e. no reaction) and consequently the inert mixing property values (except for reaction rates) are used above the autoignition limit $\psi_{st} > \chi_{st,\mathrm{AI}}$:

$$\mathcal{Q}_{|\chi_{st}}\left(\widetilde{Z}, S, \psi_{st}\right) = \langle \mathcal{Q}|\chi_{st}\rangle \left(\widetilde{Z}, S, \chi_{st,\mathrm{AI}}, Y_{c,\mathrm{MIN}}\right). \tag{3.32}$$

The above assumption implies that reaction rates are zero for $\psi_{st} > \chi_{st,\mathrm{AI}}$ which also applies to the PV source term: $\langle \dot{Y}_c|\chi_{st}\rangle(\psi_{st}) = 0$ for $\psi_{st} > \chi_{st,\mathrm{AI}}$.

Final parametrization

The unconditional mean properties are finally stored as functions of $\widetilde{Z}$, S, $\widetilde{\chi}_{st}$ and $\widetilde{Y}_c$. The replacement of $\langle Y_c|\chi_{st}\rangle$ by $\widetilde{Y}_c$ is done through a re-interpolation of the final table, since Eq. (3.29) and (3.30) are also applied to $\hat{y}_c$ in the case of synchronization with non-normalized PV. In a similar way a re-interpolation is made in the case of time synchronization in order to replace τ by $\widetilde{Y}_c$, since Eq. (3.32) and the integration (3.31) is also applied to $\hat{y}_c$ (which is a bijective function of time τ). So any mean property

$$\widetilde{\mathcal{Q}}\left(\widetilde{Z},\, S,\, \widetilde{\chi}_{st},\, \widetilde{Y}_c\right) \tag{3.33}$$

can eventually be obtained by an interpolation of the final 4D table for a given set of lookup parameters $\widetilde{Z}$, S, $\widetilde{\chi}_{st}$ and $\widetilde{Y}_c$.

From the CFD code the mean value of χ is estimated (Eq. (3.37)), but the mean of χ_{st} is actually needed as a lookup parameter. The scalar dissipation rate is related to stoichiometric scalar dissipation rate by Eq. (3.4), which has to be integrated in Z-space in order to obtain the mean values:

$$\widetilde{\chi}\left(\widetilde{Z},\, S,\, \widetilde{\chi}_{st}\right) = \widetilde{\chi}_{st} \int_{[Z]} \frac{\mathcal{F}(z)}{\mathcal{F}(z_{st})}\, P^{\beta}_{\widetilde{Z},\widetilde{Z''^2}}(z)\,\mathrm{d}z = \widetilde{\chi}_{st}\,\mathcal{J}\left(\widetilde{Z}, S\right). \tag{3.34}$$

The mean conversion factor $\mathcal{J}(\widetilde{Z}, S)$ which relates $\widetilde{\chi}$ and $\widetilde{\chi}_{st}$ is stored in a table and used in the CFD code to get $\widetilde{\chi}_{st}$.

A final flamelet table eventually requires about 30 MB to 400 MB of disc space when stored in human-readable ASCII format. The relatively wide spectrum of required memory arises from its dependence on the number of properties stored in the table and the discretization interval and considered range of the independent table lookup parameters. For instance in the case of the hydrogen jet flame presented in Chapter 4, the whole range of mixture fraction from zero to unity is considered in the table. On the contrary, the range of consider mixture fraction is significantly reduced in the "Spray H" cases as described in Chapter 5. Moreover, the number of considered properties stored in the tables of the hydrogen flame doubles since also their squared values are stored (see Chapter 4). As a consequence, the size of the tables for the "Spray H" cases is situated at the lower end of the specified range. This shows how it is possible to reduce memory requirements of the flamelet table by a reasonable choice of the above mentioned factors, an advantage of the implemented modeling approach.

3.5 Coupling with the CFD code

In this section the coupling of the combustion model with the CFD code is explained. This step represents the actual implementation of the combustion model into the existent *dieselFoam* solver of OpenFOAM 1.6 [34]. The *dieselFoam* application is a compressible, transient RANS solver suitable for reactive flow simulations, which comes with all basic equations (discussed in Section 2.3) needed to describe turbulent reactive flow including energy and species transport.

3.5.1 Implementation of model equations in OpenFOAM

The implementation of the additionally necessary model equations into the OpenFOAM environment is briefly described here. The OpenFOAM CFD platform is written in C++, an object-oriented programming language. This platform provides different applications such as solvers or postprocessing tools and a wide range of different models (e.g. turbulence models, spray models, etc.) implemented as classes. OpenFOAM 1.6 comes with a great variety of numerical schemes for the treatment of temporal and spatial derivatives [35]. The schemes adopted in this work can be considered as a standard choice in the scope of the *dieselFoam* solver, which represents the starting point of the implementation. The Euler scheme (first order, bounded, implicit) is retained for the time derivatives, while the *linear* scheme, a second order central differencing scheme, is chosen for the rest. In particular, the *limited* version of this scheme is used for divergence terms and the *corrected* version for the Laplacian terms of the equations.

Model equations that are not implemented in the original version of the *dieselFoam* solver are resumed below and presented in a usual index notation as well as in the corresponding OpenFOAM syntax. A direct comparison between the two presented notations can be made, since the terms of each equation are written in the same order for both notations.

Transport equation for the mean mixture fraction

The equation for the mean mixture fraction $\widetilde{Z}$ is given by

$$\frac{\partial \overline{\rho}\widetilde{Z}}{\partial t} + \frac{\partial \overline{\rho}\widetilde{u}_j\widetilde{Z}}{\partial x_j} - \frac{\partial}{\partial x_j}\left(\frac{\mu_{\text{eff}}}{\text{Sc}_t}\frac{\partial \widetilde{Z}}{\partial x_j}\right) = S_Z. \tag{3.35}$$

In general, the transport equation for the mixture fraction has no source term, since the mixture fraction is a conserved property. However, the source term that appears on the right-hand side of Eq. (3.35) corresponds to the evaporation source which is present in multiphase cases such as reactive sprays. For this work, this means that $S_Z = 0$ for the H_2/N_2 jet flame, but in the case of "Spray H" flames $S_Z \neq 0$.
The above equation for the mean mixture fraction is implemented in OpenFOAM as:

```
fvScalarMatrix ZEqn
(
    fvm::ddt(rho, Z)
  + fvm::div(phi, Z)
  - fvm::laplacian(turbulence->mut()/Sc_t, Z)
  ==
  Sevap
);
ZEqn.solve();
```

The equation `ZEqn` is defined as type `fvScalarMatrix` since the mixture fraction is a scalar. Mathematical operations such as time derivative, divergence or the Laplace operator (in the order they are used in the equation above) are pre-implemented functions in OpenFOAM, which facilitates the readability of equations written in OpenFOAM syntax.

Transport equation for the mixture fraction variance

The equation for the mixture fraction variance $\widetilde{Z''^2}$ is given by:

$$\frac{\partial \overline{\rho}\widetilde{Z''^2}}{\partial t} + \frac{\partial \overline{\rho}\widetilde{u}_j\widetilde{Z''^2}}{\partial x_j} - \frac{\partial}{\partial x_j}\left(\frac{\mu_{\text{eff}}}{\text{Sc}_t}\frac{\partial \widetilde{Z''^2}}{\partial x_j}\right) = 2\,\frac{\mu_{\text{eff}}}{\text{Sc}_t}\left(\frac{\partial \widetilde{Z}}{\partial x_j}\right)^2 - \overline{\rho}\widetilde{\chi}. \tag{3.36}$$

This equation reads in OpenFOAM syntax as:

```
fvScalarMatrix ZvarEqn
(
    fvm::ddt(rho, Zvar)
  + fvm::div(phi, Zvar)
  - fvm::laplacian(turbulence->muEff()/Sc_t, Zvar)
  ==
```

```
    + 2.0 * turbulence->muEff()/(Sc_t)*sqr(mag(fvc::grad(Z)))
    - rho*chi
  );
  ZvarEqn.solve();
```

The equation `ZvarEqn` is also of type `fvScalarMatrix` as the mixture fraction equation before, since the variance is a scalar too. The actual solution process of the equation is called by `ZvarEqn.solve();`.

Model for the mean scalar dissipation rate

The mean scalar dissipation rate is modeled in a standard way as:

$$\widetilde{\chi} = C_\chi \frac{\varepsilon}{k} \widetilde{Z''^2}, \tag{3.37}$$

where the turbulent dissipation ε and the turbulent kinetic energy k are directly obtained from the employed $k-\varepsilon$ turbulence model. The constant C_χ represents a parameter of the combustion model. This equation is implemented in OpenFOAM as:

```
chi = Cchi*turbulence->epsilon()/turbulence->k()*Zvar;
```

The above syntax `turbulence->epsilon()` and `turbulence->k()` shows how ε and k are directly passed from the turbulence model class by calling the respective return functions for the private variables of the class.

Transport equation for the mean non-normalized PV

The non-normalized progress variable is composed of a linear combination of species and consequently its transport equation is the same as for any other reactive species:

$$\frac{\partial \overline{\rho}\widetilde{Y}_c}{\partial t} + \frac{\partial \overline{\rho}\widetilde{u}_j\widetilde{Y}_c}{\partial x_j} - \frac{\mu_{\text{eff}}}{\text{Sc}_t}\frac{\partial^2 \widetilde{Y}_c}{\partial x_j^2} = \overline{\rho} S_{Y_c}. \tag{3.38}$$

As a source term S_{Y_c} in the above equation either

- the pure chemical source term $\widetilde{\dot{\omega}}_{Y_c}$ or
- the combined chemical-diffusion source term $\widetilde{\dot{Y}}_c$.

will be used. Different possibilities of how to make use of a progress variable within a CFD code exist. A first choice may be a direct use of the progress variable by the implementation of Eq. (3.38) in the CFD code, or, an adapted method developed for more complex problems (on an industrial scale) and its use in multi-species solvers represents an alternative way. Both methods are presented in the following two subsections.

3.5.2 Coupling with direct lookup of thermo-chemical properties

The straightforward way of connecting the combustion model with the existent CFD solver is to solve for the properties that represent the table parameters and lookup all other chemical and thermodynamic properties from the pre-integrated table. More specifically, this means that beside the governing equations of fluid flow, the above stated equations (3.35) – (3.38) for $\widetilde{Z}$, $\widetilde{Z''^2}$, $\widetilde{\chi}_{st}$ and $\widetilde{Y}_c$ are solved by the CFD code. For known values of those table parameters any tabulated property (e.g. density, temperature, species mass fraction, etc.) can then be looked up in the pre-integrated turbulent flamelet table.

The storage of the table is implemented by means of a so-called *hash table*, which is a data structure where keys are mapped to values. Here the table parameters represent the keys for which a set of properties, the values, are stored. The key for the combustion progress-direction is actually the normalized progress variable

$$\widetilde{c} = \frac{\widetilde{Y}_c - \widetilde{Y}_c^{\mathrm{INI}}}{\widetilde{Y}_c^{\mathrm{STD}} - \widetilde{Y}_c^{\mathrm{INI}}}, \tag{3.39}$$

that ranges from zero to unity and represents the grade of combustion progress. $\widetilde{Y}_c^{\mathrm{STD}}$ is the upper steady value of the progress variable for given values of $\widetilde{Z}$, S, $\widetilde{\chi}_{st}$, which can be understood as the turbulent equivalent to the value of Y_c on the upper stable branch (represented in Fig. 3.4). $\widetilde{Y}_c^{\mathrm{INI}}$ is the progress variable at initial state, i.e. its value at inert adiabatic mixture. The use of the normalized progress variable as table key has practical reasons that become clear further below.
In practice any property ϕ_i is stored for given discrete values of $\widetilde{Z}$, S, $\widetilde{\chi}_{st}$ and $\widetilde{c}$ in the hash table `TFT` as:

```
TFT.insert(TKey(Z, S, xSt, c, i), q);
```

where `q` is the value of ϕ_i at the stated keys. These five keys are used during

a simulation run to calculate the hash function which then gives the location of the desired value within the hash table. The first four keys are indeed the independent table parameters and the last key `i` is the index of the i-th property stored in the table. Hence, `i` takes values between 0 and $N_i - 1$, where N_i is the total number of stored properties[2]. The size of the hash table is determined by the discretization of the different table dimensions—in other words the number of grid points of the table—and the total number of properties N_i stored in the table: $N_{\mathtt{TFT}} = N_Z.N_S.N_\chi.N_{Y_c}.N_i$. This makes clear how the table discretization and the number of stored properties effects the size of the hash table and consequently the memory requirements. The table size $N_{\mathtt{TFT}}$ typically ranges from several million upwards.

The straightforward coupling procedure is illustrated in Fig. 3.14, which also points up the data exchange between the CFD code, including the turbulence model, and the turbulent combustion model. The so-called conversion table holds the conversion factor $\mathcal{J}(\widetilde{Z}, S)$ that relates by Eq. (3.34) the mean scalar dissipation rate $\widetilde{\chi}$, that is actually modeled in the CFD simulation, and the mean stoichiometric scalar dissipation rate $\widetilde{\chi}_{st}$, which is the actual table lookup parameter. Moreover, the rigid and direct coupling of the table output values to the table input parameters become apparent.

The procedure how to obtain a mean property $\phi_i(\widetilde{Z}, S, \widetilde{\chi}_{st}, \widetilde{Y}_c)$ from the table in practice is explained in the following. Since properties are only stored at discrete values of the independent lookup parameters in the table, multidimensional linear interpolation is employed to get properties at intermediate values of those parameters. The first step is to get the lower and upper bordering table parameters $\Pi^{\Updownarrow}$ (with '$\Updownarrow$' as place holder for 'Lo' and 'Hi') of the parameters $\widetilde{Z}$, S, $\widetilde{\chi}_{st}$ and $\widetilde{c}$:

$$\begin{aligned} Z^{\mathrm{Lo}} &\leqslant \widetilde{Z} < Z^{\mathrm{Hi}} \\ S^{\mathrm{Lo}} &\leqslant S < S^{\mathrm{Hi}} \\ \chi_{st}^{\mathrm{Lo}} &\leqslant \widetilde{\chi}_{st} < \chi_{st}^{\mathrm{Hi}} \\ c^{\mathrm{Lo}} &\leqslant \widetilde{c} < c^{\mathrm{Hi}}. \end{aligned}$$

Values of the steady progress variable $\widetilde{Y}_c^{\mathrm{STD}}(\widetilde{Z}^{\Updownarrow}, S^{\Updownarrow}, \widetilde{\chi}_{st}^{\Updownarrow})$ can then be looked up for all possible combinations of bordering table parameters $\Pi^{\Updownarrow}$ by looping over them, implemented as:

```
V[m] = TFT[TKey(ZSxLoHi[j], ZSxLoHi[k], ZSxLoHi[l], 1, i)]; ,
```

[2]Note that indexing in C++ is zero based.

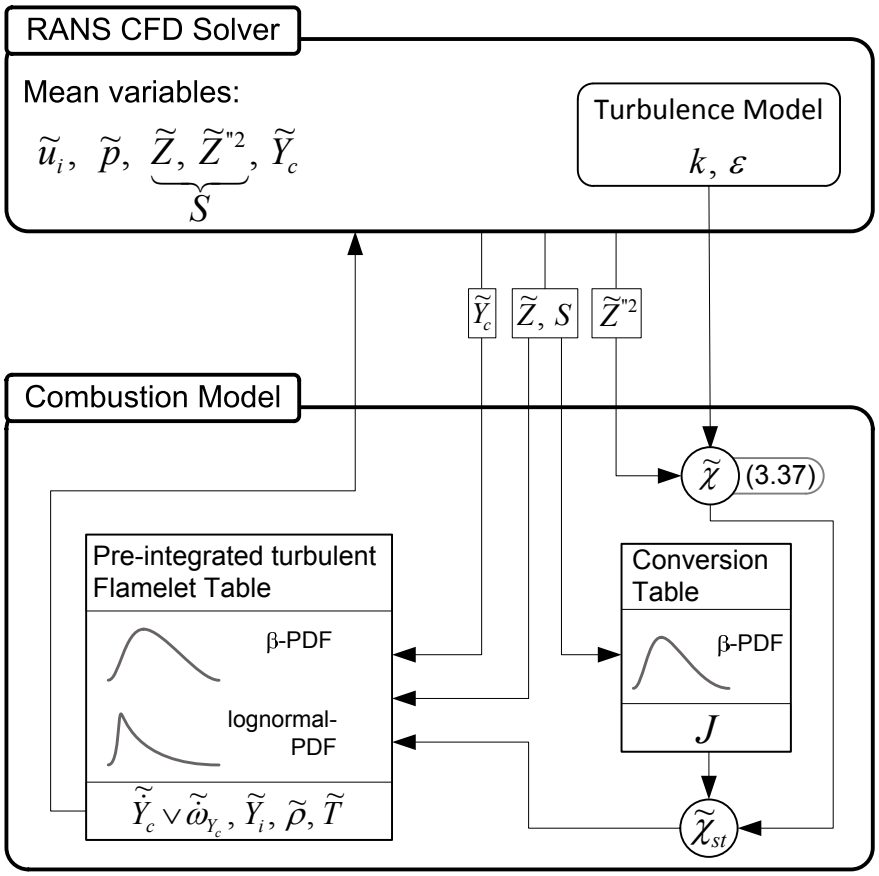

Figure 3.14. *Calculation scheme based on direct coupling of the combustion model with the CFD code.*

which leads to eight values in the case of this three-dimensional dependence. Note that the value for the key of the progress variable is fixed to `1`, which corresponds to the reactive steady state. Subsequently, a tri-linear interpolation is made to get $\widetilde{Y}_c^{\mathrm{STD}}(\widetilde{Z}, S, \widetilde{\chi}_{st})$, and Eq. (3.39) finally gives the normalized progress variable $\widetilde{c}(\widetilde{Z},\ S,\ \widetilde{\chi}_{st},\ \widetilde{Y}_c)$.
This interpolated normalized progress variable is then used to obtain all further properties at $\widetilde{Z}$, S, $\widetilde{\chi}_{st}$ and $\widetilde{c}$. Thus, the lookup process is actually performed for the same grade of combustion progress rather than the same value of progress variable. More precisely, any property ϕ_i is looked up at its corresponding bordering parameters $Z^{\Updownarrow}$, $S^{\Updownarrow}$, $\chi_{st}^{\Updownarrow}$ and $c^{\Updownarrow}$, which gives (in this case) 16 tabulated values of ϕ_i. Those tabulated values are subsequently

interpolated to finally obtain ϕ_i at the current independent table parameters $\widetilde{Z}$, S, $\widetilde{\chi}_{st}$ and $\widetilde{c}$ (corresponding to $\widetilde{Y}_c$) that are again functions of position $\boldsymbol{x}$ and time t. This interpolation process is not explicitly represented in Fig. 3.14, where the focus lies on the illustration of the coupling of the different procedure steps.

Since the table is calculated at constant pressure conditions and temperature as well as density are then directly read from the table, density changes only due to temperature variations but remains independent of pressure. By adopting this direct coupling, compressibility effects can not be taken into account. This may be acceptable in cases with so-called low-Mach number flow where compressibility effects (i.e. acoustic waves) are not present or negligible. Moreover, since temperature is directly read from the table, effects like heat loss neither can be treated. However, in many industrial applications, for instance aircraft gas turbines and internal combustion engines, such effects may have important impact on the reactive flow. Different coupling methods [36] exist to address these issues and the one used in this work is presented in the next subsection.

3.5.3 Coupling by tabulation of species mass fractions

The method chosen for the coupling of the chemistry table with the compressible solver follows closely the one presented in [37] and is outlined in the following. This method was developed for application to engine simulations, which involve numerous unsteady operating conditions over a wide range. The simulation of a full engine as well as the investigation of acoustic effects is out of the scope of this (in this sense preliminary) work; nevertheless, the implemented model shall be suitable for such applications and capable to treat such effects on a medium-term perspective.
In this method the CFD code solves the governing equations of turbulent fluid flow and the energy equation, which as a matter of course requires the mixture composition. However, the tabulation and especially transport of all species involved in the combustion process of heavy hydrocarbons is not feasible. Therefore, a limited number N_M of carefully chosen species, which represent the total mixture are considered in the CFD solver. The selection has to be made in a way that their combined contributions to the energy budget dominate over that of the remaining (not directly considered) species [36]. From the N_M considered species only $N_t = N_M - N_r$ species are stored in the chemistry table, while the remaining ones are reconstructed. The reason is that in order to fully conserve mass, atomic mass conservation equations are solved for H, O and C atoms. So in the case of hydrocarbon combustion the

number of reconstructed species is in general $N_r = 3$ for such methods.
Since this coupling method is applied here to simulate the "Spray H" cases where n-heptane is used as a surrogate for diesel, the method is detailed for that fuel in the following. Nine species are transported in the CFD code similar to those proposed in [37], of which CO, CO_2, C_7H_{16}, H, H_2 and OH are tabulated and C_7H_{14}, H_2, O_2 represent the reconstructed species responsible for mass conservation. The last three species are obtained from the atomic balance equations:

$$Y_{O_2} = -\frac{\mathcal{W}_{O_2}}{2}\left(\frac{Y_{CO}}{\mathcal{W}_{CO}} + 2\frac{Y_{CO_2}}{\mathcal{W}_{CO_2}} + \frac{Y_{H_2O}}{\mathcal{W}_{H_2O}}\right) + Y^0_{O_2}, \tag{3.40}$$

$$Y_{C_7H_{14}} = -\frac{\mathcal{W}_{C_7H_{14}}}{7}\left(-7\frac{Y^0_{C_7H_{16}} - Y_{C_7H_{16}}}{\mathcal{W}_{C_7H_{16}}} + \frac{Y_{CO}}{\mathcal{W}_{CO}} + \frac{Y_{CO_2}}{\mathcal{W}_{CO_2}}\right), \tag{3.41}$$

$$\begin{aligned} Y_{H_2} = -\frac{\mathcal{W}_{H_2}}{2}\Bigg(&-16\frac{Y^0_{C_7H_{16}} - Y_{C_7H_{16}}}{\mathcal{W}_{C_7H_{16}}} + 14\frac{Y_{C_7H_{14}}}{\mathcal{W}_{C_7H_{14}}} \\ &+ 2\frac{Y_{H_2O}}{\mathcal{W}_{H_2O}} + \frac{Y_H}{\mathcal{W}_H} + \frac{Y_{OH}}{\mathcal{W}_{OH}}\Bigg) \end{aligned} \tag{3.42}$$

In these equations Y_k and $\mathcal{W}_k$ denote the mass fraction and the molar weight of species k and Y^0_k is the mass fraction of the tracer of species k, necessary for the correct balance. Note that the species mass fractions of these three species deviate from their real concentration in the mixture, since they contain contributions from other species that are not considered in the mixture. Those species are therefore sometimes referred to as *dummy species*. Moreover, this chosen set of species may not be considered as a generally adequate choice for any hydrocarbon fuel. This fact may represent a drawback of this method, since different fuels might require certain adaptations.
The progress variable is not explicitly solved in this method but deduced from from the mass fractions of the transported, tabulated species CO and CO_2 as $Y_c = Y_{CO} + Y_{CO_2}$. For methods that are based on species transport, two different ways can be used in principle to obtain the reaction rates of species. The first approach consists of a tabulation of species reaction rates (that can later be directly read from the table), whereas species mass fractions are tabulated in the second approach. In a basic study, [33] showed that the latter one is more appropriate because the species mass fraction are relaxed towards the tabulated solution which ensures that they stay on the low dimensional manifold (LDM). This means for the practical implementation, that the mass fractions of the $N_t = 6$ tabulated species are stored in the table, and the only reaction rate stored in the table is the one of the progress variable.

The reaction rate $\widetilde{\dot{\omega}}_k$ of species k is then calculated as

$$\widetilde{\dot{\omega}}_k(t) = \frac{\widetilde{Y}_k^{\mathrm{tab}}\left(\widetilde{Z}, S, \widetilde{\chi}_{st}, \widetilde{c}(t+\tau)\right) - \widetilde{Y}_k(t)}{\tau}, \tag{3.43}$$

where $\widetilde{c}(t+\tau)$ is the normalized progress variable after a time advancement τ that is obtained by

$$\widetilde{c}(t+\tau) = \widetilde{c}(t) + \frac{\widetilde{\dot{Y}}_c^{\mathrm{tab}}\left(\widetilde{Z}, S, \widetilde{\chi}_{st}, \widetilde{c}\right)\ \tau}{\widetilde{Y}_c^{\mathrm{STD}}\left(\widetilde{Z}, S, \widetilde{\chi}_{st}\right)}. \tag{3.44}$$

The characteristic relaxation time τ is usually chosen close to the computational time step size or slightly above: $\tau \gtrsim \Delta t^{\mathrm{CFD}}$. The mean values $\widetilde{Z}$, S, $\widetilde{\chi}_{st}$ and $\widetilde{c}$ in the above equations are evaluated at position $\boldsymbol{x}$ and time t, which is not explicitly stated for simplicity. The normalized progress variable $\widetilde{c}$ is obtained in exactly the same way as explained in Section 3.5.2. However, since the progress variable is here composed of combustion products (CO and CO_2) only, its initial value $\widetilde{Y}_c^{\mathrm{INI}} = 0$. The current mass fraction $\widetilde{Y}_k$ of species k and its value after an increment $\Delta\widetilde{c}$, corresponding to the time increment τ, are thus used to calculate the respective reaction rate $\widetilde{\dot{\omega}}_k$. In doing so, the relaxation of the mixture composition towards the tabulated value is assured.

An illustration of the coupling and the whole calculation procedure based on the tabulation of species mass fractions is given in Fig. 3.15, where also the corresponding equation numbers are stated. This coupling scheme looks different and slightly more complicated compared to the direct coupling procedure. However, the application of the conversion table, used to obtain the mean stoichiometric scalar dissipation rate $\widetilde{\chi}_{st}$, works in the completely same way. A main difference is the internal loop with the relaxation time in the pre-integrated flamelet table, that is followed by the reconstruction of the non-tabulated species. At the end of a calculation cycle, the combustion model returns the reaction rates for all transported species to the CFD solver.

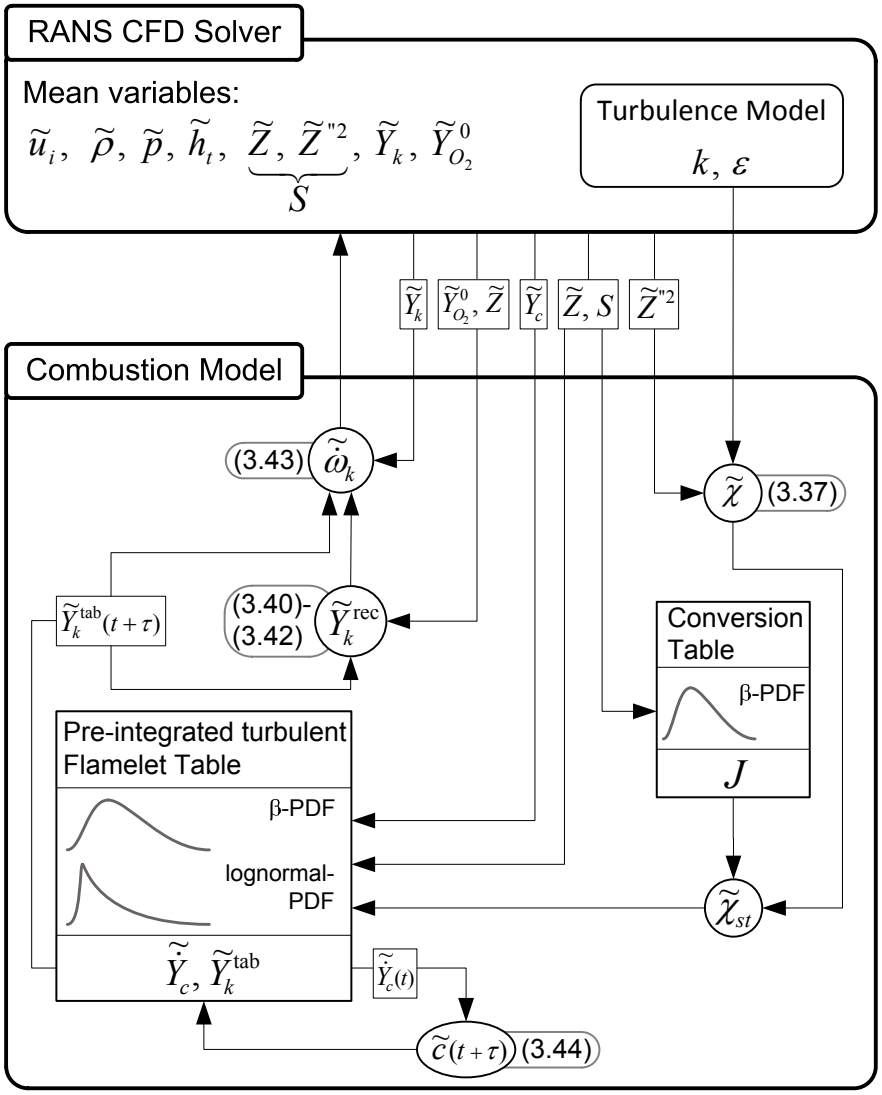

Figure 3.15. *Coupling of the combustion model with the CFD code based on species mass fraction tabulation.*

3.6 Final remarks

Some concluding final remarks concerning the implemented combustion model are given here in order to point out several important characteristics of this modeling strategy.

The adopted modeling strategy consists of two main parts, the table generation, which includes the calculation of flamelet solutions, the presumed PDF modeling and the pre-tabulation of these results, on the one hand, and the coupling of the combustion model with the CFD code on the other hand. The generation of a chemistry table is done prior and independently of a CFD simulation and though represents a completely separated step in the whole simulation process.
Moreover, it is even possible to use different types of tables, i.e. different grade of complexity, as long as the same coupling method is used. This means that chemistry tables are fully exchangeable. Not only is it possible to employ flamelet tables based on DF or ADF solutions as done in Chapter 4, but also the application of tables with reduced complexity can be realized. Reduced complexity refers in this case to a dimension reduction of the table, where for example the influence of the scalar dissipation rate is neglected which leads to a chemistry table with only three dimensions—corresponding to degrees of freedom of the table—instead of four. The implementation is elaborated in a way such that a change in the table structure does not require any further change to the combustion model or the CFD solver.
A further important fact of such a modeling strategy is the dependence of the results on a reduced set of independent parameters, the degrees of freedom of the combustion model. The mixture fraction and the scalar dissipation rate play a key role in combustion models based on the flamelet concept. These two properties are particularly influenced by the quality of the employed turbulence model and the spray modeling in case of multi-phase problems. Therefore, the combustion model has to be seen as one part of an interaction of models necessary to describe complex, multidisciplinary problems such as turbulent combustion processes.

Bibliography

[1] Pitsch H. and Ihme M. "An Unsteady/Flamelet Progress Variable Method for LES of Nonpremixed Turbulent Combustion". *43rd AIAA Aerospace Sciences Meeting and Exhibit*, Vol. Paper 2004–557, 2005.

[2] Ihme M. and See Y. C. "Prediction of autoignition in a lifted methane/air flame using an unsteady flamelet/progress variable model". *Combust. Flame*, Vol. 157, pp. 1850–1862, 2010.

[3] Vicquelin R. *Tabulation de la cinétique chimique pour la modélisation et la simulation de la combustion turbulente.* Doctoral Thesis, Ecole Centrale Paris, 2010.

[4] Sadasivuni S. K. *LES Modelling of Non-premixed and Partially Premixed Turbulent Flames.* Doctoral Thesis, Loughborough University, 2009.

[5] Peters N. *Turbulent Combustion.* Cambridge University Press, 2000.

[6] Pickett L. M., Siebers D. L. and Idicheria C. A. "Relationship Between Ignition Processes and the Lift-Off Length of Diesel Fuel Jets". *SAE Technical Paper 2005–01–3843*, 2005.

[7] Wang W. and Echekki T. "Investigation of lifted jet flames stabilization mechanism using RANS simulations". *Fire Safety Journal*, Vol. 46, pp. 254–261, 2011.

[8] Ameen M. M. and Abraham J. "RANS and LES Study of Lift-Off Physics in Reacting Diesel Jets". *SAE Technical Paper 2014–01–1118*, 2014.

[9] Siebers D. and Higgins B. "Flame Lift-Off on Direct-Injection Diesel Sprays Under Quiescent Conditions". *SAE Technical Paper 2001-01-0530*, 2001.

[10] Venugopal R. and Abraham J. "A Review of Fundamental Studies Relevant to Flame Lift–off in Diesel Jets". *SAE Technical Paper 2007–01–0134*, 2007.

[11] Cabra R., Myhrvold T., Chen J. Y., Dibble R. W., Karpetis A. N. and Barlow R. S. "Simultaneous Laser Raman-Rayleigh-LIF Measurements and Numerical Modeling Results of a Lifted Turbulent H2/N2 Jet Flame in a Vitiated Coflow". *Proc. Combust. Inst.*, Vol. 29, pp. 1881–1888, 2002.

[12] Lutz A. E., Kee R. J., Grcar J. F. and Rupley F. M. "OPPDIF: A Fortran program for computing opposed-flow diffusion flames". *SAND96-8243*, 1997.

[13] Naud B., Novella R., Pastor J. M. and Winklinger J. F. "Comparison of Different Assumptions for Tabulated Chemistry Based on Laminar Igniting and Extinguishing Diffusion Flamelets". *Proc. European Comb. Meeting*, 2013.

[14] Kee R. J., Miller J. A. and Evans G. H. "A computational model of the structure and extinction of strained, opposed flow, premixed methane-air flames". *Proc. Combust. Inst.*, Vol. 22, pp. 1479–1494, 1988.

[15] Peters N. "Laminar diffusion flamelet models in non-premixed turbulent combustion". *Prog. Energy Combust. Sci.*, Vol. 10, pp. 319–339, 1984.

[16] Kim J. S. and Williams F. A. "Extinction of diffusion flames with nonunity Lewis numbers". *J. Engng. Math.*, Vol. 31, pp. 101–118, 1997.

[17] Grcar J. F. "The Twopnt Program for Boundary Value Problems". *SAND91-8230*, 1992.

[18] Petzold L. R. "A Description of DASSL: A Differential/Algebraic System Solver". *SAND82-8637*, 1982.

[19] Saxena P. and Williams F. A. "Testing a small detailed chemical-kinetic mechanism for the combustion of hydrogen and carbon monoxide". *Combust. Flame*, Vol. 145, pp. 316–323, 2006.

[20] Zeuch T., Moréac G., Ahmed S. S. and Mauss F. "A comprehensive skeletal mechanism for the oxidation of n-heptane generated by chemistry-guided reduction". *Combust. Flame*, Vol. 155, pp. 651–674, 2008.

[21] Michel J.-B., Colin O. and Veynante D. "Modeling ignition and chemical structure of partially premixed turbulent flames using tabulated chemistry". *Combust. Flame*, Vol. 152, pp. 80–99, 2008.

[22] CHEMKIN-PRO. *Reaction Design.* San Diego, 2008.

[23] Gicquel O., Darabiha N. and Thévenin D. "Laminar premixed hydrogen/air counterflow flame simulations using flame prolongation of ILDM with differential diffusion". *Proc. Combust. Inst.*, Vol. 28, pp. 1901–1908, 2000.

[24] van Oijen J. A., Lammers F. A. and de Goey L. P. H. "Modeling of Complex Premixed Burner Systems by Using Flamelet-Generated Manifolds". *Combust. Flame*, Vol. 127, pp. 2124–2134, 2001.

[25] Fiorina B., Baron R., Gicquel O., Thevenin D., Carpentier S. and Darabiha N. "Modelling non-adiabatic partially premixed flames using flame-prolongation of ILDM". *Combust. Theory Modelling*, Vol. 7, pp. 449–470, 2003.

[26] Veynante D. and Vervisch L. "Turbulent combustion modeling". *Prog. Energy Combust. Sci.*, Vol. 28, pp. 193–266, 2002.

[27] Bradley D., Gaskell P. H. and Gu X. J. "The mathematical modeling of liftoff and blowoff of turbulent non-premixed methane jet flames at high strain rates". *Symposium (International) on Combustion*, Vol. 27, pp. 1199–1206, 1998.

[28] Vervisch L., Hauguel R., Domingo P. and Rullaud M. "Three facets of turbulent combustion modelling: DNS of premixed V-flame, LES of lifted nonpremixed flame and RANS of jet-flame". *Journal of Turbulence*, Vol. 4, pp. 1–36, 2004.

[29] Girimaji S. S. "Assumed β-pdf Model for Turbulent Mixing: Validation and Extension to Multiple Scalar Mixing". *Combust. Sci. Technol.*, Vol. 78, pp. 177–196, 1991.

[30] Libby P. A. and Williams F. A. "Turbulent combustion: fundamental aspects and a review". In Libby P. A. and Williams F. A., editors, *Turbulent reacting Flows*, pp. 2–61. Academic Press, London, 1994.

[31] Effelsberg E. and Peters N. "Scalar dissipation rates in turbulent jets and jet diffusion flames". *Proc. Combust. Inst.*, Vol. 22, pp. 693–700, 1988.

[32] Michel J.-B., Colin O. and Veynante D. "Comparison of Differing Formulations of the PCM Model by their Application to the Simulation of an Auto-igniting H2/air Jet". *Flow Turb. Combust.*, Vol. 83, pp. 33–60, 2009.

[33] Michel J.-B., Colin O. and Angelberger C. "On the formulation of species reaction rates in the context of multi-species CFD codes using complex chemistry tabulation techniques". *Combust. Flame*, Vol. 157, pp. 701–714, 2010.

[34] http://www.openfoam.org/archive/1.6/download/. *The OpenFOAM Foundation.* Download OpenFOAM® v1.6, looked up on 22.06.2014.

[35] OpenFOAM The Open Source CFD Toolbox. *User Gide Version 1.6*, 2009.

[36] Galpin J., Naudin A., Vervisch L., Angelberger C., Colin O. and Domingo P. "Large-eddy simulation of a fuel-lean premixed turbulent swirl-burner". *Combust. Flame*, Vol. 155, pp. 247–266, 2008.

[37] Pera C., Colin O. and Jay S. "Development of a FPI Detailed Chemistry Tabulation Methodology for Internal Combustion Engines". *Oil Gas Sci. Technol.*, Vol. 64, pp. 243–258, 2009.

Chapter 4

Lifted turbulent H2/N2 jet flame

Contents

4.1 Introduction

A first application of the implemented turbulent combustion model is presented in this chapter. The combustion model is applied to a laboratory

flame configuration designed at Berkeley University, the lifted turbulent H_2/N_2 jet flame in a vitiated coflow [1], sometimes referred to as the "Berkeley flame". This flame is a widely used reference case employed to study the behavior of combustion models. Some reasons why this flame was chosen for a first model test, the objectives and the methodology of this preliminary test and an outline of this chapter are given in the following.

4.1.1 Motivation

There are several reasons why this flame configuration is attractive for a preliminary study of a combustion model. First and very important is the simple fuel hydrogen burned in this flame. The chemical kinetics of hydrogen are well-known and thus uncertainties about the chemical mechanism of the fuel, which is usually a great issue for many other fuels, are excluded. The flame burns at atmospheric conditions, i.e. at constant ambient pressure, and consequently no compressibility effects need to be considered, which allows in turn the application of the direct coupling method. Furthermore, the fuel enters the combustion domain in form of a gaseous jet which means that this test case is about a single phase flow. Consequently, complex effects such as atomization, evaporation, etc. do not have to be considered. This fact avoids the use of additional models which would be necessary in case of liquid sprays. Moreover, the flame burns in a statistically steady state, thus one can solve for a time-independent solution. All these properties of this laboratory flame lead to an important simplification of the modeling effort.
However, the flame exhibits some basic features similar to those of reactive sprays (present in diesel engines and gas turbines). The flame structure is mainly a diffusion flame with some local partially premixed regions close to the flame base. This flame shows furthermore a characteristic lift-off height, which is supposed to be determined by autoignition phenomena occurring at the flame base [1].
A further advantage is the comprehensive set of experimental data available for this benchmark case due to multi-scalar measurements. The data includes detailed information about the spatial distribution of mean and variance of species and temperature, which may be compared to computational results. Such detailed information is rarely available for reactive sprays for instance.

4.1.2 Objectives of the study

The main objective of this preliminary study is to test the conventional combustion model, i.e. with the adoption of DF solutions, and its

implementation in the CFD code. Moreover, the model's response to model parameter variations shall be studied. This first test implicitly includes the validation of the assumptions made in the presumed PDF modeling. Furthermore, the predictive capabilities of the model concerning the flame lift-off height is investigated. This important property of lifted flames is reported to be highly sensitive to temperature variations in this particular case.
Since a quite simple fuel is considered in this example, the use of flamelet tables based on diffusion flame solutions is feasible. Therefore, the adoption of the ADF method is in principle not indicated for this rather simple configuration. However, this flame represents an adequate configuration for a preliminary performance check of the simplified model and allows a qualitative comparison with the conventional model.

4.1.3 Methodology of the study

Several calculations based on DF solutions are made with both $\dot{Y}_c$ and $\dot{\omega}_{Y_c}$ as possible reaction term in the modeled transport equation for the mean progress variable. Different values for C_χ (Eq. (3.37)) and σ (Eq. (3.26)) are used in these calculations together with different coflow temperatures T_c within a range of 1045 K to 1090 K in order to adjust the model setup and the obtained lift-off height. Reference cases are then chosen for both reaction terms, $\dot{Y}_c$ and $\dot{\omega}_{Y_c}$, depending on the best accordance of the predicted lift-off height with the experimental value of about 10 nozzle diameters. The setup of the two reference cases is shown in Tab. 4.1. It shall be noted, that those reference cases represent the outcome of a considerable number of calculations, and that they are stated here for clarity.

Table 4.1. *Setup of the two reference cases.*

Reference case	Reaction term	T_c	C_χ	σ
A	$\dot{Y}_c$	1062 K	3	1
B	$\dot{\omega}_{Y_c}$	1053 K	3	1

Then, calculations based on ADF solutions are made for the same coflow temperatures and with the previously found reference values for C_χ and σ. This calculations are conducted with $\dot{Y}_c$ as reaction term in the transport equation for the progress variable, since $\dot{\omega}_{Y_c}$ can not be used with the ADF method.

In the next section the case setup, the main simulation parameters and the boundary conditions are resumed. The section of the results obtained with conventional combustion model is introduced with a representation of the predicted flame structure. The influence of the model parameters on the model predictions is then discussed. In order to do so, radial profiles of the mixture fraction, the temperature and the main species are presented and compared with experimental data. Also differences in the results due to the use of different source terms are pointed out. Finally, the influence of the coflow temperature on the lift-off height is compared for both source terms with experiments.
The second part of results is about the comparison of results the conventional combustion model and of those of its approximated version. First the sensitivity of the lift-off height to coflow temperature variations when using ADF solutions is shown. With the information of those results two cases are chosen for a further comparison. Spatial distributions of the main species as well as radial profiles of mixture fraction and temperature are presented for both types of flamelet solutions. This chapter is closed with some preliminary conclusions about the implemented model and the obtained results.

4.2 Case setup and boundary conditions

A simplified sketch of the Berkeley H_2/N_2 flame configuration is given in Fig. 4.1, which is adapted from [1]. The central turbulent H_2/N_2 jet exits from a nozzle with $d = 4.57$ mm This fuel jet is enclosed by the coaxial hot coflow, which enters through a perforated disk with an outer diameter of 210 mm. This coflow consist of combustion products from a lean premixed H_2/air flame. The actually modeled region in the CFD simulations of this configuration is represented by the light grey, dashed bordered rectangle in Fig. 4.1. The computational domain—$50d$ long (in axial direction) and $20d$ wide (in radial direction)—is a half plane of the considered 2D axisymmetric geometry. A 108x108 cell non-uniform structured mesh [1] is used, stretched in both axial and radial direction with 13 uniform grid cells in radial direction above the fuel exit: between $r = 0$ and $r = R = d/2$.

Symmetry conditions are imposed on the symmetry axis, a free-slip boundary is specified on the outer boundary, and a convective outlet condition together with a constant mean pressure of 1.01325 bar is used. The inlet profiles are specified in such a way that the fluctuating axial and radial velocity

[1] The mesh is actually a 10° wedge consisting of 3D cells with symmetry conditions in circumferential direction, since OpenFoam 1.6 does not offer real 2D meshes.

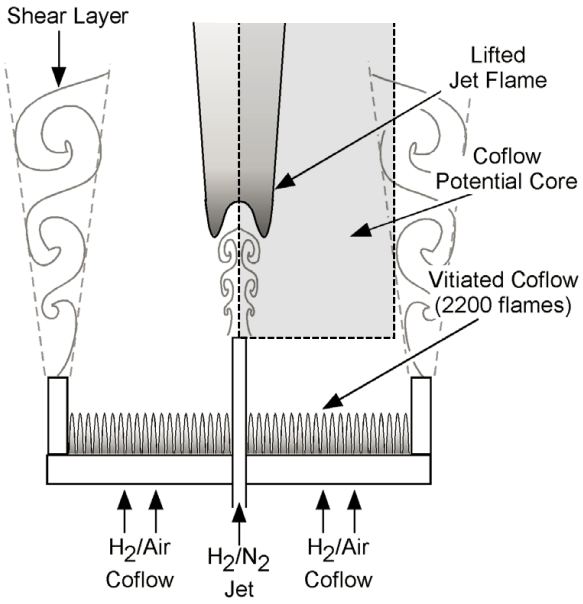

Figure 4.1. *Sketch of the H_2/N_2 jet flame configuration with CFD domain marked by light grey, dashed bordered rectangle.*

profiles, u' and v', are similar to the experimental profiles used in [2], where the influence of the inlet boundary conditions was carefully studied. In this RANS framework, the influence of the wall flows on the inner and outer sides of the fuel nozzle are simply accounted for at the injector exit by specifying the turbulent profiles for mean velocity components, turbulent kinetic energy and turbulent dissipation. The axial mean velocity profile at the injector exit is specified as $\widetilde{U} = \overline{U}(1.01 - r/R)^{1/6}$, the coflow mean velocity $\widetilde{U} = 3.5$ m/s is imposed at $r > 1.88R$. For $R < r < 1.88R$, both profiles are connected with an exponential decay $\overline{U} = a + b \cdot \exp(-cr^2)$, with $c \approx 480000$, leading to a similar profile as used in [2]. This axial mean velocity profile is normalized with U' such that the correct experimental bulk velocity of 107 m/s is imposed at the injector exit (i.e. correct fuel mass flow rate). The radial mean velocity is set to zero. The Reynolds stresses are specified as $\widetilde{u''^2} = u'u'$ in axial, $\widetilde{v''^2} = v'v'$ in radial and $\widetilde{w''^2} = \widetilde{v''^2}$ in azimuthal direction similar to [2], whereby the turbulent kinetic energy $k = \frac{1}{2}(\widetilde{u''^2} + \widetilde{v''^2} + \widetilde{w''^2})$ is given. The turbulent shear stress is specified in a similar way as in [2] such that $\widetilde{u''v''} = \rho_{uv}u'v'$, with $\rho_{uv} = 0.4(r/R)$ for $r \leqslant R$ and $\rho_{uv} = 0.4$ for $r > R$. Finally, the turbulent dissipation profile is specified by supposing that the dissipation term is equal

to the production term in the turbulent kinetic energy transport equation: $\varepsilon = -\widetilde{u''v''}\,\partial\widetilde{U}/\partial r$. The resulting boundary condition profiles for the axial mean velocity, the turbulent kinetic energy and the turbulent dissipation are represented for $r \leqslant 2R$ (since constant above this radial position) in Fig. 4.2.

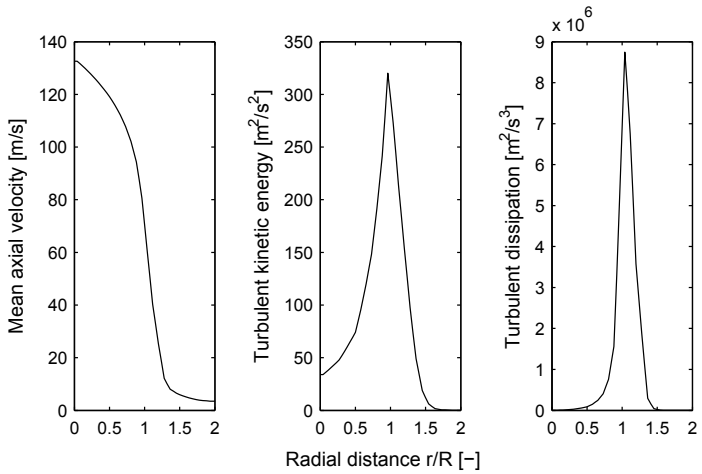

Figure 4.2. *Boundary condition profiles for radial distance* $0 < r \leqslant 2R$.

The mean temperature T_j of the central fuel jet is maintained constant at 305 K. As already mentioned, the mean temperature T_c of the coflow is varied between its nominal experimental value of 1045 K, for which a measurement uncertainty of 3% is reported in [1], and 1090 K. Different values for T_c are not only imposed as boundary condition of the CFD simulation, but also for the pre-calculation of the turbulent flamelet table. However, the composition of the fuel and coflow stream, listed in Tab. 4.2, are maintained constant for all calculations. These species mass fractions represent the initial condition for the calculation of the flamelet tables at different values of T_c. The chemical mechanism of [3], which involves 9 species (H_2, H, O_2, OH, O, H_2O, HO_2, H_2O_2 and N_2) and 21 reactions, is used to describe the chemical kinetics of this flame. Though already explained in Chapter 3, it shall be reminded that the progress variable is defined here as: $Y_c = Y_{H_2O} + 10\,Y_{HO_2} + 3\,Y_{H_2}$.
The chemistry lookup table is discretized in 50 uniform intervals in Z between 0 and 1, 20 uniform intervals in S between 0 and 0.2 and 50 uniform intervals in $\widetilde{Y}_c$ between $\widetilde{Y}_c^{\min}(\widetilde{Z}, S)$ and $\widetilde{Y}_c^{\max}(\widetilde{Z}, S)$. A logarithmic grid is used to store the lookup table in $\widetilde{\chi}_{st}$, using 41 uniform intervals between $\ln(\chi_{st,\mathrm{MIN}})$

and $\ln(\chi_{st,\mathrm{MAX}})$ (corresponding to approximately 10 intervals per order of magnitude).

Table 4.2. *Composition of the fuel jet (f) and the hot coflow (c) of the lifted H_2/N_2 turbulent jet flame.*

	Fuel jet (Z=1)	Coflow (Z=0)
Mole fractions	$X_{H_2,f} = 0.25$	$X_{O_2,c} = 0.14744$
	$X_{N_2,f} = 0.75$	$X_{H_2O,c} = 0.09893$
		$X_{N_2,c} = 0.75363$

The standard $k-\varepsilon$ turbulence model is used with the modified constant $C_{\varepsilon 1} = 1.6$, an usual modification for round jets. Good predictions of the mixing of the turbulent jet are obtained with a turbulent Schmidt[2] number of $Sc_t = 0.9$, which is maintained for all calculations.

4.3 Results of the conventional combustion model

4.3.1 Basic flame structure

In order to give a first impression of the predicted flame structure, the spatial distribution of the mean temperature is shown for the reference case A. Moreover, the mixture fraction and its variance are presented since they mark important parameters in the description of diffusion flames and play a key role in this modeling strategy as already pointed out before. For the sake of completeness, the distribution of the mean mass fraction of four main species is given. The dimensions of the shown contour plots do not represent the whole computational domain but a detail of the flame around lift-off. The contour plot on the left in Fig. 4.3.1 gives an idea of the mean mixture fraction field. $\widetilde{Z}$ equals unity (representing pure fuel stream) at the central nozzle exit, whereas radially further outside at the hot coflow it is zero (representing pure oxidizer). With increasing axial distance from the orifice the two streams mix which leads to decreased values of mean mixture fraction. Steep radial gradients of mean mixture fraction are present close to the orifice.
The rms fluctuation of the mixture fraction is shown in the contour plot on the right in Fig. 4.3.1. The driving force behind the fluctuations are gradients

[2]Ernst Schmidt (1892–1975), German engineer and professor. Sc is defined as the ratio of momentum diffusivity to mass diffusivity.

of mean mixture fraction (compare Eq. (3.36)) and consequently high values of rms fluctuation can be found in regions of steep mixture fraction gradients. A further impact on the mixture fraction fluctuations is due to the mean scalar dissipation rate which has a reducing effect on the fluctuations. Here it is important to remember, that the mixture fraction variance on the other hand also interacts with the mean scalar dissipation rate (compare Eq. (3.37)), which is analyzed in the next section. Even further, turbulence directly affects the mean scalar dissipation rate through the turbulent frequency $\omega = \varepsilon/k$. This means that k and ε, provided by the turbulence model, also have direct influence on the mixture fraction fluctuations and not only via the turbulent viscosity. In summary, the turbulence model has a vital role in the whole modeling process, since it has important influence on the most basic parameters of the combustion model.

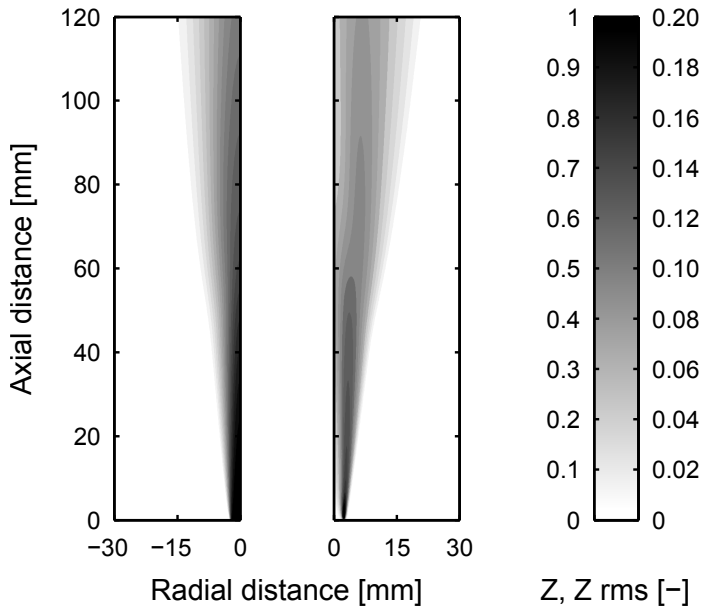

Figure 4.3. *Mean mixture fraction (left and left scale) and its rms fluctuation (right and right scale) for the reference case A.*

Figure 4.4 shows the predicted mean temperature distribution of the reference case A and some other important information. The stoichiometric mean mixture fraction is represented by the black line. The white line represents the isoline of $\widetilde{Y}_{OH} = 2 \cdot 10^{-4}$, the threshold used for the evaluation of the lift-off height as in [2]. The lift-off height, defined as minimum axial distance where the threshold of OH mean mass fraction is reached, is marked

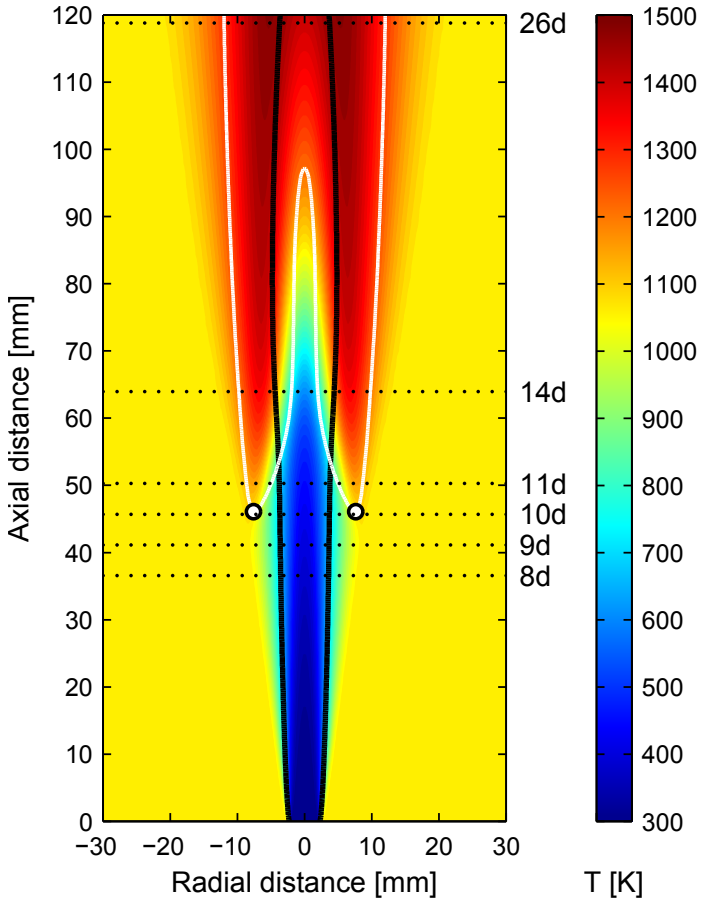

Figure 4.4. *Mean temperature distribution for the reference case A (using $\dot{Y}_c$, $T_c = 1062$ K, $C_\chi = 3$ and $\sigma = 1$). Black line: $\widetilde{Z}_{st}$, white line: $\widetilde{Y}_{OH} = 2 \cdot 10^{-4}$, black circles: lift-off height.*

by the two black circles. Good accordance of the predicted lift-off height with the nominal experimental value of $10d$ can be observed for the represented reference case A. Moreover, it can be stated that the lift-off is located in a lean mixture. The black dotted lines indicate the axial heights at which experimental data from [1] in the form of radial profiles are available and compared with modeling results further below. In this contour plot one can further observe how the stoichiometric mean mixture fraction isoline is distorted by combustion, which occurs about where the black line crosses the white line. This happens due to thermal expansion when entering reactive

regions with high temperatures where the density drops.

An overview of the spatial distribution of the mean mass fractions of H_2, OH, H_2O and O_2 is given in Fig. 4.5. First, one can observe in Fig. 4.5(a) how the fuel H_2 exhausts from the central nozzle and further downstream decreases its concentration due to combustion. Fig. 4.5(b) in contrary shows that OH, which is considered a precursor of combustion processes, is generated at regions where hydrogen is oxidized. Medium concentrations of the combustion product H_2O emerge from the hot coflow stream (Fig. 4.5(c)) as a of the lean H_2/air combustion taking place further upstream (outside of the computational domain). Increased concentrations of water vapor are generated due to the primary combustion process within the diffusion flame. Finally, Fig. 4.5(d) shows that the oxygen mean mass fraction is zero inside the fuel stream and the diffusion flame and increases to its coflow concentration elsewhere. Note that close to the flame base low concentrations of O_2 can be observed, which indicates a certain grade of partial premixing. This means that the flame base is located in a partially-premixed region, which is a typical characteristic of lifted flames.

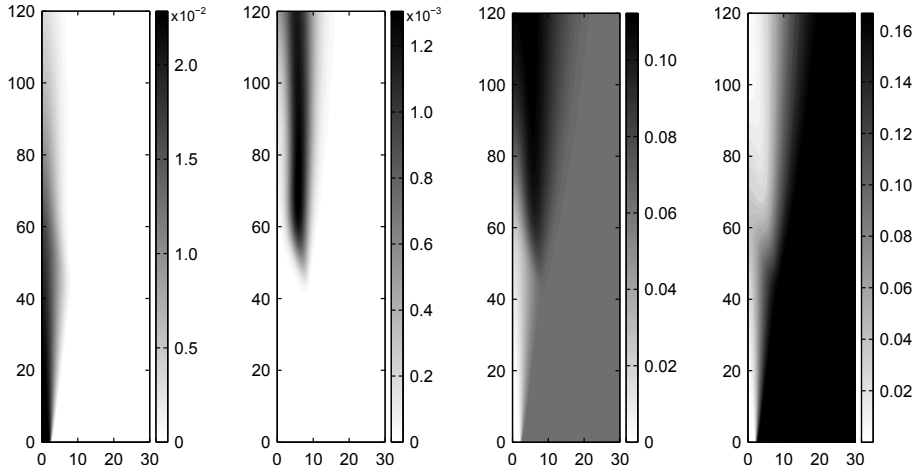

(a) $\widetilde{Y}_{H_2}$ (b) $\widetilde{Y}_{OH}$ (c) $\widetilde{Y}_{H_2O}$ (d) $\widetilde{Y}_{O_2}$

Figure 4.5. *Spatial distribution of mean mass fractions of main species for the reference case A. Axial and radial distances are stated in mm.*

4.3.2 Influence of model parameters

Influence of C_χ and main model properties

The influence of C_χ is exemplarily shown for the reference case A in the following, however, the same observations are made for other cases. Figure 4.6 shows the influence of C_χ on the results. First of all, it should

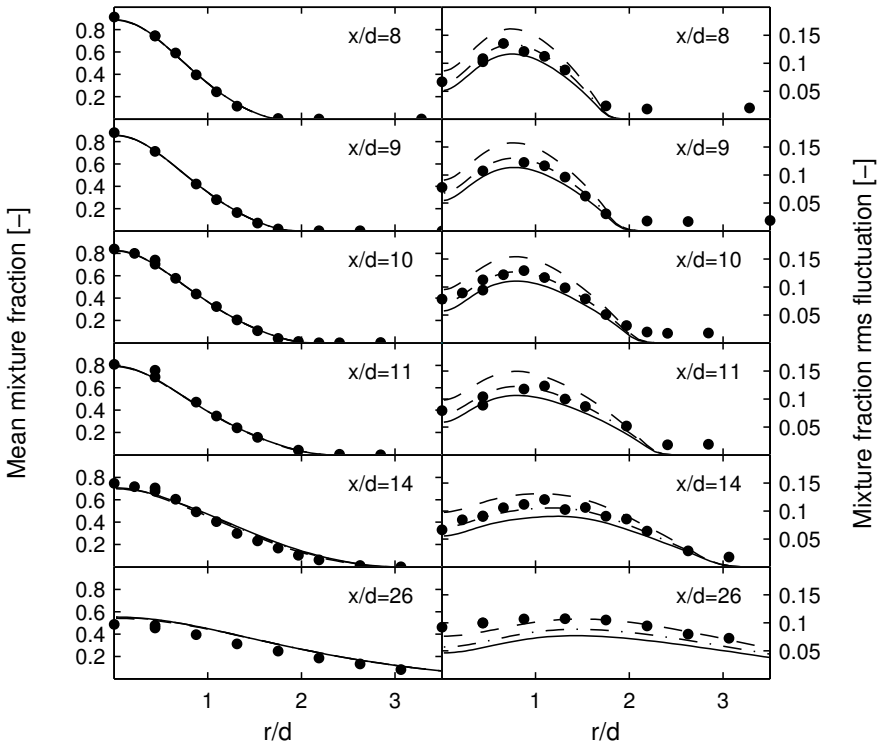

Figure 4.6. *Radial profiles of mean mixture fraction and its rms fluctuation. Symbols: experimental data / Lines: results for the reference case A. Dashed lines: $C_\chi = 2$. Dashed-dotted lines: $C_\chi = 3$. Solid lines: $C_\chi = 4$.*

be pointed out that very good results are obtained for the mean mixture fraction due to the usual adjustment of the constant $C_{\varepsilon 1} = 1.6$ for round jets and using $Sc_t = 0.9$ especially in the inert part of the flow. However, small deviations can be observed for $x/d > 11$, i.e. within the reactive part of the flow. This observations are also discussed for instance in [4], where more advanced turbulence models are suggested as possible solution. A potential explanation for these small differences in the mixing fields in combination with

the $k-\varepsilon$ model is given in [5], where density gradients are suggested as possible source. A critical examination of results and the knowledge of possible weak points in the modeling setup is certainly important, nevertheless, the observed differences can be considered small enough and not contradictory to further studies. Moreover, the obtained results do well when compared with other published modeling results [2, 4–8].
The impact of the choice of C_χ on the results for mixture fraction variance can be observed, where higher values of C_χ lead to lower values of variance. The best agreement with experimental data is found with $C_\chi = 3$, which was consequently chosen for the two reference cases.

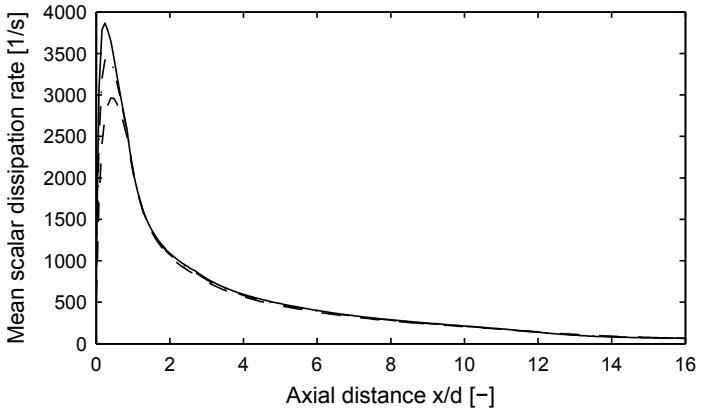

Figure 4.7. *Mean scalar dissipation rate along the mean stoichiometric isoline in the case of using $\dot{Y}_c$, $T_c = 1062$ K and $\sigma = 1$. Dashed line: $C_\chi = 2$, dashed-dotted line: $C_\chi = 3$, solid line: $C_\chi = 4$.*

In Fig. 4.7, the value of the mean scalar dissipation rate following the stoichiometric isoline as a function of the axial distance is plotted. It can be observed, that the value of C_χ has almost no influence on the mean scalar dissipation rate anywhere in the flow field, except very close to the nozzle exit. The explanation can be found in Eq. (3.37) where two effects counterbalance, since increasing values of C_χ imply lower values of $\widetilde{Z''^2}$ as observed in Fig. 4.6.

Figure 4.8 and 4.9 show the radial profiles of mean temperature and mean mass fraction of H_2O and their fluctuations. The results for these properties are similar and provide a good estimate for the quality of the predicted progress variable. The mean values are in general well predicted for both reference cases, i.e. for $\dot{Y}_c$ and $T_c = 1062$ K and $\dot{\omega}_{Y_c}$ and $T_c = 1053$ K. However, different adjusted coflow temperatures are necessary depending on

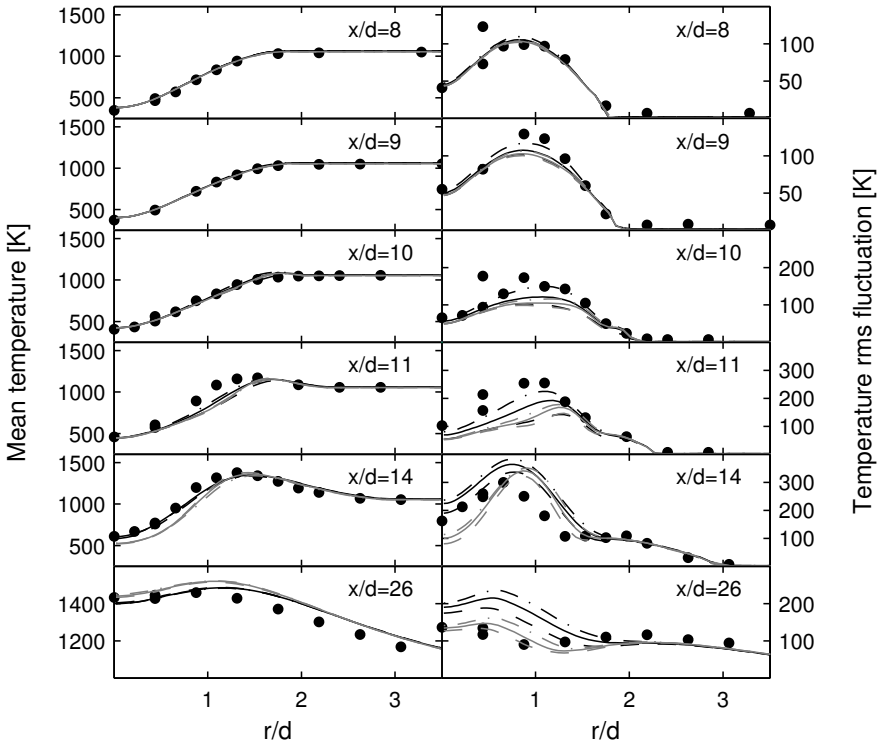

Figure 4.8. *Radial profiles of mean temperature and its rms fluctuation. Symbols: experimental data / Black lines: results using $\dot{Y}_c$, T_c = 1062 K and C_χ = 3, gray lines: results using $\dot{\omega}_{Y_c}$, T_c = 1053 K and C_χ = 3. Dashed lines: δ-PDF. Solid lines: σ = 1. Dashed-dotted lines: $\sigma = \sqrt{2}$.*

the employed reaction term in order to correctly predict the experimental lift-off height. The reason for this 9 K difference can be found in the reactivity of the laminar flamelets: the use of $\dot{Y}_c$, including diffusion effects, leads to a "less reactive flame" than when using $\dot{\omega}_{Y_c}$ as can be seen in Fig. 3.7. That is why the calculations made with $\dot{Y}_c$ require a higher coflow temperature in order to lead to the same lift-off height. Note that both values of coflow temperature lie within the 3% measurement uncertainty reported for this parameter.

The results obtained for the mean temperature and its fluctuation can also be plotted as a function of the predicted mean mixture fraction as done in Fig. 4.10. Indeed, this does not represent new information, nonetheless, it allows another insight on the modeling results. The mean temperature profiles in the inert part of the flow (x/d = 8 and x/d = 9) represent the

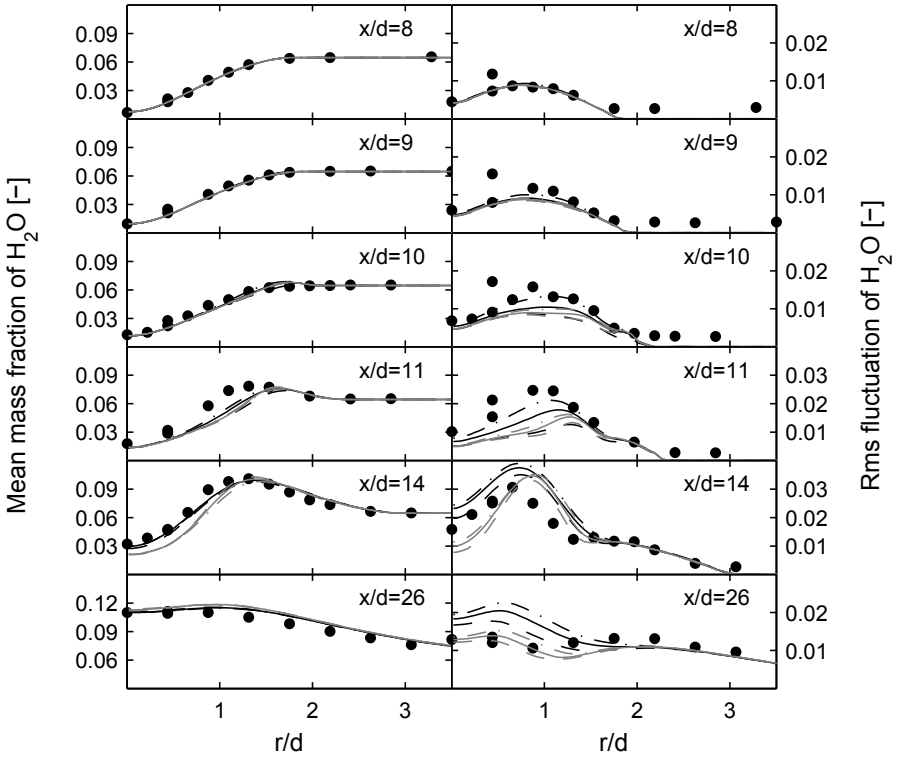

Figure 4.9. *Radial profiles of mean mass fraction of H_2O and its rms fluctuation. Symbols: experimental data / Black lines: results using $\dot{Y}_c$, T_c = 1062 K and C_χ = 3, gray lines: results using $\dot{\omega}_{Y_c}$, T_c = 1053 K and C_χ = 3. Dashed lines: δ-PDF. Solid lines: σ = 1. Dashed-dotted lines: $\sigma = \sqrt{2}$.*

inert mixture and thus the initial condition for the flamelet calculations. The good agreement with the experimental data confirms the correctness of the initial conditions. Looking at the radial profiles of $x/d = 10$ and $x/d = 11$, one can observe that close to the lift-off only lean mixtures are reactive. The most downstream profile indicates good prediction of the quasi-steady state temperature distribution. At this point, it may be noted that the obtained results are in good correspondence with experimental data for three of the four properties on which the turbulent combustion model relies: $\widetilde{Z}$, $\widetilde{Z''^2}$ and $\widetilde{Y}_c$. These results are obtained with $C_\chi = 3$, for both using $\dot{Y}_c$ or $\dot{\omega}_{Y_c}$ as reaction term in the mean progress variable transport equation, by adjusting the coflow temperature. No data is available concerning $\widetilde{\chi}$ and the standard model (Eq. (3.37)) with the adjusted constant is employed. The predictive capability of the implemented turbulent combustion model for the

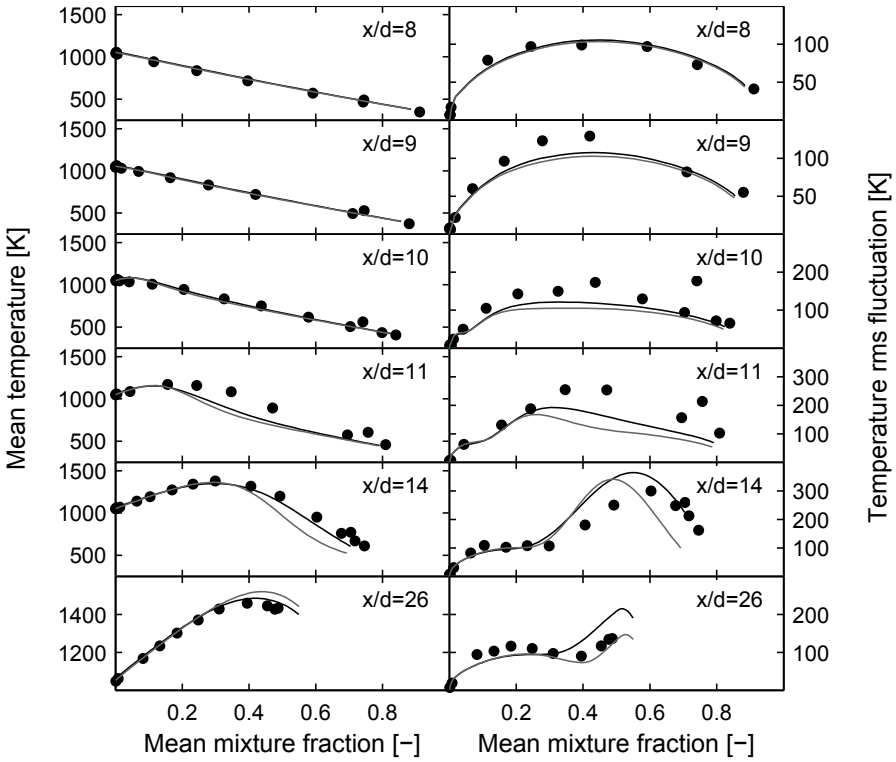

Figure 4.10. *Radial profiles of mean temperature and its rms fluctuation as function of mean mixture fraction. Symbols: experimental data / Black lines: results for reference case A. Gray lines: results for reference case B.*

other properties and their fluctuations can now be studied. As described in Chapter 3, the results for all other properties are direct consequences of the UFPV assumption together with the model for presumed shape of the joint PDF. In particular, the fluctuations of the progress variable and the tabulated properties are directly related to the model for the fluctuations of Z and χ.

Influence of fluctuation of χ_{st}

The columns of the right-hand side of Fig. 4.8 and 4.9 give an idea of the fluctuations of the progress variable. The variances are obtained from the tabulated mean properties and the mean of the square, for example for for the temperature: $\widetilde{T''^2} = \widetilde{T^2} - \widetilde{T}^2$. Close to the nozzle exit, no big differences can be found between using $\dot{Y}_c$ or $\dot{\omega}_{Y_c}$ since the mixture is still in its inert state. In the vicinity to the lift-off, both the centerline value and the peak

value are slightly better captured when using $\dot{Y}_c$, whereas further downstream results obtained with $\dot{\omega}_{Y_c}$ show better agreement with experimental data. The fluctuation predictions are sensitive to the prescribed fixed variance σ^2 in the PDF of the logarithm of χ_{st} (Eq. (3.26)), while mean values are not sensitive to this model parameter. The sensitivity of the results is observably higher when using $\dot{Y}_c$.

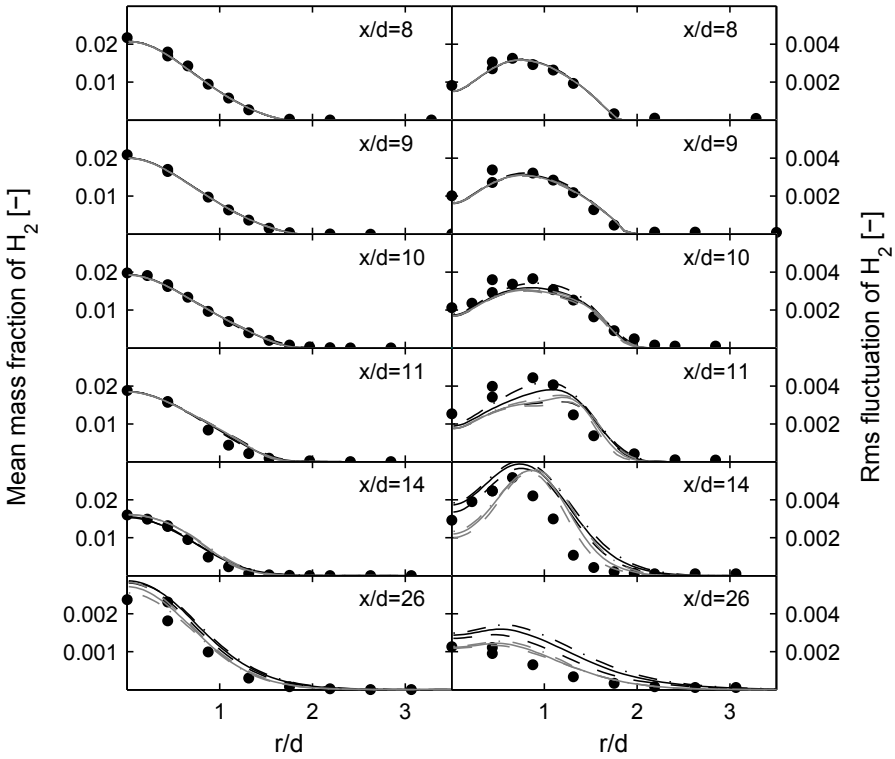

Figure 4.11. *Radial profiles of mean mass fraction of H_2 and its rms fluctuation. Symbols: experimental data / Black lines: results using $\dot{Y}_c$, T_c = 1062 K and C_χ = 3, gray lines: results using $\dot{\omega}_{Y_c}$, T_c = 1053 K and C_χ = 3. Dashed lines: δ-PDF. Solid lines: σ = 1. Dashed-dotted lines: $\sigma = \sqrt{2}$.*

The fuel and oxidizer mass fraction predictions are shown in Fig. 4.11 and 4.12. Good agreement with experimental data is obtained for the mean radial profiles. Concerning the fluctuations, similar observations can be made as for temperature. However, for these reactants which are consumed in the reaction zone, less sensitivity to σ or the use of $\dot{Y}_c$ or $\dot{\omega}_{Y_c}$ is observed as compared to the main combustion product and the temperature.

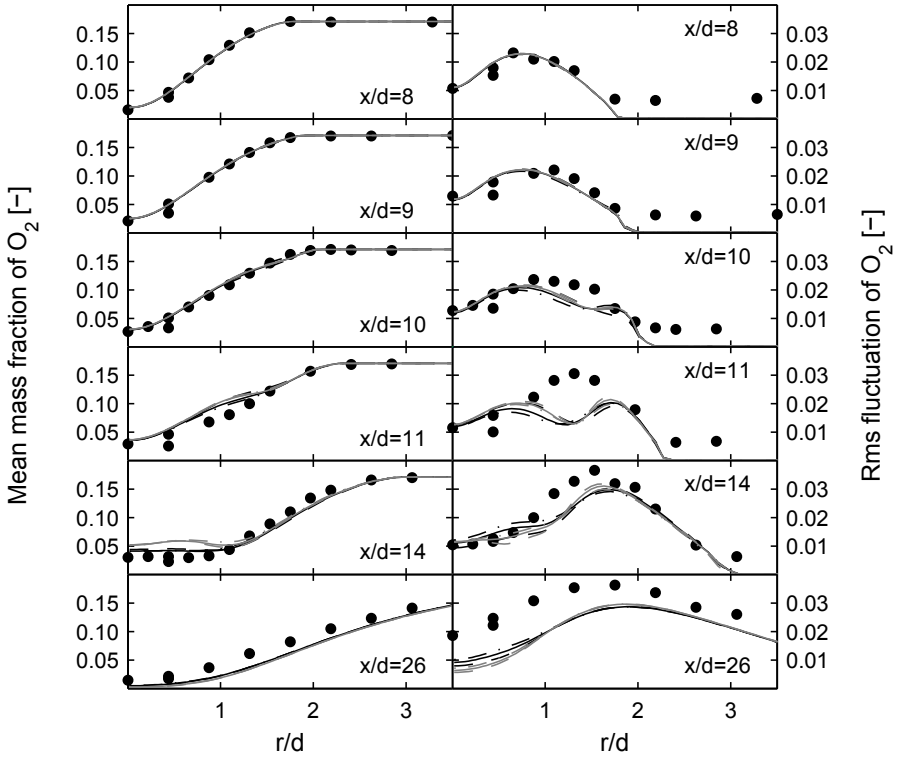

Figure 4.12. *Radial profiles of mean mass fraction of O_2 and its rms fluctuation. Symbols: experimental data / Black lines: results using $\dot{Y}_c$, T_c = 1062 K and C_χ = 3, gray lines: results using $\dot{\omega}_{Y_c}$, T_c = 1053 K and C_χ = 3. Dashed lines: δ-PDF. Solid lines: σ = 1. Dashed-dotted lines: $\sigma = \sqrt{2}$.*

As could be expected, the most sensitive property is the mean mass fraction of the OH radical as shown in Fig. 4.13. The differences are especially important at the flame base and become similar further downstream. Important differences even for the mean values can be found in this case whether $\dot{Y}_c$ or $\dot{\omega}_{Y_c}$ is used as reaction term. In general, the peak of the mean mass fraction seems to be predicted slightly too far away from the centerline right before the onset of combustion. It is interesting to note, that similar findings are obtained in [2], where a different combustion model was employed to simulate this flame, but the same turbulence model as in this work was used. Better agreement with experimental data is obtained with $\dot{Y}_c$, both for the mean and the fluctuations. The choice of σ also has a strong impact on the results (especially when using $\dot{Y}_c$), even for the mean mass fraction. Again, the values $\sigma^2 = 1$ and $\sigma^2 = 2$ seem reasonable, with the best results obtained

with $\sigma^2 = 2$ just before the flame base. However, the δ-PDF assumption for χ_{st} performs poor for the fluctuations before the flame base.

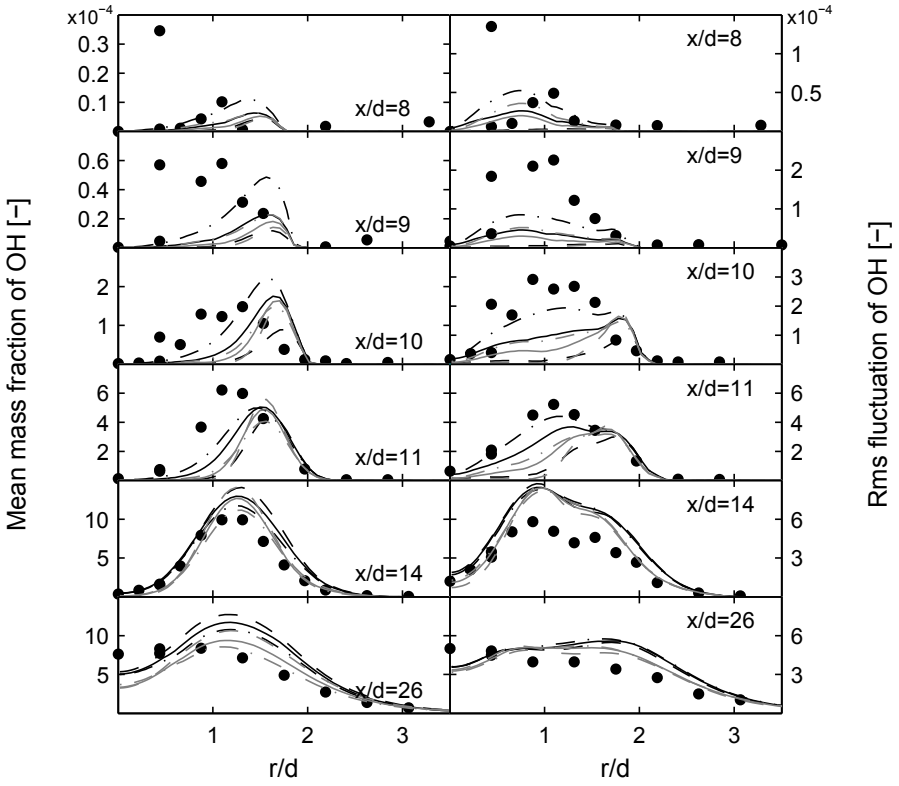

Figure 4.13. *Radial profiles of mean mass fraction of OH and its rms fluctuation. Symbols: experimental data / Black lines: results using $\dot{Y}_c$, T_c = 1062 K and C_χ = 3, gray lines: results using $\dot{\omega}_{Y_c}$, T_c = 1053 K and C_χ = 3. Dashed lines: δ-PDF. Solid lines: σ = 1. Dashed-dotted lines: $\sigma = \sqrt{2}$.*

4.3.3 Sensitivity of lift-off height

Figure 4.14 shows the dependence of the flame lift-off height h_{LO} on the coflow temperature T_c. The distance h_{LO} corresponding to the base of the modeled lifted flame is evaluated as the axial distance where $\widetilde{Y}_{OH} = 2 \cdot 10^{-4}$ as in [2]. Results are shown for both reference cases, i.e. using $\dot{Y}_c$ or $\dot{\omega}_{Y_c}$ as reaction term (similar trends are obtained with the δ-PDF assumption for χ_{st} or with $\sigma = \sqrt{2}$). The symbols on the curves for the simulation results mark the coflow temperatures at which calculations have been made. The horizontal line in Fig. 4.14 marks the measurement uncertainty of the coflow temperature

reported in the original work on this flame [1]. Experimental data from Wu et al. [9] and Gordon et al. [10] are additionally represented. The differences between the experimental data sets illustrate the high sensitivity of this flame to the coflow temperature. Moreover, they suggest that the reproducibility of the experiment might be challenging. This justifies the adjustment of the coflow temperature in the modeling in order to match a given lift-off height. On the other hand, the significant information given by these data sets is the trend of the dependence of h_{LO} on T_c. The model should be able to reproduce this dependence. The trend of both curves (using $\dot{Y}_c$ or $\dot{\omega}_{Y_c}$) is in correspondence with the experimental data for high coflow temperatures. The similar model presented in [7] using $\dot{\omega}_{Y_c}$ leads to results very similar to the ones shown here. However, at low coflow temperatures the calculations do not predict an increase in lift-off height as high as expected.

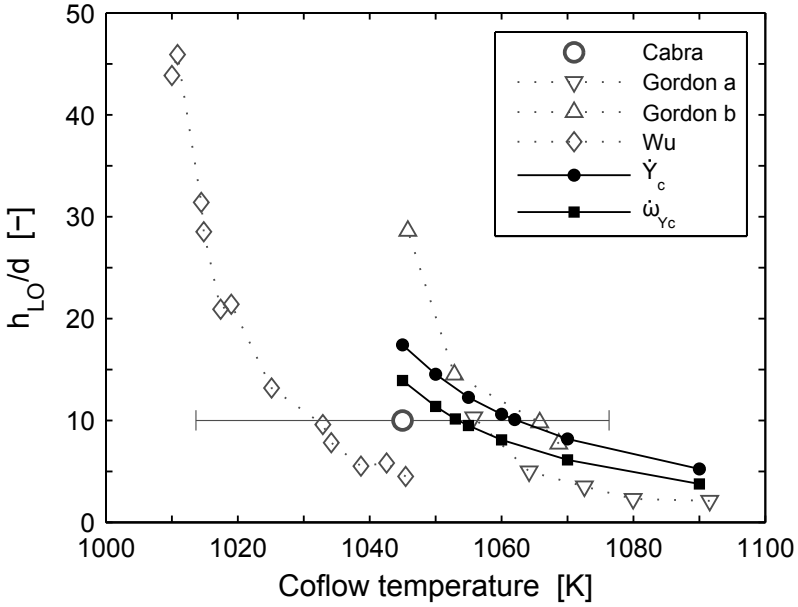

Figure 4.14. *Lift-off height as function of coflow temperature. Comparison of results when using $\dot{Y}_c$ or $\dot{\omega}_{Y_c}$ as reaction term. Symbols: experimental data / Lines: model predictions.*

4.4 Results of the conventional and the simplified combustion model

In this section results obtained with the simplified version of the turbulent combustion model, i.e. with flamelet tables based on the ADF approach, are compared with those of the conventional model presented above. It is about a primarily qualitative comparison of results with the aim to check the aptitude and correct implementation of the approximation. For this purpose, the model parameters of the reference case A ($C_\chi = 3$ and $\sigma = 1$) are used together with ADF based flamelet tables. Calculations are then made for the same values of coflow temperature as before with the conventional combustion model when using $\dot{Y}_c$.

4.4.1 Sensitivity of lift-off height

First, a comparison of the predicted lift-off height h_{LO} as a function of T_c for both the conventional (DF solutions) and the simplified (ADF solutions) combustion model is given in Fig. 4.15. The first observation is that the sensitivity of the lift-off height on the coflow temperature is predicted very similar with the simplified model. However, the calculated lift-off height lies generally above the values obtained with the conventional model. The explanation for this can be found in different "reactivity" of the laminar flamelet solutions obtained for DF and ADF. When comparing unsteady DF solutions (see Fig 3.6) with their ADF counterpart (see Fig 3.10), one can observe that for the same time increment Y_c increases stronger in case of the DF solutions than ADF solutions. This difference in reactivity becomes also noticeable in the different values obtained for χ_{AI} and χ_{Q} (compare Fig. 3.5 and 3.9). Thus, a different adjustment of T_c is necessary for the simplified combustion model. This is somehow similar to what was already discussed before for $\dot{Y}_c$ or $\dot{\omega}_{Y_c}$ as possible reaction terms in the conventional model. Although in this case none of the calculations made for different values of T_c predicted the exact nominal lift-off height, Fig. 4.15 shows that the value of T_c that would give $h_{LO}/d = 10$ still lies within the uncertainty range of the coflow temperature (marked by the gray line).

On the basis of these results, the case with $T_c = 1070$ K for the conventional model and the one with $T_c = 1090$ K for the simplified model are chosen for further comparative studies. The difference in the predicted lift-off height for these two cases is slightly above $1d$. Other potential pairs of cases are excluded

because the predicted lift-off is considered too high for an evaluation of the radial profiles at the similar axial distances as before.

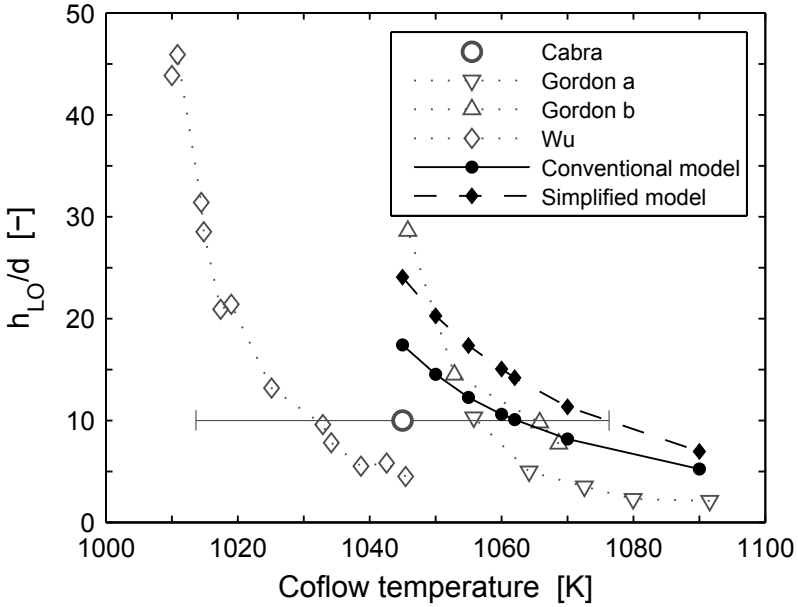

Figure 4.15. *Lift-off height as function of coflow temperature. Comparison of results of different versions of the combustion model. Symbols: experimental data / Lines: model predictions.*

4.4.2 Comparison of species predictions

At first, the spatial distribution of the mean mass fractions of H_2, OH, H_2O and O_2 obtained with the conventional combustion model are shown in Fig. 4.16, which are of course very similar to those shown in Fig. 4.5 but with a lower lift-off height. The equivalent representation for the results of the simplified combustion model are shown in Fig. 4.17. The explanation for the respective contour plot of each species given in Section 4.3.1 is certainly valid here again. No significant differences can be observed between the presented results obtained with the two different versions of the turbulent combustion model. The predicted species fields look very similar on a qualitative analysis. Indeed, the slightly lower flame base can be identified for the results of the simplified combustion model. However, apart of this distinction, the general trends are alike.

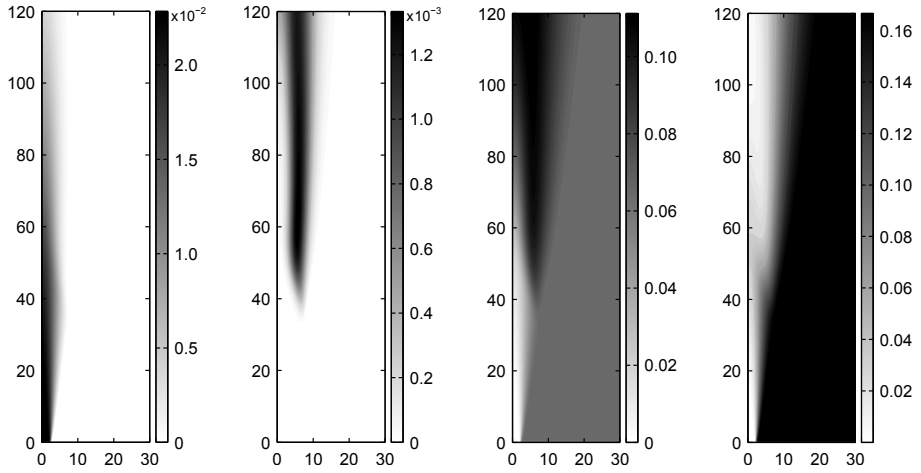

(a) $\widetilde{Y}_{H_2}$ (b) $\widetilde{Y}_{OH}$ (c) $\widetilde{Y}_{H_2O}$ (d) $\widetilde{Y}_{O_2}$

Figure 4.16. *Spatial distribution of mean mass fractions obtained with the conventional model with T_c = 1070 K. Axial and radial distances are stated in mm.*

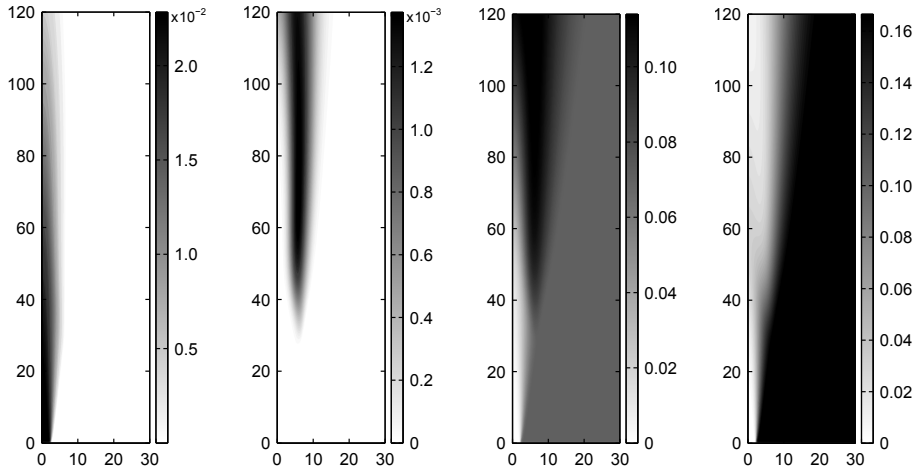

(a) $\widetilde{Y}_{H_2}$ (b) $\widetilde{Y}_{OH}$ (c) $\widetilde{Y}_{H_2O}$ (d) $\widetilde{Y}_{O_2}$

Figure 4.17. *Spatial distribution of mean mass fractions obtained with the simplified model with T_c = 1090 K. Axial and radial distances are stated in mm.*

4.4.3 Comparison of radial profiles

As a final comparison, the radial profiles of the mean mixture fraction and its fluctuation as well as the mean temperature and its fluctuation are contrasted. These properties have been chosen since the two first represent key parameters of the combustion model and the latter two give a good estimate of the prediction of the progress variable. Results of the mean mixture

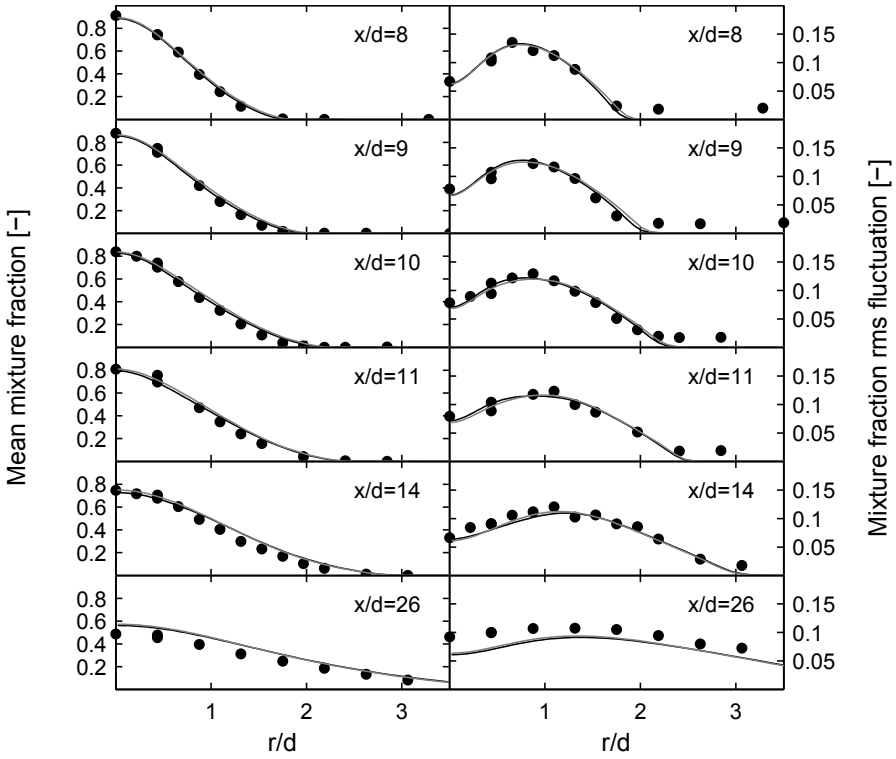

Figure 4.18. *Radial profiles of mean mixture fraction and its rms fluctuation. Black lines: results of the conventional combustion model with T_c = 1070 K, gray lines: results of the simplified combustion model with T_c = 1090 K.*

fraction and its fluctuation are compared for both combustion model versions in Fig. 4.18. As might be expected, no major difference can be found neither for the mean values of the mixture fraction nor for its fluctuations. This is not surprising, since the modeling of the mixing (primarily governed by the turbulence model) is not directly affected by the adoption of different flamelet solutions. However, secondary effects due to combustion and the slightly different lift-off height cause very small deviations. In the same

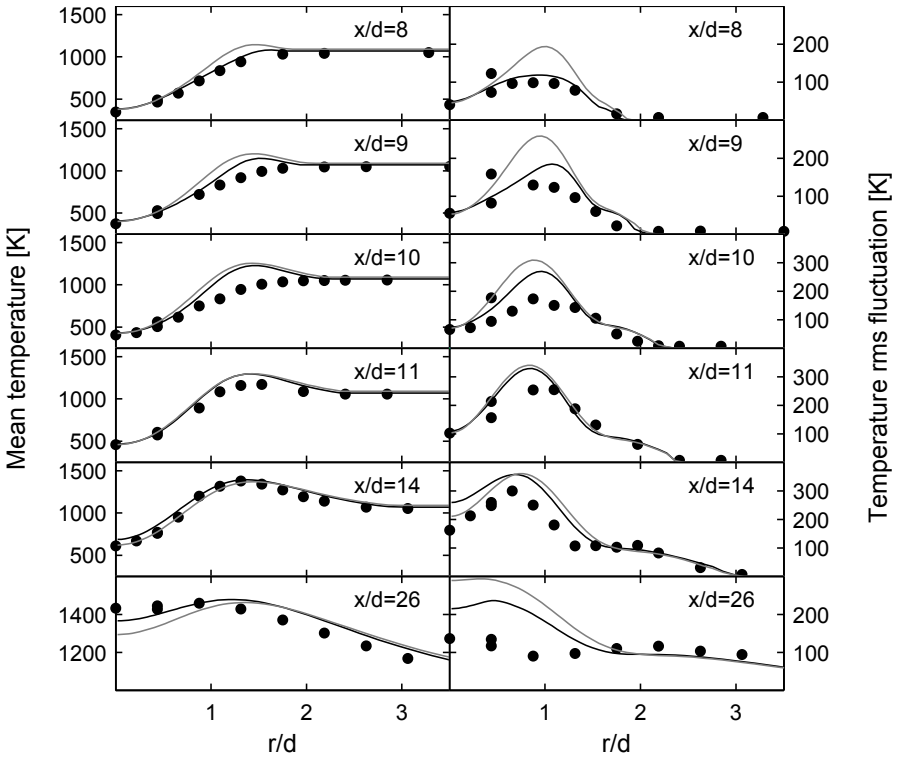

Figure 4.19. *Radial profiles of mean temperature and its rms fluctuation. Black lines: results of the conventional combustion model with T_c = 1070 K, gray lines: results of the simplified combustion model with T_c = 1090 K.*

way, the predicted mean temperature and its fluctuation are compared for the same cases in Fig. 4.19. Very similar profiles can be observed for the mean values of the temperature, with the small difference in the lift-off height slightly reflected. Significant differences in the peak values of the temperature fluctuations are found in the radial profiles close to the flame base (probably due to lift-off difference), although, the centerline value and the flame edge value are almost identical. Moreover, the general trend of the results of the simplified combustion model are in reasonable accordance with results of the conventional model. Further downstream, when entering the reaction zone, the fluctuation profiles become very similar. This encourages the conclusion that the internal structure of the flame is predicted very similar with the simplified combustion model and that in principle only an "offset in reactivity" exists between the two versions of the combustion model. This theory is further supported by the fact that the internal structure of laminar diffusion flames

and their approximated counterparts are very similar (compare Fig. 3.6 and 3.10).

4.5 First conclusions about the implemented model

The implemented turbulent combustion model based on igniting and extinguishing laminar diffusion flamelets (at unity Lewis number) has been subjected to a first test. In the considered UFPV approach proposed for autoignition problems, the progress variable is in this case defined including the main combustion product (H_2O) and a key radical species for autoignition (HO_2). The presumed-PDF model, presented in a detailed way in Chapter 3, leads to a formulation of the problem in a RANS framework in terms of mean mixture fraction $\widetilde{Z}$ and its variance $\widetilde{Z''^2}$ as two of the key parameters of the model. Solid prediction of the mean mixture is obtained with the usual adjustment of the constant $C_{\varepsilon 1} = 1.6$ in the $k-\varepsilon$ turbulence model and an adequate choice of the turbulent Schmidt number on the one hand. Good results for the mixture fraction variance can be obtained on the other hand by setting the model constant $C_\chi = 3$. Though mixing is affected by combustion, it has to be pointed out that the turbulence model plays the key role in the prediction of these two mixture properties. In this context it can be noted that the $k-\varepsilon$ model performed reasonably good. An alike study was conducted with the same combustion model but with a more sophisticated turbulence model namely the LRR-IPM second moment closure approach and presented in [11]. The results presented therein are in good agreement with those of this work though some small differences might be observed in the radial profiles close to the flame base. The LRR model seems to perform slightly better in some regions of the flame especially where density gradients are present. The implemented formulation implies a model for the fluctuations of the progress variable and of the other flamelet properties which only depend on the fluctuations in Z due to the β-PDF and the fluctuations in χ_{st} due to the log-normal distribution with fixed variance σ. In this framework, one may consider in a straightforward way the use of different presumed PDF shapes for Z or χ_{st} in the future, in particular if the model would be extended to LES.

The turbulent combustion model was applied to a H_2/N_2 turbulent lifted jet flame in a vitiate coflow. At first, it was shown that the conventional model leads to very good results compared to the experimental data for the flame stabilized around ten nozzle diameters, after adjusting the coflow temperature. Both formulations of reaction terms, $\dot{Y}_c$ and $\dot{\omega}_{Y_c}$, lead to good agreement

with experimental data, although with different adjustments of the coflow temperature. It is further demonstrated that the results for fluctuations of temperature and H_2O mass fraction are quite sensitive to the choice of the model parameter σ, and that both the mean and the fluctuations of OH mass fraction are sensitive to this parameter. Moreover, the predicted trend for the dependence of the flame lift-off height is predicted correctly (especially at high coflow temperatures). However, at low coflow temperatures the combustion model slightly underestimates the liftoff height. A possible reason is discussed in [11], but further investigations are indeed needed to better understand these trend. A first résumé of the implemented turbulent combustion model turns out satisfactory. All obtained results for this test case are comparable with results published by others and obtained with similar or even quite different modeling approaches. The combustion model can be considered well-suited to model turbulent combustion problems dominated by autoignition effects.

In a second step, the simplified version of the combustion model based on the ADF method is applied to model this hydrogen flame and subjected to a first qualitative comparison. The good quality of the results obtained with the simplified combustion model is certainly linked closely to the careful choice of the progress variable Y_c for which the flamelet equation is solved in this case. Indeed, deeper investigations of the two different combustion model versions might be made in order to obtain amplified insight on possible further differences between the different approaches. However, the observed performance of the simplified combustion model encourages its application to a more complex configuration and fuel, for what this approximation was originally developed. Moreover, [12] also demonstrated the applicability of the ADF approach in combination with a quite similar combustion model in a lifted methan-air jet flame in an almost identical configuration [13].

Bibliography

[1] Cabra R., Myhrvold T., Chen J. Y., Dibble R. W., Karpetis A. N. and Barlow R. S. "Simultaneous Laser Raman-Rayleigh-LIF Measurements and Numerical Modeling Results of a Lifted Turbulent H2/N2 Jet Flame in a Vitiated Coflow". *Proc. Combust. Inst.*, Vol. 29, pp. 1881–1888, 2002.

[2] Cao R. R., Pope S. B. and Masri A. R. "Turbulent lifted flames in a vitiated coflow investigated using joint PDF calculations". *Combust. Flame*, Vol. 142, pp. 438–453, 2005.

[3] Saxena P. and Williams F. A. "Testing a small detailed chemical-kinetic mechanism for the combustion of hydrogen and carbon monoxide". *Combust. Flame*, Vol. 145, pp. 316–323, 2006.

[4] Najafizadeh S. M. M., Sadeghi M. T., Sotudeh-Gharebagh R. and Roekaerts D. J. E. M. "Chemical structure of autoignition in a turbulent lifted H2/N2 jet flame issuing into a vitiated coflow". *Combust. Flame*, Vol. 160, pp. 2928–2940, 2013.

[5] Masri A. R., Pope R. Cao S. B. and Goldin G. M. "PDF calculations of turbulent lifted flames of H2/N2 fuel issuing into a vitiated co-flow". *Combust. Theory Modelling*, Vol. 8, pp. 1–22, 2004.

[6] Patwardhan S. S., De S., Lakshmisha K. N. and Raghunandan B. N. "CMC simulations of lifted turbulent jet flame in a vitiated coflow". *Proc. Combust. Inst.*, Vol. 32, pp. 1705–1712, 2009.

[7] Vicquelin R. *Tabulation de la cinétique chimique pour la modélisation et la simulation de la combustion turbulente.* Doctoral Thesis, Ecole Centrale Paris, 2010.

[8] Najafizadeh S. M. M., Sadeghi M. T. and Sotudeh-Gharebagh R. "Analysis of autoignition of a turbulent lifted H2/N2 jet flame issuing into a vitiated coflow". *Int Journal Hydrogen Energy*, Vol. 38, pp. 2510–2522, 2013.

[9] Wu Z. J., Starner S. H. and Bilger R. W. "Lift-off heights of turbulent H2/N2 jet flames in a vitiated co-flow". *Australian Symposium on Combustion and the 8th Australian Flame Days*, pp. 142–147, Melbourne, 2003.

[10] Gordon R. L., Masri A. R., Pope S. B. and Goldin G. M. "A numerical study of auto-ignition in turbulent lifted flames issuing into a vitiated co-flow". *Combust. Theory Modelling*, Vol. 11, pp. 351–376, 2007.

[11] Naud B., Novella R., Pastor J. M. and Winklinger J. F. "RANS modelling of a lifted H2/N2 flame using an unsteady flamelet / progress variable approach with presumed PDF". *Combust. Flame*, 2014. (accepted for publication).

[12] Michel J.-B., Colin O., Angelberger C. and Veynante D. "Using the tabulated diffusion flamelet model ADF-PCM to simulate a lifted methane-air jet flame". *Combust. Flame*, Vol. 156, pp. 1318–1331, 2009.

[13] Cabra R., Chen J.-Y., Dibble R. W., Karpetis A. N. and Barlow R. S. "Lifted methane-air jet flames in a vitiated coflow". *Combust. Flame*, Vol. 143, pp. 491–506, 2005.

Chapter 5

Reactive diesel-like sprays

Contents

5.1 Introduction

The application of the implemented turbulent combustion model to the modeling of reactive sprays is presented in this chapter. In this introduction, the motivation and objectives of this study are outlined and, furthermore, the methodology and some useful adaptations of the modeling strategy are resumed. The combustion model as it is applied here may be interpreted as further development of the more basic combustion models applied to the same configuration in [1].

5.1.1 Motivation

As already discussed in detail in Chapter 1, liquid fuels are applied in the vast majority of industrial applications, amongst which internal combustion engines and gas turbines are certainly the most famous examples. It is therefore of especial interest to study such multi-phase combustion problems (i.e. reactive sprays), which represent an extensive field of investigation. In this work the focus lies on combustion processes under conditions similar to those of diesel engines.
Combustion processes in multi-phase flow, however, are even more complicated than in single-phase flows. Moreover, the realization of experiments, often based on optical studies, in this area is also much more complicated. That is why less and especial not so detailed experimental data is available for such problems as for example laboratory flames such as the one presented in the previous chapter. Due to this fact, investigation by means of computational models is even more important.
The Engine Combustion Network (ECN) [2] was founded several years ago with the aim to concentrate the investigation efforts and to coordinate experimental and computational research in the complex area of engine research. This network provides a noteworthy database [3] of experiments of reactive sprays under diesel-like conditions. The one considered in this work is the so-called "Spray H" which uses n-heptane as a surrogate for diesel fuel. Hence, it is reasonable to apply the combustion model to a set of cases of the "Spray H" type documented in this database.

5.1.2 Objectives of the study

The final objective of this chapter coincides in principle with the main objective of this work, the simulation of reactive sprays under diesel-like conditions. For this purpose, the first objective is the adaptation of turbulent combustion model to the configuration of such reactive sprays. A further direct consequence of the main objective is the prediction of global properties of the flame, principally the ignition delay and the lift-off length. These properties can furthermore be compared with available experimental data. Beyond the comparison with experiments, an analysis of the predicted igniting and quasi-steady flame structure shall be conducted.

5.1.3 Methodology of the study

The methodology of this study is explained in the following as well as some useful and suitable adaptations of the modeling strategy to the characteristics of the considered combustion problem, namely the transient and multi-phase flow and the complex fuel.

Since this study concerns multi-phase flow, spray modeling needs to be considered in a first step. Modeling of sprays, which is in principle out of the scope of this work, by itself is a wide and complex field of research with abundant literature about it [4–8]. However, correct and reliable predictions of the spray are a necessary basis for the subsequent combustion modeling. Hence, the focus in this work lies on a good adjustment of the spray modeling with available experimental data of the inert, vaporizing spray [3]. For this purpose it is resorted to the default spray model of OpenFoam 1.6, the implemented discrete droplet model (DDM) approach, which is employed together with the "blobs"-atomization model [9, 10], Reitz' KHRT breakup model [11] and the Ranz-Marshall model [12] for droplet evaporation. DDM is based on an Lagrangian approach, and it is described in detail together with its submodels in [13], a work performed in the OpenFoam environment too. Once a satisfying setup of the spray modeling was found for the inert spray, it will be used throughout the following simulations of reacting sprays. The most important parameters of the model setup are resumed in Section 5.2.

As already mentioned above, n-heptane is the applied fuel in the "Spray H" cases. It was shown for instance in [14], that n-heptane can be considered an adequate choice to act as surrogate for diesel fuel. Problems arise in the calculation of the flamelet solutions due to the comprehensive chemical mechanisms needed to describe the complex oxidation process of n-heptane. The chemical mechanism of [15] used in this work includes 110 species and 1170 reactions. This is prohibitive for the use of DF solutions at reasonable effort, for which reason the ADF method described in Section 3.3 is adopted in this study. Then, the coupling by means of tabulated species mass fractions described in Section 3.5.3 is employed to link the compressible CFD solver with the simplified version of the turbulent combustion model that is based on the ADF solutions.

The advised adaptations of the modeling strategy concern the range and the handling of the set of approximated flamelets. First, the range of the considered mixture fraction values is limited between zero and the saturation mixture fraction Z_s, which corresponds to the local maximum mixture fraction

close to the droplet surface. This saturation mixture fraction depends on the oxidizer and fuel temperature, the ambient pressure, and the composition [16]. Z_s finds its way in the PDF of the mixture fraction (Eq. (3.17)) as discussed in Section 3.4.3. Note that a value of $Z = 1$ corresponds to liquid fuel in this case, while Z_s takes values close to 0.5 under the considered conditions. The stoichiometric mixture fraction Z_{st} is about 0.062 for the given conditions, thus far below the saturation mixture fraction.
Second, only auto-igniting ADF solutions are considered as suggested in [17]. Flamelets with strain rates above the auto-ignition range, are supposed to remain in their inert state and, therefore, their reaction rate is supposed to be zero. This assumption is critically analyzed in the section of results, but it might be considered practicable in advance in the considered auto-igniting configuration. Moreover, findings of experimental studies [18] suggest that flame lift-off under similar conditions seems to be affected by ignition phenomena. The use of chemistry tables based on auto-igniting flamelets only, reduces significantly the effort needed to obtain ADF solutions. On the one hand less flamelets have to be calculated due to the reduced range of strain rates considered. On the other hand, and even more important, there is no need to calculate the S-curve which may be quite laborious and not straightforward in some cases. Moreover, the limitation to auto-igniting flamelets allows their synchronization in time (discussed in Section 3.4.3) as originally suggested for the ADF approach in [19] and also applied in [17].
Third, a delay criterion is introduced for the ADF method in this case in order to improve the predictions of the ignition delay (especially for high values of mixture fraction). The need and the benefit of such a criterion in the ADF approach was investigated in detail in [19] for n-heptane. A simplified but robust criterion is applied in this work, which acts on the source term of the flamelet equation of the PV (Eq. (3.8)):

$$\dot{\omega}_{Y_c}(Z, c) = \begin{cases} 0, & t < \tau^*(Z) \\ \dot{\omega}_{Y_c}^{\mathrm{HR}}(Z, c(t)), & t \geqslant \tau^*(Z) \end{cases} \tag{5.1}$$

The time τ^* is defined as the time needed by a homogeneous reactor with mixture fraction Z to reach $c = 5 \cdot 10^{-4}$.

With this adapted modeling strategy, the turbulent combustion model is applied to simulate a chosen base case of the “Spray H”. Similar to the study of the hydrogen flame, the influence of the main model parameters are investigated. Since less detailed experimental data is available in this case compared to the jet flame of Chapter 4, only the predictions of the ignition delay and the lift-off length can be compared with experiments.

Finally, the influence of the ambient temperature on the ignition process and the quasi-steady flame structure is studied. For this purpose, the initial ambient temperature is varied within a range of 800 K to 1200 K.

5.2 Case setup and boundary conditions

The "Spray H" experiments have been performed in the constant volume combustion vessel at Sandia National Laboratories (Livermore (CA), USA). Detailed specifications about this vessel can be found in [20]. The simulations are performed on the assumption of 2D axial symmetry in order to save computational effort. The resolution of the structured, uniform 2D computational mesh is 0.25 mm in radial direction and 0.5 mm in axial direction, and is actually a 10° wedge consisting of 3D cells similar to the mesh used for the jet flame. The mesh resolution is primarily determined by the spray modeling, since the DDM results depend on the combination of mesh size and time step size. The time step size of the transient calculation is maintained constant at a value of 0.2 μs. Both basic calculation parameters were found in previous parameter studies.

The most important boundary conditions are resumed for all considered cases in Table 5.1, where the case with an ambient temperature of $T_0 = 1000$ K represents the base case. More detailed information on further parameters of

Table 5.1. *Boundary conditions of reactive "Spray H" cases.*

Ambient temperature T_0 [K]	800	900	**1000**	1100	1200
Ambient pressure p_0 [MPa]	3.37	3.79	4.21	4.64	5.06
Fuel temperature T_f [K]			373		
Mole fraction of O_2 [%]			21		
Nozzle diameter d [mm]			0.1		

the experimental setup can be found in the Data Search Utility of the ECN [3]. In the calculations, the ambient temperature and the ambient pressure are set as initial conditions in the computational domain. Those values yield an initial density of about 14.6 kg/m^3, which lies close to the so-called "gas density in the core region of the vessel" stated with 14.8 kg/m^3 in the Data Search Utility. Note, that for the inert case with $T_0 = 1000$ K (calculated for adjustment of the spray setup) the ambient pressure is changed to 4.39 MPa in order to

obtain the same density as in the experiment, since the ambient composition is pure nitrogen in this case.

For the fuel mass flow rate through the injector nozzle, the recommended rate of injection (ROI) profile stated in [21] is imposed as suggested by the ECN. This injection profile has a mean value of 2.7 mg/ms and a ramp at the start and the end of injection. The injector nozzle diameter and the fuel temperature are specified as stated in Table 5.1. Certainly, the injector axes coincides with the symmetry axis of the computational mesh.

The default values are retained for most of the parameters of the spray submodels. However, some parameters are adjusted in order to obtain better agreement with the available experimental data. The spray angle is set to 15°, the droplet-nozzle-diameter ratio is fixed with 0.95 and the constant B_1 of the breakup model is set to 30. The turbulent Schmidt number is 0.9 for the whole study (as for the hydrogen jet flame). At this point it shall be noted again, that all these parameters are adjusted together with the mesh size and the time step size in order to improve the spatial and temporal predictions of the spray evolution. Furthermore, the turbulence model plays indeed an important role in the modeling of the spray. As in the hydrogen jet flame, the standard $k - \varepsilon$ turbulence model is employed again. The constant $C_{\varepsilon 1}$ is set to 1.52 in this study, a value that is also suggested in [22].

As before, the unity Lewis number assumption is employ here. The validity of this assumption was studied for n-heptane flames under similar conditions of those found in this work by [23]. In a further study [24], a comparison of results from a flamelet calculation with unity Le assumption and results from a DNS without unity Le assumption showed that predicted ignition delays are within 5%.

5.3 Results

At the beginning, the results of the inert spray are presented. These results allow an evaluation of the quality of the spray modeling, which is the basis for reliable modeling of the actual combustion process. Moreover, more detailed experimental data is available for the inert, vaporizing spray. Then, the transient behavior of the igniting flame is investigated. Finally, results of the flame structure in its quasi-steady state are presented.
In contrast to the previous chapter, the equivalence ratio ϕ is used here instead of the mixture fraction Z for the representation of results, since ϕ is more common in the area of engines.

5.3.1 Distribution of the inert spray

The temporal evolution of the liquid length (LL) and the vapor penetration (VP) are shown in Fig. 5.1. Very good agreement can be observed for the liquid length. Despite some small deviations, also the global trend of the vapor penetration is well captured.

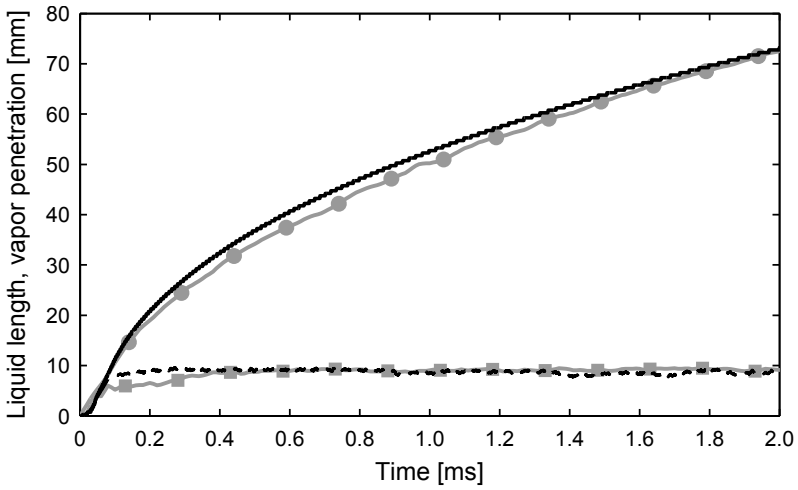

Figure 5.1. *Liquid length and vapor penetration under inert conditions. Gray: experimental data of LL (squares) and VP (dots) / Black: modeling results of LL (dashed) and VP (solid).*

The concentration of the mean mixture fraction along the symmetry axis at two different instants—0.9 ms and 1.13 ms—is presented in Fig. 5.2. In

general, satisfactory agreement with experimental data can be obtained with the adjusted setup. The observable differences at 0.9 ms at the tip of the spray coincide with the previously detected deviations in the vapor penetration. Concerning the differences in the near field of the injector (below 20 mm axial distance), one has to keep in mind that measurements in high-density regions of the spray are very complicated and subjected to measuring errors. This could be a possible explanation for the observed differences, which are however within an acceptable range. Especially at 1.13 ms, a similar trend can be observed. Radial profiles of the mean mixture fraction and its variance for

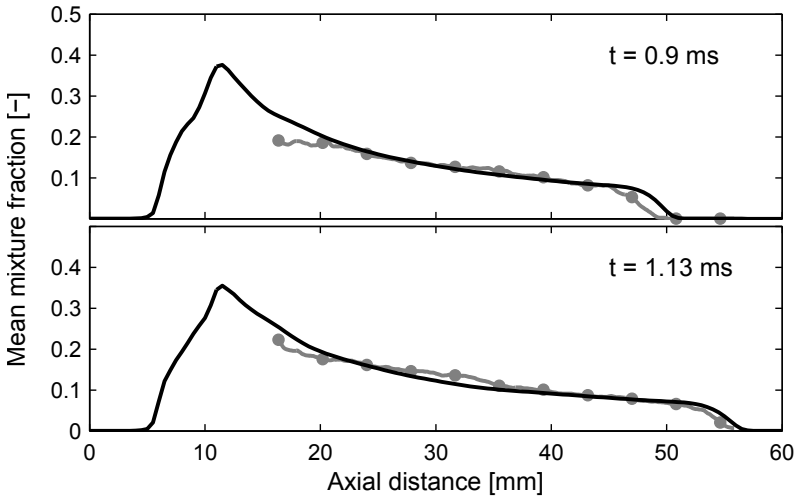

Figure 5.2. *Mean mixture fraction along the centerline at two different instants. Symbols: experimental data / Black lines: modeling results.*

the same instants as before are shown in Fig. 5.3 and 5.4. Concentrating at first on the profiles of the mean mixture fraction in the columns on the left, one can observe generally reasonable agreement of the calculated distribution with experimental data. The measured profiles show a slight asymmetry, whereas the calculated profiles are perfectly symmetric due to the applied assumption of axial symmetry. Furthermore, better accordance between simulation and experiment can be noticed for the profiles closer to the injector, at an axial distance of 20 mm and 25 mm. The reason for this is that special attention is payed on this region of the spray during the adjustment of the modeling setup, since expected lift-off lengths lie around this distance. Although great effort was made in the fine tuning of the spray modeling, no better results could be obtained for a wider range with the adopted DDM approach. The variance of the mixture fraction is depicted in the right column of Fig. 5.3

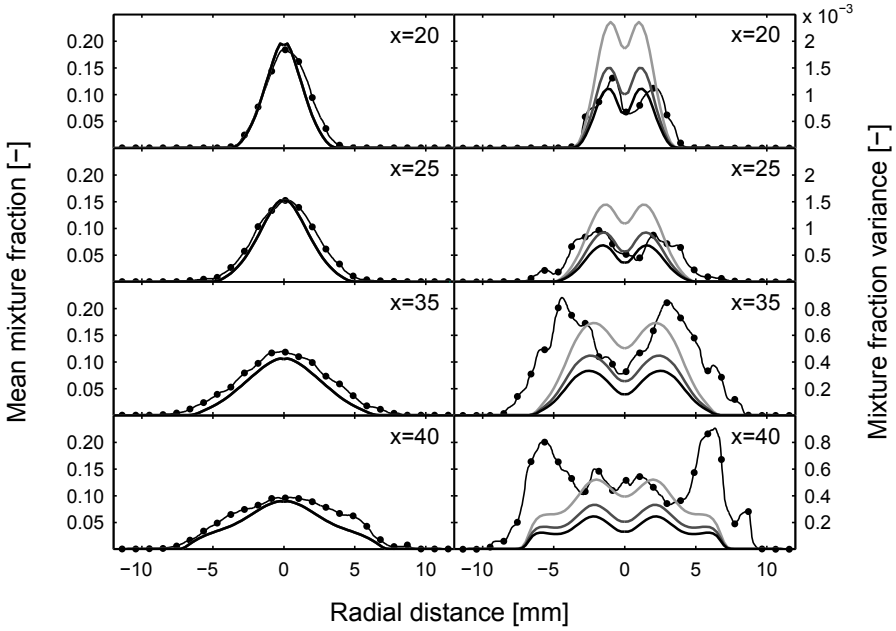

Figure 5.3. *Radial profiles of mean mixture fraction and its variance at 0.9 ms after start of injection. Symbols: experimental data / Lines: modeling results with $C_\chi = 2$ (light-gray), $C_\chi = 3$ (gray) and $C_\chi = 4$ (black).*

and 5.4 for different values of C_χ. A similar trend can be observed as for the previously presented hydrogen jet flame, an increase of C_χ leads to an decrease of the variance. In general, a value of $C_\chi = 3$ seems to be a reasonable compromise. However, especially in the far field of the spray lower values of this parameter seem to perform better, whereas in the near field of the spray slightly higher values might be a preferential. With the same argumentation as before, more importance is given to good agreement of the model predictions with experiments closer to the injector. The differences observed for the two most downstream profiles, are probably linked to the before noticed differences for the mean mixture fraction for these axial positions. Concluding, the mean mixture fraction and its variance, particularly in the near field of the spray, are predicted with reasonable accuracy. The setup of the spray modeling can therefore be considered well adjusted and suitable for its subsequent use in the modeling of the reactive sprays.

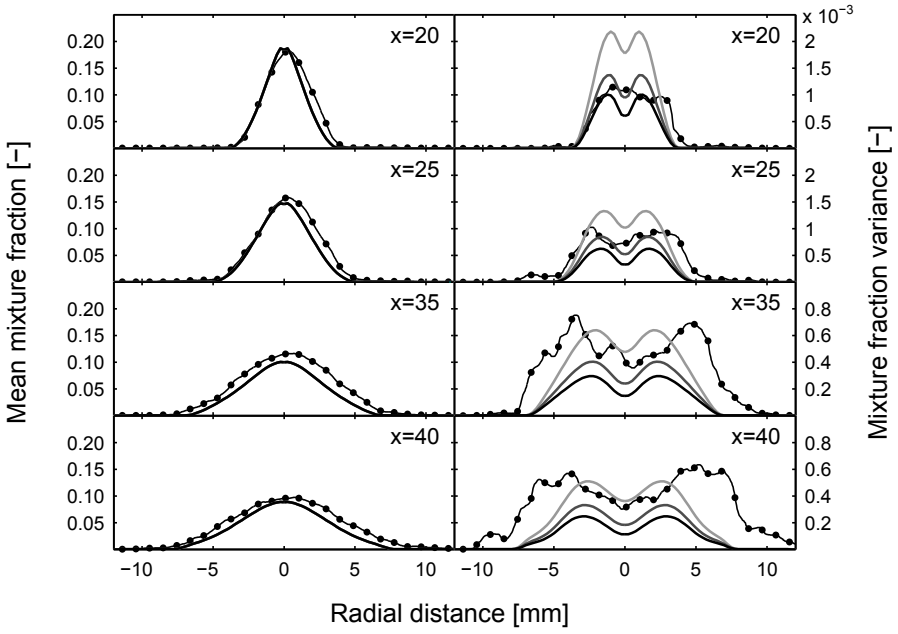

Figure 5.4. *Radial profiles of mean mixture fraction and its variance at 1.13 ms after start of injection. Symbols: experimental data / Lines: modeling results with $C_\chi = 2$ (light-gray), $C_\chi = 3$ (gray) and $C_\chi = 4$ (black).*

5.3.2 Transient igniting flame structure

In this subsection, the influence of C_χ and σ on the transient igniting flame structure is studied at first on the basis of the base case ($T_0 = 1000$ K). Then, the influence of the ambient temperature on the ignition process is presented.

Influence of C_χ

The mean temperature distribution of the igniting flame for three different values of C_χ is plotted at instants close to the ignition delay (ID) in Fig. 5.5. It is immediately apparent that using $C_\chi = 2$ leads to very different ignition behavior. Considering the results obtained for the inert spray configuration, such differences could be expected in advance. Not only the ignition location is quite different, also the ignition delay of about 0.78 ms is predicted much higher compared to the two other cases. In contrary, no big difference can be found between using $C_\chi = 3$ or $C_\chi = 4$, neither for the spatial structure of the ignition nor for the ID, which is predicted with about 0.63 ms and 0.6 ms, respectively.

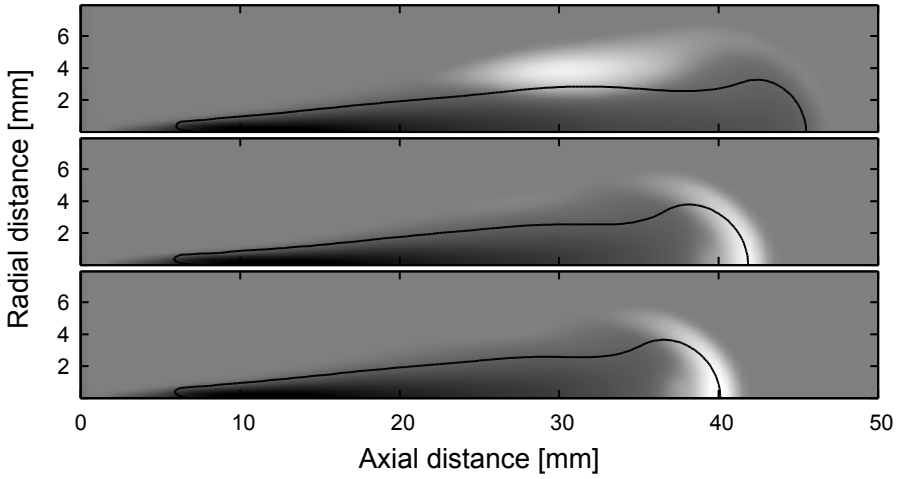

Figure 5.5. *Mean temperature around autoignition with $T_0 = 1000$ K and $\sigma = 1$. Top: $C_\chi = 2$ / Middle: $C_\chi = 3$ / Bottom: $C_\chi = 4$. Black line: stoichiometric isoline.*

Precaution is indeed demanded when comparing unsteady RANS results with experimental data such as luminosity images, since in doing so, calculated mean values are compared to snapshots of the combustion problem. However, an experimental study [25] made under comparable conditions in the same

vessel based on such images, suggests similar trends of the spatial structure of igniting diesel-like sprays then those found here. But as already said before, unsteady RANS results might not be the most adequate type for such investigations, whereas results obtained in a LES environment would certainly be more appropriate.

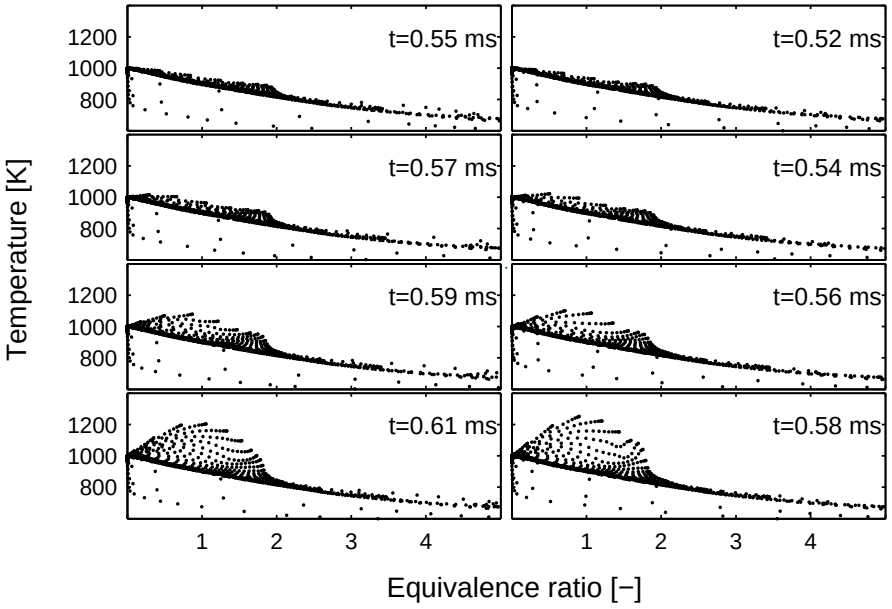

Figure 5.6. *Mean temperature as function of the mean equivalence ratio for different instants around autoignition with $T_0 = 1000$ K and $\sigma = 1$. Left: $C_\chi = 3$ / Right: $C_\chi = 4$.*

A representation of the ignition process in the equivalence ratio space is given in Fig. 5.6 for the cases with $C_\chi = 3$ and $C_\chi = 4$. As already observed before, no major difference exists between these two cases apart from a small offset in time (stated in the figure). The mean temperature distribution as a function of the mean equivalence ratio due to mixing can be seen at the top $\phi - T$ maps. In both cases a small onset of temperature rise indicating reaction can be observed at about $\phi = 2$. Consequently, this equivalence ratio is referred to be the most reactive equivalence ratio. The ignition process advances then towards lower equivalence ratios, with very similar combustion progress observable for the two considered cases. Akin findings are presented in [26] where the same flame was simulated by means of a combustion model based on the TPDF approach. Considering the obtained results in the inert

spray configuration and those presented above, a value of $C_\chi = 3$ is retained for further studies.

Influence of fluctuation of χ_{st}

Just to remind, the fluctuation of stoichiometric scalar dissipation rate is model by means of presumed PDF. Two different assumptions are adopted in this study, the log-normal PDF with a fixed variance of $\sigma^2 = 1$ (i.e. a standard deviation of $\sigma = 1$) and a δ-PDF which means to assume no fluctuation at all.

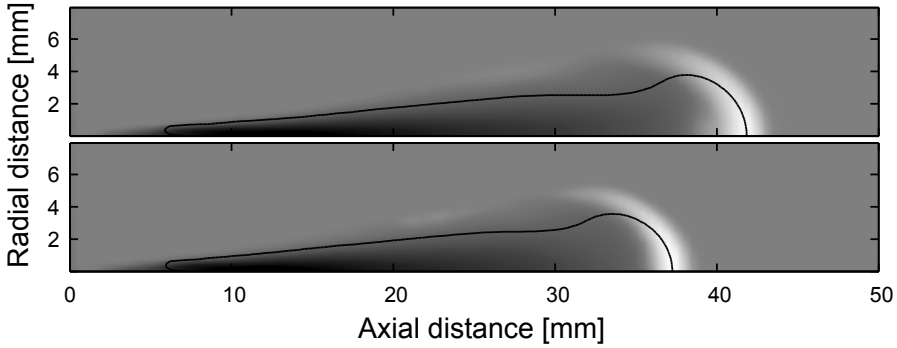

Figure 5.7. *Mean temperature around autoignition with $T_0 = 1000$ K and $C\chi = 3$. Top: $\sigma = 1$ / Bottom: δ-PDF. Black line: stoichiometric isoline.*

The transient flame structure at $T_0 = 1000$ K close to the point of autoignition is shown in Fig. 5.7 as predicted when using $C_\chi = 3$. At the top the result obtained with $\sigma = 1$ is presented, and at the bottom the result based on the assumption of a δ-PDF for χ_{st} is shown. No major differences in the predicted distributions can be found between the two solutions. Just different penetration can be noticed, since the solutions are plotted at different time—at 0.63 ms the result with $\sigma = 1$ and at 0.52 ms the one with the δ-PDF—due to differences in the ID. It was found that the assumption of δ-PDF leads to slightly shorter ignition delay compared to the case where a log-normal distribution is assumed for χ_{st}.

Looking at Fig. 5.8, where additionally to the temperature distribution also isolines of χ_{st} are shown at the same time again for the case with $\sigma = 1$, one can observe that ignition occurs at low to moderate values of χ_{st}. The ignition delay of transient ADF solutions as a function of the stoichiometric scalar dissipation rate is shown in Fig. 5.9 for the base case. The ignition delay

is here defined as the time needed by a flamelet at a given strain rate (i.e. χ_{st}) to reach 10% of the normalized PV. This ID varies little over a wide range of χ_{st}, but rises rapidly at a certain value of scalar dissipation rate which lies close to χ_{AI}. Despite this characteristic of igniting flamelets, assuming different

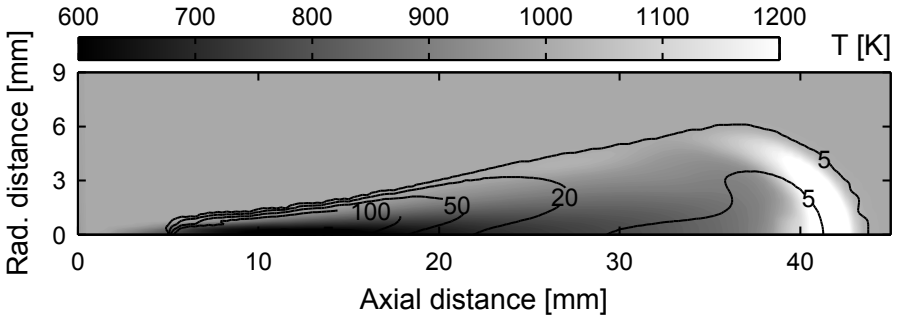

Figure 5.8. *Mean temperature of base case (using $\sigma = 1$) around autoignition and isolines of stoichiometric scalar dissipation rate.*

distributions of χ_{st} results in different combustion progress. The use of $\sigma = 1$ leads to a contribution of less reactive—interpreted as "slower"—flamelets as if only the chemical information at $\widetilde{\chi}_{st}$ is taken from the turbulent flamelet table as done with the δ-PDF assumption. The differences might be small at the beginning of the process, but different chemicals paths are taken from the first instant. Since from the first moment, different chemical information is read from the table for the different PDFs, the resulting chemical path of the transient combustion process is different. In a further consequence this

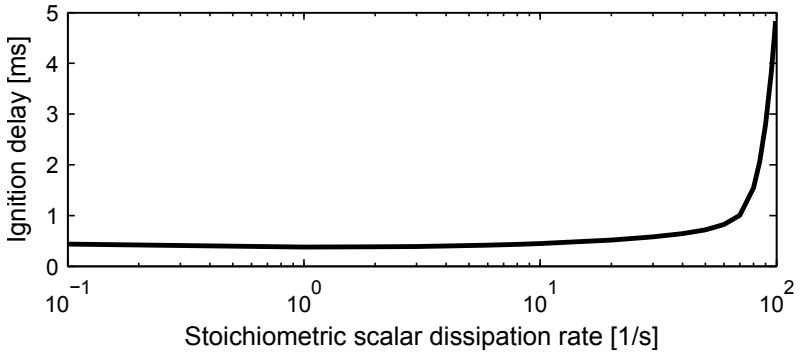

Figure 5.9. *Ignition delay as a function of the stoichiometric scalar dissipation rate for the set of ADFs of the base case.*

leads to different heat release, which in turn has influence on the turbulent

flow field, e.g. density, as touched in Chapter 2. It could be observed that the scalar dissipation rate decreases in high temperature regions, i.e. where combustion occurs, which again has impact on the chemistry. So there exists complex interaction with back coupling and mutual influence of the different phenomena involved in the ignition process as for instance discussed in [27].

Influence of ambient temperature

Finally, a quantitative comparison of simulation results with experimental data is made for different ambient temperatures in order to verify the predictive capability of the turbulent combustion model. The ignition delay as a function of the ambient temperature is plotted in Fig. 5.10 for both assumptions for the PDF of χ_{st} together with experimental data.

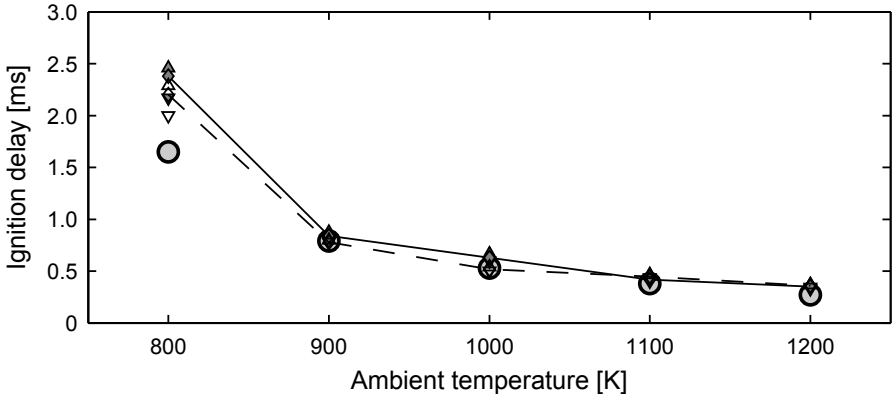

Figure 5.10. *Ignition delay as function of the ambient temperature using C_χ = 3 for σ = 1 (solid, filled symbols) and δ-PDF (dashed, empty symbols). Circles: experimental data / Evaluated with different criteria: diamonds: T_0 + 400 K, upward triangles: $(T_{max} + T_0)$ / 2 and downward triangles: 20% of steady HRR.*

First of all, no unique criteria for the evaluation of the ID exists [1], quite the contrary, many different definitions can be found in the literature (e.g. in [28]). For that reason, in this work several criteria are employed for the evaluation of the ID in order to estimate the impact of the criteria definition. The three criteria are, (1) the time needed to reach a maximum temperature of $T_0 + 400\,K$, (2) the time needed to reach a maximum temperature of $(T_{max} + T_0)/2$, and (3) the time needed to reach 20% of the mean heat release

[1] It may be noted, that the comparability or the way how to compare computational results with experimental data is an important issue within the ECN.

rate (HRR), which is about 24 J/ms in this case. The resulting ignition delays are all shown in Fig. 5.10. The trend of the ignition delay for different ambient temperature is in general well predicted with both assumptions for distribution of the stoichiometric scalar dissipation rate. Just for the case with $T_0 = 800$ K too long ID is predicted with both assumptions. It is interesting to mention, that very similar results are presented for the ID in [29] where a TPDF approach was used together with the reduced mechanism of Lu [30].
Concerning the three different criteria for the ID, no important impact can be observed at high ambient temperatures, i.e. low ID and fast ignition process. Indeed, some scattering in the ID values can be noticed in the case of $T_0 = 800$ K, which shows a relatively slow ignition process.
The use of a log-normal distribution for χ_{st} leads to clearly longer ID for low to medium ambient temperature, while the differences are less distinctive in case of the two high ambient temperatures.

Besides the expected influence of the ambient temperature of the ignition delay, a further observation could be made concerning the location of autoignition. This location is found to be close to the tip of the spray (see Fig. 5.12 and 5.8), i.e. relatively far away from the liquid length, for the base case and those with lower ambient temperature. However, at increased ambient temperature (apart from shorter ID) the ignition location moved further upstream along the sides of the spray in a region of high species and temperature gradients as shown in Fig. 5.11 for $T_0 = 1200$ K. A qualitatively similar trend is reported in an experimental study of diesel spray ignition under similar conditions [25]. The ignition location is also located in a region with

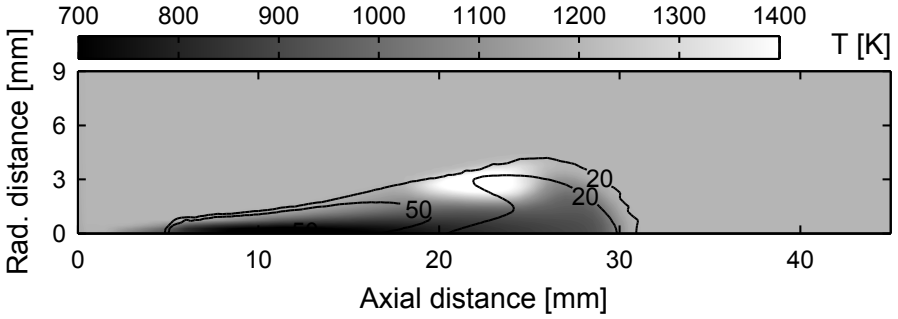

Figure 5.11. *Mean temperature for $T_0 = 1200$ K (using $\sigma = 1$) around autoignition and isolines of stoichiometric scalar dissipation rate.*

significantly higher stoichiometric scalar dissipation rate—the autoignition limit is shifted to higher values of χ_{st} with increasing temperature—compared

to the base case. As a consequence of the noticeably reduced ignition delay at high ambient temperatures, the ignition location lies closer to the liquid length and low temperature regions are present especially in the center of the spray. This fact seems to play are role in the shift of the ignition location outward into regions of higher temperature.

The obtained results for the transient flame structure encourage the conclusion that the applied adaptations—limitation to autoignition range and delay criterion—of the modeling strategy, which effect those findings, are reasonable (at least) for the considered conditions.

5.3.3 Quasi-steady flame structure

Lastly, the flame structure at quasi-steady state is investigated in the following. The quasi-steady state is here defined by means of a temporally constant lift-off length. First, the influence of the two principle modeling parameters is studied on the basis of the base case ($T_0 = 1000$ K) again. Then, the impact of diverse ambient temperature on the lift-off length as well as the quasi-steady flame structure is analyzed. As for the ID, different criteria for the evaluation of the lift-off length (LOL) are employed. The lift-off is then the shortest axial distance between the injector tip and a certain threshold value in the flame domain defined as (1) 2% of the maximum of the mean mass fraction of OH in the flame, (2) an OH mean mass fraction of $1 \cdot 10^{-4}$, and (3) a mean temperature of $T_0 + 400$ K.

Influence of C_χ

At first, during the study of the inert spray configuration (Section 5.3.1) a value of $C_\chi = 3$ was found to be the best compromise concerning the variance of the mixture fraction, particularly at axial distances where lift-off is expected. Anyhow, no major influence of this model parameter on the lift-off length could be observed when changing C_χ to a value of 4, which also gave reasonable predictions of the variance. The observed differences lie at least within the range of the axial resolution of the computational mesh (0.5 mm). Hence, a value of $C_\chi = 3$ is retained for the rest of this study.

Influence of fluctuation of χ_{st}

The mean temperature distribution of the base case at quasi-steady state is shown in Fig. 5.12 when using a log-normal PDF with $\sigma = 1$ and a δ-PDF to model the distribution of χ_{st}. The adoption of the δ-PDF leads to a shorter lift-off length, compared to the experimental value actually too short. The rest of the flame structure is virtually identical. A similar behavior is documented in [17] for a methane/air jet flame. Indeed, a shorter lift-off length suggests higher reactivity.

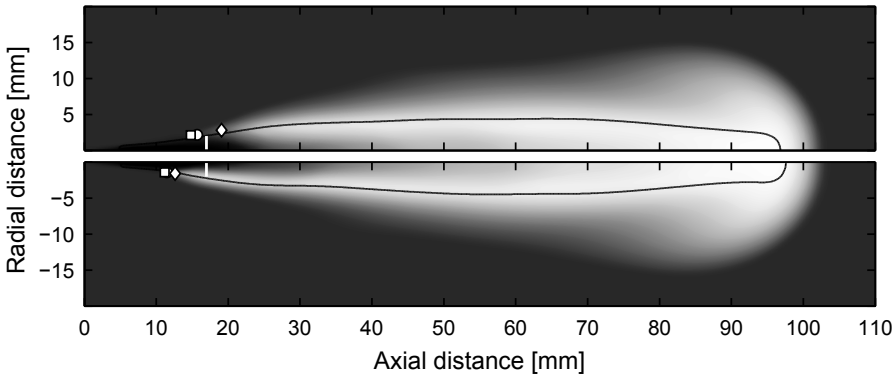

Figure 5.12. *Mean temperature of the base case at quasi-steady state when using σ = 1 (top) and when assuming a δ-PDF for χ_{st} (bottom). White line: experimental data / Square: 2% of max. of $\widetilde{Y}_{OH}$ / Circle: $\widetilde{Y}_{OH} = 1 \cdot 10^{-4}$ / Diamond: T_0 + 400 K. Black line: stoichiometric isoline.*

Another difference can be revealed by plotting the mean temperature as a function of the mean equivalence ratio as done in Fig. 5.13 for the same cases. From this $\phi - T$ map, one can observe that use of the δ-PDF leads to higher reactivity of rich mixtures with values of ϕ up to about 5 within the reactive region. The adoption of a log-normal distribution with $\sigma = 1$ on the contrary gives $\phi \sim 3$ as richest reactive equivalence ratio.
This observation is in accordance with the differences found in the lift-off length, since a flame base stabilized closer to the injector is naturally situated at regions of higher equivalence ratio. Note, however, that the maximum mean temperature obtained close to stoichiometric conditions is the same as well as the lean slope of the $\phi - T$ map. Furthermore, the predictions of the rich slope coincide up to a value of $\phi \sim 3$. The only difference can be observed at even richer mixtures which correspond the rich (partially) premixed flame base. Exactly this difference can be crucial concerning the formation of soot as shown in [31]. In this basic study of DI diesel combustion it is shown that

the initial soot formation occurs in the rich premixed base of the flame. Owing to the lack of detailed experimental data about the composition in the flame (e.g. in form of a $\phi - T$ map), a verification of the modeling results can only be made based on a comparison of the lift-off length. Thus, considering the quasi-steady flame structures shown in Fig. 5.12, an internal flame structure related to the one shown on the left of Fig. 5.13 seems to be more probable. Continuing observations concerning the internal structure of the flame and possible consequences are discussed further below.

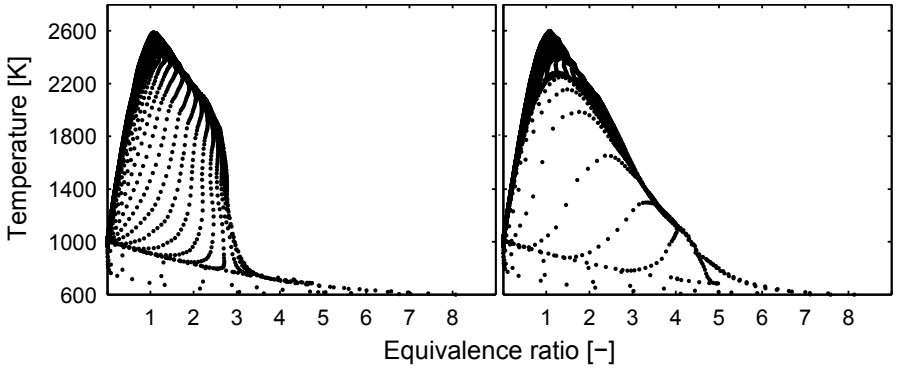

Figure 5.13. *Mean temperature as function of mean equivalence ratio of the base case at quasi-steady state when using $\sigma = 1$ (left) and when assuming a δ-PDF (right).*

An explanation for the differences found in the LOL for different χ_{st}-PDF assumptions may be given by means of the contour plot at the bottom of Fig. 5.14. This is a detailed view in the vicinity of the lift-off of the flame shown at the top of Fig. 5.12. At this ambient temperature the flame base is situated in a region of high scalar dissipation rate due to strong radial gradients and elevated turbulent dissipation. The autoignition limit ($\chi_{\mathrm{AI}} = 80\ {}^{1}/_{\mathrm{s}}$) is marked with white dots in this plot. Additionally, three isolines each marked with a percentage value are shown. These values represent the percentage of the probability of χ_{st} that lies above the autoignition limit χ_{AI}. More in detail, the value of the mean stoichiometric scalar dissipation rate $\widetilde{\chi}_{st}$ at any given location in the domain determines the shape of the log-normal PDF for χ_{st} (see Eq. (3.26)). Integration over this PDF naturally gives unity. Though, the integration over this PDF from χ_{AI} to infinity gives the values indicated in the contour plot. This percentages indicate then the weight of flamelets that are assumed to remain in inert state. The white point marks the lift-off length according to criterion (2), which lies in region of $\widetilde{\chi}_{st} < \chi_{\mathrm{AI}}$, but where inert flamelets weight almost 20%. This contribution of non-reactive

flamelets leads to an increased lift-off length. If on the other hand for the same $\widetilde{\chi}_{st} < \chi_{\mathrm{AI}}$ the assumption of a δ-PDF is used, only the chemical information at this mean stoichiometric scalar dissipation rate is read from the table without any contribution of flamelets at diverse strain rates.

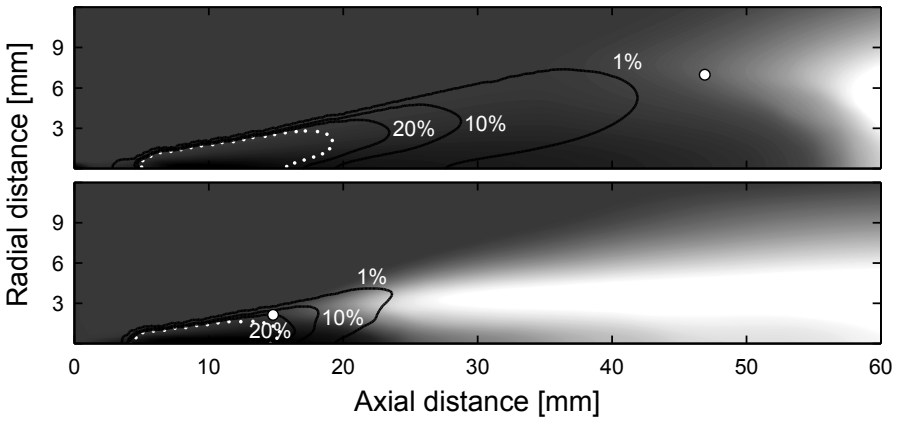

Figure 5.14. *Mean temperature of case with T_0 = 800 K (top) and T_0 = 1000 K at quasi-steady state, and isolines with indicated percentage of the log-normal PDF above χ_{AI}. White dots: isoline of χ_{AI} / White point: predicted lift-off length.*

Influence of ambient temperature

A quantitative comparison of calculated lift-off lengths with experimental data is made in Fig. 5.15. Values of LOL evaluated with the before mentioned criteria are shown for both assumptions of the χ_{st}-PDF. The experiments show that the lift-off length increases with decreasing ambient temperature, though it reacts more pronounced to temperature changes in the low temperature range than at high ambient temperatures.
At first, this non-linear relation between lift-off length and ambient temperature is reasonably reproduced with both modeling assumptions. However, the lift-off length is overall predicted too short when assuming a δ-PDF shape for the χ_{st} distribution. The calculations with a log-normal PDF perform in general significantly better, also in terms of absolute values. As already concluded in the section of the transient results, the obtained findings suggest that the employed adaptations of the modeling strategy are reasonable.
The difference in LOL for the two assumptions is indeed less distinctive in the case of T_0 = 800 K. The reason for this can be found when looking at

the contour plot at the top of Fig. 5.14. It shows a detailed view in the vicinity of the flame base of that case. In contrary to the explanation given before for the flame with $T_0 = 1000$ K (bottom contour plot in the figure), one can observe that in this case the flame base is stabilized far away from the injector. Consequently, low values of scalar dissipation rate—far away from indicated autoignition limit—exist in this region. Non-reactive flamelets have minor importance in this regions as can be deduced from the isolines with indicated weight percentages. Therefore, the shape of the χ_{st}-PDF appears to have less impact on the lift-off length at low ambient temperature. In the case with the highest ambient temperature tough, the lift-off length almost doubles when adopting the log-normal PDF compared to the value obtained with the δ-PDF. The explanation given before for the case with $T_0 = 1000$ K by means of Fig. 5.14 applies here too.

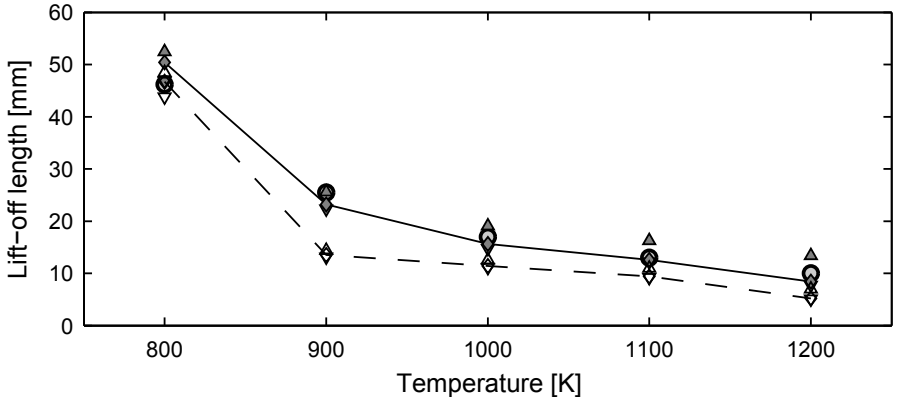

Figure 5.15. *Lift-off length as function of the ambient temperature using $C_\chi = 3$ for $\sigma = 1$ (solid, filled symbols) and $\sigma = 0$ (dashed, empty symbols). Circles: experimental data / Evaluated with different criteria: diamonds: $\widetilde{Y}_{OH} = 1 \cdot 10^{-4}$, upward triangles: T_0 + 400 K and downward triangles: 2% of max. $\widetilde{Y}_{OH}$.*

Several different theories of flame lift-off stabilization exist in the literature and till today also lively discussions goes on about this complex issue within the scientific community. A good review of some important theories is given in [32]. In the area of diesel-like sprays like those considered in this work, experimental findings suggest that autoignition phenomena play a major role in flame lift-off stabilization [18]. The influence of different parameters on the LOL in diesel sprays is resumed in the interesting review of [33]. The good agreement of modeling results and experimental data encourage the conclusion that igniting (approximated) diffusion flames are an adequate choice to model

such flames and retain fundamental physics and chemistry involved in the present combustion problem.
Furthermore, increasing influence of the modeling of the scalar dissipation rate distribution is observed in cases with high ambient temperature and consequently short lift-off length. As already discussed before, different assumptions for the χ_{st}-PDFs give quite different LOL results, since highly strained and non-reactive flamelets are weighted differently. Better results for the LOL are obtained when considering flamelets in a wider range of scalar dissipation rate, i.e. also those at higher strain rate. This finding suggests the following speculation that goes into the direction of the critical scalar dissipation concept [34]. When lift-off stabilization occurs in regions of high scalar dissipation rate (presence of strong gradients and turbulent dissipation), local extinction effects might play a role in the lift-off stabilization.
Based on the good agreement found between modeling results and experimental data in terms of the global flame parameter lift-off length, some further investigations try to give more detailed insight on the quasi-steady flame structure. Moreover, the following results and accompanying conclusions show the potential of combining CFD calculations and experimental studies.

The quasi-steady flame structure computed with $C_\chi = 3$ and $\sigma = 1$ at different ambient temperatures is plotted in Fig. 5.16 together with the stoichiometric isoline. Moreover, the predicted lift-off lengths evaluated according to different criteria are marked together with the corresponding experimental values. The two criteria based on the OH mass fraction yield very similar values of LOL, while the temperature criterion gives generally longer LOL. Note that the different flames are presented at different time, the three cases with high T_0 at 3 ms, the case with $T_0 = 900$ K at 4 ms, and the case with $T_0 = 800$ K at 7 ms. Since the injection duration is slightly below 7 ms, the 800 K case does hardly reach a quasi-steady state within this time. At first sight, the flame structures of the cases with $T_0 = 900$ K and upwards are quite similar apart from the different lift-off lengths. The typical structure of a lifted diffusion flame situated around the stoichiometric isosurface can be observed. The flame structure at 800 K ambient temperature, however, appears to be somehow different. The reaction zone hardly reaches regions of stoichiometric conditions and burns virtually entirely in a lean mixture. Such a flame structure might be of unstable nature as discussed further below.
As already observed, the ambient temperature has crucial impact on the lift-off length which again involves important consequences. One is the mixture composition at the flame base and, consequently, also the richest mixture in reactive state within the flame in such configurations. A better insight on

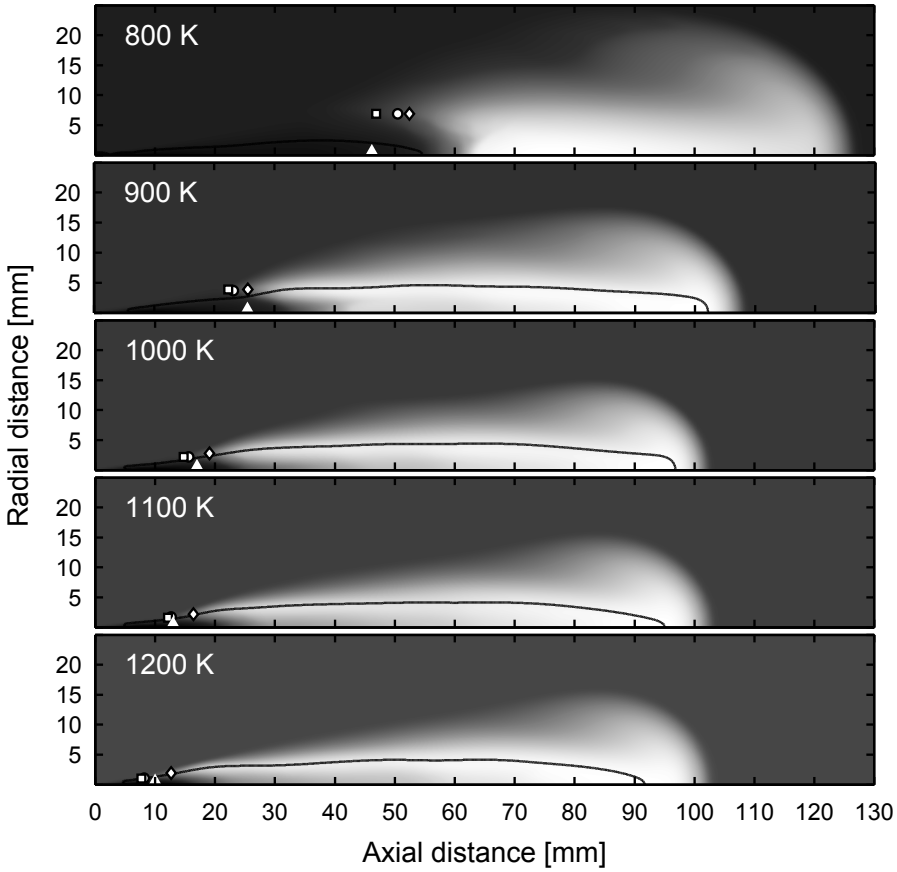

Figure 5.16. *Mean temperature for indicated ambient temperature at quasi-steady state using $C_\chi = 3$ and $\sigma = 1$. White triangles: experimental data / Squares: 2% of max. $\widetilde{Y}_{OH}$ / Circles: $\widetilde{Y}_{OH} = 1 \cdot 10^{-4}$ / Diamonds: T_0 + 400 K. Black line: stoichiometric isoline.*

the internal structure of the flame can be obtained by representing virtually the same information as before in equivalence ratio space again. This is done with the $\phi - T$ maps of the same cases shown in Fig. 5.17, which enable the analysis of the quasi-steady flame structure from a different point of view. The temperature at $\phi = 0$ corresponds obviously to the ambient temperature (indicated in the figure) in the vessel. The steep rising slope between equivalence ratios of zero to unity corresponds to the lean oxidizer side of the diffusion flame. The maximum flame temperature of about 2600 K is reached in the vicinity of stoichiometry. Small differences in the order of about 200 K can be observed in the peak value between the diverse cases due

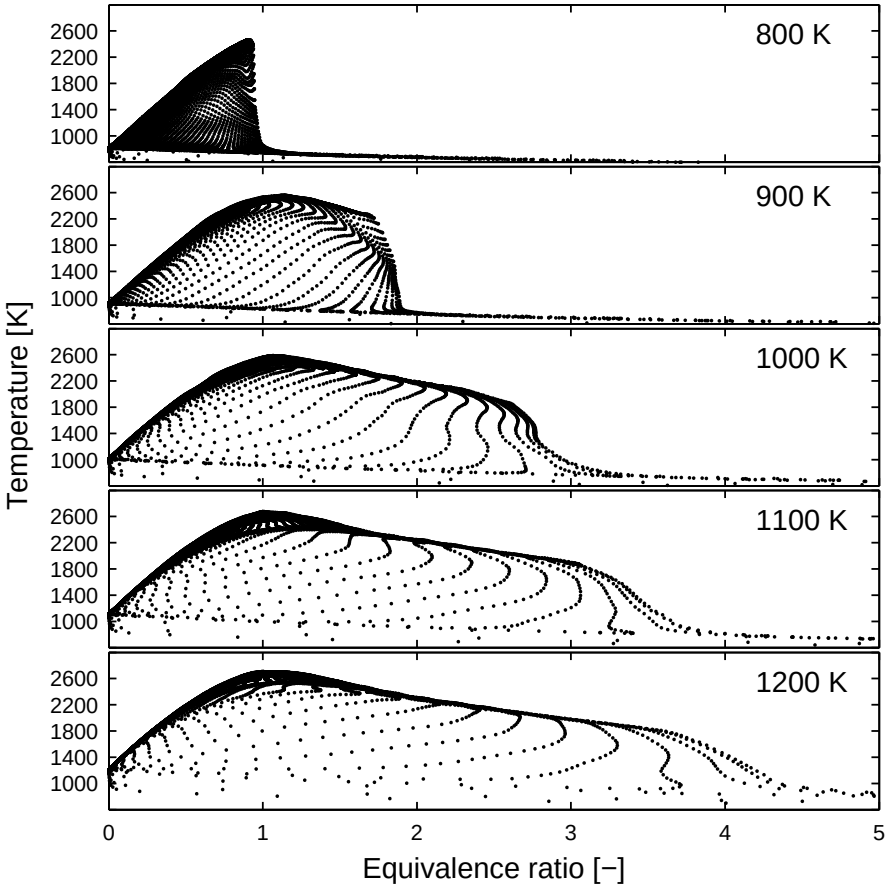

Figure 5.17. *Mean temperature as function of mean equivalence ratio for cases with indicated T_0 at quasi-steady state using $C_\chi = 3$ and $\sigma = 1$.*

to the considered ambient temperature ranging from 800 K to 1200 K. The maximum temperature in the flame is of major importance when it comes to the generation of NOx. As could be expected though, the peak value of the flame temperature is not very strongly affected by the ambient temperature. The temperature decreases again for increasing values of ϕ above stoichiometry. This relatively flat slope corresponds to the rich fuel side of the diffusion flame. The temperature then drops rapidly at a certain equivalence ratio. This more or less pronounced slope (depending on T_0) corresponds to the rich (partially) premixed region where the flame base is situated. From a spatial point of view, this is the region from the lift-off to the centerline of the flame. The maximum equivalence ratio at the flame base—where

the abrupt temperature change occurs—varies significantly over the different cases due to the different lift-off length. So the most outstanding difference between the diverse cases is certainly the range of equivalence ratio within high temperature regions. Higher ambient temperature leads to shorter flame lift-off and consequently to richer mixtures in reactive state, while the maximum mean temperature remains almost unchanged.
Moreover, it can be observed that the temperature drop is steeper at lower ambient temperature. For the cases of 800 K and 900 K this drop occurs almost at one distinct equivalence ratio, while the temperature declines over a wider range of ϕ at higher ambient temperature. This means that the flame base stabilizes along an ϕ-isosurface in low temperature cases.
A reduction of the ambient temperature can drastically reduce the reactivity of rich mixtures which in turn has important impact on soot formation. Modeling of soot is in principle out of the scope of this work, though further conclusions can be drawn at this point by means of experimental findings. In an experimental study of sprays under comparable conditions to those considered here, it is reported for instance that in a flame with $\phi \sim 2$ at the lift-off length almost no soot incandescence could be measured [35]. The influence of the ambient gas temperature on the soot level was also evidenced in [36], where increasing ambient temperature was found to cause an increased peak level of soot. Different ways to obtain non-sooting flames have been investigated in [37] and a conceptual model of soot formation was presented in [38].
In summary, reducing the ambient temperature is an effective measure to avoid the generation of soot in the considered flame configurations. From this point of view, the case with $T_0 = 800$ K seems to be preferable against those with higher ambient temperature. However, one has to keep in mind the relatively long—concerning characteristic times of diesel engines—ignition delay of about 2 ms and even further the approximately 7 ms needed to reach quasi-steady state under the considered conditions. Moreover, lift-off lengths of the order of 50 mm are not feasible in today's conventional diesel engines. Lastly and as already suggested before, the flame at $T_0 = 800$ K might be at risk to become unstable, since an increase in flame lift-off, i.e. towards leaner mixtures, goes along with a drastic temperature decrease (see top $\phi - T$ map in Fig. 5.17), which might finally lead to the termination of combustion.

At last, the influence of the ambient temperature on the heat release rate (HRR) shall be studied. For this purpose, the computational results are subjected to a qualitative comparison with experimental data. The temporal evolution of the vessel pressure was measured in the "Spray H" test series [3],

which allows to deduce the heat release rate by means of basic thermodynamic relations (1st law of thermodynamics). This deduced and filtered experimental HRR is represented by the gray curves in Fig. 5.18 for the base case and the two limiting cases. The black curves represent the computational results obtained with $C_\chi = 3$ and the log-normal with $\sigma = 1$. In the left column of Fig. 5.18, the HRR is represented as function of time after start of injection (ASI). From this representation one can observe different temporal shift between experiment and simulation due to the differences in the ignition delay (already discussed above). In order to improve comparability, the heat release rates are plot versus time after start of combustion (ASC) in the right column.

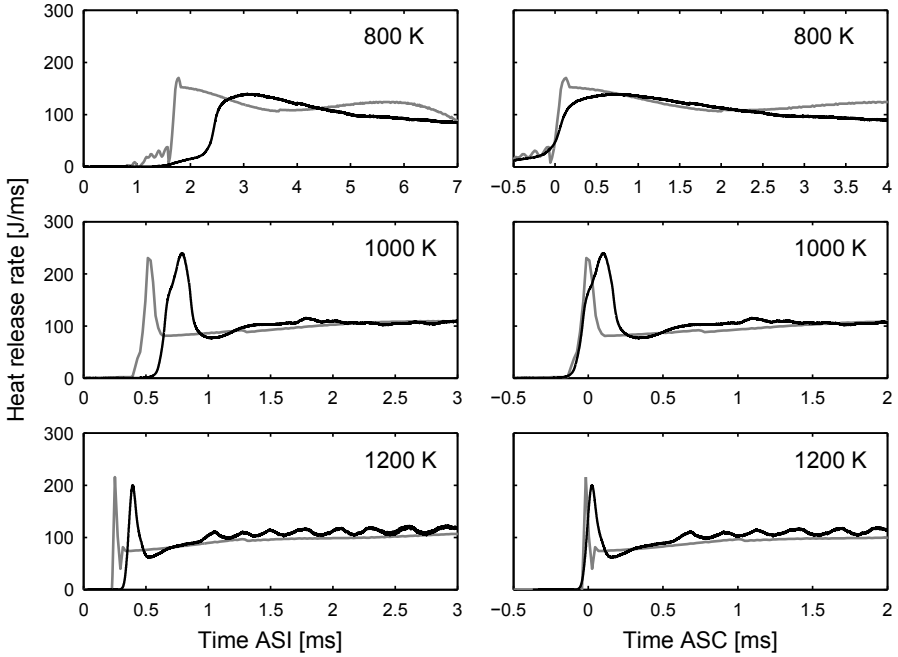

Figure 5.18. *Heat release rate at different ambient temperature as function of time after start of injection (ASI) (left) and time after start of combustion (ASC) (right). Gray line: experimental data / Black line: computational results obtained with $C_\chi = 3$ and $\sigma = 1$.*

Focusing first on the experimental results, there is no heat release observable for a certain period of time after SOI independent of the ambient temperature. During this time the spray formation process including phenomena such as atomization, breakup, and evaporation takes place at the same time as the evaporated fuel mixes with surrounding air which leads to

a flammable mixture. At a certain instant of time—after the temperature-dependent ignition delay—this formed mixture ignites which causes a sudden increase in heat release. In cases of moderate to high ambient temperature (here 1000 K and 1200 K), the onset of heat release rise is abrupt and steep and manifests in a characteristic peak in the HRR curve. This peak corresponds to the premixed burnout that marks the first stage of combustion typical for diesel sprays. The peak value increases as ambient temperature and consequently also the ignition delay decrease, since a higher amount of flammable mixture has been formed (compare cases with T_0 = 1000 K and 1200 K). Then, the HRR decreases relatively fast after the first combustion stage and stabilizes at an almost constant value. This phase corresponds to the second non-premixed combustion phase. The characteristic peak in HRR is virtually not present in the case of law ambient temperature (800 K case) probably due to the reduced reactivity of the mixture. Moreover, the onset of heat release rise is rather smooth compared to high temperature cases. Consequently, also the two combustion phases are less distinct. All these described trends are overall acceptably reproduced by the combustion model. The quality of the results is comparable to those presented for instance in [39]. In this numerical study, the influence of EGR variation on the heat release rate of the "Spray H" base case is investigated by means of a similar modeling approach but in a LES environment. Despite the satisfying results obtained with the combustion model in in its present state, further studies may certainly lead to an enhancement of the predictions. An improvement of the considered results might be achieved by better prediction of the ignition delay.

Predicted species distribution

Finally, a qualitative analysis of the calculated species mass fractions presented in Fig. 5.19 is made. The black/white line indicates stoichiometric conditions. Starting with the fuel, one can observe high concentration of n-heptane in the gas phase at upstream regions which are rapidly consumed. Since evaporation takes some time, no fuel vapor exists directly at the injector nozzle and the peak of fuel vapor concentration lies close to the liquid length. The mean mass fraction of C_7H_{14}—a dummy species—is here representative for all hydrocarbons apart of the proper fuel. Its concentration rises as the fuel is oxidized, i.e. broken down to smaller hydrocarbon chains. The distribution of OH, which is a precursor for combustion, shows high concentrations in the vicinity of stoichiometric conditions. Subsequently, high concentration of CO can be found in the regions of rich mixtures within the diffusion flame (inside the stoichiometric iso-surface). Carbon monoxide is generated at the flame

base due to rich partially-premixed combustion and high concentrations of CO remain present within the diffusion flame due to the lack of oxygen. Oxidation of CO occurs in regions close to stoichiometric conditions and, consequently, CO_2 is generated. Concluding, the model is not only capable to correctly reproduce the lifted flame structure but also the distribution of the species considered during tabulation.

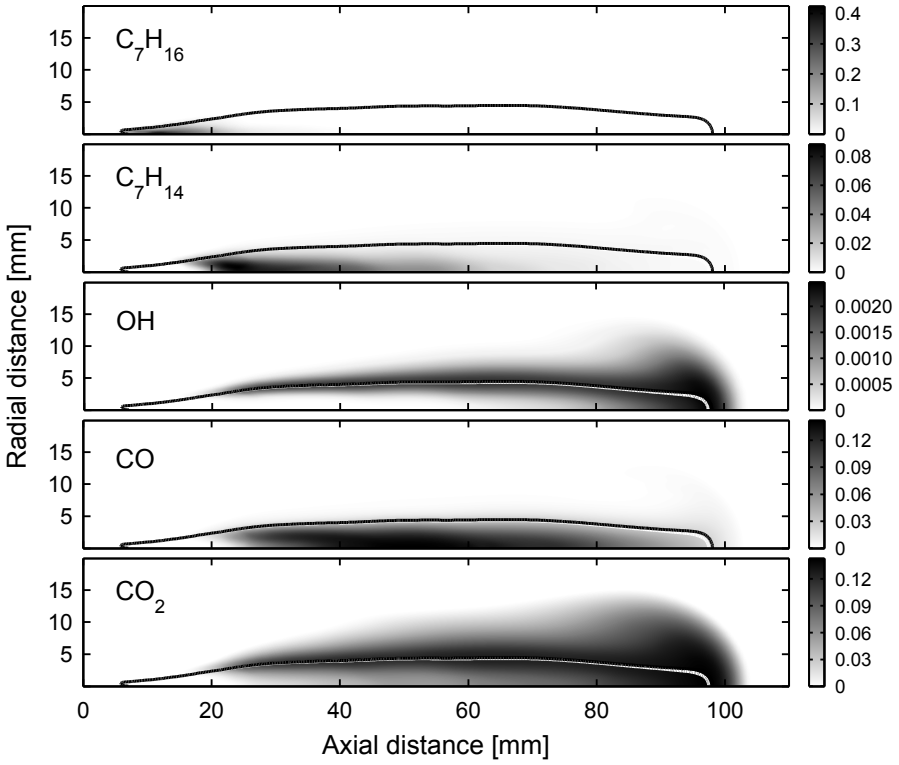

Figure 5.19. *Mean mass fractions of main species of the base case. White/black line: stoichiometric isoline.*

5.4 Conclusions

The turbulent combustion model in its simplified version, i.e. based on ADF solutions, was applied to simulate reactive sprays under diesel-like conditions. Prior to the study, some useful adaptations of the modeling strategy as proposed in the literature were presented. Especially the limitation to auto-igniting ADFs represents an important reduction of computational

effort. Moreover, the employed spray modeling by means of the DDM approach was briefly touched.
Before the actual study, the spray was modeled in inert conditions in order to adjust the setup of the spray model. Solid spray predictions are the basis for reliable results of the combustion simulation. Reasonable results for two main combustion model properties, namely the mean mixture fraction and its variance, could by obtained by introducing small changes in some parameters of the spray submodels and an thorough adjustment of the mesh and the time step size. The DDM approach is still widely used even in commercial coeds although it imposes quite strong limitations on mesh and time step size. New spray models based on Eulerian-Eulerian approaches like the σ-Y model [40] are developed in recent years and promising improvements in spray modeling may be expected from this advances [41]. Furthermore, it was found in the pre-study of the inert spray that good agreement for the computed mixture fraction variance with experimental data can be obtained for C_χ close to 3, which coincides with the findings of the hydrogen jet flame.

Subsequently the influence of C_χ and the assumed shape of the PDF for χ_{st} on the transient and the quasi-steady state flame structure was studied on the basis of the case with an ambient temperature of 1000 K. The value of C_χ is in principle determined by adjustment of the mixture fraction variance. However, equally well adjustment of the variance in the near and the far field of the spray with a constant value of C_χ is hardly achievable. The focus was therefore laid on the near field, where the lift-off is expected. Decreasing values of C_χ lead to longer ignition delay. The use of $C_\chi = 2$, which gave poor prediction of the variance in the near field, led to very long ID and even different spatial structure of the igniting flame. No big difference could be found though between $C_\chi = 3$ and $C_\chi = 4$, just a slightly decreased ID when using the latter value. The assumption of a δ-PDF for the distribution of the stoichiometric scalar dissipation rate predicted slightly shorter ignition delay compared to the use of a log-normal distribution with $\sigma = 1$. This trend is slightly more distinctive for low to medium ambient temperatures. The influence of the ambient temperature on the ignition delay is generally well reproduced with both PDF assumptions. The ignition delay is overall slightly overestimated with the biggest differences in the case with $T_0 = 800$ K.

Concerning the predictions of the lift-off length, it could be observed that the adoption of a log-normal distribution for χ_{st} leads to a shift of the LOL towards higher values and to better agreement with experimental data. The reason for the longer lift-off length was found to be due to the contribution of

non-reactive flamelets already at moderate scalar dissipation rates, while this is not the case when a δ-PDF is assumed. This effect is more significant at high ambient temperature leading to short lift-off length where the flame base stabilizes at regions high scalar dissipation rate. On the contrary, the influence of the χ_{st}-PDF is less distinctive in flames with long lift-off length, i.e. at low ambient temperature. This is because the flame base is situated in regions with low scalar dissipation rate away from the autoignition limit. The global trend of the lift-off length with the ambient temperature is well predicted with considerably better agreement wit experiments when using $\sigma = 1$. No significant influence on the lift-off length could be observed for C_χ.

The general trends of the heat release rate are reasonable captured by the combustion model. Also the influence of ambient temperature variation is well reproduced. The observed differences are most likely related to discrepancy in ignition delay predictions. Furthermore, the combustion model provides insight on the spatial distribution of the main species concentrations in the flame. The predicted species concentrations are consistent with what may be considered the commonly known picture of the structure of a diffusion flame under the considered configuration according to experimental findings [42].

Concluding, the planned modeling strategy was found to be appropriate to simulate reactive sprays under conditions similar to diesel engines. Moreover, the introduced adaptations appear to be reasonable for the considered conditions, as confirmed by the obtained results. This is an important finding in view of the fact that the limitation to autoigniting approximated diffusion flames represents an important computational saving and a general reduction of the modeling effort. Additionally, also the ADF method turned out to be adequate for such configurations. The common and quasi-standard PV definition for such fuels applied in this study seems to work fair though an advanced definition including some intermediate species might be beneficial.

Bibliography

[1] García-Oliver J. M., Novella R., Pastor J. M. and Winklinger J. F. "Evaluation of combustion models based on tabulated chemistry and presumed probability density function approach for diesel spray simulation". *Int. J. Comp. Mathematics*, Vol. 91, pp. 14–23, 2014.

[2] http://www.sandia.gov/ecn/. *Engine Combustion Network*, looked up in August 2014.

[3] http://www.sandia.gov/ecn/cvdata/dsearch/frameset.php. *ECN Data Search Utility*, looked up in August 2014.

[4] Pita E. G. *Heat and Mass Transfer in Evaporating Sprays*. University of Maryland, College Park, 1969.

[5] Chitre S. *Turbulent Evaporating Sprays: Comparison Vaporization Models*. University of Illinois at Chicago, 1990.

[6] Sirignano W. A. *Fluid Dynamics and Transport of Droplets and Sprays*. Cambridge University Press, 2010.

[7] Ashgriz N. *Handbook of Atomization and Sprays: Theory and Applications*. Springer, 2011.

[8] Sazhin S. *Droplets and Sprays*. Springer London, 2014.

[9] Han Z., Parrish S., Farrell P. V. and Reitz R. D. "Modeling Atomization Processes Of Pressure Swirl Hollow-Cone Fuel Sprays". *Atomization Sprays*, Vol. 7, pp. 663–684, 1997.

[10] Allocca L., Bella G., Vita A. De and Angelo L. Di. "Experimental Validation of a GDI Spray Model". *SAE Technical Paper 2002-01-1137*, 2002.

[11] Reitz R. D. "Modeling Atomization Processes in High-Pressure Vaporizing Sprays". *Atomisation Spray Technol.*, Vol. 3, pp. 309–337, 1987.

[12] Crowe C. T., Schwarzkopf J. D., Sommerfield M. and Tsuji Y. *Multiphase Flows with Droplets and Particles*. CRC Press, 1997.

[13] Kärrholm F. B. *Numerical Modelling of Diesel Spray Injection, Turbulence Interaction and Combustion*. Doctoral Thesis, Chalmers Tekniska Hogskola, Göteborg, 2008.

[14] Ra Y. and Reitz R. D. "A reduced chemical kinetic model for IC engine combustion simulations with primary reference fuels". *Combust. Flame*, Vol. 155, pp. 713–738, 2008.

[15] Zeuch T., Moréac G., Ahmed S. S. and Mauss F. "A comprehensive skeletal mechanism for the oxidation of n-heptane generated by chemistry-guided reduction". *Combust. Flame*, Vol. 155, pp. 651–674, 2008.

[16] Pastor J. V., García-Oliver J. M., Pastor J. M. and Vera-Tudela W. "1D diesel spray modelling of multi-component fuels". *Atomization Sprays*, 2014. (accepted, in press).

[17] Michel J.-B., Colin O., Angelberger C. and Veynante D. "Using the tabulated diffusion flamelet model ADF-PCM to simulate a lifted methane-air jet flame". *Combust. Flame*, Vol. 156, pp. 1318–1331, 2009.

[18] Pickett L. M., Siebers D. L. and Idicheria C. A. "Relationship Between Ignition Processes and the Lift-Off Length of Diesel Fuel Jets". *SAE Technical Paper 2005–01–3843*, 2005.

[19] Michel J.-B., Colin O. and Veynante D. "Modeling ignition and chemical structure of partially premixed turbulent flames using tabulated chemistry". *Combust. Flame*, Vol. 152, pp. 80–99, 2008.

[20] http://www.sandia.gov/ecn/cvdata/sandiaCV/vesselGeometry 2009.php. *Combustion Vessel Geometry*, looked up in August 2014.

[21] http://www.sandia.gov/ecn/cvdata/sandiaCV/SprayHroi.php. *Spray H: Recommended rate of injection*, looked up in August 2014.

[22] Janicka J. and Peters N. "Prediction of turbulent jet diffusion flame lift-off using a pdf transport equation". In *19th Symposium (Int.) on Combustion*, pp. 367–374, Pittsburgh, 1982. The Combustion Institute.

[23] Gopalakrishnan V. and Abraham J. "Effects of multicomponent diffusion on predicted ignition characteristics of an n-heptane diffusion flame". *Combust. Flame*, Vol. 136, pp. 557–566, 2004.

[24] Mukhopadhyay S. and Abraham J. "Influence of compositional stratification on autoignition in n-heptane/air mixtures". *Combust. Flame*, Vol. 158, pp. 1064–1075, 2011.

[25] Higgins B., Siebers D. and Aradi A. "Diesel-Spray Ignition and Premixed-Burn Behavior". *SAE Technical Paper 2000-01-0940*, 2000.

[26] Bhattacharjee S. and Haworth D. C. "Simulations of transient n-heptane and n-dodecane spray flames under engine-relevant conditions using a transported PDF method". *Combust. Flame*, Vol. 160, pp. 2083–2102, 2013.

[27] Heywood J. *Internal Combustion Engines*. McGraw-Hill, New York, 1988.

[28] Bajaj C., Ameen M. and Abraham J. "Evaluation of an Unsteady Flamelet Progress Variable Model for Autoignition and Flame Lift-Off in Diesel Jets". *Combust. Sci. Technol.*, Vol. 185, pp. 454–472, 2013.

[29] Pei Y., Hawkes E. R. and Kook S. "A Comprehensive Study of Effects of Mixing and Chemical Kinetic Models on Predictions of n-heptane Jet Ignitions with the PDF Method". *Flow Turb. Combust.*, Vol. 91, pp. 249–280, 2013.

[30] Lu T., Law C. K., Yoo C. S. and Chen J. H. "Dynamic stiffness removal for direct numerical simulations". *Combust. Flame*, Vol. 156, pp. 1542–1551, 2009.

[31] Dec J. E. "A Conceptual Model of DI Diesel Combustion Based on Laser-Sheet Imaging". *SAE Technical Paper 970873*, 1997.

[32] Lyons K. M. "Toward an understanding of the stabilization mechanisms of lifted turbulent jet flames: Experiments". *Progr. Energy Comb. Sci.*, Vol. 33, pp. 211–231, 2007.

[33] Venugopal R. and Abraham J. "A Review of Fundamental Studies Relevant to Flame Lift–off in Diesel Jets". *SAE Technical Paper 2007–01–0134*, 2007.

[34] Peters N. and Williams F. A. "Liftoff Characteristics of Turbulent Jet Diffusion Flames". *AIAA*, Vol. 21, pp. 423–429, 1983.

[35] Siebers D. and Higgins B. "Flame Lift-Off on Direct-Injection Diesel Sprays Under Quiescent Conditions". *SAE Technical Paper 2001-01-0530*, 2001.

[36] Pickett L. M. and Siebers D. L. "Soot in diesel fuel jets: effects of ambient temperature, ambient density, and injection pressure". *Combust. Flame*, Vol. 138, pp. 114–135, 2004.

[37] Pickett L. M. and Siebers D. L. "Non-Sooting, Low Flame Temperature Mixing-Controlled DI Diesel Combustion". *SAE Technical Paper 2004-01-1399*, 2004.

[38] Idicheria C. A. and Pickett L. M. "Formaldehyde Visualization Near Lift-off Location in a Diesel Jet". *SAE Technical Paper 2006-01-3434*, 2006.

[39] Tillou J., Michel J.-B., Angelberger C., Bekdemir C. and Veynante D. "Large-Eddy Simulation of Diesel Spray Combustion with Exhaust Gas Recirculation". *Oil Gas Sci. Technol.*, Vol. 69, pp. 155–165, 2014.

[40] García-Oliver J. M., Pastor J. M., Pandal A., Trask N., Baldwin E. and Schmidt D. P. "Diesel spray CFD simulations based on the Σ-Y Eulerian atomization model". *Atomization Sprays*, Vol. 23, pp. 71–95, 2013.

[41] García-Oliver J. M., Pastor J. M. and Pandal A. "A comparison of diesel sprays CFD modelling approaches: DDM vs Σ-Y Eulerian atomization model". *Submitted to J. Multiphase Flow*, 2014. (private communication).

[42] Flynn P. F., Durret R. P., Hunter G. L., zur Loye A. O., Akinyemi O. C., Dec J. E. and Westbrook C. K. "Diesel Combustion: An Integrated View Combining Laser Diagnostics, Chemical Kinetics, And Empirical Validation". *SAE Technical Paper 1999-01-0509*, 1999.

Chapter 6

General conclusions and future work

Contents

6.1 General conclusions

A turbulent combustion model based on laminar diffusion flames—the so-called flamelet concept—was implemented in the CFD platform OpenFOAM in this work. The turbulence-chemistry interaction is accounted for by means of presumed PDF modeling. A tabulation technique is adopted to store pre-calculated turbulent flamelet solutions in order to allow the use of detailed chemical mechanisms at reasonable computational cost. The combustion model is designed to be applied to simulate turbulent combustion processes in a mainly non-premixed combustion regime including problems with a certain degree of partial premixing. Moreover, it is capable to reproduce phenomena like autoignition and flame lift-off.

The behavior of laminar diffusion flames (DF) in opposed jet configuration was first studied on the basis of hydrogen. Furthermore, the ADF approach, an approximation of laminar diffusion flames proposed for complex fuels, was implemented and applied to calculate approximated flamelet solutions

for the same fuel. This approximation leads to an important reduction of computational effort, since the flamelet equation is solved only once for a progress variable rather than for each species included in the chemical mechanism. Hence, the ADF method is of particular interest for combustion processes of complex fuels whose chemical description requires a large number of species. Indeed, the progress variable plays an important role in this approach and has to fulfill certain criteria like being unique and strictly monotonically increasing. Satisfactory basic accordance was found for the two kind of flamelet solutions especially for the internal structure of the laminar hydrogen diffusion flames.

A presumed-PDF approach was developed to account for the turbulence-chemistry interaction with assumed distributions of the mixture fraction Z, the progress variable Y_c and the stoichiometric scalar dissipation rate χ_{st}. A β-distribution is assumed for the mixture fraction as common practice, and a δ-PDF for the non-normalized progress variable. The distribution of χ_{st} is modeled with a log-normal PDF with constant variance and a δ-PDF. Integration of a set of laminar flamelet solutions at different strain rates over the described PDFs results in the turbulent flamelet solutions. These solutions can be stored in a 4D lookup table that is parametrized by the mean mixture fraction $\widetilde{Z}$ and its variance $\widetilde{Z''^2}$, the mean progress variable $\widetilde{Y}_c$, and the mean of the stoichiometric scalar dissipation rate $\widetilde{\chi}_{st}$. The whole process until here is independent of the actual CFD calculation and is done in a pre-processing step.

Two different ways of coupling of the combustion model with the CFD code are presented and adopted in this work. First, a direct coupling where the source term for the transport equation of the progress variable is directly read from the turbulent flamelet tables as well as other dependent properties such as temperature or species mass fractions. The second method uses coupling based on the tabulation of species mass fraction adapted for fully compressible problems. In this coupling method a relaxation of the mixture composition towards the tabulated values is achieved. Transport equations for a carefully chosen subset of species are solved instead of an equation of the progress variable. A detailed description of the combustion model and all its components is given in Chapter 3.

The implemented turbulent combustion model was first applied to model the turbulent lifted H_2/N_2 jet flame from Berkeley University, an widely

used reference case in the area of turbulent combustion modeling. This configurations shows important similarities to diesel sprays such as the lifted flame base but with a much simpler and well-known fuel, which makes it an attractive test case. After an investigation of the influence of the main model parameters and an corresponding adjustment, very good agreement with experimental data was obtained when DF solutions were employed. Also the well-known sensitivity of this flame to variations in the coflow temperature are reasonably reproduced. In a second step, the simplified version of the combustion model—based on ADF solutions—was applied to the same configuration. Since the ADF solutions were found to be slightly less reactive, higher lift-off heights were predicted for the same coflow temperature compared to the results of the conventional combustion model. However, good predictions of the lift-off height sensitivity to the coflow temperature and the correct reproduction of the flame structure encouraged the further use of the simplified combustion model.

After the successful assessment of the combustion model on basis of the hydrogen jet flame, it was finally applied in its simplified version to the modeling of reactive n-heptane sprays in the so-called "Spray H" configuration of the ECN. Some useful adaptations were introduced to the combustion model in accordance to the considered problem. At first, an adjustment of the spray modeling setup under inert conditions, for which measured mixture fraction and variance profiles exist, was made in order to obtain a solid basis for the subsequent combustion modeling. Again, the influence of the main model parameters were investigated and similar trends could be observed as before. The predicted ignition delay and the lift-off length for different ambient temperatures have been compared to available experimental data. Good agreement could be observed not only for the predicted trend of these global flame parameters as a function of the temperature but also in absolute values. Moreover, the model gives solid predictions of the transient and quasi-steady flame structure, and the spatial distribution of species mass fractions. The results confirm the adequacy of the introduced adaptations for the considered configurations. Especially the limitation to autoigniting flamelet solutions represents considerable savings in the modeling process.

Concluding, the overall performance of the combustion model both in the conventional and in the simplified version is satisfactory at feasible computational effort. It has to be pointed out that the presented modeling strategy is relatively simple and economic compared to other combustion models proposed in the literature. The implemented model offers great

flexibility considering the adoption of chemical mechanisms of different complexity. The most critical issues of the combustion model are probably the progress variable definition and the election of considered species in case the species mass fraction tabulation is chosen. The implemented model in its current state is fully operational, however, further improvements of the modeling strategy and the current implementation are certainly possible and necessary. The obtained results surely encourage the further development of the turbulent combustion model. Some potential enhancements are proposed in the following section.

6.2 Future work

Some suggestion for future work may be given according to the logical structure of the present research, from the implementation of the combustion model to its operational stage and subsequent application to technical problems. With respect to the proper implementation of the presented combustion model it has to be noted, that the model was implemented virtually without any basis. In other words, almost all the development of necessary numerical routines as well as the programming work, in particular for the chemistry tabulation, started without previously existing code. All subroutines and steps of the whole modeling environment have of course been thoroughly tested and debugged. However, improvements in the computational performance of the combustion model seem to be possible. An improvement opportunity for instance might be the implementation of a more efficient hash function in order to accelerate the calculation of the keys required for the lookup process in the turbulent flamelet table. The hash function might represent a small and profound part of the whole implementation, but it is of considerable importance since it continuously called during a simulation run.

Concerning the calculation process of approximated laminar flamelet solutions with the ADF approach, the stability of the resolution of the stiff ODE is for sure an important issue. The impact of the progress variable definition on the results of the ADF approach should be carefully studied for its further development. In this context also the research for possible improvements of the progress variable definition for different fuels might be of use. Moreover, the accurate limitations of this approach and its appropriate area of application are not completely defined.

Another interesting and still unresolved question to look at, is the way of synchronizing a set of flamelets at different strain rates. Different approaches are used in different versions of flamelet based combustion models, as done in this work, and there exists no unique method. Indeed, the time-synchronization approach might be tied to restrictions due to its ambiguity in the unstable flamelet range, although, it seems to be adequate in certain flame configurations dominated be autoignition phenomena. On the other side there exist the possibility to synchronize by means of a progress variable. But even in doing so it is not clear whether normalized or non-normalized PV is physically more reasonable.

In view of the conventional combustion model (employing the DF solutions), a next logical step could be the application of the model to an analog configuration of the H_2/N_2 jet flame that uses methane as fuel. This turbulent lifted methane/air jet flame is another widely used test case that shows similar features as the flame modeled in this work. However, the characteristics of methane are more alike to real fuels as for instance the value of the stoichiometric mixture fraction. Fortunately, the chemical mechanism is quite well-known and of manageable size, which reduces uncertainties of the chemistry on the one hand and promotes the extension of the flamelet solution process to more complex fuels on the other hand. In the area of reactive sprays, the experimental cases of the "Spray A" attract a lot of attention lately and may be considered as further examples of study. Furthermore, the coupling of the implemented combustion model with an advanced Eulerian spray model inside the OpenFoam platform will surely lead to a considerable improvement of the modeling of reactive sprays.

Finally, the possible transfer of the combustion model to a LES environment might be seriously considered in the mid-term. Improvements may be expected not only in issues with the relatively simple turbulence modeling of a RANS approach but also in the prediction of unsteady combustion phenomena such as extinction and re-ignition. In this context, the modeling of the so-called "Flame F" configuration might be an adequate example in order to investigate the model's capability to predict such phenomena. Of course, the increased computational effort due to necessary reduction of the mesh size and the time step size has to be balanced with the expected results and possible increase in the quality of the predictions.

Bibliography

Abdel-Gayed R. G. and Bradley D.
Combustion regimes and the straining of turbulent premixed flames.
Combust. Flame, Vol. 76, pp. 213–218, 1989. (cited on p. 16)

Airbus S.A.S.
Global Market Forecast Future Journeys 2013 2032.
2013. (cited on p. 4)

Allocca L., Bella G., Vita A. De and Angelo L. Di.
Experimental Validation of a GDI Spray Model.
SAE Technical Paper 2002-01-1137, 2002. (cited on p. 131)

Ameen M. M. and Abraham J.
RANS and LES Study of Lift-Off Physics in Reacting Diesel Jets.
SAE Technical Paper 2014–01–1118, 2014. (cited on p. 58)

Anderson J. D.
Computational Fluid Dynamics.
McGraw-Hill, 1995. (cited on p. 29)

Arrhenius S.
On the reaction rate of the inversion of non-refined sugar upon souring.
Z. Phys. Chem., Vol. 4, pp. 226–248, 1889. (cited on p. 41)

Ashgriz N.
Handbook of Atomization and Sprays: Theory and Applications.
Springer, 2011. (cited on p. 131)

Bajaj C., Ameen M. and Abraham J.
Evaluation of an Unsteady Flamelet Progress Variable Model for Autoignition and Flame Lift-Off in Diesel Jets.
Combust. Sci. Technol., Vol. 185, pp. 454–472, 2013. (cited on p. 143)

Bekdemir C., Somers L. M. T. and de Goey L. P.H.
Modeling diesel engine combustion using pressure dependent Flamelet Generated Manifolds.
Proc. Combust. Inst., Vol. 33, pp. 2887–2894, 2011. (cited on p. 45)

Bhattacharjee S. and Haworth D. C.
Simulations of transient n-heptane and n-dodecane spray flames under engine-relevant conditions using a transported PDF method.
Combust. Flame, Vol. 160, pp. 2083–2102, 2013. (cited on p. 140)

Bilger R. W.
The structure of turbulent nonpremixed flames.
In *22nd Symposium (Int.) on Combustion*, pp. 475–488, Pittsburgh, 1988. The Combustion Institute. (cited on pp. 21, 24)

Bilger R. W.
Conditional moment closure for turbulent reacting flows.
Phys. Fluids, Vol. A5, pp. 436–444, 1993. (cited on p. 46)

Bodek K. and Heywood J.
Europe's evolving passenger vehicle fleet: Fuel use and GHG emissions scenarios through 2035.
Laboratory for Energy and Environment, Massachusetts Institue of Technology, 2008. (cited on p. 4)

Bodenstein M. and Lind S. C.
Geschwindigkeit der Bildung des Bromwasserstoffs aus seinen Elementen.
Z. Phys. Chem., Vol. 57, pp. 168, 1906. (cited on p. 43)

Bongers H.
Analysis of Flamelet-Based Methods to Reduce Chemical Kinetics in Flame Computations.
Doctoral Thesis, Technische Universiteit Eindhoven, 2005. (cited on p. 44)

Borghi R.
On the structure and morphology of turbulent premixed flames.
In Casci C., editor, *Recent Advances in the Aerospace Science*, pp. 117–138. Plenum Press, New York, 1985. (cited on p. 16)

Borghi R.
Turbulent combustion modelling.
Prog. Energy Combust. Sci., Vol. 14, pp. 245–292, 1988. (cited on pp. 24, 25)

Borghi R. and Destriau M.
Combustion and flames.
(Translated from French). Editions Technip, 1998. (cited on p. 19)

Boulanger J., Vervisch L., Reveillon J. and Ghosal S.
Effects of heat release in laminar diffusion flames lifted on round jets.
Combust. Flame, Vol. 134, pp. 355–368, 2003. (cited on p. 27)

Bourlioux A., Cuenot B. and Poinsot T.
Asymptotic and Numerical Study of the Stabilization of Diffusion Flames by Hot Gas.
Combust. Flame, Vol. 120, pp. 143–159, 2000. (cited on p. 27)

Bradley D., Gaskell P. H. and Gu X. J.
The mathematical modeling of liftoff and blowoff of turbulent non-premixed methane jet flames at high strain rates.
Symposium (International) on Combustion, Vol. 27, pp. 1199–1206, 1998. (cited on p. 78)

Bray K. N. C.
Turbulent flows with premixed reactants in turbulent reacting flows.
In Libby P. A. and Williams F. A., editors, *Topics in Applied Physics*, pp. 115–183. Springer Verlag, New York, 1980. (cited on p. 16)

Bray K. N. C. and Peters N.
Laminar Flamelets in turbulent Flames.
In Libby P. A. and Williams F. A., editors, *Turbulent reacting flows*, pp. 63–113. Academic Press, London, 1994. (cited on pp. 24, 25)

Brown C. D., Watson K. A. and Lyons K. M.
Studies on Lifted Jet Flames in Coflow: The Stabilization Mechanism in the Near– and Far–Fields.
Flow Turb. Combust., Vol. 62, pp. 249–273, 1999. (cited on p. 26)

Burke S. P. and Schumann T. E. W.
Diffusion flames.
In *1st Symposium (Int.) on Combustion*, pp. 2–11, Pittsburgh, 1928. The Combustion Institute. (cited on p. 21)

Bykov V. and Maas U.
The extension of the ILDM concept to reaction–diffusion manifolds.
Combust. Theory Modelling, Vol. 11, pp. 839–862, 2007. (cited on p. 44)

Cabra R., Chen J.-Y., Dibble R. W., Karpetis A. N. and Barlow R. S.
Lifted methane-air jet flames in a vitiated coflow.
Combust. Flame, Vol. 143, pp. 491–506, 2005. (cited on p. 126)

Cabra R., Myhrvold T., Chen J. Y., Dibble R. W., Karpetis A. N. and Barlow R. S.
Simultaneous Laser Raman-Rayleigh-LIF Measurements and Numerical Modeling Results of a Lifted Turbulent H2/N2 Jet Flame in a Vitiated Coflow.
Proc. Combust. Inst., Vol. 29, pp. 1881–1888, 2002.
(cited on pp. 60, 102, 104, 106, 109, 119)

Cao R. R., Pope S. B. and Masri A. R.
Turbulent lifted flames in a vitiated coflow investigated using joint PDF calculations.
Combust. Flame, Vol. 142, pp. 438–453, 2005. (cited on pp. 105, 108, 112, 117, 118)

CHEMKIN-PRO.
Reaction Design.
San Diego, 2008. (cited on p. 70)

Chen M., Herrmann M. and Peters N.
Flamelet modeling of lifted turbulent methane/air and propane/air jet diffusion flames.
Proc. Combust. Inst., Vol. 28, pp. 167–174, 2000. (cited on p. 45)

Chen T. H., Goss L. P., Talley D. G. and Mikolaitis D. W.
Dynamic Stabilization Zone Structure of Jet Diffusion Flames from Liftoff to Blowout.
J. of Propulsion and Power, Vol. 8, pp. 548–552, 1992. (cited on p. 26)

Chen Y.-C. and Bilger R. W.
Stabilization Mechanisms of Lifted Laminar Flames in Axisymmetric Jet Flows.
Combust. Flame, Vol. 123, pp. 23–45, 2000. (cited on p. 26)

Chitre S.
Turbulent Evaporating Sprays: Comparison Vaporization Models.
University of Illinois at Chicago, 1990. (cited on p. 131)

Colin O., Pera C. and Jay S.
Detailed chemistry tabulation based on a FPI approach adapted and applied to 3-D internal combustion engine calculations.
In *Third European Combustion Meeting*, 2007. (cited on p. 45)

Connors K. A.
Chemical Kinetics.
VCH Publishers, 1990. (cited on p. 41)

Crowe C. T., Schwarzkopf J. D., Sommerfield M. and Tsuji Y.
Multiphase Flows with Droplets and Particles.
CRC Press, 1997. (cited on p. 131)

Cuenot B. and Poinsot T.
Effects of curvature and unsteadiness in diffusion flames. Implications for turbulent diffusioncombustion.
In *25th Symposium (Int.) on Combustion*, Pittsburgh, 1994. The Combustion Institute. (cited on pp. 24, 25)

Curl R. L.
Dispersed phase mixing: I. Theory and effects of simple reactors.
AIChE J., Vol. 9, pp. 175–181, 1963. (cited on p. 46)

Curran H. J., Gaffuri P. and Westbrook C. K.
A Comprehensive Modeling Study of n-Heptane Oxidation.
Combust. Flame, Vol. 114, pp. 149–177, 1998. (cited on p. 42)

Damköhler G.
Der Einfluss der Turbulenz auf die Flammengeschwindigkeit in Gasgemischen.
Z. Elektrochem. Angew. Phys. Chem., Vol. 46, pp. 601–626, 1940. (cited on p. 16)

Dec J. E.
A Conceptual Model of DI Diesel Combustion Based on Laser-Sheet Imaging.
SAE Technical Paper 970873, 1997. (cited on p. 146)

Devaud C. B. and Bray K. N. C.
Assessment of the applicability of conditional moment closure to a lifted turbulent flame: first order model.
Combust. Flame, Vol. 132, pp. 102–114, 2003. (cited on p. 46)

Dietzschold C.
Der Cornelius Nepos der Uhrmacher.
C. Dietzschold's Verlag, 1910. (cited on p. 2)

DIW Berlin and Energy Analysis Environment Forecast.
Auswertungstabellen zur Energiebilanz fur die Bundesrepublik Deutschland 1990 bis 2012.
Arbeitsgemeinschaft Energiebilanzen e.V., 2013. (cited on p. 4)

Domingo P. and Vervisch L.
Triple flames and partially premixed combustion in autoignition of non–premixed mixtures.
In *26th Symposium (Int.) on Combustion*, pp. 233–240, Pittsburgh, 1996. The Combustion Institute. (cited on pp. 26, 27)

Dopazo C.
Recent developments in PDF methods.
In Libby P. A. and Williams F. A., editors, *Turbulent reacting flows*, pp. 375–474. Academic Press, London, 1994. (cited on p. 45)

Dopazo C. and O'Brien E. E.
An approach to the autoignition of a turbulent mixture.
Acta Astronaut., Vol. 1, pp. 1239–1266, 1974. (cited on p. 46)

Echekki T. and Mastorakos E.
Turbulent Combustion Modeling, volume 95.
Springer, 2011. (cited on pp. 42, 45, 47)

Effelsberg E. and Peters N.
Scalar dissipation rates in turbulent jets and jet diffusion flames.
Proc. Combust. Inst., Vol. 22, pp. 693–700, 1988. (cited on p. 79)

European Comission.
Panorama of Energy - Energy statistics to support EU policies and solutions.
Office for Official Publications of the European Communities, 2009. (cited on p. 4)

European Comission.
Flightpath 2050 Europe's Vision for Aviation.
Publications Office of the European Union, 2011. (cited on p. 4)

European Comission.
EU Energy in Figures - Statistical Pocketbook 2013.
Publications Office of the European Union, 2013. (cited on p. 4)

Fairweather M. and Woolley R. M.
First-order conditional moment closure modeling of turbulent, nonpremixed hydrogen flames.
Combust. Flame, Vol. 133, pp. 393–405, 2003. (cited on p. 46)

Fairweather M. and Woolley R. M.
First- and second-order elliptic conditional moment closure calculations of piloted methane diffusion flames.
Combust. Flame, Vol. 150, pp. 92–107, 2007. (cited on p. 46)

Favre A.
Équations des gaz turbulents compressibles.
Jour. Méc., Vol. 4, pp. 361–390, 1965. (cited on p. 36)

Favre A.
Statistical equations of turbulent gases.
In *Problems of Hydrodynamics and Continuum Mechanics*, pp. 231–266, Philadelphia, 1969.
Soc. for Ind. and Appl. Mathematics. (cited on p. 36)

Fiorina B., Baron R., Gicquel O., Thevenin D., Carpentier S. and Darabiha N.
Modelling non-adiabatic partially premixed flames using flame-prolongation of ILDM.
Combust. Theory Modelling, Vol. 7, pp. 449–470, 2003. (cited on p. 72)

Flynn P. F., Durret R. P., Hunter G. L., zur Loye A. O., Akinyemi O. C., Dec J. E. and Westbrook C. K.
Diesel Combustion: An Integrated View Combining Laser Diagnostics, Chemical Kinetics, And Empirical Validation.
SAE Technical Paper 1999-01-0509, 1999. (cited on p. 158)

Galpin J., Naudin A., Vervisch L., Angelberger C., Colin O. and Domingo P.
Large-eddy simulation of a fuel-lean premixed turbulent swirl-burner.
Combust. Flame, Vol. 155, pp. 247–266, 2008. (cited on p. 94)

García-Oliver J. M., Novella R., Pastor J. M. and Winklinger J. F.
Evaluation of combustion models based on tabulated chemistry and presumed probability density function approach for diesel spray simulation.
Int. J. Comp. Mathematics, Vol. 91, pp. 14–23, 2014. (cited on p. 129)

García-Oliver J. M., Pastor J. M. and Pandal A.
A comparison of diesel sprays CFD modelling approaches: DDM vs Σ-Y Eulerian atomization model.
Submitted to J. Multiphase Flow, 2014.
(private communication). (cited on p. 157)

García-Oliver J. M., Pastor J. M., Pandal A., Trask N., Baldwin E. and Schmidt D. P.
Diesel spray CFD simulations based on the Σ-Y Eulerian atomization model.
Atomization Sprays, Vol. 23, pp. 71–95, 2013. (cited on p. 157)

Ghosal S. and Vervisch L.
Stability Diagram for Lift-Off and Blowout of a Round Jet Laminar Diffusion Flame.
Combust. Flame, Vol. 123, pp. 646–655, 2001. (cited on p. 26)

Gicquel O., Darabiha N. and Thévenin D.
Laminar premixed hydrogen/air counterflow flame simulations using flame prolongation of ILDM with differential diffusion.
Proc. Combust. Inst., Vol. 28, pp. 1901–1908, 2000. (cited on pp. 44, 71)

Gicquel O., Thévenin D., Hilka M. and Darabiha N.
Direct numerical simulation of turbulent premixed flames using intrinsic low-dimensional manifolds.
Combust. Theory Modelling, Vol. 3, pp. 479–502, 1999. (cited on p. 44)

Girimaji S. S.
Assumed β-pdf Model for Turbulent Mixing: Validation and Extension to Multiple Scalar Mixing.
Combust. Sci. Technol., Vol. 78, pp. 177–196, 1991. (cited on p. 79)

Gopalakrishnan V. and Abraham J.
Effects of multicomponent diffusion on predicted ignition characteristics of an n-heptane diffusion flame.
Combust. Flame, Vol. 136, pp. 557–566, 2004. (cited on p. 134)

Gordon R. L., Masri A. R., Pope S. B. and Goldin G. M.
A numerical study of auto-ignition in turbulent lifted flames issuing into a vitiated co-flow.
Combust. Theory Modelling, Vol. 11, pp. 351–376, 2007. (cited on p. 119)

Grcar J. F.
The Twopnt Program for Boundary Value Problems.
SAND91-8230, 1992. (cited on p. 62)

Han Z., Parrish S., Farrell P. V. and Reitz R. D.
Modeling Atomization Processes Of Pressure Swirl Hollow-Cone Fuel Sprays.
Atomization Sprays, Vol. 7, pp. 663–684, 1997. (cited on p. 131)

Hawkes E. R., Sankaran R., Sutherland J. C. and Chen J. H.
Direct numerical simulation of turbulent combustion: fundamental insights towards predictive models.
J. Phys.: Conf. Ser., Vol. 16, pp. 65–79, 2005. (cited on p. 33)

Haworth D. C.
Progress in probability density function methods for turbulent reacting flows.
Prog. Energy Combust. Sci., Vol. 36, pp. 168–259, 2010. (cited on p. 47)

Heywood J.
Internal Combustion Engines.
McGraw-Hill, New York, 1988. (cited on p. 143)

Higgins B., Siebers D. and Aradi A.
Diesel-Spray Ignition and Premixed-Burn Behavior.
SAE Technical Paper 2000-01-0940, 2000. (cited on pp. 139, 144)

Hirschfelder J. O., Curtiss C. F. and Byrd R. B.
Molecular theory of gases and liquids.
John Wiley & Sons, New York, 1969. (cited on p. 39)

Höök M.
Fuelling Future Emissions - Examining fossil fuel production outlooks used in climate models.
InTech, 2011. (cited on p. 3)

http://www.openfoam.org/archive/1.6/download/.
The OpenFOAM Foundation.
Download OpenFOAM® v1.6, looked up on 22.06.2014. (cited on p. 88)

http://www.sandia.gov/ecn/.
Engine Combustion Network, looked up in August 2014. (cited on p. 130)

http://www.sandia.gov/ecn/cvdata/dsearch/frameset.php.
ECN Data Search Utility, looked up in August 2014. (cited on pp. 130, 131, 133, 153)

http://www.sandia.gov/ecn/cvdata/sandiaCV/SprayHroi.php.
Spray H: Recommended rate of injection, looked up in August 2014. (cited on p. 134)

http://www.sandia.gov/ecn/cvdata/sandiaCV/vesselGeometry 2009.php.
Combustion Vessel Geometry, looked up in August 2014. (cited on p. 133)

Idicheria C. A. and Pickett L. M.
Formaldehyde Visualization Near Lift-off Location in a Diesel Jet.
SAE Technical Paper 2006-01-3434, 2006. (cited on p. 153)

IEA.
World Energy Outlook 2011.
International Energy Agency (IEA), 2011. (cited on p. 4)

IEA.
Key World Energy Statistics 2013.
International Energy Agency (IEA), 2013. (cited on p. 3)

Ihme M. and Pitsch H.
Prediction of extinction and reignition in nonpremixed turbulent flames using a flamelet/progress variable model 1. A priori study and presumed PDF closure.
Combust. Flame, Vol. 155, pp. 70–89, 2008. (cited on p. 45)

Ihme M. and Pitsch H.
Prediction of extinction and reignition in nonpremixed turbulent flames using a flamelet/progress variable model 2. Application in LES of Sandia flames D and E.
Combust. Flame, Vol. 155, pp. 90–107, 2008. (cited on p. 45)

Ihme M. and See Y. C.
Prediction of autoignition in a lifted methane/air flame using an unsteady flamelet/progress variable model.
Combust. Flame, Vol. 157, pp. 1850–1862, 2010. (cited on pp. 56, 83)

Janicka J., Kolbe W. and Kollmann W.
Closure of the transport equation for the probability density function of turbulent scalar fields.
J. Non-Equilib. Thermodyn., Vol. 4, pp. 47–66, 1977. (cited on p. 46)

Janicka J. and Peters N.
Prediction of turbulent jet diffusion flame lift-off using a pdf transport equation.
In *19th Symposium (Int.) on Combustion*, pp. 367–374, Pittsburgh, 1982. The Combustion Institute. (cited on p. 134)

Jones W. P. and Launder B. E.
The prediction of laminarization with a two–equation model of turbulence.
International Journal of Heat and Mass Transfer, Vol. 15, pp. 301–314, 1972. (cited on p. 38)

K. Kuan–yun Kuo.
Principles of Combustion.
John Wiley & Sons, 1986. (cited on pp. 14, 15)

Kärrholm F. B.
Numerical Modelling of Diesel Spray Injection, Turbulence Interaction and Combustion.
Doctoral Thesis, Chalmers Tekniska Hogskola, Göteborg, 2008. (cited on p. 131)

Kee R. J., Miller J. A. and Evans G. H.
A computational model of the structure and extinction of strained, opposed flow, premixed methane-air flames.
Proc. Combust. Inst., Vol. 22, pp. 1479–1494, 1988. (cited on p. 61)

Kim J. S. and Williams F. A.
Extinction of diffusion flames with nonunity Lewis numbers.
J. Engng. Math., Vol. 31, pp. 101–118, 1997. (cited on p. 62)

Kim W. T. and Huh K. Y.
Numerical simulation of spray autoignition by the first order conditional moment closure model.
Proc. Combust. Inst., Vol. 29, pp. 569–576, 2002. (cited on p. 46)

Klimenko A. Y.
Multicomponent diffusion of various scalars in turbulent flows.
Fluid Dyn., Vol. 25, pp. 327–334, 1990. (cited on p. 46)

Klimenko A. Y. and Bilger R. W.
Conditional moment closure for turbulent combustion.
Prog. Energy Combust. Sci., Vol. 25, pp. 595–688, 1999. (cited on p. 46)

Klimenko A. Y. and Pope S. B.
A model for turbulent reactive flows based on multiple mapping conditioning.
Phys. Fluids, Vol. 15, pp. 1907–1925, 2003. (cited on p. 46)

Kolmogorov A. N.
A refinement of previous hypotheses concerning the local structure of turbulence in a viscous incompressible fluid at high Reynolds number.
J. Fluid Mech., Vol. 13, pp. 82–85, 1962. (cited on p. 32)

Kolmogorov A. N.
The Local Structure of Turbulence in Incompressible Viscous Fluid for Very Large Reynolds Numbers.
Proc. R. Soc. London, Vol. 434, pp. 9–13, 1991. (cited on p. 32)

Kronenburg A., Bilger R. W. and Kent J. H.
Second Order Conditional Moment Closure for Turbulent Jet Diffusion Flames.
Proc. Combust. Inst., Vol. 29, pp. 1097–1104, 1998. (cited on p. 46)

Kuznetsov V. R.
Effect of turbulence on the formation of large superequilibrium concentration of atoms and free radicals in diffusion flames.
Mehan. Zhidkosti Gasa, Vol. 6, pp. 3–9, 1982. (cited on p. 22)

Launder B. E., Reece G. J. and Rodi W.
Progress in the Development of a Reynolds-Stress Turbulence Closure.
J. Fluid Mech., Vol. 68, pp. 537–566, 1975. (cited on p. 37)

Launder B. E. and Sharma B. I.
Application of the Energy Dissipation Model of Turbulence to the Calculation of Flow Near a Spinning Disc.
Letters in Heat and Mass Transfer, Vol. 1, pp. 131–138, 1974. (cited on p. 38)

Launder B. E. and Spalding D. B.
The Numerical Computation of Turbulent Flows.
Comput. Methods Appl. Mech. Eng., Vol. 3, pp. 269–289, 1974. (cited on p. 38)

Law C. K.
Combustion Physics.
Cambridge University Press, New York, 2006. (cited on p. 43)

Libby P. A. and Williams F. A.
Turbulent combustion: fundamental aspects and a review.
In Libby P. A. and Williams F. A., editors, *Turbulent reacting Flows*, pp. 2–61. Academic Press, London, 1994. (cited on pp. 25, 79)

Liñán A.
Ignition and flame spread in laminar mixing lauyers.
In Buckmaster J., Jackson T. L. and Kumar A., editors, *Combustion in High–Speed Flows*, pp. 461–476. Kluwer Academic, Dordrecht, 1994. (cited on p. 26)

Lu T., Law C. K., Yoo C. S. and Chen J. H.
Dynamic stiffness removal for direct numerical simulations.
Combust. Flame, Vol. 156, pp. 1542–1551, 2009. (cited on p. 144)

Lutz A. E., Kee R. J., Grcar J. F. and Rupley F. M.
OPPDIF: A Fortran program for computing opposed-flow diffusion flames.
SAND96-8243, 1997. (cited on p. 61)

Lyons K. M.
Toward an understanding of the stabilization mechanisms of lifted turbulent jet flames: Experiments.
Progr. Energy Comb. Sci., Vol. 33, pp. 211–231, 2007. (cited on p. 149)

Maas U. and Pope S. B.
Simplifying chemical kinetics: Intrinsic low-dimensional manifolds in composition space.
Combust. Flame, Vol. 88, pp. 239–264, 1992. (cited on p. 44)

Martin S. M., Kramlich J. C., Kosály G. and Riley J. J.
The premixed conditional moment closure method applied to idealized lean premixed gas turbine combustors.
J. Eng. Gas Turb. Power, Vol. 125, pp. 895–900, 2003. (cited on p. 46)

Masri A. R., Pope R. Cao S. B. and Goldin G. M.
PDF calculations of turbulent lifted flames of H2/N2 fuel issuing into a vitiated co-flow.
Combust. Theory Modelling, Vol. 8, pp. 1–22, 2004. (cited on p. 112)

Mastorakos E. and Bilger R. W.
Second-order conditional moment closure for the auto-ignition of turbulent flows.
Physics of Fluids, Vol. 10, pp. 1246–1248, 1998. (cited on p. 46)

Michel J.-B., Colin O. and Angelberger C.
On the formulation of species reaction rates in the context of multi-species CFD codes using complex chemistry tabulation techniques.
Combust. Flame, Vol. 157, pp. 701–714, 2010. (cited on pp. 83, 95)

Michel J.-B., Colin O., Angelberger C. and Veynante D.
Using the tabulated diffusion flamelet model ADF-PCM to simulate a lifted methane-air jet flame.
Combust. Flame, Vol. 156, pp. 1318–1331, 2009. (cited on pp. 126, 132, 146)

Michel J.-B., Colin O. and Veynante D.
Modeling ignition and chemical structure of partially premixed turbulent flames using tabulated chemistry.
Combust. Flame, Vol. 152, pp. 80–99, 2008. (cited on pp. 69, 75, 77, 85, 132)

Michel J.-B., Colin O. and Veynante D.
Comparison of Differing Formulations of the PCM Model by their Application to the Simulation of an Auto-igniting H2/air Jet.
Flow Turb. Combust., Vol. 83, pp. 33–60, 2009. (cited on p. 83)

Mortensen M. and Bilger R. W.
Derivation of the conditionalmoment closure equations for spray combustion.
Combust. Flame, Vol. 156, pp. 62–72, 2009. (cited on p. 46)

Mukhopadhyay S. and Abraham J.
Influence of compositional stratification on autoignition in n-heptane/air mixtures.
Combust. Flame, Vol. 158, pp. 1064–1075, 2011. (cited on p. 134)

Najafizadeh S. M. M., Sadeghi M. T. and Sotudeh-Gharebagh R.
Analysis of autoignition of a turbulent lifted H2/N2 jet flame issuing into a vitiated coflow.
Int Journal Hydrogen Energy, Vol. 38, pp. 2510–2522, 2013. (cited on p. 112)

Najafizadeh S. M. M., Sadeghi M. T., Sotudeh-Gharebagh R. and Roekaerts D. J. E. M.
Chemical structure of autoignition in a turbulent lifted H2/N2 jet flame issuing into a vitiated coflow.
Combust. Flame, Vol. 160, pp. 2928–2940, 2013. (cited on pp. 111, 112)

Naud B., Novella R., Pastor J. M. and Winklinger J. F.
Comparison of Different Assumptions for Tabulated Chemistry Based on Laminar Igniting and Extinguishing Diffusion Flamelets.
Proc. European Comb. Meeting, 2013. (cited on p. 61)

Naud B., Novella R., Pastor J. M. and Winklinger J. F.
RANS modelling of a lifted H2/N2 flame using an unsteady flamelet / progress variable approach with presumed PDF.
Combust. Flame, 2014.
(accepted for publication). (cited on pp. 125, 126)

Nooren P. A., Wouters H. A., Peeters T. W. J., Roekaerts D., Maas U. and Schmidt D.
Monte Carlo PDF modeling of a turbulent natural-gas diffusion flame.
Combust. Theory Modelling, Vol. 1, pp. 79–96, 1997. (cited on p. 46)

Norris A. T. and Pope S. B.
Modeling of Extinction in Turbulent Diffusion Flames by the Velocity-Dissipation-Composition PDF Method.
Combust. Flame, Vol. 100, pp. 211–220, 1995. (cited on p. 44)

O'Brien E. E.
The probability density function (PDF) approach to reacting turbulent flows.
In Libby P. A. and Williams F. A., editors, *Turbulent reacting flows*, pp. 185–218. Academic Press, London, 1980. (cited on p. 45)

OpenFOAM The Open Source CFD Toolbox.
User Gide Version 1.6, 2009. (cited on p. 88)

Pastor J. V., García-Oliver J. M., Pastor J. M. and Vera-Tudela W.
1D diesel spray modelling of multi-component fuels.
Atomization Sprays, 2014.
(accepted, in press). (cited on p. 132)

Patwardhan S. S., De S., Lakshmisha K. N. and Raghunandan B. N.
CMC simulations of lifted turbulent jet flame in a vitiated coflow.
Proc. Combust. Inst., Vol. 32, pp. 1705–1712, 2009. (cited on p. 112)

Pei Y., Hawkes E. R. and Kook S.
A Comprehensive Study of Effects of Mixing and Chemical Kinetic Models on Predictions of n-heptane Jet Ignitions with the PDF Method.
Flow Turb. Combust., Vol. 91, pp. 249–280, 2013. (cited on p. 144)

Pera C., Colin O. and Jay S.
Development of a FPI Detailed Chemistry Tabulation Methodology for Internal Combustion Engines.
Oil Gas Sci. Technol., Vol. 64, pp. 243–258, 2009. (cited on pp. 94, 95)

Peters N.
Local quenching of diffusion flamelets and non-premixed turbulent combustion.
In *Western States Section of the Combustion Institute*, WSS 80-4, Spring Meeting, Irvine, CA, 1980. (cited on p. 22)

Peters N.
Laminar diffusion flamelet models in non-premixed turbulent combustion.
Prog. Energy Combust. Sci., Vol. 10, pp. 319–339, 1984. (cited on pp. 45, 62)

Peters N.
The turbulent burning velocity for large–scale and small–scale turbulence.
J. Fluid Mech., Vol. 384, pp. 107–132, 1999. (cited on p. 19)

Peters N.
Turbulent Combustion.
Cambridge University Press, 2000. (cited on pp. 14, 17, 21, 22, 45, 46, 58, 62)

Peters N. and Williams F. A.
Liftoff Characteristics of Turbulent Jet Diffusion Flames.
AIAA, Vol. 21, pp. 423–429, 1983. (cited on p. 150)

Petzold L. R.
A Description of DASSL: A Differential/Algebraic System Solver.
SAND82-8637, 1982. (cited on p. 62)

Phillips H.
Flame in a buoyant methane layer.
In *10th Symposium (Int.) on Combustion*, pp. 1277–1283, Pittsburgh, 1965. The Combustion Institute. (cited on p. 26)

Pickett L. M. and Siebers D. L.
Non-Sooting, Low Flame Temperature Mixing-Controlled DI Diesel Combustion.
SAE Technical Paper 2004-01-1399, 2004. (cited on p. 153)

Pickett L. M. and Siebers D. L.
Soot in diesel fuel jets: effects of ambient temperature, ambient density, and injection pressure.
Combust. Flame, Vol. 138, pp. 114–135, 2004. (cited on p. 153)

Pickett L. M., Siebers D. L. and Idicheria C. A.
Relationship Between Ignition Processes and the Lift-Off Length of Diesel Fuel Jets.
SAE Technical Paper 2005–01–3843, 2005. (cited on pp. 26, 58, 132, 149)

Pierce C. D. and Moin P.
Progress–variable approach for large–eddy simulation of non–premixed turbulent combustion.
J. Fluid Mech., Vol. 504, pp. 73–79, 2004. (cited on p. 45)

Pita E. G.
Heat and Mass Transfer in Evaporating Sprays.
University of Maryland, College Park, 1969. (cited on p. 131)

Pitsch H.
Large-Eddy Simulation of Turbulent Combustion.
Ann. Rev. Fluid Mech., Vol. 38, pp. 453–482, 2006. (cited on p. 33)

Pitsch H. and Ihme M.
An Unsteady/Flamelet Progress Variable Method for LES of Nonpremixed Turbulent Combustion.
43rd AIAA Aerospace Sciences Meeting and Exhibit, Vol. Paper 2004–557, 2005. (cited on p. 56)

Pitsch H. and Peters N.
A consistent flamelet formulation for non-premixed combustion considering differential diffusion effects.
Combust. Flame, Vol. 114, pp. 26–40, 1998. (cited on p. 22)

Pitsch H. and Peters N.
Unsteady flamelet modeling of turbulent hydrogen-air diffusion flames.
In *27th Symposium (Int.) on Combustion*, pp. 1057–1064, Pittsburgh, 1998. The Combustion Institute. (cited on p. 22)

Pitts W. M.
Assessment of theories for the behaviourand blowout of lifted turbulent jet diffusion flames.
In *22nd Symposium (Int.) on Combustion*, pp. 809–816, Pittsburgh, 1988. The Combustion Institute. (cited on p. 26)

Plessing T., Terhoeven P., Peters N. and Mansour M. S.
An Experimental and Numerical Study of a Laminar Triple Flame.
Combust. Flame, Vol. 115, pp. 335–353, 1998. (cited on p. 27)

Poinsot T. and Veynante D.
Theoretical and Numerical Combustion.
Edwards, 2005. (cited on pp. 14, 16, 17, 21, 24, 39, 41)

Poinsot T., Veynante D. and Candel S.
Diagrams of premixed turbulent combustion based on direct simulation.
Proc. Combust. Inst., Vol. 23, pp. 613–619, 1990. (cited on p. 16)

Poinsot T., Veynante D. and Candel S.
Quenching process and premixed turbulent combustion diagrams.
J. Fluid Mech., Vol. 228, pp. 561–605, 1991. (cited on p. 19)

Pope S. B.
A Monte Carlo method for the pdf equations of turbulent reactive flow.
Combust. Sci. Technol., Vol. 25, pp. 159–174, 1981. (cited on p. 47)

Pope S. B.
PDF method for turbulent reacting flows.
Prog. Energy Combust. Sci., Vol. 11, pp. 119–192, 1985. (cited on pp. 45, 46)

Pope S. B.
Computationally efficient implementation of combustion chemistry using in situ adaptive tabulation.
Combust. Theory Modelling, Vol. 1, pp. 41–63, 1997. (cited on p. 43)

Pope S. B.
Turbulent Flows.
Cambridge University Press, 2000. (cited on pp. 31, 33, 38, 39, 40)

Ra Y. and Reitz R. D.
A reduced chemical kinetic model for IC engine combustion simulations with primary reference fuels.
Combust. Flame, Vol. 155, pp. 713–738, 2008. (cited on p. 131)

Reitz R. D.
Modeling Atomization Processes in High-Pressure Vaporizing Sprays.
Atomisation Spray Technol., Vol. 3, pp. 309–337, 1987. (cited on p. 131)

Ren Z. and Pope S. B.
An investigation of the performance of turbulent mixing models.
Combust. Flame, Vol. 136, pp. 208–216, 2004. (cited on p. 46)

Richardson L. F.
Weather Prediction by Numerical Process.
Cambridge University Press, 1922. (cited on p. 31)

Roberts W. L., Driscoll J. F., Drake M. C. and Goss L. P.
Images of the quenching of a flame by a vortex—To quantify regimes of turbulent combustion.
Combust. Flame, Vol. 94, pp. 58–69, 1993. (cited on p. 19)

Sadasivuni S. K.
LES Modelling of Non-premixed and Partially Premixed Turbulent Flames.
Doctoral Thesis, Loughborough University, 2009. (cited on p. 56)

Saxena P. and Williams F. A.
Testing a small detailed chemical-kinetic mechanism for the combustion of hydrogen and carbon monoxide.
Combust. Flame, Vol. 145, pp. 316–323, 2006. (cited on pp. 63, 106)

Sazhin S.
Droplets and Sprays.
Springer London, 2014. (cited on p. 131)

Senouci M., Bounif A., Abidat M., Belkaid N. M., Mansour C. and Gokalp I.
Transported-PDF (IEM, EMST) micromixing models in a hydrogen-air nonpremixed turbulent flame.
Acta Mech, Vol. 224, pp. 3111–3124, 2013. (cited on p. 46)

Siebers D. and Higgins B.
Flame Lift-Off on Direct-Injection Diesel Sprays Under Quiescent Conditions.
SAE Technical Paper 2001-01-0530, 2001. (cited on pp. 58, 153)

Sirignano W. A.
Fluid Dynamics and Transport of Droplets and Sprays.
Cambridge University Press, 2010. (cited on p. 131)

Subramaniam S. and Pope S. B.
A mixing model for turbulent reactive flows based on Euclidean minimum spanning trees.
Combust. Flame, Vol. 115, pp. 487–514, 1998. (cited on p. 46)

Tennekes H. and Lumley J. L.
A first course in turbulence.
MIT Press, 1972. (cited on p. 30)

Tillou J., Michel J.-B., Angelberger C., Bekdemir C. and Veynante D.
Large-Eddy Simulation of Diesel Spray Combustion with Exhaust Gas Recirculation.
Oil Gas Sci. Technol., Vol. 69, pp. 155–165, 2014. (cited on p. 155)

Turns S. R.
An Introduction to Combustion.
MacGraw–Hill, 2000. (cited on pp. 12, 18)

van Oijen J. A. and de Goey L. P. H.
Modelling of premixed laminar flames using flamelet-generated manifolds.
Combust. Sci. Technol., Vol. 161, pp. 113–137, 2000. (cited on p. 44)

van Oijen J. A. and de Goey L. P. H.
Modelling of premixed counterflow flames using the flamelet-generated manifold method.
Combust. Theory Modelling, Vol. 6, pp. 463–478, 2002. (cited on p. 44)

van Oijen J. A. and de Goey L. P. H.
A numerical study of confined triple flames using a flamelet-generated manifold.
Combust. Theory Modelling, Vol. 8, pp. 141–163, 2004. (cited on p. 44)

van Oijen J. A., Lammers F. A. and de Goey L. P. H.
Modeling of Complex Premixed Burner Systems by Using Flamelet-Generated Manifolds.
Combust. Flame, Vol. 127, pp. 2124–2134, 2001. (cited on pp. 44, 71)

Venugopal R. and Abraham J.
A Review of Fundamental Studies Relevant to Flame Lift–off in Diesel Jets.
SAE Technical Paper 2007–01–0134, 2007. (cited on pp. 26, 58, 149)

Versteeg H. K. and Malalasekera W.
An Introduction to Computational Fluid Dynamics.
Pearson, 2007. (cited on pp. 30, 38)

Vervisch L.
Using numerics to help the understanding of non–remixed turbulent flames.
Proc. Combust. Inst., Vol. 28, pp. 11–24, 2000. (cited on p. 27)

Vervisch L., Hauguel R., Domingo P. and Rullaud M.
Three facets of turbulent combustion modelling: DNS of premixed V-flame, LES of lifted nonpremixed flame and RANS of jet-flame.
Journal of Turbulence, Vol. 4, pp. 1–36, 2004. (cited on pp. 44, 78)

Vervisch L. and Poinsot T.
Direct numerical simulation of non-premixed turbulent flames.
Ann. Rev. Fluid Mech., Vol. 30, pp. 655–691, 1998. (cited on p. 33)

Veynante D. and Vervisch L.
Turbulent combustion modeling.
Prog. Energy Combust. Sci., Vol. 28, pp. 193–266, 2002. (cited on pp. 33, 42, 47, 78)

Vicquelin R.
Tabulation de la cinétique chimique pour la modélisation et la simulation de la combustion turbulente.
Doctoral Thesis, Ecole Centrale Paris, 2010. (cited on pp. 56, 83, 112, 119)

Villermaux J. and Devillon J. C.
Représentation de la coalescence et de la redispersion des domaines de ségrégation dans un fluide par un modèle d'interaction phénoménologique.
In *Proc. Second Intern'l. Symp. on Chemical Reaction Engineering*, pp. 1–13, New York, 1972. Elsevier. (cited on p. 46)

Vreman A. W., Albrecht B. A., van Oijen J. A., de Goey L. P. H. and Bastiaans R. J. M.
Premixed and nonpremixed generated manifolds in large-eddy simulation of Sandia flame D and F.
Combust. Flame, Vol. 153, pp. 394–416, 2008. (cited on p. 44)

Wang W. and Echekki T.
Investigation of lifted jet flames stabilization mechanism using RANS simulations.
Fire Safety Journal, Vol. 46, pp. 254–261, 2011. (cited on p. 58)

Warnatz J., Maas U. and Dibble R. W.
Combustion.
Springer, 2006. (cited on pp. 16, 17, 20, 37, 42, 43)

White F. M.
Viscous Fluid Flow.
McGraw-Hill, 1991. (cited on pp. 28, 30)

Wilcox D. C.
Turbulence Modeling for CFD.
DCW Industries, 1994. (cited on pp. 35, 37)

Williams F. A.
Turbulent Mixing in Nonreactive and Reactive Flows.
In Murthy S. N. B., editor, *Recent advances in theoretical descriptions of turbulent diffusion flames*, pp. 189–208. Plenum Press, New York, 1975. (cited on p. 23)

Williams F. A.
Combustion Theory.
Addison-Wesley, 1985. (cited on p. 16)

Wu Z. J., Starner S. H. and Bilger R. W.
Lift-off heights of turbulent H2/N2 jet flames in a vitiated co-flow.
Australian Symposium on Combustion and the 8th Australian Flame Days, pp. 142–147, Melbourne, 2003. (cited on p. 119)

Xiao K., Schmidt D. and Maas U.
PDF simulations of turbulent non-premixed CH4/H2-air flames using automatically reduced chemical kinetics.
Proc. Combust. Inst., Vol. 27, pp. 1073–1080, 1998. (cited on p. 44)

Zeuch T., Moréac G., Ahmed S. S. and Mauss F.
A comprehensive skeletal mechanism for the oxidation of n-heptane generated by chemistry-guided reduction.
Combust. Flame, Vol. 155, pp. 651–674, 2008. (cited on pp. 43, 69, 131)